Development of Simultaneous Electroencephalography and Near-Infrared Optical Topography for Applications to Neurovascular Coupling and Neonatal Seizures

Robert J Cooper, MPhys
Department of Medical Physics and Bioengineering, UCL.

A thesis submitted for the degree of Doctor of Philosophy (Ph.D.) at University College London

I hereby declare that the work presented in this thesis is my own, and where information has been derived from other sources, those sources are credited.

Robert J Cooper

Abstract

This thesis describes the development and preliminary application of methods for performing simultaneous electroencephalography (EEG) and near-infrared (NIR) imaging of the brain. The simultaneous application of EEG and NIR imaging has many benefits because of the complementary nature of the two modalities, and has significant potential in the study of the relationship between neuronal activity and cerebral haemodynamics.

This work goes beyond previous experiments which have combined EEG and limited-channel near-infrared spectroscopy by designing and implementing an arrangement which allows dense near-infrared optical topography and EEG to be performed over the same cortical area, with as simple an application method as possible. These application methods are described in detail, as is their extensive testing using novel dual-modality phantoms and an in-vivo EEG-NIR imaging experiment in a healthy adult.

These methods are subsequently applied to the study of neonates in the clinical environment. An intricate EEG-NIR imaging experiment is designed and implemented in an investigation of functional activation in the healthy neonatal visual cortex. This series of experiments also acts as a further test of the suitability of our EEG-NIR imaging methods for clinical application. The results of these experiments are presented.

The EEG-NIR imaging arrangement is then applied to four neurologically damaged infants in the neonatal intensive care unit, each of whom had been diagnosed with seizures. The results of these studies are presented, and a potentially significant haemodynamic feature, which is not present in age-matched controls, is identified. The importance and physiological implications of our findings are discussed, as is the suitability of a combined EEG and NIR imaging approach to the study and monitoring of neonatal brain injury.

Acknowledgements

I consider myself extremely lucky to have had access to the expertise and constant support of a large number of UCL scientists throughout my PhD. This includes my supervisors, Prof. Jem Hebden and Dr. Adam Gibson, who have been outstanding, and to whom I owe a great deal. It also includes Dr. Nick Everdell who, despite having no obligation, has provided me with continual advice and assistance and has fielded the majority of my more stupid enquiries. I would also like to thank all those in the department who have assisted me in the last three years, particularly Dr. Louise Enfield, Prof. Clare Elwell, and Dr. Salavat Magazov.

Without the collaboration and enthusiasm of Dr. Topun Austin, this thesis would have been impossible and I am very grateful for his continued encouragement. I must also thank the Rosie Hospital research team, Dr. Helen O'Reilly and Dr. Subha Mitra, who were essential to all our clinical experiments and contributed a great deal of time and effort.

I would also like to thank my parents, Jill and Steve Cooper, for without their generous and unwavering supply of tea this thesis would never have been completed. Finally I would like to thank Andrea Zitna for putting up with me still being a student.

This work has been supported by the EPSRC.

Publications resulting from this work

Peer-reviewed journal papers

Cooper, R J, Jeremy C Hebden, H O'Reilly, S Mitra, A Mitchell, N L Everdell, A P Gibson and T Austin. "**Transient haemodynamic events in neurologically compromised infants: a simultaneous EEG and diffuse optical imaging study."** (submitted)

Cooper, R J and T Austin. "**Combining EEG and Diffuse Optical Imaging: A new approach to monitoring neonatal seizures?**" *Advances in Clinical Neuroscience and Rehabilitation.*10, no. 4 (2010).

Cooper, R J, R Eames, J Brunker, L C Enfield, A P Gibson, and Jeremy C Hebden. "**A tissue equivalent phantom for simultaneous near-infrared optical tomography and EEG.**" *Biomedical Optics Express* 1, no. 2 (2010): 425-430.

Cooper, R J, D Bhatt, N L Everdell, and Jeremy C Hebden. "**A tissue-like optically turbid and electrically conducting phantom for simultaneous EEG and near-infrared imaging.**" *Physics in Medicine and Biology* 54, no. 18 (2009): N403-408.

Cooper, R J, N L Everdell, L C Enfield, A P Gibson, Alan Worley, and Jeremy C Hebden. "**Design and evaluation of a probe for simultaneous EEG and near-infrared imaging of cortical activation**." *Physics in Medicine and Biology* 54, no. 7 (2009): 2093-2102.

Conference proceedings

Cooper, R J, T Austin, N L Everdell, A P Gibson, and J C Hebden. "**Simultaneous EEG and Near-Infrared Imaging for Investigation of Neurovascular Coupling and Neonatal Seizure**." *Biomedical Optics*, OSA Technical Digest, (Optical Society of America, 2010).

Conference posters

Cooper, R J and Jeremy C Hebden. "**Simultaneous EEG and near-infrared imaging for studies of neonatal seizure**". **Advances in Optics** for **Biotechnology**, **Medicine and Surgery** XI, Burlington, Vermont, USA. July 2009.

Table of Contents

Table of Figures and Tables

Chapter 1

Chapter 2

Project Motivation and Objectives

Current technologies for the investigation of functional activity in the human brain can be placed into two distinct groups by the nature of the signal they observe. Electroencephalography (EEG) and Magnetoencephalography (MEG) are direct measures of the electromagnetic dynamics of synchronously firing of groups of neurons, whilst functional Magnetic Resonance Imaging (fMRI), Positron Emission Tomography (PET), Single Photon Emission Computed Tomography (SPECT) and Near-Infrared (NIR) techniques are used to observe the metabolic or haemodynamic changes which result from a pronounced increase in neuronal activity.

In the last ten years there has been a great increase in research aiming to take advantage of the complementary information present in these two fundamental types of functional brain imaging. Despite the many technical difficulties, simultaneous fMRI and EEG has now become a standard neuro-imaging technique, and has been used extensively in the study of resting cortical activity (Goldman et al. 2002), epilepsy (Gotman et al. 2006, Vuilliemoz et al. 2010) and visual and auditory function (e.g. Bonmassar et al. 1999, Portas et al. 2000).

The virtues which allow NIR techniques to thrive despite the prevalence of fMRI also apply to the simultaneous use of EEG and NIR techniques in a field where EEG-fMRI is common. Ease of application, portability, cost and a relatively high tolerance to movement artifact allow NIR techniques to be used at the bedside, and applied to many vulnerable subject groups which may not be suited to fMRI, PET or SPECT. Near-infrared techniques typically have a significantly higher temporal resolution than fMRI, and also have the advantage of being able to accurately quantify concentration changes in oxy and deoxy-haemoglobin.

Electroencephalography continues to be the dominant technique for the study and diagnosis of epileptic disorders. Techniques which employ EEG concurrently with other methods of interrogating the brain will therefore find many of their applications in study of epileptic seizures. A seizure is a transient period of excessive, often extreme, neuronal firing or synchrony. Clinical signs of seizures typically consist of an altered mental state and/or involuntary movements or convulsions.

Seizures in neonates are particularly common, especially in those who have suffered hypoxic-ischemia or other forms of encephalopathy. Neonatal seizures are very difficult to diagnose for several reasons, but primarily because only one third of electrographic seizures (that is, seizures which can be observed using EEG) manifest themselves physically. Seizures in neonates are often associated with some failure of the cerebrovascular system, but the haemodynamic response to seizures themselves is poorly understood. Given that there is growing evidence that seizures can cause damage to the developing brain (Thibeault et al. 2009, Glass et al. 2009) there has been increasing interest in the use of simultaneous EEG and NIR techniques in the study of neonatal seizures (Toet and Lemmers 2009, Wallois et al. 2009).

Simultaneous EEG and NIR imaging also has a more general application in providing functional information about the brain. EEG techniques have been used for decades to study all aspects of brain function, both in a resting state and in response to particular stimuli. A combined EEG-NIR system has the advantage of measuring both the electro-cortical and haemodynamic activity associated with particular cortical processes as well as having the potential to provide a spatial resolution far better than is possible with EEG alone.

This project has several aims. The first, and most fundamental, is to develop methods which allow high quality EEG recording to be performed

simultaneously with NIR imaging over the same areas of the scalp. These methods must be extensively tested to ensure they are suitable for use in the clinical environment. The second is to apply these methods to the investigation of functional activation in the healthy newborn infant. This will provide further evidence of the suitability of the technique and has the potential to elicit new information about functional processing in the developing brain.

The long-term objective of this work is the development of the technique of EEG-NIR imaging for application to neonatal medicine. To this end, the final aim of this project is to explicitly prove that EEG-NIR imaging techniques are suitable for application to newborn infants in intensive care, and take the first steps towards the study of the haemodynamic changes associated with seizures in the neonate.

This thesis is divided into four chapters. The first outlines the fundamentals of both EEG and near-infrared techniques. The second contains a description of the advantages of a combined EEG-NIR imaging system, discusses some specific applications and details the work that has already been done to combine these two modalities. Chapter two then goes on to describe the work of the author in the development of practical methods of performing simultaneous EEG and NIR imaging and the vigorous testing of these methods. Chapter three describes the direct application of EEG-NIR imaging to two separate series of experiments in neonates: the first designed to study neonatal functional activation and the second to study neonatal seizures. The fourth and final chapter briefly describes the work which remains to be done, and the likely direction that EEG-NIR research will take, particularly with respect to neonatal medicine.

Chapter 1

1.1 Electroencephalography

1.1.1 Introduction and the Origin of the Signal

Electroencephalography is the measurement of variations in electrical potential difference at the scalp. The human cerebral cortex contains billions of neurons, each of which is connected to thousands of others via complex, branch-like extensions of the neuronal cell body. The vast network of neurons that makes up the cerebral cortex is the site of constant electrochemical activity. Neurons are electrically polarised at rest, and transmit and process information by the propagation (or inhibition) of waves of depolarisation of the neuronal cell membrane. As such, electrical activity could not be more fundamental to the function of the brain.

Recorded at the scalp, typical, adult EEG activity will have an amplitude of tens of microvolts. Although all electrochemical processes within the brain produce an electric field, the depolarisation of a single neuron will not produce a signal which is observable at the scalp. However, the summation of the electric fields created by thousands of neurons across a given volume of brain tissue can result in an electrical potential difference large enough to be measured at the scalp. Whether the electro-chemical activity of groups of neurons is observable by EEG is therefore dependent on whether the electric fields created by individual neurons combine constructively or otherwise. Constructive combination of the transient electric fields which result from neuronal activation can only occur if the contributing neurons are approximately aligned (i.e. not orthogonal) and, most importantly, if those neurons are firing in synchrony. Groups of neurons can become increasingly active during the performance of a particular functional task, but this will not be observable as an increase in EEG signal unless that activity is synchronous across that group of neurons. Certain cognitive tasks are known to result in a decrease in EEG activity, because, although they cause an increase in neuronal electro-chemical activity, they remove those neurons from a previously synchronised state (Niedermeyer and Silva 2004).

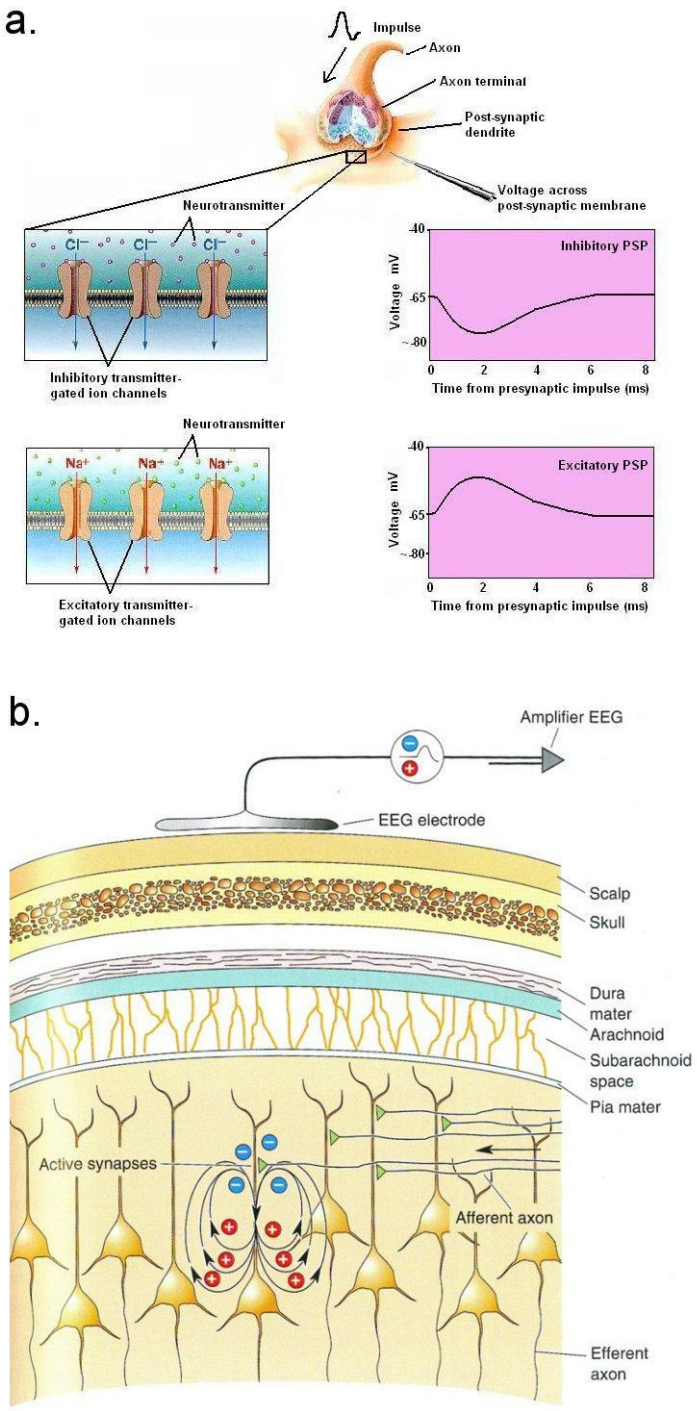

Figure 1.1.1. The resting membrane potential of ~ -70 mV must be depolarised beyond a threshold (~ -40 mV) in order for an action potential to be transmitted. The effects of inhibitory and excitatory neurotransmitters on the post synaptic membrane are shown in figure a. Figure b indicates how current flow in and around a pyramidal neuron due to the creation of a PSP can result in the creation of dipole-like electric field. Only if thousands of neurons contribute to such a field will the result be observable at the scalp (adapted from Bear et al. 2007).

The EEG signal is thought to primarily result from the synchronisation of the electric fields generated by post-synaptic potentials in pyramidal neurons (Schaul 1998, Niedermeyer and Silva 2004). Pyramidal neurons are large, vertically orientated neurons which are abundant in the human cerebral cortex. Post-synaptic potentials (PSPs) are an alteration of the resting potential of the neuronal membrane on the receptor side of a synaptic cleft, which can be in the form of either a depolarisation (an excitatory PSP) or a hyperpolarisation (an inhibitory PSP). Excitatory and inhibitory PSPs induce current to flow in the neuron and in the surrounding extra-cellular space, it is synchronisation of many of these current flows which produces the electric fields observable at the scalp (see figure 1.1.1).

Although neuronal action potentials are higher in amplitude than synaptic potentials, their short duration and the fact that they are transmitted very quickly along the neuronal membrane prevents their synchronisation across a large number of neurons. The spatially integrated electric field which results from asynchronous action potentials is therefore not significant at the scalp. Figure 1.1.2 illustrates how individual neurons contribute to the electric field observable by EEG, and shows the importance of synchronicity.

The electric field produced in and about pyramidal neurons is well approximated by an electrical dipole (Gloor 1985). The solid angle theorem of volume conduction provides a simple explanation of the relationship between the cortical generators of EEG, the location of an electrode and the measured scalp potential. It states that the potential generated at an electrode (relative to a reference at infinity) will be proportional to the solid angle subtended by the poles of the dipole generator.

As stated by Schaul (1998), there are four fundamental factors which influence the size, shape and duration of EEG potentials: (1) the distance of the recording electrode from the pyramidal neurons in question, (2) the

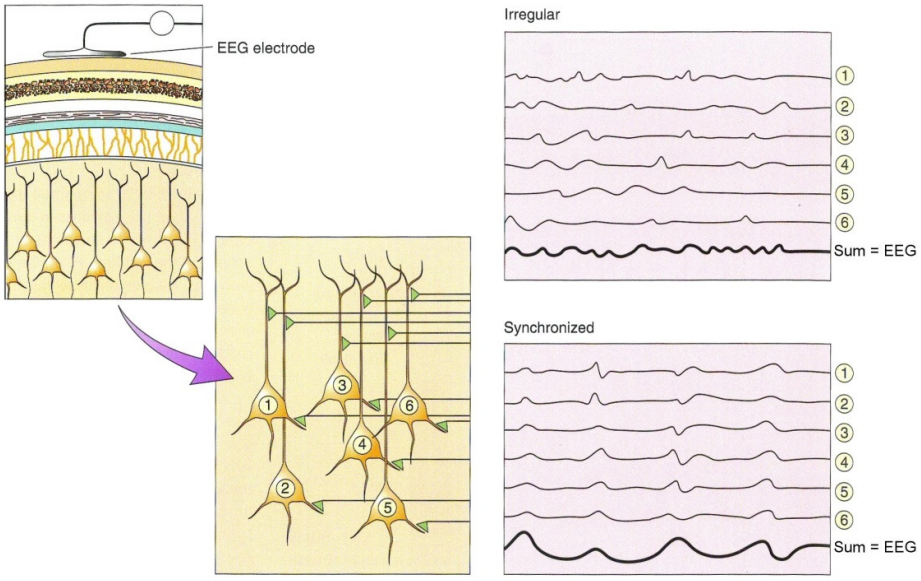

Figure 1.1.2. An illustration of the importance of synchronisation of synaptic input to the recorded EEG. In a given group of pyramidal neurons, all receive many synaptic inputs. If those inputs are irregular, the total electric field will be small, and will not produce significant EEG variation. However, if those inputs are synchronised, the total electric field can be large enough to produce observable signal at the scalp (adapted from Bear et al. 2007).

duration of PSPs in these neurons, (3) the number of PSPs which are synchronous and (4) the orientation of this neuronal layer relative to the electrode.

Although there are dominant generators of electrocortical activity, the EEG should be thought of as resulting from the sum of all electrochemical activity throughout the whole volume of the brain, recorded across an inhomogeneous, non-isotropic, partially-conducting medium. The presence of the skull, cerebo-spinal fluid and scalp between the source of the electric fields and the EEG electrodes limits the amplitude (and therefore signal-to-noise ratio) of any given neuronal activity but also results in a loss of spatial information. In the case of epileptic discharges, it has been reported that as much as 6 cm^2 of cortical surface must exhibit synchronous neuronal

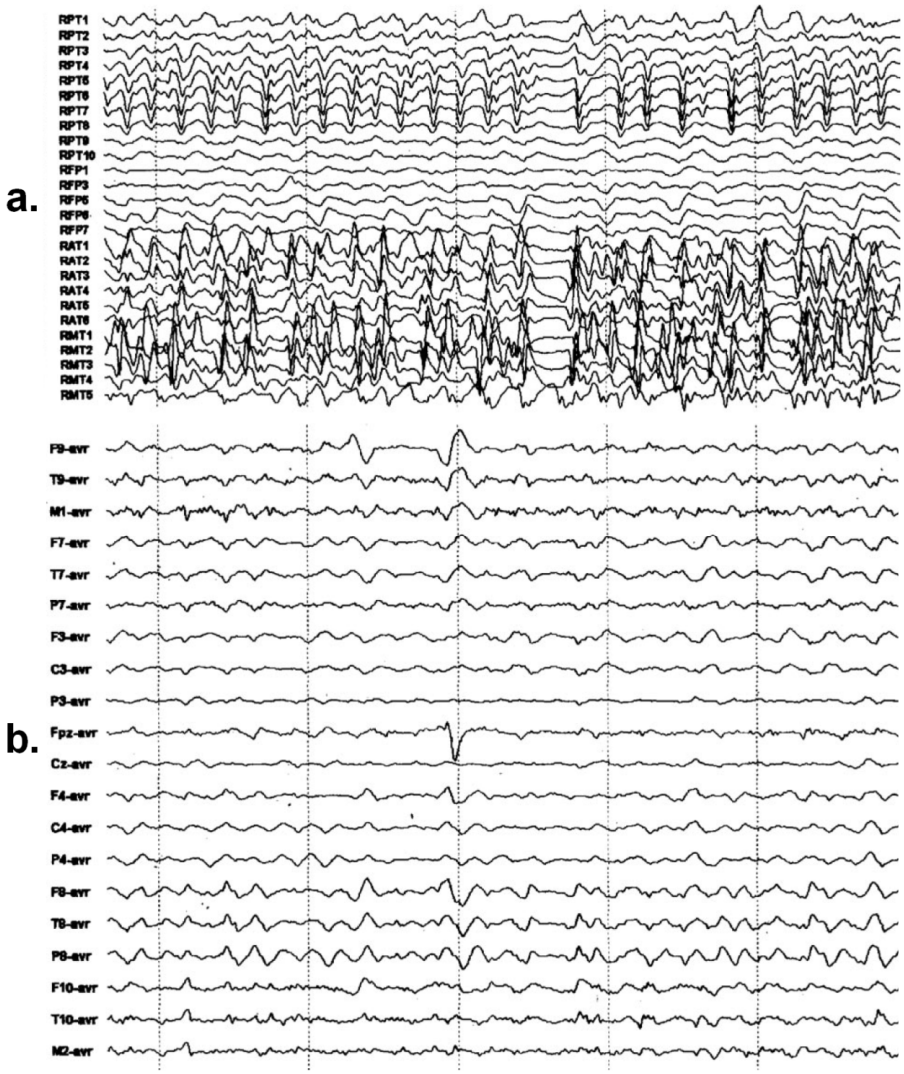

Figure 1.1.3. Simultaneous inter-cranial EEG (a) and scalp EEG (b) of a temporal lobe seizure. The seizure rhythm in the scalp EEG is fairly poorly developed despite the high amplitude, synchronous cortical activity shown in the inter-cranial data. Note that these figures are plotted on the same scale, though no absolute scale is given (Ebersole 2003).

activity in order that that activity can be observed by scalp EEG (Tao et al. 2005). Figure 1.1.3 shows a comparison between inter-cranial EEG (which uses surgically implanted electrodes directly in contact with the cortex) and scalp EEG recording (Ebersole 2003).

The scale of the EEG signal necessitates amplification by a factor of 10^6 in order that measurement can occur and as a result EEG is vulnerable to electrical noise and many forms of artifact. However, EEG offers a sub-millisecond temporal resolution, is relatively easy to perform and is the only clinically available technique which directly and non-invasively measures the electrochemical activity of brain cells.

Electroencephalography is the oldest method of non-invasively studying human brain disorder and in the past was used to aid the diagnosis of a variety of pathologies, including stroke, haemorrhage, Alzheimer's disease and cancer. The use of EEG in such cases today is less common, primarily because of the development of superior structural imaging methods, particularly magnetic resonance imaging (MRI) and x-ray computed tomography (CT). However, EEG remains essential to the diagnosis and study of epilepsy and seizures because of its temporal resolution, its ease of application and the nature of epileptic conditions themselves (Niedermeyer and Silva 2004).

EEG also remains of great value to the study of healthy brain function, as it allows the intricate millisecond-duration cortical responses to functional stimuli to be recorded directly. As such EEG remains a commonly used tool amongst neuroscientists, cognitive scientists and psychologists and physiologists.

1.1.2 EEG in Practice

1.1.2.1 Electrode application, impedance and amplification

Standard EEG is performed by fixing a number of sensing electrodes, a reference electrode and a common earth electrode to the scalp and then amplifying and recording the variations of electrical potential difference between each sensing electrode and the reference electrode. In the majority of clinical systems, the electrodes themselves consist of small metal cups made from a highly conductive, non-reactive metal such as gold or silver-chloride coated silver (Ag/AgCl), an example is shown in figure 1.1.4.

To measure the electrical potential difference across two points, it is necessary for a current to flow between those two points. A large impedance to this flow of current can seriously affect the accuracy and noise susceptibility of the measurement of electrical potential difference. For EEG, it is therefore desirable to minimise the electrical impedance between

Figure 1.1.4. A standard, clinical, silver/silver-chloride 'cup' electrode. The cup is 9mm in diameter.

each sensing electrode and the reference electrode by making as good an electrical connection to the scalp as possible. In practice this is done by removing excess skin cells from the contact site by lightly abrading the skin with a granular paste and introducing a conductive gel in to the electrode cup before applying the electrode to the contact site. It is typically stated that the electrical impedance measured between each sensing electrode and reference electrode should not exceed 5 kΩ in order to produce an acceptable signal-to-noise ratio (Odom et al. 2004).

Electrical impedance is thus often used as a generic measure of the quality of electrode contact, though it is important to note that (depending on the

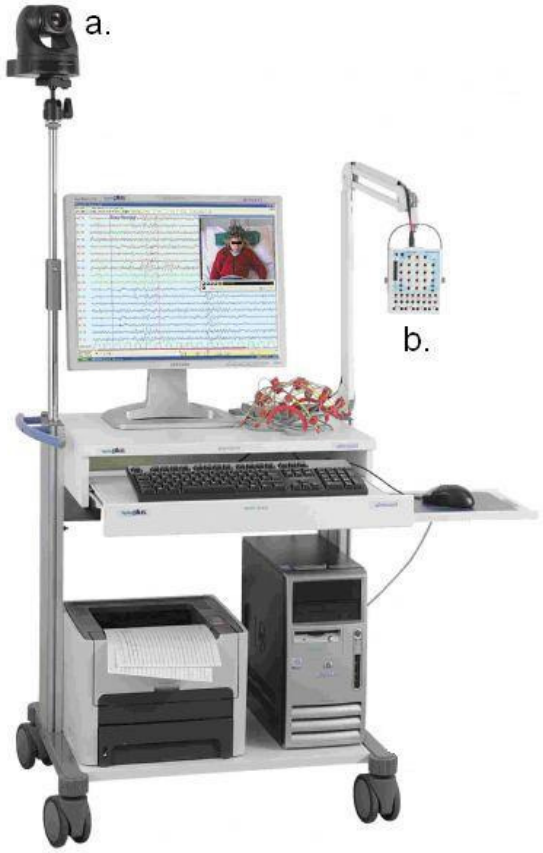

Figure 1.1.5. A standard clinical EEG system. Note the inclusion of a PC-linked video camera (point a.) which allows clinical symptoms and movement to be monitored. The digital amplification occurs at the 'headbox' (point b.), to which the EEG electrodes are attached.

input impedance of the EEG amplifier) it is often possible to obtain a good signal-to-noise ratio with contact impedances higher than 5 kΩ. Equally, good contact impedances do not guarantee a noise-free EEG, as this is often more dependent on the electrical characteristics of the room in which recording is taking place. A standard clinical EEG system is shown in figure 1.1.5.

There are many commercially available EEG systems which use a fundamentally different design of electrode and method to make contact with the scalp. These include systems which use pre-soaked sponges (Electrical Geodesics Inc. OR, USA) and conductive gelatinous pads (Hydro Dot Inc. MA, USA) to act as sensing electrodes. These designs usually avoid the use abrasion of the contact site in order to maximise the comfort of the subject. As abrasion of individual electrode sites is unnecessary, it is possible to apply dense caps or head-nets containing hundreds of electrodes. Such systems can maximise the available spatial information but the limited quality of the electrode contact (relative to the clinical abrading system) usually necessitates electrical isolation of the subject and the amplifiers. Isolation from electrical noise using a Faraday cage is impossible in most clinical settings and as a result, high-density EEG systems have not yet been accepted for standard clinical use in the UK. As amplifier technology develops, it is likely that the acceptable contact impedance will rise, which may allow such dense-array EEG systems to become clinically commonplace. However, a further important advantage of individual application of electrodes is that it is flexible; electrode positions can be added or omitted depending on the clinical circumstances.

Clinical EEG usually involves the application of around 20 sensing electrodes in positions across the whole scalp defined in a standardised fashion by the 10-20 international system of electrode placement (Klem et

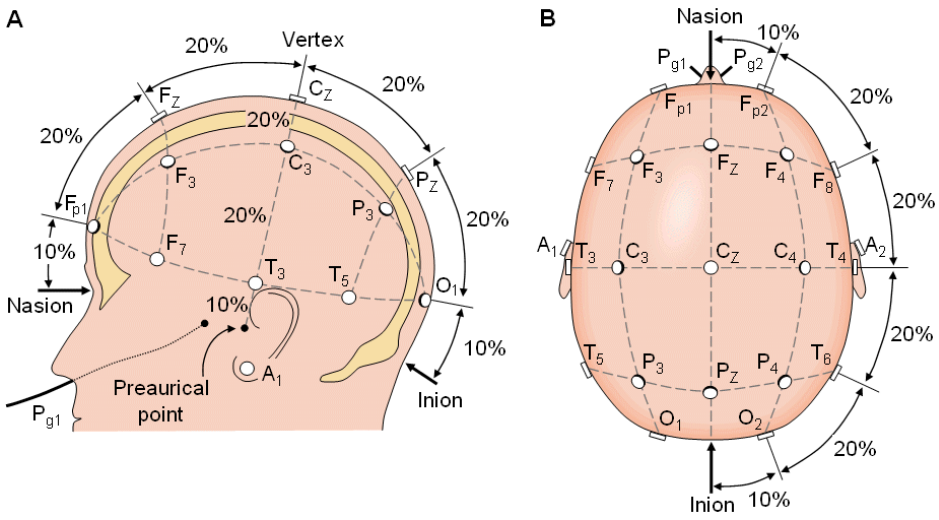

Figure 1.1.6. The 10-20 international system of electrode placement. (Figure adapted from www.BCI2000.org).

al. 1999). This system defines 19 main electrode sites in terms of 10 % and 20 % divisions of the nasion-to-inion sagittal and left-to-right pre-aurical coronal distances, as is shown in figure 1.1.6. This method of positioning electrodes on the basis of the bony landmarks of the head maximises the validity of the assumption that a given electrode is sensitive to electrical activity in a given region of the cortex, across various subjects. In practice, application of the 10-20 system is fairly subjective, and in the author's experience, electrode positions can vary by as much as 2 cm from recording to recording. Given the limited spatial resolution of EEG, such errors are rarely considered in a clinical environment.

The position of the reference electrode is important because all variations in electrical potential difference are recorded relative to it. As the reference electrode is moved closer to a sensing electrode, the signal recorded across that channel will be reduced because the *difference* in electrical potential between the two electrodes will tend to zero. There are, however, advantages in having the reference electrode positioned somewhere on the head or face as certain noise components (such as 50 Hz mains noise for

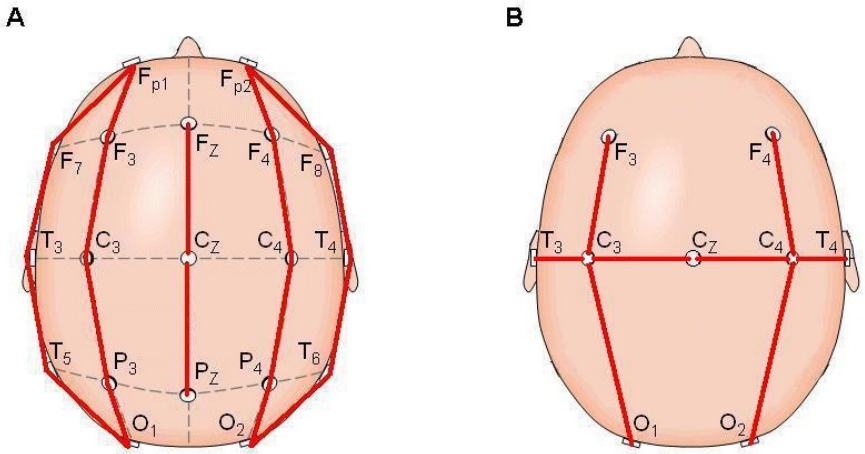

Figure 1.1.7. A typical anterior-posterior adult EEG montage is shown in image A. Each red line represents a bipolar pair, or channel, across which the electrical potential difference is recorded. Image B shows a reduced neonatal EEG montage, which typically includes 9 electrodes. (Figure adapted from www.BCI2000.org).

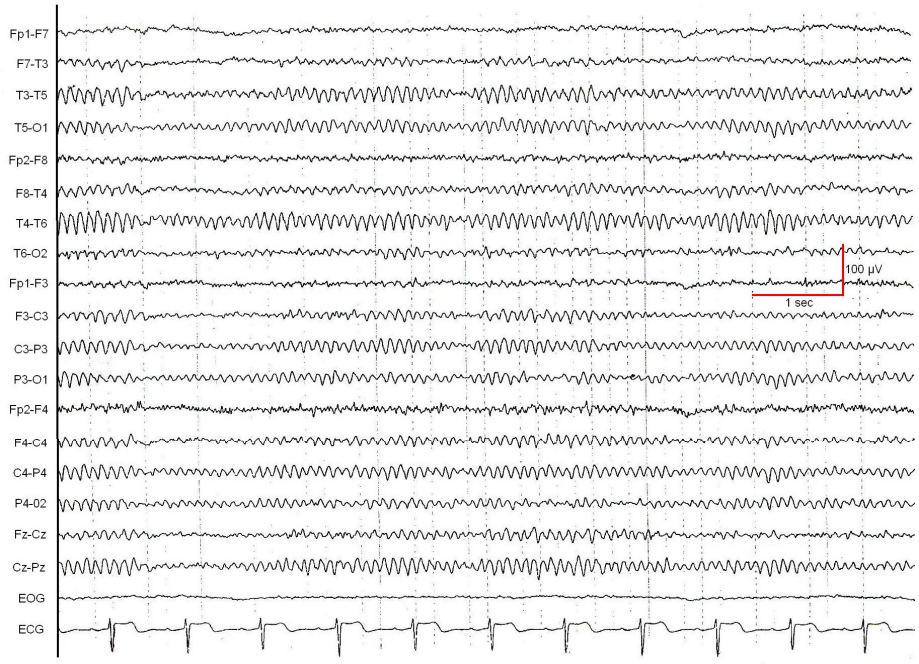

Figure 1.1.8. A normal, waking adult EEG showing a well formed alpha rhythm at ~9Hz. Note also that both the electro-oculogram (EOG) and electro-cardiogram (ECG) were recorded in addition to the EEG. (Figure adapted from emedicine.medscape.com).

example) will affect both electrodes approximately equally, and thus will be reduced by differential measurement.

Although the amplified EEG signal is usually that measured between each sensing electrode and a reference electrode, there is often an advantage in displaying the signal between different sensing electrodes. For example, differential amplification will occur between the electrodes F_3 and the reference electrode and C_3 and the reference electrode (REF), but it may be more physiologically and clinically beneficial to monitor the electrical potential difference between electrodes F_3 and C_3. The recording of the electrical potential difference between neighbouring electrodes is known as bipolar recording, and is easily achieved by subtraction of the two amplified signals:

$$(\mathrm{F_3} - \mathrm{REF}) - (\mathrm{C_3} - \mathrm{REF}) = \mathrm{F_3} - \mathrm{C_3}. \tag{1.1}$$

In this manner, the arrangement of EEG channels that is monitored can be arbitrarily chosen and altered during and after recording The arrangement of EEG channels is known as a montage, and there are several common clinical montages (figure 1.1.7). Figure 1.1.8 shows an example of a clinical EEG trace. This is the EEG of a healthy adult, displayed in the bipolar montage of figure 1.1.7a.

EEG amplifiers are essentially multi-channel differential amplifiers arranged such that the signal at each sensing electrode is amplified relative to that at the reference electrode. Modern systems typically have a sampling rate of between 500 and 2000 Hz, filters which can be applied across a range of ~0.01 to 100 Hz and various data-handling functions which allow noise effects to be minimised and the desired electro-cortical signals to be focussed upon.

1.1.2.2 Common EEG artifacts

EEG is highly sensitive to movement, changes in electrode impedance, external electrical interference and non-cerebral electrophysiological signals. There are therefore many common EEG features which are not related to cortical discharges or any brain activity. In general, such features are referred to as artifacts. Experienced electrophysiologists should be able to minimise EEG artifacts during recording, but it is difficult to produce a completely artifact-free EEG. A selection of the most common artifacts is given below.

Electrode 'Pop' (Figure 1.1.9)
This artifact results from a sudden decrease in electrode contact quality. It will typically produce a sharp, transient feature which is isolated to a single electrode, therefore producing a mirrored feature across two or more channels in a bi-polar montage. It is of clinical importance to identify these artifacts, as they can be mis-interpreted as epilepsy-related.

EMG (Muscle) Artifact (Figure 1.1.10)
Contraction of muscle produces high-amplitude (100s of microvolts), high-frequency (20-100 Hz) potentials, as recorded by electromyogram (EMG). Contraction of muscles on and around the head can therefore produce EMG artifacts within the EEG recording. It is usually straight forward to identify such artifacts, as they typically consist of bursts of high-frequency activity which have no cortical equivalent.

ECG (Cardiac) Artifact (Figure 1.1.11)
Similarly, the beating of the heart produces a high-amplitude electrophysiological signal, which can infiltrate the EEG recording. Clinical EEG is usually recorded alongside a single-channel electrocardiogram (ECG), which allows this artifact to be visually rejected.

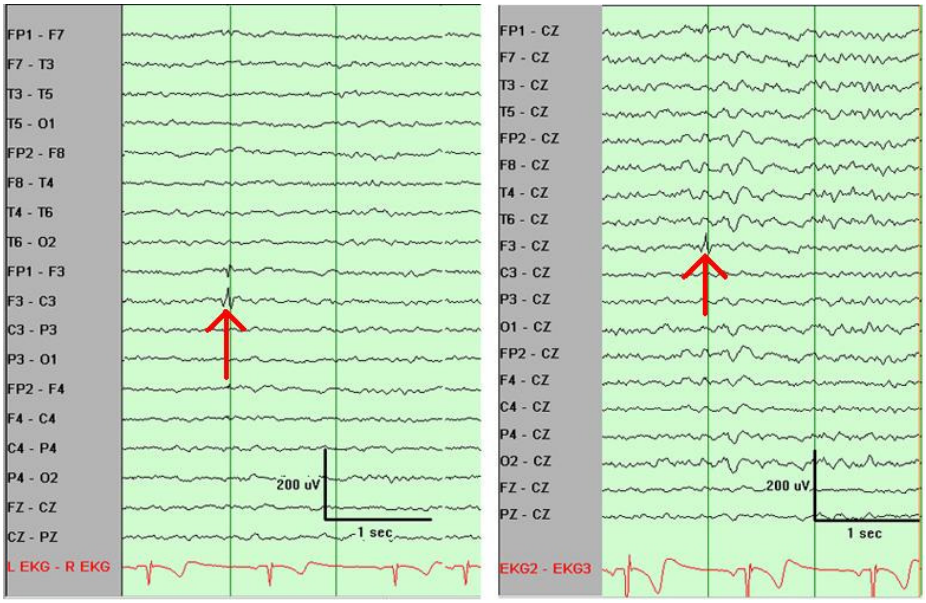

Figure 1.1.9. The Electrode 'pop' artifact. The relevant feature is identified by the arrows. The transient spike is apparent on two channels of the bi-polar montage, but by using a common reference (electrode Cz), it becomes obvious that the feature is limited to a single electrode (F_3). (Figure adapted from emedicine.medscape.com).

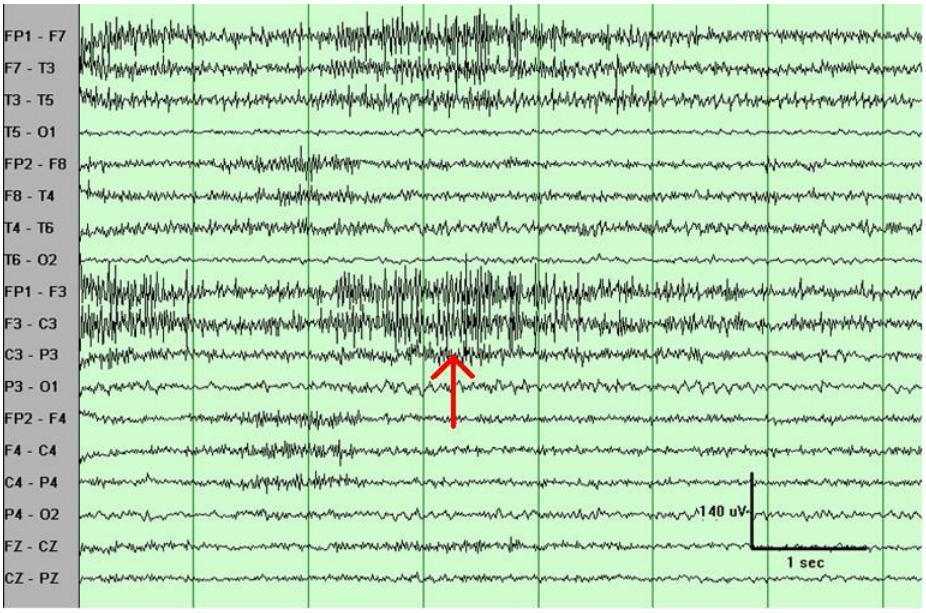

Figure 1.1.10. EMG artifact. The arrow identifies one period of high-amplitude, high frequency artifact which is apparent on several channels over the left fronto-temporal region. (Figure adapted from emedicine.medscape.com).

Figure 1.1.11. ECG artifact. The arrow identifies one ECG artifact spike, which is apparent over several channels. This feature can usually be easily identified because of it's clear periodicity, especially if it can be compared to the simultaneously recorded ECG (shown in red at the bottom of the trace). (Figure adapted from emedicine.medscape.com).

Figure 1.1.12. Eye movement artifact. The arrow identifies one artifact which, because the deflections are of opposite polarity at F7 and F8, is consistent with a lateral eye movement. (Figure adapted from emedicine.medscape.com).

Eye Movement Artifacts (Figure 1.1.12)

The retina and the cornea of the eye are charged negatively and positively respectively. As a result, movements of the eye produce a distinct change in electrical potential which can be observed by EEG recording. Lateral, vertical and blinking movements of the eye can be identified by polarity and symmetry of the changes in electrical potential difference as recorded at the frontal EEG electrodes. Eye movement artifacts are extremely common to EEG recording, to such an extent that an electro-oculogram (where electrodes are placed either side of one or both eyes, at the temple and at the nasion, see Marmor et al. 2004) is often recorded alongside the EEG and single-channel ECG to allow such artifacts to be easily identified.

Other significant artifacts include those due to movement of the mouth and tongue, interference from at the electrical mains frequency (50 Hz in the UK) and artifacts due to other medical equipment (such as intravenous drips, respirators etc.).

1.1.3 Clinical EEG

1.1.3.1 The healthy adult EEG

The healthy adult EEG is dominated by a number of rhythmical oscillations which are identified by their frequency and amplitude. These rhythms are representative of continuous, synchronous cortical neuronal activity. Hans Berger, the first man to observe the electroencephalogram in humans, named the dominant EEG components in the order he observed them (Berger 1929). The alpha wave is the principle feature of normal adult EEG and consists of a rhythmic pattern with a frequency of 8 to 13Hz. Alpha is most prominent over the posterior of the head, and is sometimes referred to as the posterior dominant rhythm (PDR). The alpha wave is most apparent for a subject in a relaxed but waking state with their eyes closed, and is known to be attenuated by eye opening and certain visual stimuli (Niedermeyer and Silva 2004). Despite having been the subject of

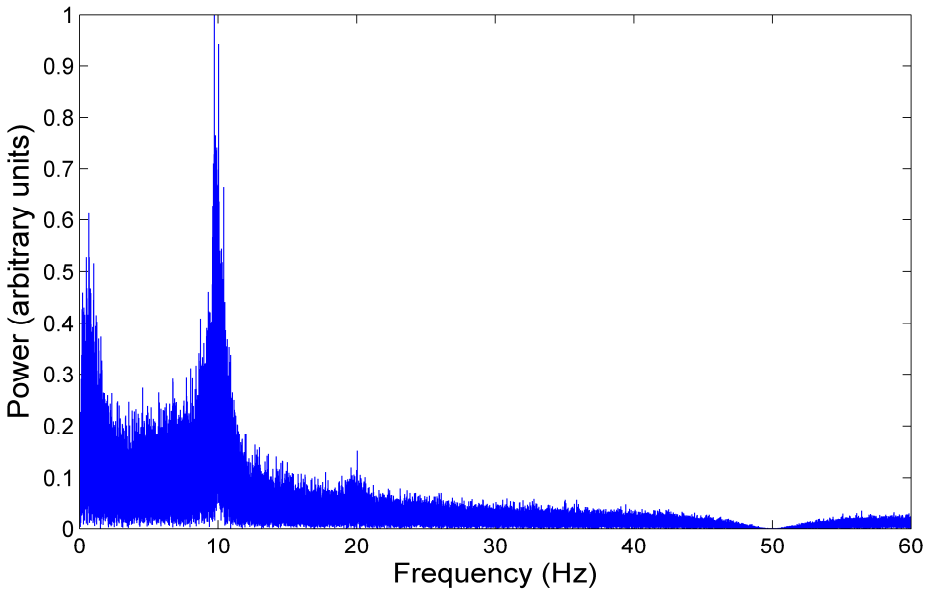

Figure 1.1.13. The normalised power spectrum of the EEG recorded at electrode Oz in a healthy adult in a resting state with his eyes closed, recorded as part of this work. The dominant peak at (almost exactly) 10 Hz corresponds to the alpha wave, which has an observable resonance at 20 Hz. There are no other prominent features, as little or no beta was apparent in this individual. Note that the result of the application of a 50 Hz notch feature is also visible.

research for over 80 years, the origin of the alpha wave is still an issue of debate (Steriade 2000). Many animal studies (both in-vitro and in-vivo) have indicated that the thalamus has a fundamental role in the creation and regulation of the alpha wave, with Morison and Basset (1945) being the first to observe a relationship between 8-13 Hz thalamic oscillations and the synchronised activity of cortical neurons. The details of cortico-thalamic interactions are complex, and are an increasing popular application of functional imaging techniques, including PET (Danos et al. 2001), PET-EEG (Schreckenberger et al. 2004), and EEG-fMRI (Goldman et al. 2002).

In a clinical context, the spatial distribution of the alpha wave across the scalp, variations in its frequency and amplitude, and persistence of the alpha wave with eye opening can all provide important clinical information. The absence of alpha over one hemisphere of the brain is almost always related to a pathological condition. A section of normal, adult EEG was shown in figure 1.1.8. In this figure the alpha pattern is very well developed and most prominent over the posterior regions of the head. Figure 1.1.13 shows a frequency-domain representation of the EEG at electrode Oz in a healthy adult.

Beta activity was the second normal EEG component observed by Berger. It is defined as activity of 14 Hz or above and is present in the background of most adult EEG recordings. Beta is usually observed bilaterally with maximum amplitude over the fronto-central regions. Due to its high frequency, it can be difficult to differentiate between beta activity and EMG artifact. Various drugs are known to affect the abundance of beta activity and hemispheric asymmetry of beta components is usually an indicator of the presence a pathological condition. An example of normal beta activity is shown in figure 1.1.14.

Theta activity is defined as that between 4 and 7 Hz and is also usually present in the waking adult EEG, though much less significantly than alpha

Figure 1.1.14. An example of beta activity in a healthy adult. As indicated, beta is particularly present over the fronto-central regions. (Figure adapted from emedicine.medscape.com).

or beta and can be completely absent without clinical significance. In adults, localised theta activity is often related to underlying structural disease.

EEG activity below 4 Hz is known as delta activity, and is only normally present in adults during deep sleep. Focal delta activity is a good indicator of localised encephalopathy. Other typical EEG components include the mu rhythm, which is associated with the sensori-motor cortex and lamda waves, which are transient, spike-like potentials occurring in the occipital regions which can be mistaken for evidence of epileptic disorder.

The study of the activity of the adult brain during sleep is a common application of EEG, and sleep patterns have their own distinct phases and forms of EEG activity (Kandel et al. 2000, Niedermeyer and Silva 2004). Knowledge of the EEG components of sleep is very important to the understanding of clinical EEG because not only does the sleeping EEG

differ markedly from its wakeful equivalent, but sleep can cause abnormal EEG features to become more prominent. This is particularly the case with epileptiform activity. In brief, sleep is divided into two broad types: non-rapid eye movement (NREM) and rapid eye movement (REM). Non-rapid eye movement sleep is further separated into three stages. Stage 1 of NREM sleep represents the transition from wakefulness to sleep and typically lasts several minutes. It is characterised by a slowing and fragmentation of the normal waking EEG components described above. Stage 2 contains well defined 'sleep spindles'; sinusoidal waveforms of between 12 and 14 Hz. Stage 3 (which was previously separated into two) is also known as deep or slow-wave sleep and is dominated by high amplitude, delta frequency waveforms. The EEG during REM sleep reverts to a low voltage pattern containing a variety of frequency components, similar to stage 1 NREM but, as the name suggests, is coincident with rapid movement of the eyes and is associated with periods of dreaming. While REM sleep is seldom encountered during an adult clinical EEG, it is very common for patients to become drowsy and enter the early stages of NREM sleep. In contrast, infant subjects will often remain in a state of deep sleep for the duration of an EEG examination. This is discussed further in the following section.

1.1.3.2 The healthy infant EEG

Neonatal electro-cortical activity is unlike that observed at any other time of life. The healthy neonatal EEG can contain features which are high in amplitude, transient, mixed-frequency and discontinuous without being indicative of encephalopathy. There is also significantly more inter-patient variability within neonatal EEG than in the adult recordings, which can make the interpretation of neonatal EEG particularly challenging.

An example of the EEG of a full term, newborn infant is shown in figure 1.1.15. In comparison with the adult, the most obvious difference is that the

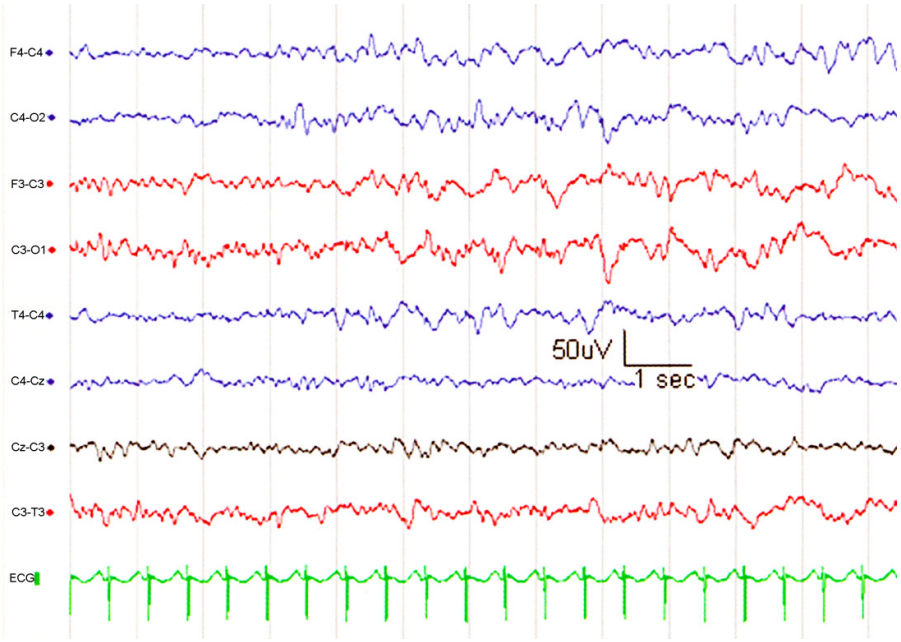

Figure 1.1.15. A typical EEG trace of a healthy term neonate during quiet sleep. Note the mixed low-frequency, high-amplitude nature of the resting EEG compared to that of the adult. (Rennie et al. 2008).

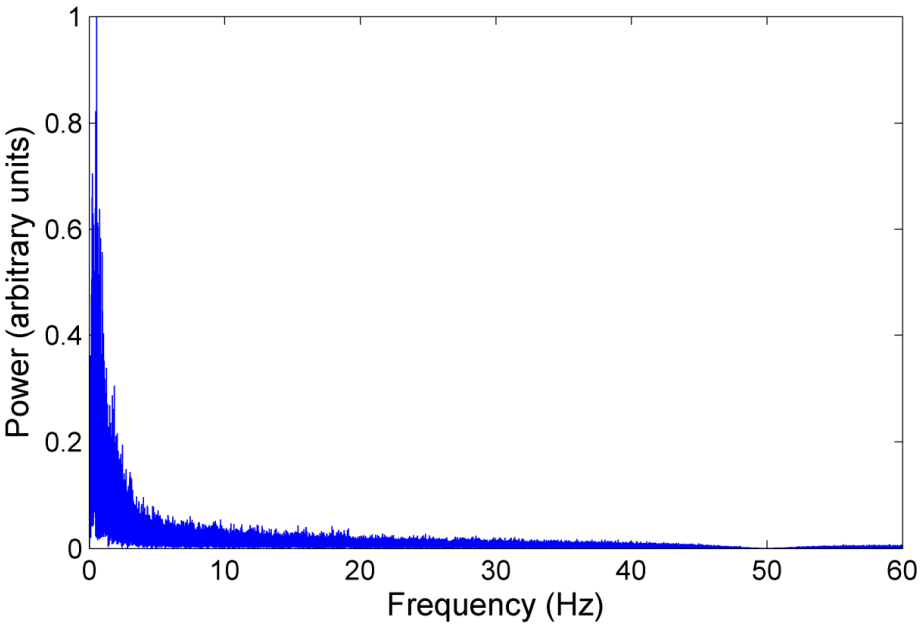

Figure 1.1.16. The normalised power spectrum of the EEG recorded at electrode Oz in a healthy sleeping, term infant. Note that the vast majority of EEG power is containing within frequencies below 5 Hz.

EEG is generally larger in amplitude (often up to 100 μV) and low in frequency (dominantly less than 5 Hz). A frequency domain representation of the EEG of a term infant recorded over the occipital lobe is shown in figure 1.1.16. The EEG of the newborn shows no posterior dominant rhythm (which is synonymous with the alpha wave in adults) at all, but rather a continuous combination of rhythmic, but variable, delta and theta activity. By the time an infant has reached 3 months, a more consistent delta wave will dominate. There is a gradual increase in the frequency of this dominant rhythm during childhood, from slow theta by the age of 1 year to a well-established slow alpha wave at 6 years.

The rapid growth and maturation of the brain from viable pre-term to term is accompanied by marked changes in EEG activity. Pre-term EEG is characterised by its discontinuity; consisting of intermittent bursts of activity occurring at a rate of 0.1 to 0.5 Hz, but containing a variety of higher-frequency components (Vanhatalo and Kaila 2006). The periods between these bursts will often show almost no discernable EEG activity at all. Both the rate of occurrence and the content of these intermittent bursts (which have recently been termed spontaneous activity transients or SATs) changes significantly with pre-term age. These SATs are only occasionally visible in the healthy term infant, because of the increase in amplitude of continuous background activity. The EEG typically obtains full continuity by 45 weeks gestational age (note that gestational age is the age of an infant measured from the approximate time of conception, usually taken as the time of a mother's last menstruation). Figure 1.1.17 shows the discontinuous EEG of a pre-term infant, whilst figure 1.1.18 shows a schematic representation of the dominant features (i.e. continuous background oscillations plus SATs) of infant EEG and how these vary with pre-term age and sleep state.

Sleep states in newborns are less well defined than those in adults (Mirmiran et al. 2003). Though NREM and REM sleep can be readily

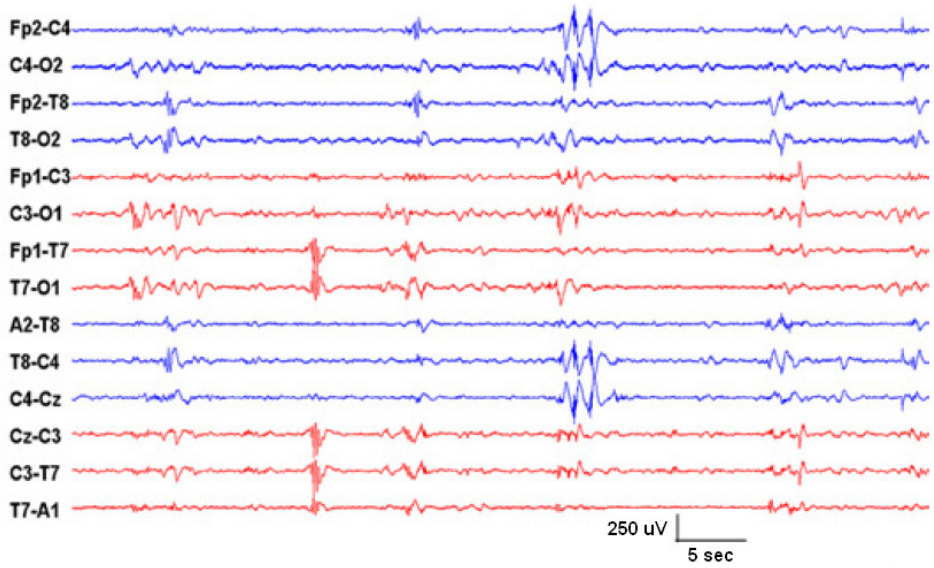

Figure 1.1.17. The EEG trace of a 32 week neonate during quiet sleep, recorded with an extended montage. Such traces are characterised by the limited-amplitude continuous background oscillations interspersed with large, transient periods of mixed frequency activity. (Vanhatalo and Kaila 2006).

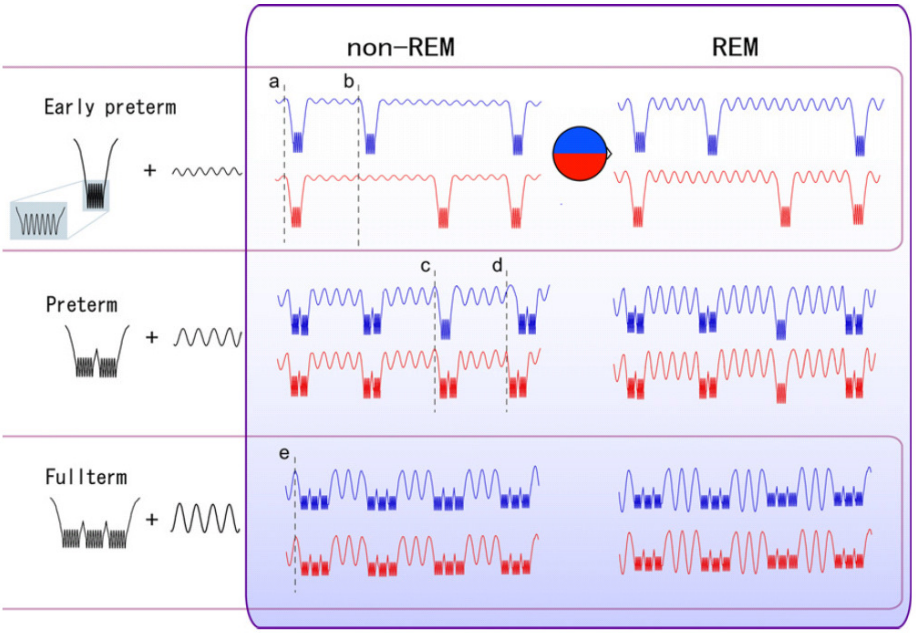

Figure 1.1.18. A simplified schematic representation of how the dominant features of the EEG trace of infants of varying ages and sleep states can be modelled as a combination of spontaneous activity transients (SATs) and background activity (of varying amplitude, frequency content, regularity and hemispheric synchronicity). (Vanhatalo and Kaila 2006). Note how the discrete SATs become less distinct as the infant ages and continuous background oscillations begin to dominate.

distinguished from as early as 32 weeks gestational age, further classification is difficult. In general, the neonatal EEG during REM sleep will show continuous, mixed-frequency activity in conjunction with irregular respiration and rapid eye movements. This continuous activity will be of a higher amplitude than that shown during wakefulness. Neonates in a NREM sleep state will exhibit either a high-voltage slow wave (of 1-2 Hz) or, as sleep progresses, bursts of high amplitude, mixed frequency activity separated by periods of decreased amplitude (less than 40 μV). Such discontinuous activity can be distinguished from that of pre-term infants by the fact that the low amplitude periods associated with NREM sleep will still show some activity, rather than complete suppression.

1.1.3.2 Epileptic disorders and seizures

As defined by the International League Against Epilepsy (Fisher et al. 2005), 'Epilepsy is a disorder of the brain characterised by an enduring predisposition to generate epileptic seizures and by the neurobiologic, cognitive, psychological and social consequences of this condition. The definition of epilepsy requires the occurrence of at least one epileptic seizure.' The same publication defines an epileptic seizure as 'a transient occurrence of signs and/or symptoms due to abnormal excessive or synchronous neuronal activity in the brain'. Note that this widely accepted definition of a seizure is based on the occurrence of symptoms pertaining to abnormal electrical activity in the brain, rather than the presence of this activity itself. Inherent to this definition is the assumption that abnormal neuronal discharges are occurring, and would be observed in conjunction with clinical symptoms if recording methods and circumstances were ideal. This subtlety is important because it must be possible to define and diagnose seizures even when the abnormal electrical activity cannot be directly observed (which may be due to the EEG being normal between (or even during) seizure events, or simply because an EEG cannot be obtained). EEG recording is the gold-standard approach to the diagnosis and classification of seizures and epileptic disorders.

Fundamentally, a seizure is a transient period of extreme neuronal firing and/or hyper-synchrony. Seizures which incorporate clinical symptoms (such as an altered mental state or involuntary, erratic movements) are broadly referred to as clinical seizures, whilst a seizure which is only apparent via EEG recording is known as a subclinical or electrographic seizure. A seizure can last for as little as a few seconds, through to extreme cases where seizure is continuous and will not relent without intervention. A patient suffering continuous, unremitting seizure for more than 30 minutes is classified as in 'status epilepticus'. The many types of seizure are categorised by whether the source of epileptiform activity is localised (partial seizure) or distributed across the cortex (generalised seizure). Partial seizures can sometimes spread to other areas of the brain, producing a secondary generalised seizure. Generalised seizures are categorised further by the effect they have on the body, but all typically involve a loss of consciousness. Partial seizures are divided into simple partial seizures, which do not invoke any loss of consciousness or awareness, and complex partial seizures which do (see Engel 2006 for a detailed classification).

It is important to note that whilst *spontaneous* seizures are inherent to epileptic disorders, seizures themselves often occur, for a variety of reasons, in people who do not have epilepsy. The causes of such provoked seizures are varied, and include traumatic head injury, stroke, hypoxic-ischemic encephalopathy, multiple sclerosis, meningitis and brain tumour (Engel et al. 2008). The hyperactivity and hypersynchronisation of neurons during a seizure is known to result from an imbalance of mechanisms which inhibit and excite the propagation of action potentials. The dominant inhibitory neurotransmitter in the adult brain is gamma-aminobutyric acid (or GABA) which typically (by binding to certain membrane-bound receptor molecules and altering the flow of chloride and potassium ions) causes a hyperpolarization of the post synaptic membrane. This hyperpolarization inhibits the transmission of an action potential to the post-synaptic neuron. Glutamate is the most abundant excitatory neurotransmitter in the human

nervous system and causes (at the vast majority of synapses) the post-synaptic membrane potential to approach the action potential threshold, thus increasing excitability. High levels of glutamate in the extra-cellular space not only increases the excitability of surrounding neurons, but can result in an excessive uptake of calcium ions, eventually leading to neuronal death. Neurons therefore exhibit a very efficient active mechanism which transports extra-cellular glutamate across the cell membrane and into the cell. Most neurons posses an average intra-cellular glutamate concentration of 10 mM (Bradford et al. 1978), which is much higher than for any other excitatory neurotransmitter.

The neurobiology and electrochemistry of seizures is complex, and many aspects are still the subject of intense research (Bradford 1995, Engel at al. 2008). However, rises in glutamate, and decreases in GABA concentration (or decreases in the effectiveness of those neurons which control GABA-mediated inhibition) have been shown repeatedly to be associated with the onset and propagation of neuronal hyperactivity and hypersynchrony (Bradford 1995, Kandel 2000).

In this section seizures have been discussed as a symptom of other neuropathology. Whether seizures are merely a symptom or whether they can cause or exacerbate neurological damage is still an issue of debate. Whilst continuous seizures are known to be potentially damaging (Wasterlain et al. 1993) millions of adult epileptics live with regular transient seizures and exhibit little or no long term neurological damage. There is growing evidence however, that even transient seizures can damage the developing brain (Scher 2003, Thibeault-Eybalin et al. 2009, Glass et al. 2009, Silverstein 2009).

1.1.3.3 The EEG in adult epilepsy and seizures

EEG is able to directly observe the excessive electro-cortical activity or synchrony which is inherent to a seizure, and as a result it is the best tool

available for the study and diagnosis of epilepsy. There are several well-defined electrophysiological indicators of epileptic activity, both during (ictal) and between (inter-ictal) periods of seizure. (Note that as duration is the only factor by which this distinction can be made, the separation of ictal and inter-ictal discharges is often problematic and sometimes meaningless). The presence of transient inter-ictal features is incredibly important to the diagnosis of epileptic disorders, as a typically hour-long EEG recording will often not include any ictal periods. Of the inter-ictal discharges, the most common and specific are classed as epileptiform. This includes the spike, sharp wave and the spike-wave complex. The spike, as its name implies, is a sudden, sharply contoured discharge with a duration of less than 70 ms. An example of an inter-ictal spike is shown in figure 1.1.19. Sharp waves differ from spikes only in duration, lasting between 70 and 200 ms) and both will typically exceed 100 μV in amplitude. The spike is usually a negative deflection at the surface, and will tend to have a steep onset and a slower return. The spike is often observed in conjunction with a slow-wave, typically lasting around 300 ms, usually negative and larger in amplitude then the spike itself. In combination, this is known as the spike-wave complex and is a classic inter-ictal determinant of epileptic disorder. Continuous repetition of any of these features is logically indistinguishable from ictal EEG activity.

Ictal EEG patterns in adults are typically identified by comparison to that individual's background EEG, as it is difficult to come to a meaningful and absolute definition of what constitutes ictal EEG activity. The onset of an ictal period is therefore identified by rapid changes in EEG amplitude or frequency content. In some cases this can be difficult to distinguish from background, because ictal patterns can appear at similar frequencies and amplitudes to background EEG activity. Classic ictal EEG recordings show the development of a rhythmical pattern of a noticeably higher amplitude than background EEG. It is also common for these waveforms to be sharp in appearance, particularly in comparison to the near-sinusoidal alpha

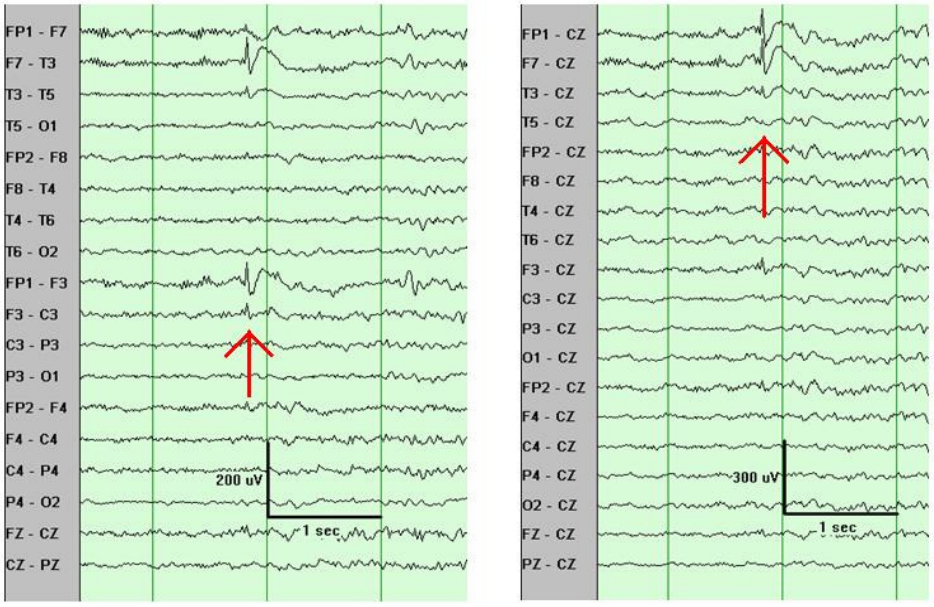

Figure 1.1.19 An example of an inter-ictal spike discharge in an adult, shown in both bipolar (left) and referential (right) montages. (Figure adapted from emedicine.medscape.com).

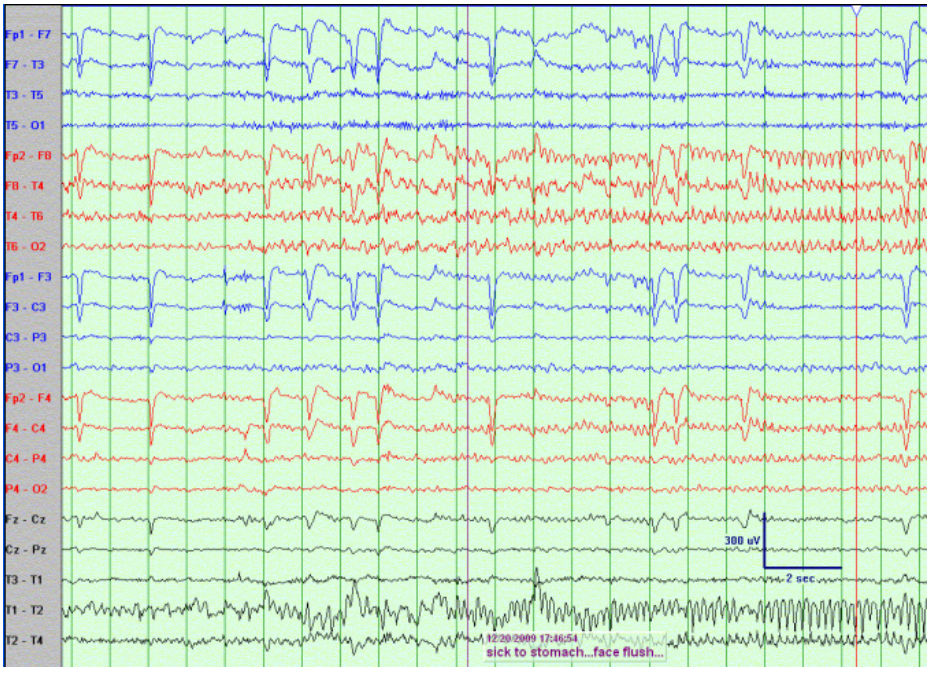

Figure 1.1.20 The onset of a lateralised temporal lobe seizure in an adult. Note the development of a distinct ~4 Hz sharp wave pattern over the right sided electrodes. (Figure adapted from emedicine.medscape.com).

Figure 1.1.21 A generalised seizure in an adult, characterised by the onset of a global, synchronous ~3 Hz spike-wave complexes. (Figure adapted from emedicine.medscape.com).

pattern. A good example of EEG during a partial seizure is shown in figure 1.1.20. Note the way the sharp wave pattern apparent on only the right-sided electrodes increases in amplitude and consistency over a period of several seconds. Figure 1.1.21 shows an EEG recording during an absence seizure in an adult. Across all channels there is an unmistakable increase in amplitude and change of form at the onset of seizure, consisting of a continuous spike-wave pattern.

1.1.3.3 The EEG in neonatal seizures

Newborn babies are exceptionally vulnerable to seizures. Seizures are diagnosed in approximately 10 % of very low birthweight, 5 % of low birthweight and around 0.3 % of full-term babies (Murray et al. 2008). However, these figures rely on clinical diagnosis, which is only possible if the seizure is accompanied by changes in movement or behaviour and even then diagnosis can be very difficult. A study showed that only 21 % of 393

electrographic seizures observed in 41 babies exhibited clinical signs (Clancy et al. 1988). There is significant evidence that a standard EEG, usually lasting 20 to 40 minutes has a good chance of detecting seizure activity but prolonged, video-EEG is considered the best diagnostic method (Glauser and Clancy 1992). Seizures in the neonate are brief, usually lasting 2-3 minutes (Rennie et al. 2008). Neonates do not exhibit sustained clinical or electrographic seizures in the same way as adults, which makes a meaningful diagnosis of status epilepticus difficult.

There are many factors which contribute towards the increased susceptibility of the developing brain to seizures. A significant number of animal and in-vivo experiments have implicated developmental differences in the expression of glutamate and GABA neurotransmitters (and in the number of the receptor molecules which are sensitive to these compounds) (Johnston 1995, Sanchez and Jensen 2001). Glutamate receptors are critical to neuroplasticity, and as a result are over-expressed in the developing brain (Silverstein & Jensen 2007). The suggestion is therefore that the increased level of neuronal excitability associated with greater expression of glutamate receptors increases seizure susceptibility, though this relationship remains unclear. Conversely, the expression and function of GABA receptors has been shown (in animal models) to be lower in the early stages of life (Swann et al. 1989), suggesting a decreased ability to inhibit the transmission of neuronal potentials. However, it is also known that (due to a limited expression of chloride ion transporters), GABA acts as an excitatory neurotransmitter in the immature brain - i.e. it's function is the inverse of that found in later life (Ben-Ari 2002). These factors partially explain the resistance of neonatal seizures to certain anti-epileptic drugs, as the primary effect of drugs such as phenobarbital is to mimic the effects of GABA by binding to GABA receptors at the synaptic membranes (Painter et al. 1999, Boylan et al. 2002).

The causes of neonatal seizures are varied, and include cerebrovascular pathologies such as ischemic stroke and haemorrhage, metabolic disorders like hypoglycaemia, and infections of the central nervous system such as meningitis. Hypoxic-ischemic encephalopathy (HIE), where the entire brain suffers a temporary lack of oxygen, is a common result of complications at birth, and is the most common cause of neonatal seizures (Silverstein and Jensen 2007).

An EEG recording in neonates is of clinical use even when the external symptoms of seizures are unequivocal. EEG can provide information about seizure type, location duration and background activity which can all inform diagnosis and prognosis. The ictal neonatal EEG will vary in location, localisation, duration amplitude and morphology, but as in adult EEG, what is usually observed is the development of a new pattern of activity, distinct from background EEG. Characteristic neonatal seizures consist of repetitive sharp or slow wave discharges, or (less commonly) spike-wave complexes. The vast majority of neonatal seizures have a focal origin (most commonly in the temporal regions) though a secondary generalised seizure can result. Due to immature hemispheric and synaptic connections, seizures in neonates often exhibit less generalisation than in adults, and different seizure patterns can be apparent in different areas of the brain simultaneously (Rennie et al. 2008). Figures 1.1.22 to 1.1.24 are examples of neonatal EEG during seizure events.

Although video-EEG monitoring is rightly considered the gold-standard method for seizure detection and observation, there have been reported cases of clinical symptoms of seizures being present without, or asynchronously with, ictal electrographic features. This phenomenon is known as electro-clinical dissociation. (Note that this term is used ambiguously: others use it to refer to all seizures where the clinical and electrographic elements do not coincide, which include what have previously been defined as electrographic seizures, i.e. those visible to EEG

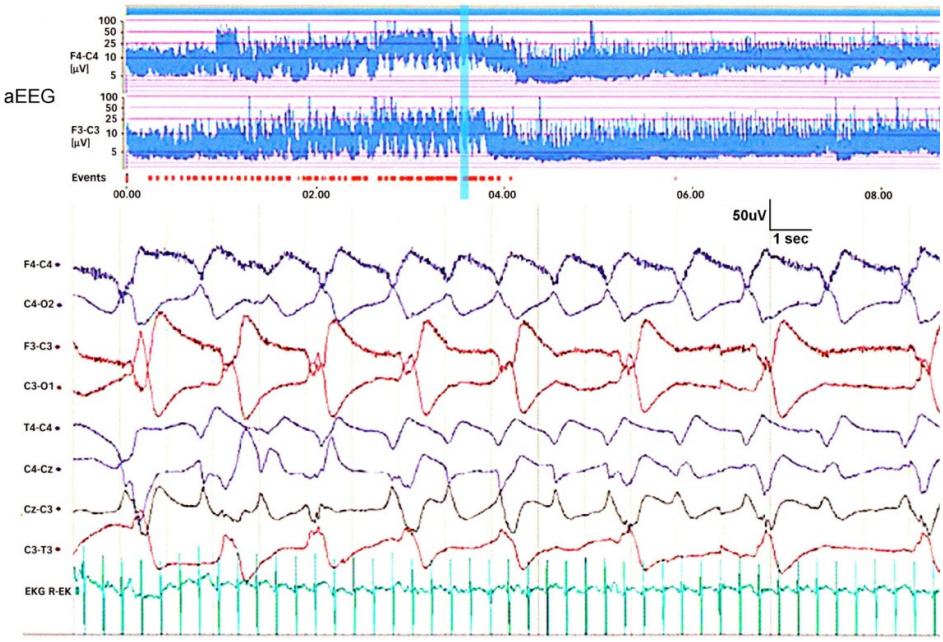

Figure 1.1.22 A high amplitude, slow wave, generalised seizure. Note how there is asynchrony between the left and right hemispheres, with the right-sided seizure pattern being of a higher frequency. The top of the figure shows a two-channelled aEEG (which shows over 8 minutes of data). The period corresponding to the EEG trace is indicated by the vertical, light-blue bar, and is seizure-positive as defined by aEEG. (Figure adapted from Rennie et al. 2008).

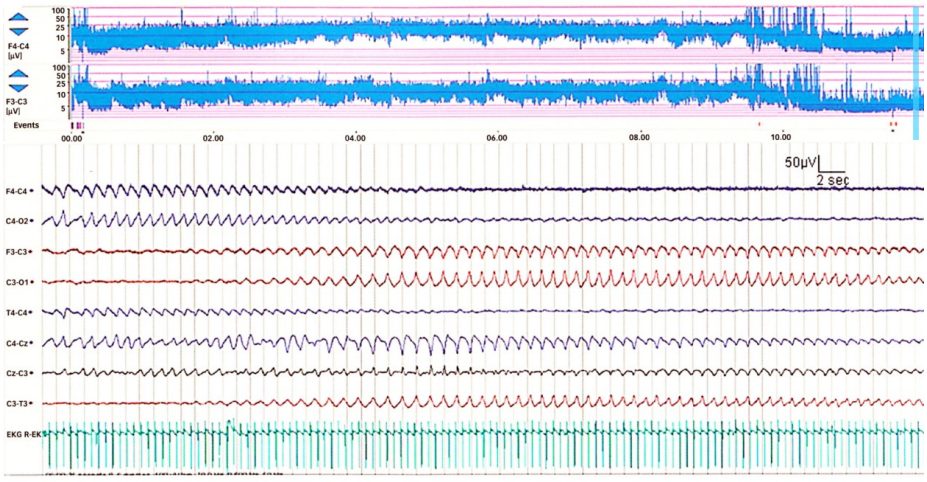

Figure 1.1.23 A repetitive sharp, ictal waveform with a relatively low amplitude. Note how early on in the trace the seizure rhythm is only apparent on right-sided electrodes, but then switches to being more apparent over the left hemisphere. (Figure adapted from Rennie et al. 2008).

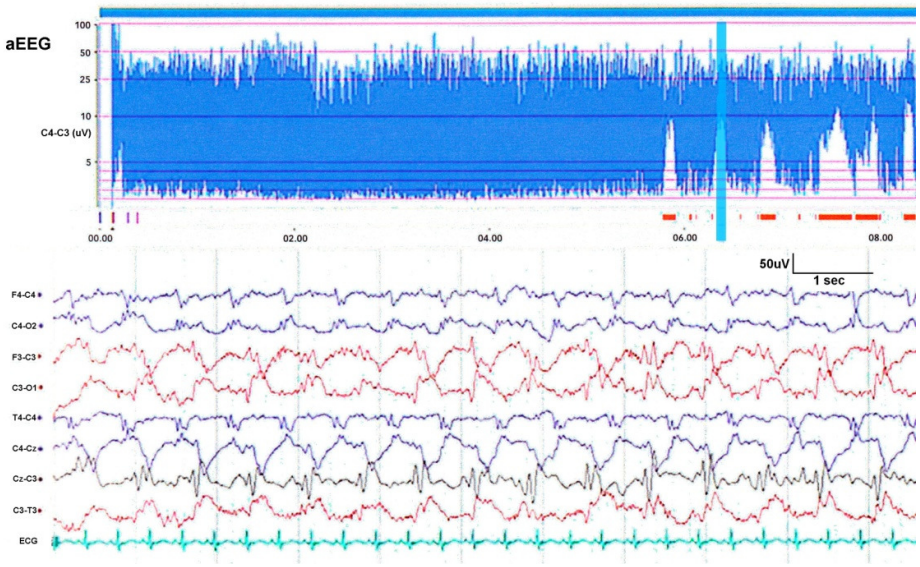

Figure 1.1.24. Relatively high amplitude, generalised spike and slow-wave ictal morphology. Note the very apparent ictal saw-tooth pattern in the aEEG. (Figure adapted from Rennie et al. 2008).

which have no clinical symptoms. Such events are particularly common in neonates after the administration of anti-epileptic medications (Scher et al. 2003). There are only two possible explanations for electro-clinical dissociation; that the clinical symptoms are not in fact associated with seizures at all (i.e. the clinical symptoms are caused by some form of brainstem release phenomena), or that the seizures in question are not visible using EEG or the EEG recording is misinterpreted. The most likely explanation for the observation of electro-clinical dissociation is, of course, a combination of both of these possibilities. Whilst many clinically-diagnosed neonatal seizures will have non-epileptic origins (Mizrahi and Kellaway 1987), there will also be cases where the neuronal hyper-activity and hyper-synchrony that defines a seizure will be present and will cause subtle clinical symptoms, but without being apparent to a limited-channel neonatal scalp EEG recording (Weiner et al. 1991, Pinto and Giliberti 2001). This is to be expected given the limitations of EEG discussed previously, particularly in terms of sensitivity to depth and neuronal orientation and is not limited to neonates. Using invasive depth electrodes

and scalp EEG in a study of adult temporal lobe epilepsies, Lieb et al. (1976) found that as little as 10 % of subclinical seizures are detectable by scalp EEG.

1.1.3.4 Amplitude integrated EEG

In the 1960s Maynard and Prior (Maynard et al. 1969) sought to develop a method of simplifying EEG in order to produce a cheap, easily interpreted, reliable and simple method of monitoring neuronal function. The result was a signal processing algorithm which takes the EEG recorded over as few as two electrodes and produces a trace which is very different to a normal EEG recording. This trace is designed to highlight changes in the power content of the EEG recording at particular frequencies, and is known as amplitude-integrated EEG (or aEEG). Originally aEEG was performed using dedicated systems known as Cerebral Function Monitors (or CFMs), but with the onset of digital EEG systems, the aEEG algorithm is now commonly available in all clinical EEG software packages. The use of aEEG is particularly common in neonatal monitoring, as it provides a reasonable sensitivity and specificity in the observation of neonatal seizures even when interpreted by the non-electrophysiologist (Toet et al. 2002). It is known however that aEEG is often insensitive to short-duration, low amplitude and focal seizure events (Rennie et al. 2004). Figures 1.1.22 to 1.1.24 all include an aEEG trace at the top of the standard EEG readout. In figure 1.1.24 the classic ictal aEEG ‘saw-tooth’ pattern is very apparent.

1.1.4 Event Related Potentials

1.1.4.1 Event Related Potentials and functional processing research

In the study of functional processing in the healthy brain it is usual that experiments are designed so as to isolate the function of interest as far as possible. This will almost always involve providing a subject with a particular stimulus which is known to invoke the cortical process of interest. As the electroencephalogram represents a summation of all the underlying electrical activity of the brain, the signal-to-noise ratio of the activity relating to any particular cortical process will typically be very low. It is however possible to isolate and study a particular cognitive function by time-locking the onset of the stimulus or task to the EEG recording. Time-locking in this way means that if the stimulus is repeated many times the

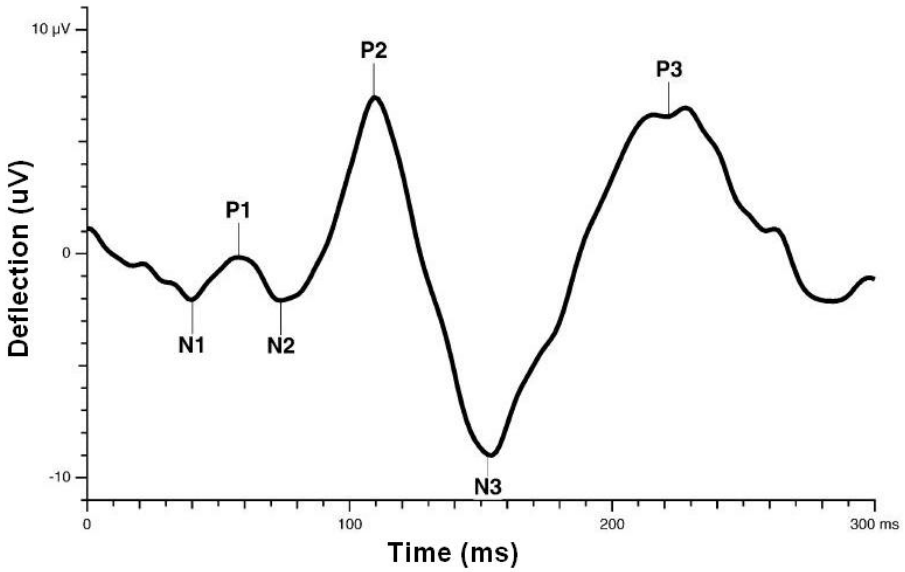

Figure 1.1.25. A stereotypical adult visual-evoked response to a flash stimulus, recorded over the occipital lobe. The stimulus occurs at zero on the time axis, and the average electro-cortical response consists of a waveform with a variety of peaks and troughs. These are usually defined by their polarity and the order in which they occur, hence the labels N1, P1 etc. This waveform is plotted with the negative downwards on the y-axis, which is contrary to ERP convention.

recording can be block-averaged around the point of stimulus onset. This allows any background EEG activity to be averaged out, leaving only the electro-cortical activity which is directly linked to the stimulus. This stimulus-linked electro-cortical activity is known as an event related potential (ERP). Obtaining an ERP is one of the most commonly used methods of studying cortical processing, and has been used for decades to study all aspects of brain function (Rugg and Coles 1996, Luck 2005). An example of an event related potential, in this case in response to a flash-based visual stimulus is shown in figure 1.1.25.

1.1.4.2 Amplification and data processing

Although there is no conceptual difference between a clinical EEG system and an ERP system, there are practical differences. Many clinical EEG systems, especially older versions, will have a sample rate of 500 Hz or less. Such a sample rate is perfectly suitable for continuous EEG monitoring, and systems with a lower sample rate are often significantly less expensive. However, systems designed to perform ERP studies are required to have a much higher sample rate (usually 2000 Hz and above) because of the fast, transient nature of stimulus-related electro-cortical activity. As ERP systems are often solely designed for research purposes, they are often able employ a high-density electrode array of the form mentioned in section 1.1.2, which are not commonly used in clinical settings.

An ERP study will typically consist of a large number of stimulus repetitions. How many are necessary will depend on the initial signal-to-noise ratio but it is common for the number of repetitions to be in the hundreds. In order to process this data, ERP software will usually allow each trial to be inspected visually and rejected if it is deemed to contain significant artifacts. The mean of the accepted trials can then be calculated. ERP software will also allow a variety of filters and data handling methods to be performed in order to remove noise and background trends and further isolate the signal of interest.

1.2 Near-Infrared Optical Imaging

1.2.1 Introduction to and Fundamentals of Biomedical Optics

Near–infrared (NIR) optical imaging constitutes an evolution of the basic principles of NIR spectroscopy (NIRS), a method which was first demonstrated over 30 years ago (Jöbsis 1977). It is thus important to discuss NIRS before moving on to the details of NIR optical imaging. NIRS uses changes in the intensity of diffusely scattered NIR light at two or more wavelengths over a volume of tissue to calculate changes in the optical properties of that tissue. These variations in optical properties are the result of a change in the concentration of certain optical absorbers (or chromophores) within the tissue, and using relatively simple models of light transport and certain assumptions, it is possible to calculate these concentration changes. The most physiologically interesting chromophores in human tissue include oxy-haemoglobin (HbO_2), deoxy-haemoglobin (HHb) and cytochrome oxidase. Haemoglobin is responsible for transportation of oxygen around the bloodstream and as a result a measurement of changes in concentrations of its oxygenated and reduced state can provide us with information about localised tissue oxygenation. A change in haemoglobin concentrations implies that the local oxygen demand has changed and this has particular implications when studying the brain and how regional cerebral blood flow is related to the activity of surrounding neurons.

NIRS can be performed with one detector and a pair of co-located NIR sources (which constitute a single channel) coupled to the body via optical fibres. The sample rate of a NIRS system is only limited by the efficiency of the optical detectors, and as a result most NIRS systems have a high temporal resolution, typically around 10Hz (Obrig and Villringer 2003). However, as most NIRS systems employ only a very small number of channels, their spatial resolution is limited to knowing broadly which area

of tissue they are applied to, be it a particular muscle or a loosely defined area of the cerebral cortex.

Near-infrared imaging techniques go beyond this limitation by using many source-detector pairs and intricate reconstruction methods to produce 2D and 3D images of changes in chromophore concentration. Many NIR imaging systems can provide an optimal resolution comparable to that of functional Magnetic Resonance Imaging (fMRI), but with the advantages of low cost, easy applicability and the potential to be employed at the bedside.

1.2.1.1 Optical properties of tissue

Biological tissue is an inhomogeneous and anisotropic medium made up of many different structures and substances. As a result, the manner in which light interacts with bulk tissue is remarkably complicated. At a fundamental level however, it can be simplified into a combination of two possible types of interaction: absorption and scattering.

Absorption is the process by which the energy of a photon is taken up by the medium in which it is travelling, typically by an atomic electron, and as such the photon will cease to exist. When traversing a purely absorbing (i.e. non-scattering) medium, the ratio of the intensity of light out (I) to the intensity of light in (I_0) is given by the Lambert-Bouger law:

$$I / I_0 = e^{-\mu_a(\lambda)x} , \tag{1.2.1}$$

where x is the distance traversed through the medium (the optical pathlength) and $\mu_a(\lambda)$ is the absorption coefficient of the medium at a given wavelength (λ). The absorption coefficient is a measure of the probability of a photon being absorbed per unit length, and is the product of the concentration of the absorbing substance and the specific absorption coefficient of that substance. If the medium consists of several different

absorbing substances, each with their own absorption coefficient and concentration, the total absorption coefficient will be a linear sum of the individual absorption coefficients, such that:

$$\mu_a(\lambda) = \sum_n k_n(\lambda) c_n \tag{1.2.2}$$

Where $k_n(\lambda)$ is the specific absorption coefficient (at wavelength λ) and c_n is the concentration, of the n^{th} substance. Biological tissue obviously does consist of many different optically absorbing substances, and in bulk tissue the most dominant of these chromophores are water, haemoglobins, lipids, melanin and cytochrome oxidase.

Water and haemoglobins are present in very high concentrations in the human body and as a result it is their absorption spectra which dominate the absorption characteristics of bulk tissue. The absorption spectrum of water exhibits a marked increase in absorption of light at wavelengths greater than approximately 900 nm. Similarly, haemoglobins absorb very strongly at wavelengths below around 600 nm. It is the presence of this absorption 'window' between 600 and 900 nm which allows NIR light to be used to interrogate human tissue. Figure 1.2.1 shows the absorption spectrum of water from 600 to 1000 nm whilst figure 1.2.2 shows the absorption spectra of oxy-haemoglobin (HbO_2) and its reduced equivalent deoxy-haemoglobin (HHb) over the range 650 to 1000 nm. It is worth noting the significant difference in the absorption spectra of HbO_2 and HHb. Their difference over the visible region of the electromagnetic spectrum (particularly around 400 nm, the blue end of visible) is the reason why well oxygenated, arterial blood is typically a much brighter colour red than lesser-oxygenated venous blood. The differences in these spectra over the NIR range are fundamental to all NIR biomedical techniques, and will be discussed in greater detail in section 3.1.2.

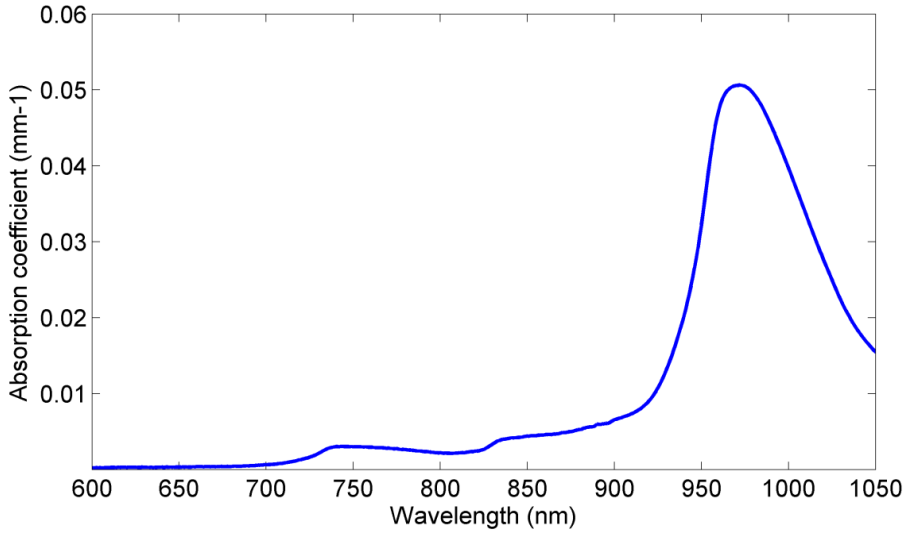

Figure 1.2.1. The absorption spectrum of water. Adapted from Matcher et al. 1995.

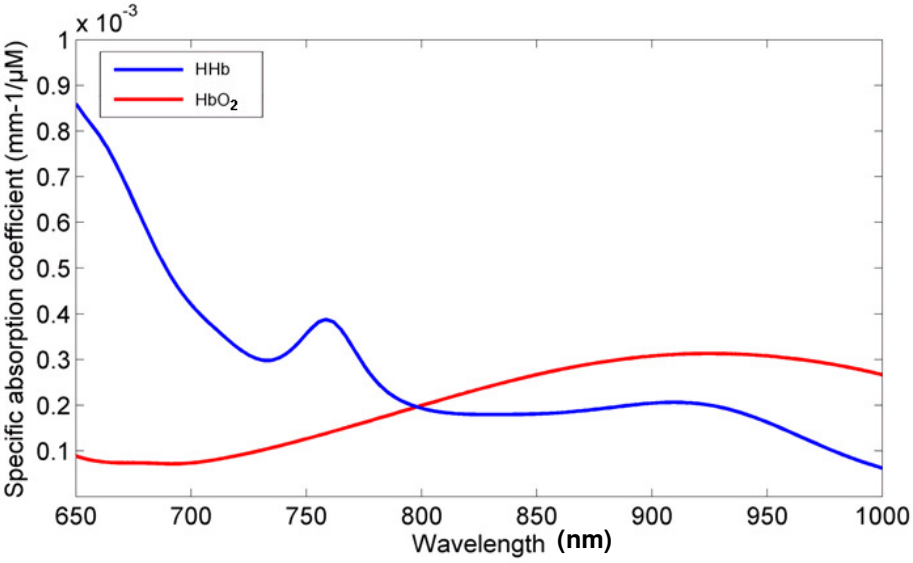

Figure 1.2.2. The specific absorption spectra of oxy and deoxy-haemoglobin over the NIR range. (Matcher et al. 1995).

Lipids (which include fats, oils, cholesterols etc.) are generally highly concentrated in tissue, but concentration varies markedly with tissue type. In a similar way to water, lipids also exhibit a 'window' of relatively low absorption around the NIR range. Melanin is a protein present in the upper surfaces of human skin and is a very efficient absorber of ultra-violet light. It is also a significant absorber over the NIR range, but is present in relatively low concentrations.

Cytochrome oxidase (CtOx) is the last enzyme in the respiratory electron transport chain, and is a fundamental element of cellular metabolism. It is responsible for the reduction of molecular oxygen, converting it to two molecules of water. It is in this manner that the vast majority of oxygen is used up in biological tissue. The concentration of CtOx in tissue is, at most, a tenth that of haemoglobin and as a result CtOx has a relatively small affect on the total absorption coefficient of tissue. It is mentioned here because of the potentially valuable physiological information which can be obtained by measuring variations in concentration of different CtOx states. The relative quantities of CtOx in a reduced or oxidised state can provide an indirect measure of the metabolic demand of a region of tissue. Because the total concentration of cytochrome oxidase does not vary, it is the difference in the absorption coefficient of reduced and oxidised CtOx which is relevant to spectroscopic measurements. However, as the concentration of CtOx is so low in comparison to haemoglobin, its contribution to variations in absorption coefficient is negligible compared to that of HbO_2 and HHb and is commonly neglected in NIRS measurements.

The second fundamental way in which light can interact with matter is through a scattering process. Scattering is the general term used to describe a variety of light-matter interactions which maintain the existence of the incoming photon but which may alter its direction of travel or (in the case of inelastic scattering) the photon's energy. Scattering is by far the most dominant light-matter interaction in biological tissue at optical wavelengths,

and as virtually all of these are elastic interactions, inelastic scattering is generally neglected in biomedical optics.

The scattering coefficient, $\mu_s(\lambda)$ represents the probability that a photon will undergo a scattering event, per unit length of medium. In the same way that the absorption coefficient is a product of an intrinsic property of a substance and the concentration of that substance, μ_s is a product of the scattering cross section of a particle (which is a measure of the likelihood of that particle causing scattering event) and the number density of those particles. Scattering of NIR light in bulk tissue tends to occur preferentially in the forward direction, that is, the initial direction of the incident photon. However, as scattering is so dominant, NIR photons will lose their original directionality after traversing only a few millimetres of tissue and the light can therefore be assumed to be isotropically distributed. This assumption is fundamental to the light-transport model based on the diffusion equation which is discussed in section 1.2.3.1. This model requires the definition of the reduced scattering coefficient (μ_s'), which is a product of μ_s and a factor pertaining to the anisotropy of tissue scattering. The reduced scattering coefficient represents the number of *isotropic* scattering events, per unit length.

The effect of scattering in biomedical optics is to prevent incident light from taking the direct path through a medium. Instead, a photon will travel a random path, from one scattering event to the next. This means that the chance of any given photon being absorbed will no longer be a simple function of the thickness of the medium (x). A photon undergoing a greater number of scatters will (on average) have to travel a greater distance to traverse the medium, and will therefore have a greater chance of being absorbed.

In order to model the attenuation of light transmitted through an absorbing and scattering medium, it is necessary to include a factor that accounts for

those photons which are rendered undetectable by being scattering away from the detector and to replace the optical pathlength *x* with a function that accounts for the increase in average pathlength due to scattering events. This approach leads us to what is known as the modified Beer-Lambert law:

$$I/I_0 = e^{-\mu_a(\lambda)Dx+G}.$$

(1.2.3)

In the above equation *G* represents the loss of intensity due to scattered photons which do not reach the detector and *D* is known as the differential pathlength factor (DPF). The DPF is dependent upon the reduced scattering coefficient $\mu_s'(\lambda)$, the absorption coefficient $\mu_a(\lambda)$ and the geometry of source and detector. The modified Beer-Lambert law is probably the most important equation in biomedical optics and it allows us to calculate several physiologically important characteristics.

1.2.1.2 What does NIRS measure?

The modified Beer-Lambert law provides us with a method of calculating the absorption coefficient of a medium given the amount of light lost through it, the DPF and the geometrical loss, *G*. The intensity loss due to scatter and the geometry of the set-up (*G*) is very difficult to calculate and as a result, the measurement of absolute values of $\mu_a(\lambda)$ becomes impossible in simple NIRS arrangements. This problem is by-passed by recording *changes* in the attenuation of NIR light over the medium, such that between state 1 and state 2 the change in attenuation is:

$$\ln\left(I_2/I_0\right) - \ln\left(I_1/I_0\right) = \ln\left(I_2/I_1\right) = Dx(\Delta\mu_{a(2-1)})$$

(1.2.4)

Note that G has been eliminated and only the product of the DPF and the optical pathlength is still required in order that the change in absorption coefficient can be calculated from measurements of change in attenuation. The product of the DPF and optical pathlength constitutes the average path-length travelled by photons within the medium. If we can measure the mean time taken by photons to traverse the medium and we know the medium's refractive index, we can calculate the DPF. This is performed continuously in certain frequency-domain NIRS systems (see 1.2.2.3). The DPF can also be approximated given knowledge of the optical properties of the medium (Arridge et al. 1992). In simple applications of NIRS, the DPF is often taken as a fixed, constant value, which will be based on previous measurements most suited to the tissue and subject being studied.

As mentioned in section 3.1.1, there are many relevant chromophores in biological tissue, but only those which vary in concentration over the timescale of an experiment will contribute to $\Delta\mu_a$ and it is these which are of physiological interest. Of the five major chromophores listed in section 3.1.1, water, lipids and melanin can be safely assumed to remain constant during any normal experiment. This leaves concentration changes of oxy and de-oxy haemoglobin and cytochrome oxidase to provide any measured variation in absorption coefficient.

Equation 1.2.4 allows us to calculate the change in absorption coefficient at a single wavelength given the variation in optical attenuation at that wavelength. Given equation 1.2.2 and the assumptions mentioned above, by measuring at two wavelengths simultaneously it is possible to calculate the concentration change in HbO_2 and that of HHb via the simultaneous equations:

$$\Delta\mu_a(\lambda_1) = \varepsilon_{HbO2}(\lambda_1)\Delta c_{HbO2} + \varepsilon_{HHb}(\lambda_1)\Delta c_{HHb}\,,$$
$$\Delta\mu_a(\lambda_2) = \varepsilon_{HbO2}(\lambda_2)\Delta c_{HbO2} + \varepsilon_{HHb}(\lambda_2)\Delta c_{HHb}\,, \quad (1.2.5)$$

where $\varepsilon_{HHb}(\lambda)$ and ε_{HbO2} (λ) are the extinction coefficients of respective chromophores at the relevant wavelength and Δc_{HHb} and Δc_{HbO2} are the relevant changes in concentration of each chromophore. The standard method for performing NIRS is therefore to measure the changes in attenuation of two wavelengths of light over the same volume of tissue, and concentration changes are then calculated by solving the equations 3.5. By adding a third wavelength it is possible to measure variations in concentration of three chromophores; HbO_2, HHb and CtOx.

1.2.1.3 Functional NIRS and the origin of the signal

Because of the manner in which NIRS is limited to observing changes in chromophore concentration, NIRS is most readily applied in experiments where a change in chromphore concentration is invoked by the application of a stimulus. The increase in electro-chemical activity of neurons associated with the performance of a cognitive task necessitates an increase in the rate of energy consumption within those neurons. Whilst the details of cellular energetics are too complex to be discussed here, they can be summarised in that cellular respiration is undertaken in order to produce the energy-rich molecule adenosine-tri-phosphate (or ATP) which is used to power almost all cellular processes. Repeated neuronal firing requires the continual re-polarisation of the cell back to its resting state potential, a process which requires ATP to power the active transportation of charged ions across the cellular membrane. Ultimately, maintenance of an increased rate of neuronal firing requires an increase in cellular respiration, a process which is fuelled by both oxygen and glucose. This increase in metabolic demand is met by a response from the localised vasculature, via an interaction which is broadly known as neurovascular coupling. Capillary dilation results in a localised increase in cerebral blood flow (CBF). (See Buxton et al. 1998 for a discussion of the associated biomechanical parameters). As NIRS is able to resolve changes in the concentrations of oxy and deoxy-haemoglobin, it is the balance between the rate at which oxygen is consumed from the blood (known as the cerebral metabolic rate

of oxygen, $CMRO_2$) and the rate at which oxygenated blood is flowing into a region of the brain which dictates the scale and form of the functional NIRS signal.

Naively one would expect an increase in functional activity of a localised group of neurons to result in a localised decrease in oxyhaemoglobin and increase in deoxy-haemoglobin concentrations because of an increase in the rate at which oxygen is extracted from the blood. In fact, the classic functional NIRS response is the result of a decrease in deoxy-haemoglobin and an increase in oxyhaemoglobin concentration. This is due to the fact that the change in $CMRO_2$, and the responding change in CBF are poorly balanced. In a seminal PET study in 1986, Fox and Raichle found that the ratio of the increase in CBF to the increase in $CMRO_2$ was approximately 6 for a somatosensory stimulation task, which represents a massive overcompensation in cerebral perfusion. Though this figure is still the subject of fierce debate (Tak et al. 2010, Hoge et al. 2005, Boas et al. 2003), functional changes in neuronal activity do result in an over-compensation in local CBF, and this is the basis for the mapping of functional activation using fMRI and NIR optical techniques. The classic functional response as recorded by NIRS therefore consists of a localised micro-molar scale increase in HbO_2 concentration, accompanied by a (somewhat more variable, and smaller) decrease in HHb concentration.

The haemodynamic response to functional stimulation is typically quite slow, beginning no sooner that 3 seconds after the onset of stimulation and usually reaching its peak within 20 seconds of stimulus onset (Obrig and Villringer 2003). Time-courses, scale, and the form of the haemodynamic response will vary for different stimuli, stimuli duration, subject group, subject age and for different regions of the brain, but a example of a classic functional haemodynamic response is shown in figure 1.2.3.

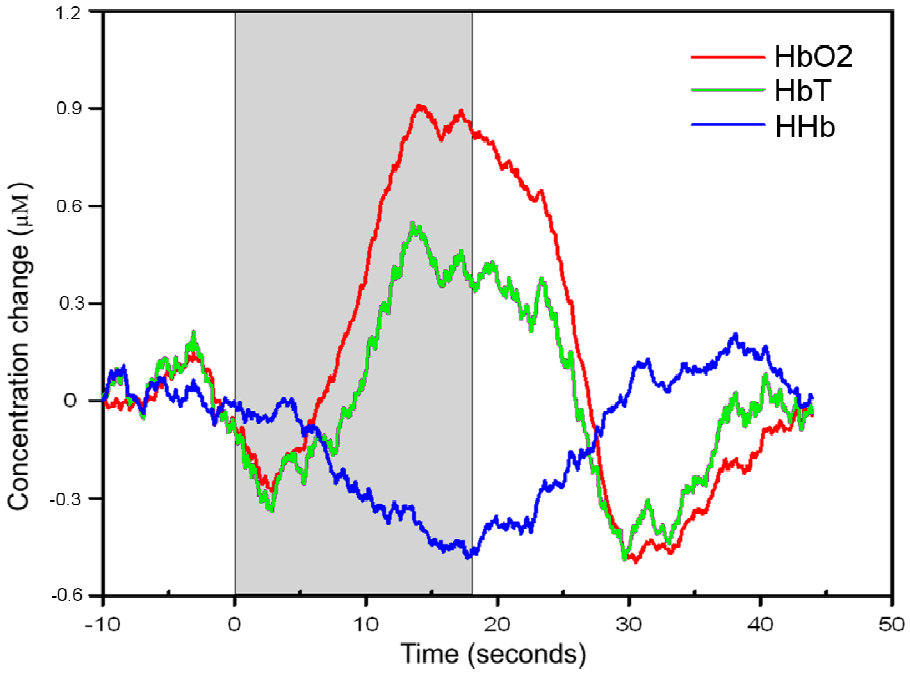

Figure 1.2.3. A classic NIRS functional activation data set in response to a visual stimulus in an adult (Meek et al. 1995). The grey box specifies the period of stimulus. Note how the increase in oxyhaemoglobin is accompanied by a decrease in deoxyhaemoglobin concentration.

Although the classical functional haemodynamic response observed by NIR methods has a time course of the order of seconds, for over ten years there have been reports of a resolvable fast optical response with a time course of the order of milliseconds. The depolarization of neurons is known to produce a change in optical attenuation, which is believed to be due to changes in optical scatter. This has been shown in single neurons ex-vivo (Cohen et al. 1972) and in animal studies in vivo (Rector et al. 1997). It is therefore possible that NIRS could not only measure the 'slow' signal due to the vascular response to neuronal activation, but also the 'fast' signal due to increased activity in the neurons themselves, with a temporal resolution analogous to that of EEG. This would render NIRS a remarkably exquisite methodology for non-invasive study of neurovascular coupling in humans. It would also negate many of the reasons for pursuing a combined EEG and NIR system. Gratton and co-workers have repeatedly reported successfully

eliciting and recording such fast optical responses (Gratton et al. 1997, 2006) though how reproducible and robust these responses are remains an issue of controversy; several experiments have failed to reproduce Gratton's results and upper-limit estimates of the expected size of such a fast optical signal have suggested it to be several orders of magnitude smaller than reported (Obrig and Villringer 2003, Franceschini and Boas 2004).

1.2.2 Types of NIR Instrumentation

1.2.2.1 Spectroscopy, topography and tomography

There are several ways in which the various NIR techniques and instrumentation can be classified. The most general is the division of NIR techniques into three types; spectroscopy, optical topography and optical tomography. This division is based upon a combination of factors, including how a system is applied to the body, whether the system is designed to produce images and whether measurements of the transmission of NIR light as well as measurements of diffusely-reflected light are obtained.

NIRS has already been described in detail, and involves the use of as little as one source-detector pair to probe a region of tissue. Optical topography will typically employ an approximately planar array of sources and detectors, so that measurements of diffusely reflected NIR light allow the haemodynamics of the area of superficial tissue directly under the array to be observed. It is important to note the subtle distinction between optical topography and multi-channel NIRS, which is that optical topography will, by definition, result in the production of a topographic map of changes in chromophore concentration, whereas multi-channel NIRS is simply a series of spectroscopic measurements (Gibson et al. 2005).

Optical tomography will also use an array of sources and detectors, but arranged so that a transverse slice or full three-dimensional (3D) image can be generated (Arridge et al. 2000a). This is only possible if a number of sources and detectors are positioned roughly opposite one another, so as to record transmission of NIR across the whole thickness of tissue. This is necessary in order that measurements are sensitive to changes in optical properties of the deepest volumes of tissue. Optical tomography will usually employ sources and detectors arranged in a ring, a series of rings or so as to cover the whole surface of the head. The latter arrangement can

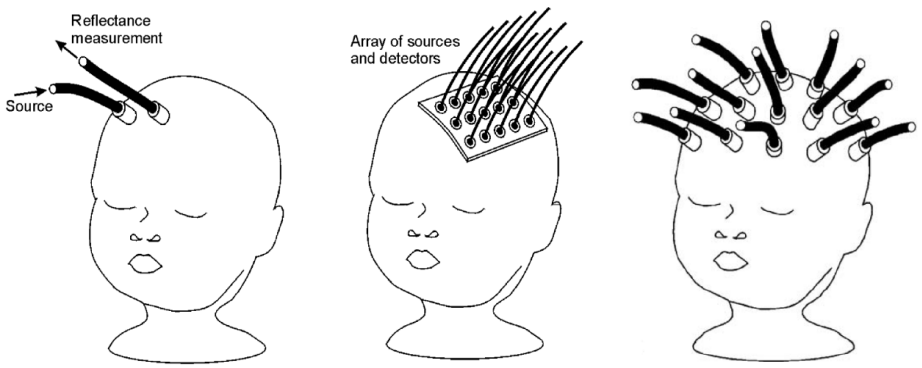

Figure 1.2.4. An illustration of the fundamental differences in application of (from left to right) NIRS, optical topography and optical tomography. (Figure courtesy of J C Hebden).

allow whole-head, 3D images of haemodynamics and oxygenation to be produced. Figure 1.2.4 illustrates the differences in application between NIRS, optical topography and optical tomography. It is worth noting that despite its name, optical topography will inherently contain some information about the depth of any chromophore concentration change, and certain optical topography systems are able to use this information to produce 3D images, albeit of a limited depth.

It is also important to mention, that there is a somewhat varied use of defining nomenclature across the NIR community. Diffuse optical imaging (DOI) is a general term which encompasses all optical imaging techniques for which scattering is the dominant photon-matter interaction, though it is typically applied (mostly in the USA) to mean either optical topography or tomography. Certain groups do not distinguish between topography and tomography at all, and often refer to planar imaging arrangements as tomographic.

There are several classes of NIR instrumentation which are categorised by the manner in which they emit and detect NIR light, and by the way

information is obtained from the light that is detected. These are defined below.

1.2.2.2 Continuous wave systems

Continuous wave (or CW) systems employ sources which emit light at a constant intensity, to allow variations in attenuation of this light to be recorded. These measurements allow chromophore concentration changes to be calculated using either the modified Beer-Lambert law (in the case of CW NIRS), or by comparing attenuation measurements with more sophisticated models of light transport (in the case of imaging applications, see section 1.2.3). CW systems are the simplest and least expensive of all NIR systems but allow a remarkable amount of physiological information to be obtained. The majority of commercial NIRS systems are CW, as are many optical topography systems.

Continuous wave optical topography systems require multiple source-detector pairs, and while the detectors tend to record continuously, the sources will either be illuminated in sequence or will be illuminated in parallel but with each intensity-modulated at a different frequency (Gibson et al. 2005). Intensity modulation in this fashion allows each source to be isolated using a Fourier transform of the detected intensity, or by using an arrangement of lock-in amplifiers. CW optical topography systems have been extensively applied to studies of haemodynamic changes in superficial tissues, especially the upper cortical surface of the brain.

As mentioned previously, CW optical topography systems probe superficial tissues by measuring diffusely back-scattered light. As such they usually employ relatively small source-detector separations. As the intensity of light successfully travelling from source to detector across a region of tissue decreases exponentially with source-detector separation, these small separations mean the intensity of light incident at a detector will be relatively high. This reduces the necessary signal integration time at the

detectors which will increase the possible sample rate of the system. CW optical topography systems typically have a sample rate of around 10Hz, but 50Hz has been demonstrated (Franceschini et al. 2003).

Continuous wave methods have also been applied to optical tomography (Schmitz et al. 2002, 2005). As optical tomography requires the use of large source-detector separations (to provide sensitivity to the deepest regions of the tissue) the intensity of light which reaches each detector will typically be extremely low. This necessitates integration of the incident light over several seconds in order to provide an adequate signal. This process will limit the acquisition speed of such a system.

Continuous wave systems have the advantage of being simple, versatile, inexpensive and able to provide a good temporal resolution. However they have two fundamental disadvantages. The first is that they tend to be very sensitive to the changes in the coupling of a source or detector fibre to the scalp. Variation of the force with which a fibre is pressed to the skin affects the intensity measurements significantly, as can the presence of hair. As with many of the inherent problems associated with a CW measurement, this problem is negated by assuming that such properties remain approximately constant during a given experiment and will not contribute to any short-term change in optical properties of the interrogated tissue.

The second fundamental issue is that for a suitably brief acquisition time, measurements of intensity are only sensitive to regions directly below a source-detector pair, as defined by the photon measurement density function (PMDF) (Arridge 1995). The PMDF constitutes a three-dimensional model of the probability that a detectable photon (i.e. one which terminates at the detector) traverses a given optical path. Photon measurement density functions have been produced for models of the scalp, skull, cerebo-spinal fluid and brain of varying complexity (Schweiger and Arridge 1999). These models provide us with an accurate assessment of the shape and size of the

volume of the cerebral cortex that a given source-detector pair applied to the scalp is able to sample. Although it varies depending on the instrument and the optical properties of the target tissues, a general experimental rule-of-thumb is that a source-detector pair separated by a distance d will only be sensitive to a depth of approximately d/2 (Arridge 1995).

The amount of light which can be coupled into the scalp is limited for safety reasons, and most NIR systems maintain an output intensity below that of the eye safety limit (10 W/m^2 for NIR wavelengths in continuous operation (British Standard EN 60825-1:2007)). Continuous wave systems are usually designed to enable a relatively high sample rate (10 Hz or above). This limits the integration time (and therefore how many photons are available) for each measurement to be performed. The maximum source-detector separation which can be achieved is therefore limited by the sensitivity (and ultimately, the cost) of the detector apparatus. There have been some recent advances made in the separation of cerebral functional activation with systemic changes of haemoglobin concentrations in superficial tissues (i.e. the scalp) using source detector separations which deliberately only sample those superficial tissues (Zeff et al. 2007). However, the majority of continuous wave systems will typically operate with source detector separations of between 15 and 45 mm, large enough to have a good chance of sampling brain tissue, but small enough to allow a suitable amount of light to be detected.

1.2.2.3 Frequency domain systems

If intensity-modulated light is used to interrogate tissue, it is possible to measure not only attenuation of this light, but by comparison with the source modulation we can measure the change in phase of the modulated light at the detector. This principle is illustrated in figure 1.2.5. Adding this measurement of phase shift has the significant advantage of allowing the actual optical pathlength (the product of the DPF and tissue thickness x, see equation 1.2.3) to be measured continuously. This means that estimates of

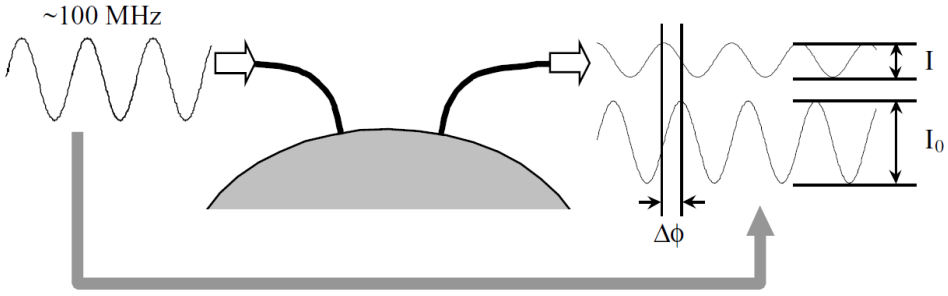

Figure 1.2.5. A representation of a frequency domain NIRS measurement. Both the drop in intensity and the change in phase of diffusely reflected, frequency-modulated NIR light are measured. (Figure courtesy of J C Hebden).

the optical pathlength based on the source-detector separation and estimates of the DPF need not be used, and this removes a significant source of error from measurements of absorption coefficient. By measuring phase shift it is also possible for the effects of absorption and scattering to be separated, which is not possible for CW systems. By comparing measurements of attenuation and phase with predictions of suitable models of light transport in tissue, the absorption and scattering coefficients can be calculated. Frequency domain systems have been designed to perform NIRS, optical topography and optical tomography (Chance et al. 1998, Franceschini et al. 2000, Culver et al. 2003).

1.2.2.4 Time domain systems

Time domain systems are the most sophisticated of NIR systems as they involve the measurement of the time taken for individual photons to traverse a volume of tissue. This is achieved by illuminating the tissue with a short duration (a few picoseconds) pulse of NIR light and measuring the time of flight of the emerging photons using very sensitive detectors. On emerging from the tissue, the NIR pulse will have broadened in duration, from a few picoseconds to several nanoseconds, because of the effect of scattering on the path of the photons. This broadened pulse (or temporal point spread

function, TPSF) represents a histogram of the time taken for each photon to travel from source to detector (Hebden and Delpy 1994).

The information contained within a TPSF will always be greater than a single wavelength measurement of attenuation and phase as obtained by frequency domain systems. The integration of the TPSF provides an intensity measurement equivalent to a CW measurement, while the Fourier transform of the TPSF provides a continuous spectrum of amplitude and phase shift data, each point of which is equivalent to a single frequency domain measurement. As with frequency domain systems, absorption and scattering components can be independently calculated using a Beer-Lambert approach or a more sophisticated approach for imaging applications (see section 1.2.3). Figure 1.2.6 illustrates how changes in optical properties of a volume of tissue will affect the associated TPSF.

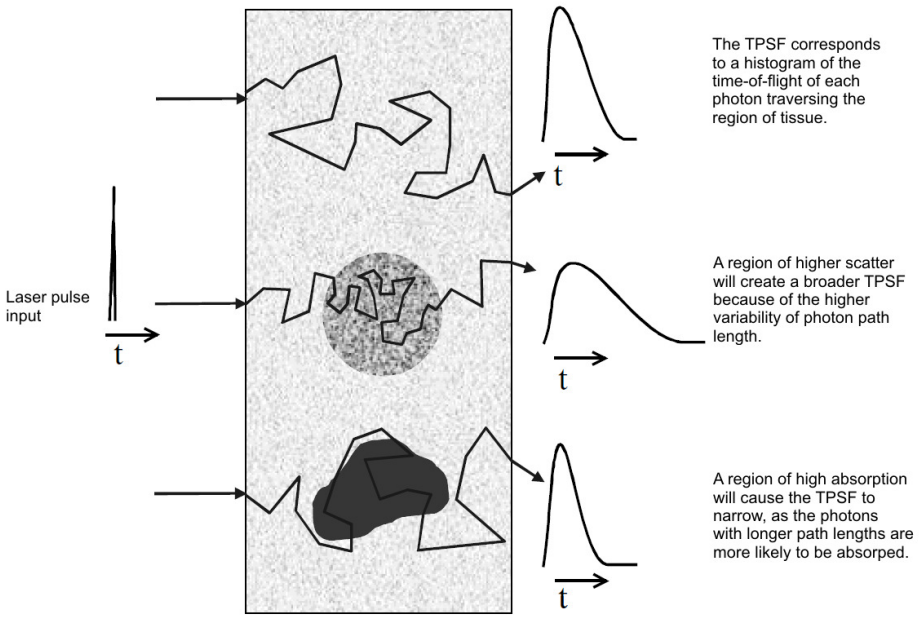

Figure 1.2.6. A summary of how the optical characteristics of tissue affect the TPSF recorded in time-domain imaging systems. (Figure courtesy of J C Hebden).

1.2.3 Photon Transport and Image Reconstruction

Producing 2D and 3D images of changes in chromophore concentrations from measurements of the TPSF, attenuation and phase shift or solely from attenuation is a very challenging mathematical problem (Arridge 1999). At x-ray wavelengths, the effect of scattering in tissue is minimal, and as a result, the path taken between source and detector can be well approximated to a straight line. As a result, the reconstruction of 3D images in x-ray computed tomography is a relatively straight-forward mathematical problem. This is not the case in NIR imaging because scattering is dominant, and the propagation of light certainly cannot be approximated to a straight line. Instead, the first stage of optical image reconstruction is to provide a model of how photons will travel through a volume of tissue. This model can then be used to calculate the distribution of light throughout a given volume of tissue, which will allow measurements to be simulated for a given arrangement of sources and detectors. The prediction of a measurement from a model of intrinsic properties in this manner is known as the *forward problem*. In solving the forward problem in NIR imaging, a sensitivity matrix is produced that relates the optical properties of a volume of tissue to the resulting measurement at the surface. Calculating the optical properties of a volume of tissue given an array of measurements at the surface constitutes an *inverse problem*, and solving this is the third and final stage of optical image reconstruction.

1.2.3.1 Modelling light transport in tissue

A complete description of light propagation through a medium is provided by the radiative transport equation (RTE) which has been successfully used to model the transport of a variety of particles through a variety of media. The RTE is a conservation equation. It states that the rate of change of the number of photons (travelling in a given direction, at a given time, per unit volume) is equal to the rate of gain of photons (travelling in a given direction, at a given time, per unit volume), minus the rate of loss of photons

(travelling in a given direction, at a given time, per unit volume). The mechanisms by which photons are gained are the presence of a source and the scattering of photons, whilst the mechanisms of loss are absorption and scattering. The time-domain RTE is shown below:

$$\left(\frac{1}{c}\frac{\partial}{\partial t} + \hat{s}.\nabla + \mu_{tr}(r)\right)\phi(r,\hat{s},t) = \mu_s(r)\int \Theta(\hat{s},\hat{s}')\phi(r,\hat{s},t)d\hat{s}' + q(r,\hat{s},t)$$

(1.2.6)

In equation 1.2.6, $\phi(r, \hat{s}, t)$ is the number of photons per unit volume which are travelling from point r in direction $\hat{s}$ at time t, $\mu_{tr} = \mu_a + \mu_s$ as defined in section 1.2.1, $\Theta(\hat{s},\hat{s}')$ is the scattering phase function, which is the probability of a photon scattering from direction $\hat{s}$ to direction $\hat{s}'$, $q(r,\hat{s},t)$ is representative of a light source and c is the speed of light in a vacuum (Arridge et al. 1999). In order to calculate the distribution of light throughout a large 3D volume, the RTE is unsuitably computationally expensive (Aydin et al. 2002). As a result, simplifications of equation 1.2.6 are often applied to optical image reconstruction. By expanding the $\hat{s}$ dependent elements of equation 1.2.6 in spherical harmonics and taking a first-order approximation, and then by approximating further using the assumptions that all sources are isotropic and photon flux varies slowly, we can obtain the diffusion approximation to the RTE (also known as the diffusion equation);

$$-\nabla.\kappa(r)\nabla\Phi(r,t) + \mu_a\Phi(r,t) + \frac{1}{c}\frac{\partial\Phi(r,t)}{\partial t} = q_0(r,t)$$

(1.2.7)

Here, $\Phi(r,t)$ is the photon density and κ is the diffusion coefficient such that $\kappa = 1/3(\mu_a+\mu_s')$. The diffusion equation is the most widely used model

of light transport in tissue for optical imaging applications. Its fundamental assumption, that NIR light travels diffusely, is valid for media in which $\mu_a \ll \mu_s'$ which is generally true in bulk tissue. However, this assumption can breakdown near sources, at internal or external boundaries, in tissue which is particularly anisotropic and in regions of particularly high absorption or low scatter. It is worth noting that there are several other approaches to the modelling of light transport in tissue and perhaps the most important of these is statistical modelling of individual photon paths using Monte Carlo simulation. Monte Carlo simulation is often used in situations where the diffusion equation is not valid and although it produces arguably the best possible model of light transport in tissue, its computational expense makes it impractical for experimental image reconstruction (Boas et al. 2002).

1.2.3.2 The forward and inverse problems and image reconstruction

The next step towards optical image reconstruction is to use the diffusion equation to calculate the light field in a given volume of tissue for a given arrangement of sources and detectors, allowing us to produce a simulated set of measurements. This constitutes solving the *forward problem* (Gibson et al. 2005). In order to solve the forward problem it is necessary to determine the forward operator F, which relates the internal optical properties of our given volume (x) to a simulated set of measurements, (y). The forward problem can therefore be described by the equation:

$$y = F(x). \tag{1.2.8}$$

Despite the simplification of the RTE into the diffusion equation, producing a model of light distribution in a 3D volume is still mathematically challenging. It has been shown that there are analytical solutions to the forward problem using Green's functions (Boas et al. 1994) but in order to model complex geometries it is usually necessary to use numerical

modelling techniques, most commonly a finite element method (Arridge et al. 2000b).

The finite element method (FEM) involves the production of a mesh, which separates the interrogated volume into a finite number of elements. FEM is used to solve partial differential equations over complex geometries by estimating, in our case, the photon density at a series of points throughout the volume, points which correspond to the nodes of the finite element mesh. Producing a mesh suitable for modelling a complex, inhomogeneous volume whilst minimising computational expense is in itself a difficult problem, and one which is the subject of active research (Schweiger et al. 2003, Elisee et al. 2010).

The FEM solution to the diffusion equation results in the production of a sensitivity matrix which is a discrete approximation to the continuous forward operator $F(x)$. Using this approximation, we can perform the final stage of optical image reconstruction by finding a solution to the *inverse problem*.

Equation 1.2.8 shows how the forward problem constitutes calculating a simulated set of data (y) given knowledge of the internal optical properties of our volume (x). In order to reconstruct an image it is necessary to calculate the internal optical properties given a measured set of data, i.e. the inverse of equation 1.2.8;

$$x = F^{-1}(y). \tag{1.2.9}$$

The inversion of the forward operator F is a non-linear problem, but it can be linearised if we are able to assume that the optical properties x are close to the initial estimate x_0 (which was an input to the forward problem) and that measured data y are similar to the simulated data set y_0 (which comes from the solution of the forward problem). Such an assumption is typically

valid when the aim is to produce an image of the difference between two states, i.e. when measurements are taken before and after a small change in optical properties occurs. This is commonly the case when performing NIR imaging of functional activation. Given this assumption, we can use a Taylor series to expand equation 1.2.8 about x_0:

$$y = y_0 + F'(x_0)(x - x_0) + F''(x_0)(x - x_0)^2 + \cdots \tag{1.2.10}$$

F' and F'' are the first and second order Fréchet derivatives of F, Fréchet derivatives being a form of linear integral operator. These derivatives can in general be represented respectively by the Jacobian (J) and Hessian (H) matrices of the forward operator. The Jacobian is calculated by solving the forward problem, and is the approximation to the forward operator which is calculated using the finite element method described above.

If we neglect the higher terms of the expansion in equation 1.2.10 and consider the changes in optical properties $\Delta x = x - x_0$, and changes in our data set $\Delta y = y - y_0$ then equation 1.2.10 becomes linear:

$$\Delta y = \mathrm{J}\Delta x. \tag{1.2.11}$$

The inverse problem now constitutes the inversion of the Jacobian matrix J which can be performed using standard matrix inversion techniques. The most suitable is to introduce a Tikhonov regularisation parameter (λ) into the generalised Moore-Penrose inverse such that:

$$\Delta x = \mathrm{J}^{\mathrm{T}}(\mathrm{J}\mathrm{J}^{\mathrm{T}} + \lambda \mathrm{I})^{-1}\Delta y \tag{1.2.12}$$

where I is the identity matrix (Gibson et al. 2005). This linear solution to the inverse problem is known as linear image reconstruction. If the assumption that we are reconstructing the difference between two similar states is not valid, either because the change is too large or because we wish

to reconstruct absolute images of optical properties, then the inverse problem cannot be linearised and the full non-linear problem must be solved. This is generally the case if the aim of optical imaging is to observe an optical inhomogeneity, as in optical mammography or forms of static brain imaging.

The non-linear image reconstruction problem does not have an analytical solution and must be solved using numerical methods. This generally involves defining what's known as an objective function, which represents the difference between measured data and that simulated in solution of the forward problem. The aim of non-linear image reconstruction is then to minimise the objective function (Arridge 1999). A software package developed at UCL (the time-resolved optical absorption and scatter tomography (TOAST)) defines a finite element mesh in order to discretely model the diffusion approximation to the radiative transfer equation and reconstructs images iteratively by adjusting the optical properties of the finite element mesh to minimise the differences between modelled and recorded data (Arridge et al. 2000a, Schwieger et al. 2003)

1.2.3.3 Optimisation of Image Reconstruction

When performing optical topography of functional activation, the functional response constitutes a small perturbation to the resting optical properties of the system. Linear image reconstruction is therefore the most suitable imaging approach (Gibson et al. 2005). A carefully performed optical image reconstruction is the only way to extract all the available information from a multi-channelled NIR recording, however the complexity of the mathematical problem of image reconstruction will always result in certain limitations. These include a propensity to produce artifacts (particularly close to the source and detector array (Stott et al. 2003) and limits to the optimum resolution. One particular issue with linear image reconstruction is a tendency to inaccurately reconstruct the scale of a change in absorption,

often producing an under-estimate (Boas 1997). A series of linearly reconstructed images of functional activation are shown in figure 1.2.7.

All image reconstruction methods are constrained in their accuracy by (among other things) the design of the sensing array, i.e. the arrangement of sources and detectors attached to the scalp. In designing an array, the aim is always to maximise the number of detectable photons which traverse a given volume of sample tissue, i.e. to maximise the volume sampling density (Boas et al. 2004, Dehgani et al. 2009). No real array design can produce completely homogenous sampling, but a poorly designed array will

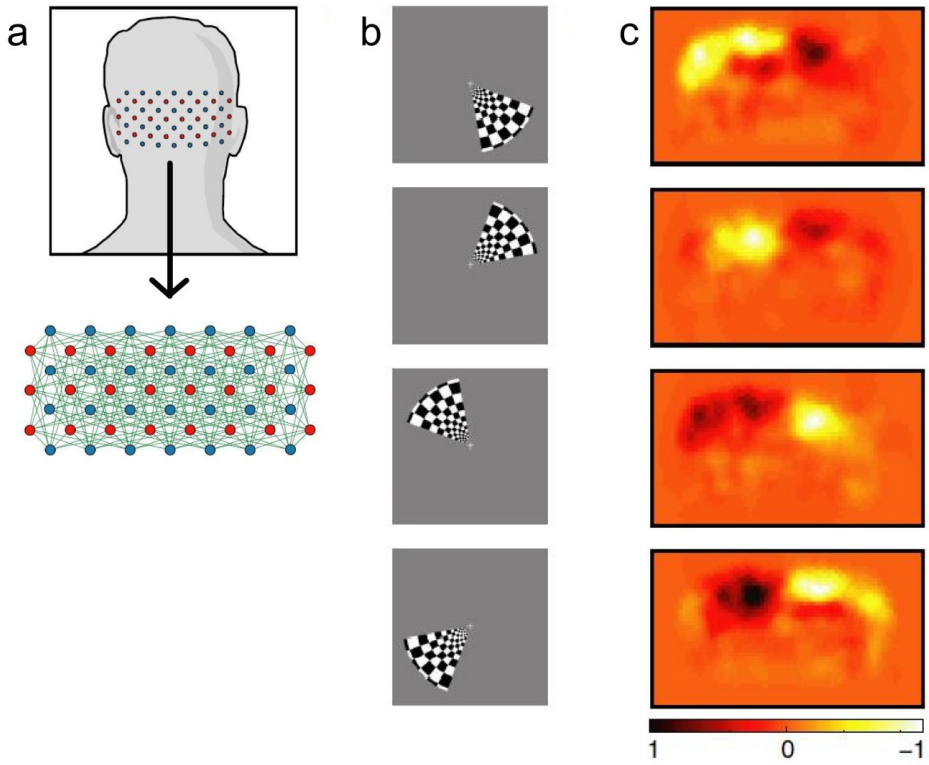

Figure 1.2.7. An example of linearly reconstructed images of functional activation taken from Zeff et al. 2007. A high-density optical imaging array over the visual cortex (a) is used to image functional activation due to a rotating, reversing checkerboard stimulus (b). The resulting reconstructed changes in oxyhaemoglobin concentration (which are normalised to each figure, the peak changes are 0.34, 0.60, 0.45 and 0.32 µM respectively) are shown (c). The high density of this imaging array resulted in images which are generally considered to be the best example of optical topography of functional activation yet produced, and as such represent a current upper limit of the quality of diffuse optical images.

produce significantly distorted reconstructed images. In practice there are several rules which must be adhered to in order to maximise an array's suitability for image reconstruction. These rules will often, in practice, be mutually incompatible, and it therefore becomes necessary to prioritise depending on the aim of the experiment in question. These rules were compiled by the author during the course of this work and are as follows: First, the number of source-detector pairs (channels) per unit surface area should be maximised. Second, these channels should be arranged so that their sampled volumes overlap; the number of channels sampling a given volume of tissue should be maximised. Third, the channels sampling a given volume of tissue should have as large a variety of source-detector separations as possible, so as to maximise the range of depths for which meaningful images can be reconstructed. These theoretical optimisations are then restricted by certain practical requirements and limitations, namely that source-detector separations larger than 50 mm are unlikely to yield a viable signal-to-noise ratio, the optical fibre bundles which carry light to and from the head are of a non-zero diameter, the number of sources and detectors is limited by the optical instrument and that the array has to be comfortable, relatively light and easy to apply.

1.3 Simultaneous EEG and NIR Techniques

1.3.1 Why Perform Simultaneous EEG and NIR Imaging?

The benefit of any multi-modality imaging system is found in the complementary information provided by each of the constituent modalities. For simultaneous EEG and NIR imaging, it is the nature of the signals which are observed and the differing spatial and temporal characteristics of these signals which make a dual-modality system beneficial.

As described in the previous chapters, EEG provides a measure of the group activity of cortical neurons with a sub-millisecond temporal resolution but a severely limited spatial resolution. NIR techniques can observe the vascular response to such neuronal activation with a good temporal resolution (10 Hz or better) and an excellent spatial resolution (potentially as good as ~5 mm in all three dimensions).

Therefore, a combined system has several fundamental advantages. The first is obvious, and it is that a dual-modality system simply provides more information about the brain. For example, obtaining an event-related potential *and* a functional haemodynamic response to a given stimulus inherently teaches us more about the brain's processing of that stimulus. The second advantage encompasses the fact that the signal observed by each modality is fundamentally different, and this allows one to inform the other. For example, a more meaningful event-related potential could be obtained if only those electrodes closest to the location of the neuronal activation were studied, and NIR optical imaging can provide that localisation. Conversely, there are many clinical scenarios where cerebral haemodynamics during particular electroencephalographic events are poorly understood, and a combined system allows for EEG-informed optical imaging of those events (for example, see Roche-Labarbe et al. 2007). This second advantage is also a result of the fact that simultaneous EEG-NIR can provide both good

temporal and good spatial resolution, a quality which is important in functional activation studies and is rare among neuro-imaging techniques.

The third advantage of a combined EEG-NIR system is that it allows the relationship between neuronal activation (be it stimulus related or spontaneous) and the resulting macroscopic vascular response to be explicitly studied in-vivo (the qualifier 'macroscopic' is used here to explicitly express that EEG-NIR systems will only ever be able to study the neurovascular coupling relationship in bulk (i.e. > 100 mm^3) brain tissue, as opposed to methods which study the microscopic responses of individual blood vessels to a localised change in neuronal activation (for example see Bouchard et al. 2008). The neuro-vascular coupling relationship is incredibly important not just for direct clinical reasons but because the assumption that an increase in cerebral blood flow is a good proxy for increased localised brain function is fundamental to the vast majority of functional neuroimaging techniques (including fMRI, PET, SPECT and NIR techniques). Simultaneous EEG-NIR recording allows models of macroscopic neurovascular coupling and neuronal metabolism to be tested in a simple and versatile fashion. Such experiments have already been performed using simultaneous EEG and NIR spectroscopy (see section 2.1.3). Variations in this relationship under different circumstances can potentially provide new information about healthy brain function and the nature of certain brain disorders, and may provide us with a better understanding of the effects of certain drugs (Franceschini et al. 2010).

The nature of these advantages, and the clinical uses of EEG, lead to three specific applications: the study of functional activation, the study of neurovascular coupling itself and the clinical study of the haemodynamics, neurovascular coupling and localisation of epileptic seizures. As this technique is in its infancy, these applications remain quite general, and much work is needed in order to identify how EEG-NIR techniques may best be used to improve our knowledge of healthy brain function and

provide clinical benefit. A brief description of these three applications is provided in section 1.3.3.

1.3.2 Simultaneity and Dual Modality Data Fusion

In the development of a dual-modality functional imaging system, it is important to understand the advantages and disadvantages of fully simultaneous dual-modality data acquisition in comparison to the sequential application of each modality. Performing two neuroimaging techniques simultaneously will always result in each data acquisition process being less than optimal. This can be the result of the two systems interfering with one another or can simply be because the application of two imaging systems is more challenging than the application of one. The extent to which simultaneous recording is detrimental to the acquisition process must be weighed against what can be gained from fully simultaneous data. Because NIR and EEG systems do not interfere with one another, it is only the additional difficulties of application and experimental design which are a detriment to a simultaneous EEG-NIR imaging model.

Simultaneous acquisition clearly has the advantage of allowing dual-modality datasets to be obtained in a single recording session, but such an arrangement is only inherently superior to sequential acquisition when the physiological feature under investigation exhibits significant inter-feature variability, and where that variability is of scientific interest. If the characteristics of a given physiological feature do not vary from one instance to the next, then the data obtained from sequential measurement is completely equivalent to that of simultaneous measurement. In such circumstances simultaneous acquisition would be superfluous. In addition, if the variability is not of scientific interest itself, then by recording a large enough number of features and taken an average, that variability can be removed and, once again, sequential acquisition will be completely equivalent to simultaneous acquisition.

A good example of a case where simultaneous acquisition is explicitly desirable in a functional activation experiment is the study performed by Obrig et al. (2002). In this study, it was the variation caused by habituation

effects, both within and across periods of visual stimulation, which was the subject of investigation and necessitated fully simultaneous EEG-NIR acquisition.

Simultaneous acquisition is also desirable when the purpose of the neuroimaging study is to investigate a feature which is well defined with one modality but not with another, which is the case in the EEG-NIR imaging study of seizures (though simultaneous acquisition is also necessary in the study of seizures because of the significant variability between seizure events and because seizures are spontaneous and unpredictable). The use of the EEG to define a seizure, and then investigating the haemodynamic variations using simultaneously recorded NIR imaging constitutes EEG-informed NIR imaging, and is an example of an asymmetric data fusion model. This purely temporal correlation approach (which could equally apply to NIR-informed EEG recording) is the simplest form of dual-modality data fusion.

The spatial information present in each modality also presents a number of other forms of asymmetric data fusion. The simplest consist of arrangements which use the spatial information available in the first modality in order to better target the second modality, for example, in circumstances where the location of focal seizures have been approximated by EEG and a NIR imaging system can be applied to the area of interest, as performed by Gallagher et al. (2008). An extension of this approach is to restrain the solutions of the inverse imaging problem of one modality using the spatial information provided by another. An example would be the use of BOLD-fMRI clusters to restrain the solutions to the EEG source localisation problem in studies using EEG-fMRI (Lui et al. 2006). Similar approaches should be possible using an EEG-NIR imaging method.

The full, symmetrical integration of two different imaging modalities requires the inversion of a forward model which encapsulates the signal

observed by both modalities, and how these signals are related. In the case of EEG-NIR imaging and EEG-fMRI, this requires a detailed model of neurovascular coupling mechanisms. The hierarchy of data fusion models in the context of EEG-fMRI are reviewed by Vuillemoz et al. 2010.

As mentioned previously, the reasons why NIR techniques have continued to thrive, despite the prevalence of fMRI (portability, cost, ease of application, suitability to vulnerable subject groups and the significant ability to resolve changes in particular chromophores) will also support the use of EEG-NIR techniques in a field where EEG-fMRI is commonplace. No discussion of the benefits of a combined NIR and EEG technique would be therefore be complete without a brief discussion of the successes and limitations of EEG-fMRI. This is included in section 1.3.5.

1.3.3 Applications

1.3.3.1 Neurovascular coupling

The relationship between neuronal activity and the localised vascular response is of incredible importance to functional brain imaging. How neuronal activation results in an increased metabolic demand and how this in turn affects haemodynamics is a very complex issue, and though various models have been proposed, there are still many aspects which are poorly understood (Sheth et al. 2004, Attwell and Iadecola 2002). High density, simultaneous EEG and NIR imaging would allow the precise temporal and spatial relationship between neuronal firing and the localised vascular response to be observed in-vivo in a manner similar to studies performed with EEG-fMRI (see Arthurs et al. 2000), but with the important advantage of being able to explicitly measure change in oxy and deoxyhaemoglobin concentrations.

How neurovascular coupling is affected by certain metabolic, cognitive and vascular disorders is also of great importance. It is known that vasodilation can be affected by hypertension, diabetes and Alzheimer's disease (D'Esposito et al. 2003, Iadecola 2004). An understanding of alterations to neurovascular coupling in such conditions could potentially lead to new methods of diagnosis and new methods of treatment and assessment.

1.3.3.2 Functional activation

The use of ERP methods to study healthy brain function is very well established but does have severe limitations, particularly in localisation of functional activity. Although fMRI is rightly considered to be the gold standard of functional image techniques (at least in terms of spatial resolution), there are certain subject groups (particularly children with developmental disorders) which are not well suited to large scale EEG-fMRI studies. The spatial localisation provided by a combined EEG and NIR imaging system would allow previous ERP studies to be extended to

specify exactly where in the brain certain processes are being performed, a question which remains unanswered for many functional processes, particularly in infants.

There is also the important question of whether neurovascular coupling itself varies with the type of functional activation. Neurovascular coupling will vary with location in the brain because of the differences in cerebral vasculature, but whether the response to a given neuronal metabolic demand varies with task and what this would tell us about brain function is not yet understood.

1.3.3.3 Epilepsy and seizures

As the study of epileptic disorders and seizures is the single most important clinical application of EEG, it will also be a dominant application of any combined EEG and NIR imaging system. The exact changes in haemodynamics related to seizure events are still the subject of active research (see sections 1.3.3 and 1.3.4), and as one would expect are variable across subjects, age groups and seizure type. Partial seizures (particularly in the temporal lobes) have long been the subject of PET and SPECT imaging studies (Casse et al. 2002, la Fougère et al. 2009), which routinely show that ictal events are associated with a localised increase in cerebral blood flow and increased glucose uptake (hypermetabolism). By measuring the same ictal increase in regional cerebral blood flow, studies have already shown that NIR imaging can provide good quality seizure focus localisation (see section 1.3.3).

As well as the ability to localise partial seizure focus, we hope that a combined system will have several other significant benefits. First, it will provide a simple method of studying the haemodynamics associated with seizures, how they differ from those of functional activation and how they vary with subject and what this could potentially mean for diagnosis and treatment. These applications are well aligned to those of EEG-fMRI,

though the limited sensitivity of combined EEG-NIR techniques to movement artifacts and their ability to applied at the bed side may prove significant, particularly in the study of ictal (as opposed to inter-ictal) epileptic events and those which manifest themselves clinically.

Second we believe it is possible that a combined system would provide a greater rate of neonatal seizure diagnosis, particularly if simultaneous EEG and whole-head optical tomography are performed. In this scenario the whole volume of the brain could be interrogated which would potentially allow seizures originating in sub-cortical regions of the brain (which would likely be invisible to EEG) be observed and studied. There is also potentially an application of a combined system to assess the suitability and effectiveness of the medication prescribed to seizure patients, and how such medications affect cerebral haemodynamics.

1.3.4 A Review of Previous Combined EEG and NIR Studies

There are already a good number of studies which have looked to take advantage of the complementary information available using combined EEG and NIR methods. These include examples from many different research areas, including studies of visual cortex activation, the relation between background electrophysiological and haemodynamic activity and a number of studies relating to epileptic seizures in adults and children.

Although in the following passage the most relevant of these studies will be described in terms of their research application, it is worth noting that they can also be arranged into three distinct categories on the basis of their protocol. There are those which use multi-channel EEG with single-site NIRS, those which have performed optical topography with a limited arrangement of EEG electrodes and finally a limited number which have used multi-channel NIRS and EEG arranged over the same area of the scalp. At the time of writing and with the exception of the work presented here, no-one has yet performed full clinical EEG and optical topography over the same cortical area in either adults or infants.

The first NIRS system became commercially available in 1986, with smaller, more advanced and more popular versions being released subsequently. As single-channel NIRS is easy to apply in conjunction with EEG, many combined NIRS-EEG experiments have been performed. A large proportion of combined EEG and NIR studies have focussed on the diagnosis, treatment and understanding of epileptic disorders. One of the earliest of these was a pilot study of the use of NIRS in the lateralisation of temporal lobe epilepsy (Steinhoff et al. 1996). Though there had been earlier assessments of the use of NIRS in the study of seizures, EEG had not been performed simultaneously and seizures were diagnosed using clinical observation (Villringer et al. 1994). In a pre-surgical evaluation of two patients suffering from intractable temporal lobe epilepsy, Steinhoff et al. concluded that NIRS had the potential to provide a simple and effective

method of lateralising the primary source of seizures in adults. This study used single-site NIRS located on alternating sides of the frontal cortex to observe a lateralised increase in oxygen saturation associated with seizures.

Between 1997 and 2000, Watanabe et al. successfully employed combined EEG and multi-channel NIRS or optical topography in a study of 28 patients exhibiting partial seizures (Watanabe et al. 2000, 2002). The ability of combined scalp EEG and NIR techniques to correctly lateralise seizure focus were compared to that of SPECT using invasive intracranial EEG as a benchmark. These studies found that EEG-informed NIR techniques successfully lateralised 96% of seizure foci and presented evidence that an observable haemodynamic shift (most commonly consisting of a large, slow increase in regional cerebral blood volume) may occur during subclinical seizures and even prior to seizure onset in some cases. The use of the Hitachi 1010 24-channel optical topography system allowed the production of rudimentary, interpolated maps of changes in haemoglobin concentration, but prevented EEG from being performed over the same area of the scalp. In 2002, Haginoya et al. performed an EEG-NIRS study of 15 children, ranging in age from 1.5 months to 16 years, with various forms of epilepsy. In this study ictal haemodynamic responses were observed consistently, and although the form of these responses varied with the type of epileptic seizure, the most common observation was an ictal increase in HbO_2 and HHb concentrations which persisted beyond the cessation of electro-clinical symptoms. The use of EEG-informed NIR techniques to localise epileptogenic foci has continued and in 2008 Gallagher et al. published a single-subject case study briefly comparing the localisation provided by optical topography with that of SPECT, PET, fMRI, MEG and EEG.

Although their methods allowed only interpolated maps of haemoglobin concentration to be produced, the optical topography results were in agreement with those of all other modalities, though no quantification of the accuracy of localisation was presented. The haemodynamic response was

found to consist of a significant increase in localised oxyhaemoglobin concentration with was sustained beyond the end of the seizure and a smaller, delayed decrease in deoxyhaemoglobin, for both clinical and subclinical seizures.

In 2004 Buchheim et al. performed NIRS and video-EEG in the study of absence seizures in adults and reported a reproducible decrease in oxy and increase in deoxy-haemoglobin consistent with a reduction in cerebral blood flow. A similar result was obtained by Roche-Labarbe et al. in 2008 in a

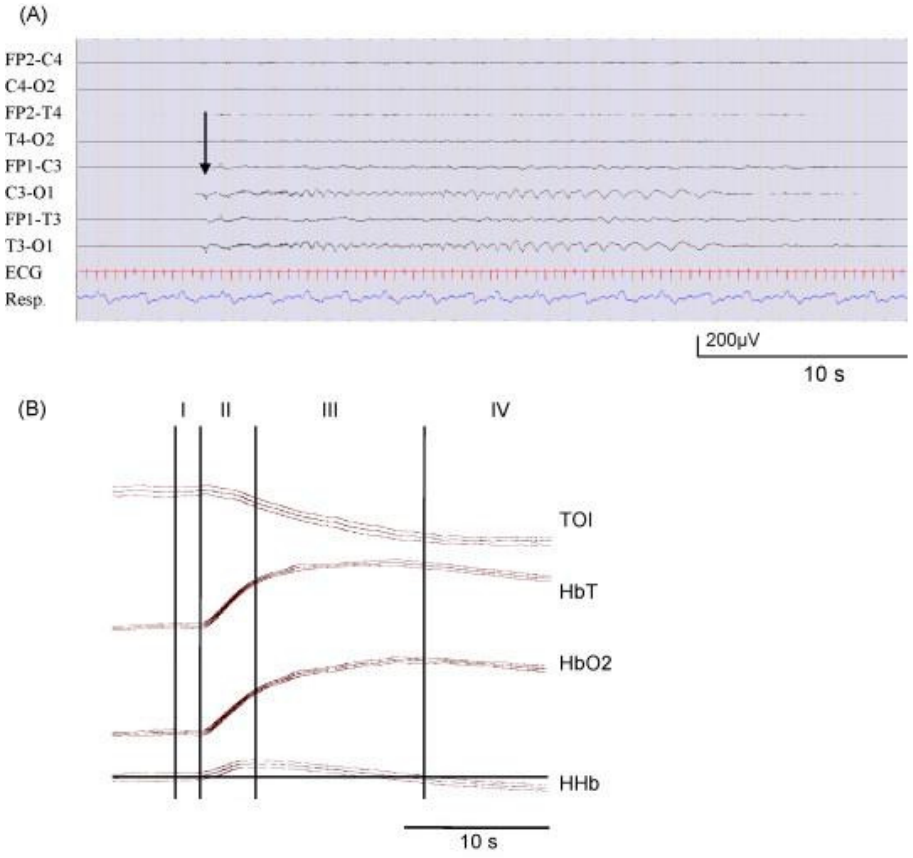

Figure 1.3.1. 'Seizure-like' activity as recorded by EEG is shown in (A). The haemodynamic response to this event, for several channels is shown in (B). The first vertical line represents the start of the seizure-like discharge, the second marks the start of HbO2 increase, the third line is related to EEG power (not shown) and the fourth gives the intercept of HHb concentration. Note that no scale was provided (Wallois et al. 2009).

study of absence epilepsy in children, though their paper also describes an initial increase and decrease in HbO_2 and HHb respectively, beginning 2-10 seconds prior to the spike and wave EEG activity associated with absence seizures. A preliminary study has also used combined EEG-NIRS as a method of assessing the effectiveness of anti-epileptic medication in an infant exhibiting status epilepticus with little clinical manifestation (Diaz et al. 2006).

In late 2009, Wallois et. al performed the first simultaneous EEG and NIRS study of 'seizure-like' activity in a single, critically ill neonate. This experiment was designed to allow the study of the interaction between neonatal epileptic discharges and haemodynamic variations in circumstances where (due to ventilation and the administration of muscle relaxants) there were no cardiorespiratory variations or clinical symptoms. This would allow the cerebrovascular response to seizure activity to be isolated, without the secondary interference of changes in respiration, heart rate or cerebral blood flow due to seizure-induced movements. This paper suggested that 'seizure-like' discharges result in an increase in oxyhaemoglobin and deoxyhaemoglobin concentration over a period of a minute or greater followed by a return to baseline and an under-shoot in deoxyhaemoglobin concentration (see figure 1.3.1).

It is also important to mention that there has recently been an explicit examination of the need for a combined NIR and EEG system for neonatal monitoring, with Toet and Lemmers (2009) concluding that a combination of EEG and NIRS will probably become the future of neonatal monitoring.

Simultaneous EEG and NIR techniques have also been used for many non-clinical applications, particularly to study the neurovascular coupling of cognitive function. In 2001, Kennan et al. were the first to perform a simultaneous optical topography and ERP study. Using an auditory odd-ball stimulus an ERP and a localised haemodynamic response (consistent

with previous fMRI studies (Bénar et al. 2007)) were successfully observed. Horovitz and Gore (2004) explored the use of combined ERP and optical topography to study semantic processing and concluded that such a combined system is suitable for the study of language function. Combined EEG and NIR techniques have also been used in several studies exploring the link between electro-cortical activity and cerebral haemodynamics in relation to sleep (Roche-Labarbe et al. 2007, Uchida-Ota et al. 2008) and in relation to functional activation of the visual cortex (Obrig et al. 2002, Koch et al. 2006 and 2008, Näsi et al. 2010). In their studies of neuro-vascular coupling in the visual cortex, Koch et al. (2006) described certain discrepancies between the maximal electro-cortical and haemodynamic responses in relation to visual stimulus frequency. It is important to note that Koch et al. are the only group to have performed EEG/ERP and multi-channel NIRS over the same cortical area. This arrangement was possible because of the use of an integrated electrode cap containing ring-electrodes allowing the necessary optical fibres to contact the scalp through the ring.

1.3.5 EEG-fMRI

Despite their vastly different approaches, functional magnetic resonance imaging and near infrared imaging are inherently similar techniques. As described previously, it is changes in localised cerebral blood flow that provide the source of both fMRI and NIR imaging signals. The current resolutions of these imaging techniques are also of a similar order. (Though it is likely that both will improve as technologies develop, particularly fMRI, which is spatially limited only by signal-to-noise ratio, whereas diffuse optics which always be somewhat limited by the scattering properties of tissue (Logothetis 2008)).

The dual modality approaches of EEG-fMRI and EEG-NIR are therefore also closely related. The number of studies performed using EEG-fMRI is vast, and a thorough review is not provided here. A brief introduction to the technique is included below, in order to highlight its successes and limitations and the variety of potential applications of EEG-NIR. The ongoing success of EEG-fMRI should be considered a reason to pursue EEG-NIR techniques, rather than as a reason to abandon them.

EEG-fMRI has several inherent compatibility issues which make it a difficult technique to perfect. Electromagnetic induction requires that a non-zero rate of change of magnetic flux through a closed, conducting path will induce a current to flow around that path. The recording of EEG in the static and time-varying magnetic fields of an fMRI system introduces two forms of EEG artifact: one due to movements of the subject and electrodes in the static magnetic field (which are apparent even in a subject who remains still, as movements due to the cardiac pulse result in what is known as the ballistocardiogram artifact) and one due to the necessary variations of the magnetic field gradients during MRI imaging sequences. Radio-frequency emissions from EEG recording apparatus also have the potential to affect fMRI image quality.

However, these difficulties have largely been overcome. Initially techniques were pursued where recording of EEG and fMRI were sequential, and timed in a manner which minimised the importance of artifact-corrupted data (e.g. Warach et al. 1996). More sophisticated inter-leaved acquisition designs, which approach simultaneity, are still in use, but EEG post-processing and synchronisation methods have been successfully developed which remove (or at least minimise) ballistocardiogram and imaging EEG artifacts and allow truly simultaneous and continuous EEG-fMRI (Allen et al. 2000, Lemieux et al. 2001, Bonmassar et al. 2002, Salek-Haddadi et al. 2003a, Mandelkow et al. 2006). However, despite these advances, movement is still a serious problem. Movement of the subject will produce EEG artifacts which, as they are less predictable than either ballistocardiogram or imaging artifacts, are difficult to remove. In addition movement of the head by as little as a few millimetres over the course of fMRI acquisition can corrupt the resulting images to the point of rejection (Gotman et al. 2006).

The vast majority of EEG-fMRI studies performed to date can be broadly grouped into three: those which have investigated functional, stimulus-related cerebral activation, those which have sought to elucidate the relationship between resting state electro-cortical activity and cerebral blood flow, and studies of the localisation and haemodynamics of ictal and inter-ictal epileptic discharges.

Early paradigms based on sequentially obtained EEG and fMRI data sets were performed in order to study various aspects of brain function, including visual processing (Linden et al. 1999), visual-spatial attention (Mangun et al. 1998, Noesselt et al. 2002, Di Russo et al. 2003), somatosensory stimulation (Grimm et al. 1998) and movement-related cortical potentials (Toma et al. 2002). Simultaneous and quasi-simultaneous methods are continuing to develop, and have been used to study auditory and visual evoked responses (Bonmassar et al. 1999, Scarff

et al. 2004, Bénar et al. 2007, Mayhew et al. 2010) and to compare and combine fMRI acquisition with EEG source localisation using both visual evoked potentials (Bonmassar et al. 2001) and somatosensory stimulation (Thees et al. 2003). Bonmassar et al. used fMRI imaging data to constrain EEG source localisation methods, an approach which could well be applied to EEG-NIR. Though there remains some debate as to how precisely EEG and BOLD signals can be assumed to result from the same neuronal activity (Nunez and Silberstein 2000, Ritter and Villringer 2006, Rosa et al. 2009), which is ultimately a question of neurovascular coupling.

The study of resting-state cerebral haemodynamics poses some particular problems for fMRI, as conventional fMRI imaging procedures are heavily dependent on paradigms with distinct periods of rest and activation, in order that statistical hypothesis testing can isolate the event-related signal contribution (Salek-Haddadi et al. 2003b). Despite these issues, EEG-fMRI has been used extensively to study the BOLD fluctuations associated with background EEG rhythms (Goldman et al. 2002, Laufs et al. 2003, de Munck et al. 2007, Laufs 2008) and with sleep (Kaufmann et al. 2006, Horovitz et al. 2007).

It is in the study of epileptic disorders that EEG-fMRI has proved most successful. In general, this research has sought to either provide a method of localising the focus of partial seizures, or to characterise the relationship between epileptic electro-cortical activity and the haemodynamic response, in both partial and general epilepsies. The majority of these studies have dealt with inter-ictal discharges, as seizures themselves are impossible to predict and rarely occur during scanning. Again, the number of significant findings is too great to list, and only an overview is given here, excellent reviews are provided by Gotman (2006 and 2008) and Vuillemoz et al. 2010.

In studies of partial seizures, the time-locking of fMRI acquisition to EEG-recorded inter-ictal spike discharges has been repeatedly shown to produce images of seizure focus (as defined by various standards, including EEG source localisation, inter-cranial EEG and structural MRI (in the case of lesional epilepsy)). However, both the reliability and form of the BOLD response to inter-ictal discharges have proved variable (Krakow et al. 1999, Krakow et al. 2001, Jager et al. 2002, Al-Asmi et al. 2003, Kobayashi et al. 2006, Salek-Haddadi et al. 2006, Thornton et al. 2009). There have also been a limited number of examples of fMRI images acquired in response to ictal epileptic events. Salek-Haddadi et al. (2002) were the first to detect a BOLD signal in response to a focal electrographic seizure. This study showed a biphasic pattern lasting ~100 seconds in response to a 41 second partial seizure. The BOLD response consisted of an initial increase which continued for several seconds after the end of the electrographic seizure, then a subsequent decrease in BOLD signal and a return to baseline. Interestingly, this single dataset suggested that the BOLD changes may actually precede the EEG-defined seizure onset, a feature which has since been pursued in relation to inter-ictal epileptic spikes (Hawco et al. 2007). Tyvaert et al. (2008) recorded ictal events in 8 patients with malformations of cortical development (MCDs) and found examples of both positive BOLD (referred to as activation) and negative BOLD (deactivation).

Studies of inter-ictal and ictal generalised epileptic discharges (commonly spike-wave discharges associated with absence seizures) have consistently shown activation of the thalamus and predominant deactivation of cortical regions. These results have begun to further elucidate the known role of thalamo-cortical interactions in the lapse in patient responsiveness characteristic of absence seizures (Salek-Haddadi et al. 2003c, Gotman et al. 2005, Hamandi et al. 2006). This negative cortical BOLD response associated with absence seizures is consistent with the increase in deoxyhaemoglobin concentration found in the limited number of EEG-

correlated NIRS studies of spike-wave activity in adults and children (Buchheim et al. 2004, Roche-Labarbe et al. 2008).

Chapter 2

2.1 Dual Modality Probe Design and Evaluation

2.1.1 Design Considerations

To allow simultaneous EEG and NIR imaging to be performed over the same cortical area in a versatile and easily applicable manner, it is first necessary to consider how to couple optical fibres and EEG electrodes to the scalp of a subject. The applications of simultaneous EEG and NIR techniques described in this work are primarily clinical, i.e. the bed-side study of electro-cortical and haemodynamic activity and their interaction in relation to functional activation and neonatal seizures. Clinical EEG is almost always performed using disposable Ag/AgCl electrodes which are affixed to the scalp using a conductive paste and a small amount of adhesive tape. The area to which they are attached is prepared using alcohol wipes and an abrasive paste. This method is widely used because it consistently produces a very good electrical contact, which is of the utmost importance in the electrically noisy environment of the hospital ward. Integrated, whole-head EEG nets and caps have struggled to gain acceptance in clinical application because of the difficulty of achieving a good electrical contact and because of the versatility of application which is required in a hospital environment. For these reasons and because of the nature of the EEG systems which will be used in forthcoming experiments, it was decided that we should aim to produce an application method which closely mimics that currently used in clinical EEG. We also did not wish to have to significantly re-design the optical fibre bundles which are used to carry light to and from the head of the subject, as these are already optimised for optical topography. By remaining as true as possible to pre-existing methodologies, it was also likely that design errors would be minimised.

2.1.2 The Opto-Electrode Probe Design and Preliminary Testing

In order to pursue clinical application of simultaneous EEG and NIR imaging, and particularly in order to study neonatal seizures, it was necessary to design an opto-electrode which a) can be used in conjunction with standard EEG systems, b) was as simple to apply as standard EEG electrodes, and c) occupied the minimum possible area of the scalp. As described in chapter 2, clinical EEG systems typically use Ag/AgCl electrode cups, coupled to the scalp using a conductive paste or gel.

The design shown in figure 2.1.1 makes use of a standard Ag/AgCl electrode cup, and allows the normal method of site preparation and use of a

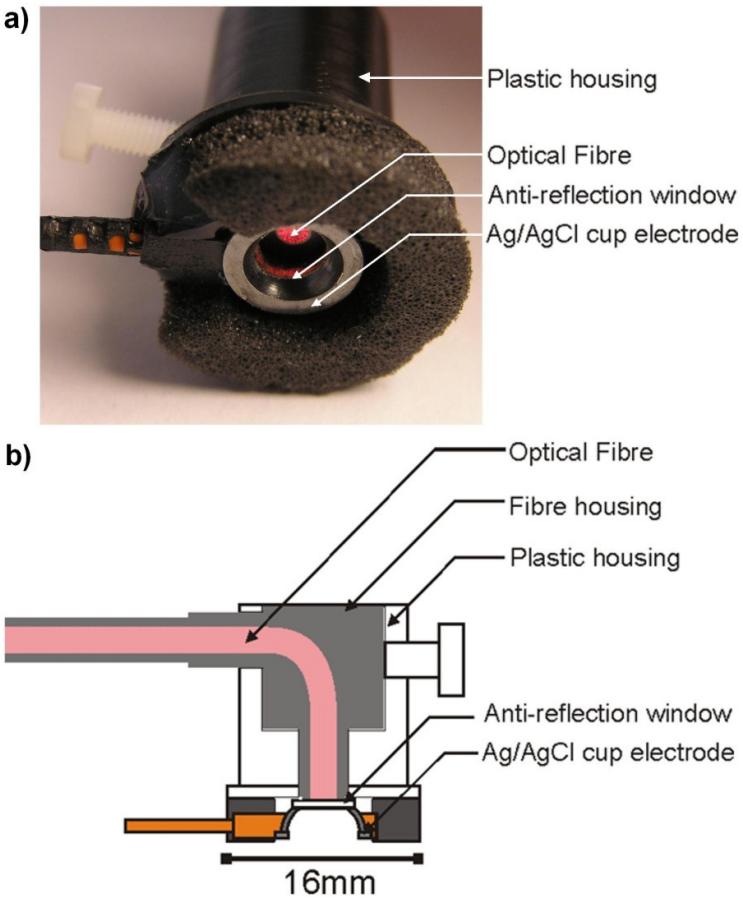

Figure 2.1.1. The opto-electrode probe design. Both a photograph (a) and a schematic (b) are provided.

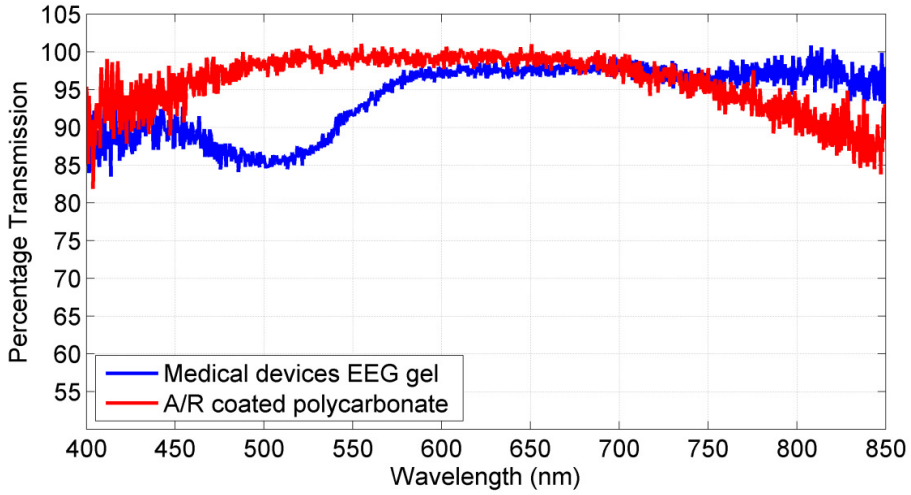

Figure 2.1.2. The transmission spectra of 1 cm of Medical Devices EEG gel (in blue) and the 1 mm thick anti-reflection coated polycarbonate (in red).

contact gel to be maintained. It also minimises the area of scalp which is occupied (which increases the possible sampling density) and, by co-locating the electrode and the optical fibre, allows for optimal co-registration of the two modalities. A standard electrode (Micromed Electronics Ltd., Italy) is modified so that the ceiling of the cup is replaced with a 4.5 mm diameter anti-reflection coated polycarbonate (VisionTek Systems Ltd., UK) window. The electrode is then fixed to a plastic housing, which holds the optical fibre bundle directly behind the polycarbonate window. When the opto-electrode is applied, the electrode cup must be filled with an electrical contact gel, as is typical in clinical application. As this design places the contact gel in the optical path, it is necessary to use a contact gel which exhibits a minimal absorption of NIR light. One particular commercially available EEG contact gel (Et Medical Devices SPA, Italy) is well suited to this task.

It is clearly possible to employ a similar arrangement of optical fibre and electrode and perform simultaneous EEG and NIR imaging without the use of a window. However, because the fibres must be removable and are typically very expensive, we believe the window is vital in order to protect

the optical fibre from repeated applications of electrode contact gel and to make the probe easier to clean and re-apply. The transmission spectra of the polycarbonate window and Medical Devices EEG contact gel are shown in figure 2.1.2, each was measured using a PC linked, white light source spectrometer (Ocean Optics, Inc., USA). During the acquisition of the transmission spectrum the Medical Devices EEG contact gel was held in a cuvette cell measuring 1 cm across.

2.1.2.1 Electrical contact

As a stable and low-impedance electrical contact is necessary to perform EEG, it was important that the electrical contact properties of the opto-electrode design were explicitly tested in vivo. Two opto-electrodes were placed 38 mm apart, on the forehead of an adult volunteer, spanning the midline just above the hairline. The contact site was carefully abraded prior to application using NuPrep abrasive paste (Weaver and Co., USA) and cleaned with a disposable alcohol wipe. A small quantity of Medical Devices EEG contact gel was placed within the electrode cup of each of the two probes, which were then held in place by light bandaging. The contact impedance across these two opto-electrodes was then measured at 10 Hz using an impedance meter (Checktrode, UFI corp., USA). Ten repetitions of this measurement at different contact sites around the frontal region of the head resulted in a mean contact impedance of 3.8 kΩ (standard deviation of 1.3 kΩ), below the clinical benchmark of 5 kΩ. The maximum recorded impedance was 5.8 kΩ. This result provides explicit proof that alterations to the electrode and the presence of the polycarbonate window do not prevent a good quality electrical contact being achieved.

2.1.2.2 Optical attenuation

As the opto-electrode design places the polycarbonate window and the electrode contact gel in the optical path, it is clearly necessary to assess how the intensity of light measured between source opto-electrodes and detector

opto-electrodes is affected. Although we have previously measured the transmission spectra of the polycarbonate and the chosen contact gel, there are additional affects such as collimation and surface reflection which need to be accounted for. In order to measure the optical attenuation due to the opto-electrode design a single-channel NIR experiment was performed on a solid, tissue-mimicking phantom (Firbank et al. 1995), with an absorption coefficient of 0.01 mm^{-1} and a reduced scattering coefficient of 1 mm^{-1}.

Ten measurements of intensity at 670 nm and 850 nm were taken using the UCL OT system (see section 2.1.4) with a pair of clinical opto-electrodes separated by 25 mm acting as source and detector. Between each measurement, the probes were removed and cleaned before being re-applied over a different region of the phantom surface. To provide a control, this experiment was repeated with two standard optodes holding the same source and detector optical fibre bundles. Standard optodes consist of a plastic housing which holds the optical fibre bundle in place. They are identical to the opto-electrode design of figure 2.1.1 but without the addition of the electrode and polycarbonate window. In order to provide a best-case measure of the intensity of the recorded light between source and detector (and thus a worse-case measure of the light loss due to our opto-electrode design) the optical fibre bundles were positioned so that their terminus was in direct contact with the phantom surface. This corresponds to the highest intensity arrangement of source and detector. However, it is worth noting that in practice the fibre bundles are often retracted slightly (by up to 5 mm) from the surface, as anecdotal evidence has shown that this can minimise the attenuation effect of hair between the fibre bundle and the scalp.

The result of this preliminary measure was that the opto-electrode arrangement recorded an average (and standard deviation) intensity equal to 54.5 (7.5) % and 46.3 (6.9) % that of the control arrangement at 670 nm and 850 nm respectively. Although this upper limit represents a significant attenuation, it is not enough to affect the usefulness of the design. The UCL

OT system allows the intensity of each source output to be adjusted as required. It is often necessary to keep the source output well below its maximum in order to prevent detector saturation, particularly with recent improvements to the efficiency of the optical fibre bundles. There is therefore some headroom with respect to the amount of light that can be lost in transmission without affecting the viability of the system. Though in-vivo testing is obviously necessary, in this phantom arrangement, despite the extra losses due to the opto-electrodes, it was still necessary to set the sources below their maximum output (which is, in turn, well below safety limits) in order to prevent saturation of the detector.

2.1.2.3 Movement artifact

A further important characteristic of the opto-electrode is how its design affects the susceptibility of NIR recording to movement artifact. It was necessary to investigate whether the presence of the electrode between the optical fibre and the target object would cause movement to have a greater effect on measured NIR intensity. Typically, the effect of movement artifact is difficult to quantify because it is hard to find a method which produces a consistent, reproducible artifact. However, an attempt was made to quantify the susceptibility of the probe to movement artifact using a pendulum. Movement artifact is caused by relative movement between the optical fibres and the object being investigated, which alters the optical path between source and detector. By attaching a small pendulum to the array which holds the opto-electrodes, reproducible movements of the array relative to the target object can be produced. The amplitude of a pendulum swing can be easily controlled and its constant oscillation frequency allows an experiment to be performed numerous times and the results averaged, as individual recordings can be shifted so as to be in phase with one another. The amplitude of the average oscillation in intensity caused by the swinging of a pendulum attached to the opto-electrode array will thus provide a measure of how vulnerable the arrangement is to movement artifact.

Such an experiment was performed using a single source and detector pair coupled to a solid, tissue-mimicking phantom using light bandaging. The bandaging was removed and re-attached for each individual measurement. The phantom has a reduced scattering coefficient of 1 mm^{-1} and an

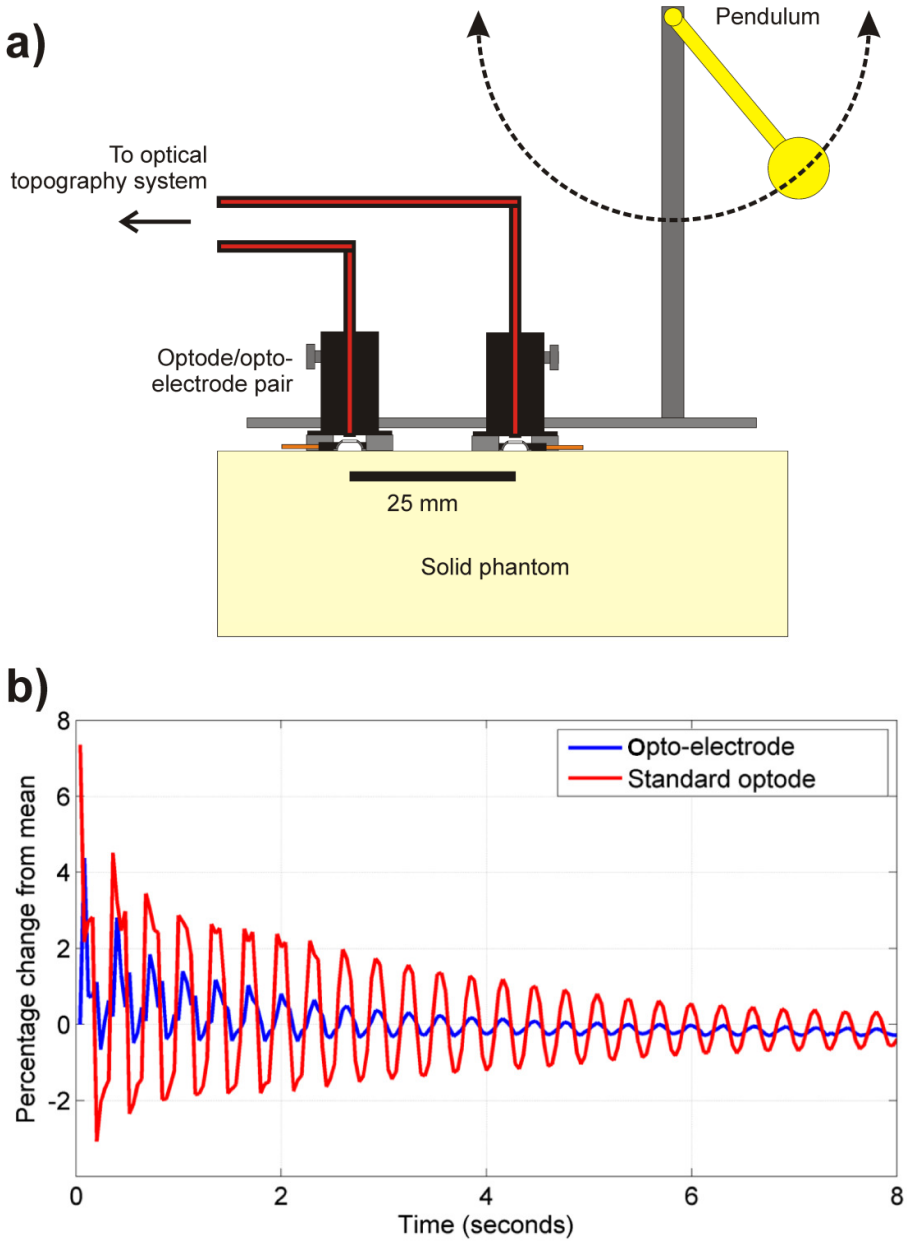

Figure 2.1.3. An illustration of the experimental arrangement is shown in a) whilst the mean percentage shift in intensity resulting from pendulum-induced movement artefact for the clinical opto-electrode and a standard optode arrangement is shown in b).

absorption coefficient of 0.01 mm^{-1}. The experiment was performed using a pair of our clinical opto-electrode probes and with a pair of standard, optical-fibre-only probes so a direct comparison could be made. Five measurements each were performed for the opto-electrode and control arrangements. In each measurement, the pendulum was held at the top of its arc and released. Single-channel NIR data were obtained using the UCL Optical Topography System until the pendulum had come to a complete stop. The arrangement is shown in figure 2.1.3a.

Each measurement was converted to a fractional change from a baseline intensity (taken as the average of 10 seconds recorded prior to pendulum swing) and the time-course of each was shifted so that the first maximum of all five measurements for the opto-electrode and control arrangements were exactly in phase prior to a mean being calculated. The result of this process is shown in figure 2.1.3b. Both the value of the maximum intensity shifts (i.e. the perturbation caused to the optical recording when the pendulum reached its extremed) and the rate of damping of the intensity oscillation suggest that the opto-electrode design is actually less susceptible to movement artifacts. The average (and standard deviation) intensity change, at the peak of each pendulum swing for the opto-electrode design is 38 (11.8) % of that recorded using the standard optode arrangement. It is likely that this additional robustness is due to the presence of the electrode coupling gel and the additional rigidity provided by the electrode itself.

2.1.3 Dual-Modality Liquid Phantom Experiment

In the development of a new medical imaging technique, it is common to test the system by applying it in the laboratory to an object which mimics the properties of in-vivo tissue. In NIR imaging, these phantoms are built to have a reduced scattering coefficient and an absorption coefficient similar to that of bulk tissue. Optical imaging phantoms will usually contain a target with a different absorption coefficient to the rest of the phantom. This target is then either moved, or made to exhibit a change in optical properties so that NIR imaging of the change can be performed. EEG phantoms have also been built (Leahy et al. 1998), and are most commonly used to test the accuracy of dipole source localisation, which is a method of localising neuronal activity by modelling the field it produces on that of a current dipole. EEG phantoms usually consist of a head-shaped object with an electrical conductance equivalent to that of tissue, sometimes with additional layers to mimic the scalp and skull. Within the phantom body will be one or more current dipoles which produce a varying electric field and provide the source of the electrical activity which can be measured via EEG electrodes at the surface of the phantom. The position of the source dipole as calculated from the surface EEG data can then be compared with the actual known position and amplitude of the current dipole.

The previous section described the preliminary evaluation of our opto-electode design. However, more rigorous testing of the design was necessary before it could be applied in a clinical environment. To that end, we designed and performed a series of dual modality phantom experiments. These experiments were performed not only to test our probe design, but also as an investigation of the construction of dual-modality EEG and optical imaging phantoms in general. We believe that the ability to construct increasingly complex and realistic dual-modality phantoms may be of use in the development of methods to optimise the integration of EEG and optical imaging data. Our first phantom design used an optically turbid and electrically conducting liquid and is described below.

2.1.3.1 Liquid phantom construction

Construction of a dual-modality EEG and optical imaging phantom requires the integration of the pre-existing phantom methodologies of each imaging modality. The target body must contain a current dipole, but also provide contrast for NIR imaging. The whole body of the phantom should optically mimic tissue, but also be electrically conductive. The simplest way to meet these requirements was to build a liquid phantom, as suitable optical scattering, optical absorption and electrical conductivity can be achieved by the addition of a scattering emulsion, an absorbing dye and sodium chloride to water. A current dipole was embedded within a polyester resin cylinder with a known optical absorption which is higher than average bulk tissue. This cylinder would thus provide 'contrast' for both modalities when moved within the liquid phantom. The liquid phantom is shown in figure 2.1.4.

A plastic tank of approximate dimensions 240 × 160 × 120 mm was used to contain a solution of 1 % Intralipid® emulsion (which provides a reduced scattering coefficient of 1 mm^{-1} (Flock et al. 1992)), a NIR absorbing dye (S109564 ICI Ltd.) (which provides an absorption coefficient of 0.01 mm^{-1} at 800 nm) and 0.2 % sodium chloride which provides a conductance similar to that of brain tissue (Tidswell et al. 2001). The target cylinder had a height of 20 mm and a diameter 20 mm and the same optical scattering properties as the solution, but with an absorption coefficient of 0.04 mm^{-1} at 800 nm. The current dipole embedded in the target cylinder consisted of two Ag/AgCl pellet electrodes, 2 mm in length and set 5.5 mm apart. The pellet electrodes were coupled to the positive and common terminals of an 11 Hz sine-wave generator (a frequency chosen to mimic adult alpha wave) so as to provide a current dipole moment of 10 μA mm. This current dipole moment was found to provide a maximum electrical p.d. oscillation amplitude of around 20 μV as measured at the surface of the liquid, equivalent in amplitude to in-vivo EEG signals. The target cylinder

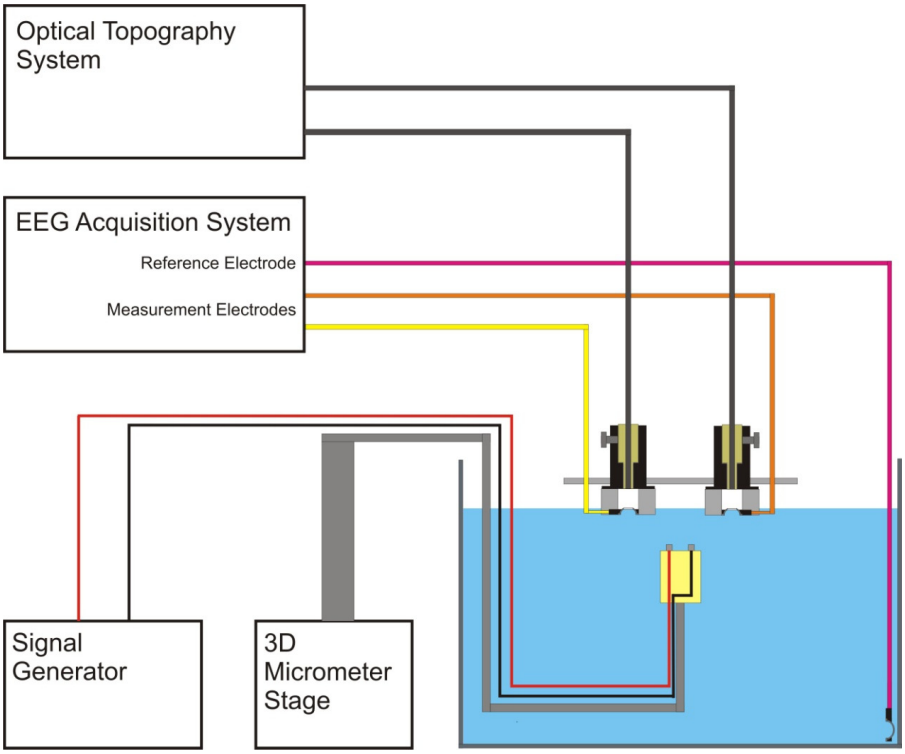

Figure 2.1.4. The dual-modality liquid phantom arrangement.

was suspended in the solution using an electrically insulated arm connected to a three-axis micrometer stage, allowing the target cylinder's position to be precisely controlled.

An array containing 8 opto-electrodes, arranged in a simple 2 × 4 grid, providing ten viable source-detector pairs at each wavelength was suspended at the surface of the liquid phantom such that all 8 electrodes were submerged and no air gaps remained between the liquid and the polycarbonate window. The opto-electrode array is shown in figures 2.1.5a and 2.1.6a.

2.1.3.2 Experimental Methods

Optical data were recorded using the University College London Optical Topography System, (Everdell et al. 2005). This system can employ up to 32 laser diode sources (16 at 770 nm (or 670 nm depending on the version) and 16 at 850 nm) and 16 avalanche photodiode detectors. All sources are illuminated simultaneously, with each modulated at a different frequency which allows a Fourier transform of the diffusely reflected intensity measured at each detector to isolate the contribution from each source. Optical images were reconstructed using the linear reconstruction methods described in section 1.2.3.

EEG recording was performed using a Grass-Telefactor H2O 32-channel EEG system, which has a sample rate of 400 Hz, and a PC interface running the EEG Twin 2.6 acquisition software package (Grass Technologies, AstroMed inc.). Data were recorded over the range 1-70 Hz with no filters applied. Data were exported in a raw format and processed offline using Matlab (The Mathworks Inc.).

The target cylinder was positioned at a depth suitable for imaging via optical topography, extending from between approximately 4 to 24 mm beneath the opto-electrode array. The cylinder was then translated along the path dissecting the short axis of the array in 5 mm steps, with 10 seconds of optical topography and EEG data recorded at each position. A further 10 second set of optical data was recorded with the target absent from the liquid phantom tank in order to provide a reference measurement for difference image reconstruction. Note that the signal at each EEG electrode was recorded relative to a common reference electrode placed in the bottom corner of the phantom tank. The impedance of each EEG channel was measured at the start of the experiment and all were found to be below 1 kΩ.

Figure 2.1.5

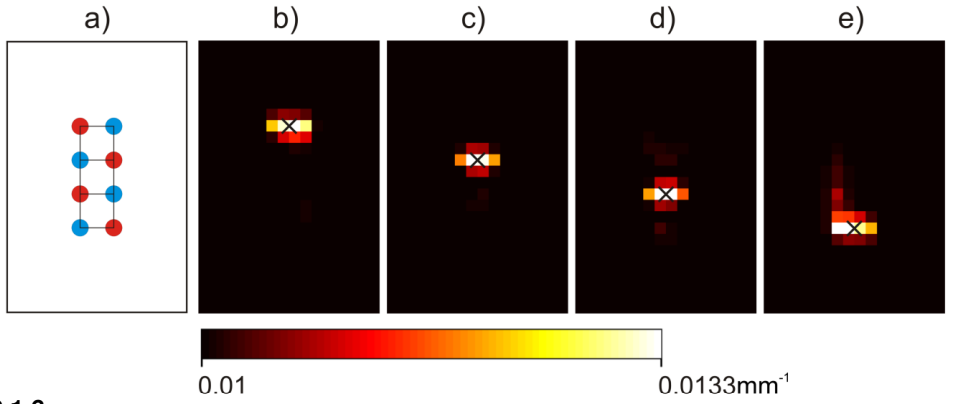

Figure 2.1.6

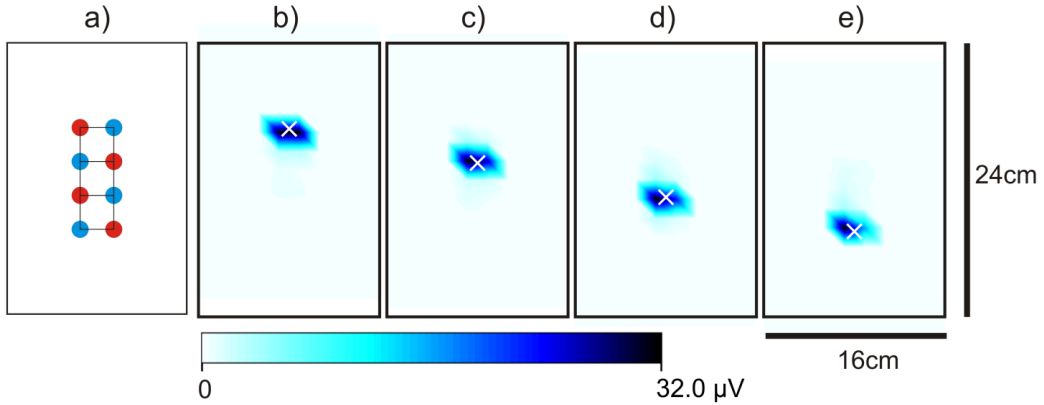

Figures 2.1.5 and 2.1.6. Figures 2.1.5a and 2.1.6a show the 8-point opto-electrode array, where red circles correspond to sources and blue circles to detectors. Figures 2.1.5 b–e are the reconstructed images of changes in optical absorption at 850 nm in the dual-modality liquid phantom for four target positions, scaled to the maximum range across all four images and viewed from above. The black cross denotes the actual position of the optically absorbing, current-dipole target. Figures 2.1.6 b-e are interpolated representations of the simultaneously recorded EEG data for the same four target positions.

2.1.3.3 Results

Figures 2.1.5b to 2.1.5e show the reconstructed images of the change in optical absorption coefficient as measured at 850 nm for four positions of the target cylinder at a depth of 10 to 20 mm. The mean (and standard deviation) two-dimensional error between the peak reconstructed change in optical absorption and the actual target centre was found to be 3.8 (1.9) mm. Note that the scale of these absorption changes significantly underestimates the size of the change in optical absorption, this is due to the limitations of optical image reconstruction and was discussed in section 1.2.3. Figures 2.1.6b to 2.1.6e show the equivalent interpolated RMS amplitude images calculated from the EEG data. Rather than a dipole-localisation, these images are a simple representation of the peak of the measured amplitude of electrical potential difference oscillation. They only represent the position of the dipole to within a distance equal to half the electrode separation (15 mm) in each dimension. The error in the position is not therefore quoted as it would be of little relevance.

2.1.3.4 Discussion and conclusions

The results summarised in figures 2.1.5 and 2.1.6 demonstrate that it is possible to simultaneously record EEG and NIR imaging data over the same volume using our clinical opto-electrode design. The localisation provided by optical reconstruction, even with this low sampling-density array, is very good. This experiment has proven that the opto-electrode design provides sufficient optical signal to perform image reconstruction and that alterations to the electrode and the simultaneous use of the UCL Optical Topography System do not prevent the recording of EEG-mimicking electrical potential difference signals.

2.1.4 Solid-Surface Dual-Modality Phantoms

Once the liquid phantom experiments had proved successful, we began to consider whether it was possible to produce an EEG-NIR imaging phantom that was reusable and, ultimately, more stable. Liquid phantoms are not ideal for such experiments primarily because direct contact with a conducting fluid is a poor representation of the conductivity of the human scalp. It also removes the need for introduction of an electrode contact gel and therefore does not provide an optical arrangement comparable to an in-vivo experiment.

If a more stable and reusable phantom could be constructed that also provides an electrode contact impedance comparable to that of the human scalp, it would provide a better test of the suitability of current and future opto-electrode designs. A stable and re-usable phantom may also prove useful in the future development of reconstruction methods which take advantage of the spatial information present in both the optical and EEG data, such as in the testing of algorithms which perform optically constrained dipole source localisation.

An ideal dual-modality phantom would consist of a solid, optically turbid, translucent electrically conducting material into which an optical inhomogeneity and dipole source could be embedded. However, solid, electrically conducting and (at least approximately) transparent materials are extremely rare. In fact the pursuit of such materials is a very active area of condensed matter physics (Ginley 2010). We therefore began to consider whether it would be possible to design and build a phantom with a solid, conducting, and optically turbid interface, which would house a liquid core identical to that described in section 2.1.3. This could potentially provide a more suitable electrode contact impedance, would prevent the opto-electrodes and optical fibres from coming into contact with the liquid and would hopefully be easier to use and re-use. It does not, however, solve the

problem of stability, as phantoms based on scattering emulsions (Flock et al. 1992) can only be used for few days before the liquid needs to be replaced.

2.1.4.1 Solid-surface phantom construction

A number of phantoms were designed which utilise an optically scattering and electrically conducting interface. This interface is based on a polyester resin (Alec Tiranti Ltd., UK) to which an absorbing dye (pro-jet, Avecia Inc., USA) and a scattering compound (superwhite resin pigment, Alec Tiranti Ltd., UK) are added prior to curing so as to provide optical absorption and scattering properties equivalent to that of bulk tissue ($\mu_a = 0.01$ mm^{-1}, $\mu_s' = 1$ mm^{-1} at a wavelength of 800 nm). The resin mixture can be formed into almost any shape using a suitable mould design.

In order to make the interface electrically conducting, a dense array of 0.25 mm diameter gold-plated copper wires (Griffin, Germany) is embedded in the mould prior to the addition of the resin mixture. The lengths of wire are arranged so as to traverse the polyester resin layer, with one end flush to the surface of the resin, and with the other protruding by approximately 5 mm. Once cured, this resin interface is designed to form one wall of the container which holds the liquid component of the phantom. This design allows an array of opto-electrodes to be coupled to the smooth surface of the interface, with the gold wires providing an electrical contact between the opto-electrodes and the liquid core of the phantom. In this arrangement the gold plated wires lie parallel to the optical path of the NIR light coupled in to and out of the phantom via optical fibre bundles. Because the wires are fine, their affect on the optical characteristics of the interface is likely to be negligible. The presence of the wires will not affect optical imaging of the phantom because the arrangement is designed to allow NIR optical imaging of a change in absorption, and the optical properties of the interface will remain constant throughout any experiment. Gold plated wire was chosen because of its high conductivity, chemical stability and availability.

The density of the array of gold plated wires dictates the contact impedance of the interface surface. After some trial and error, we found that a square grid array with a separation of 2.5 mm provided a suitable electrode contact impedance for a planar interface arrangement. The electrode contact impedance was measured using two standard silver/silver-chloride EEG electrodes connected to an electrode impedance meter operating at 10 Hz (Checktrode, UFI Inc., USA). The electrodes were positioned 30 mm apart and coupled to the interface surface using a standard EEG contact gel. The contact impedance was measured at twenty random locations on the interface. The mean contact impedance was found to be 6.1 kΩ with a standard deviation of 1.1 kΩ.

This interface design has, to date, been applied in two different phantom constructions. The first consisted of a rectangular tank arrangement where the interface constituted one wall. This planar arrangement was designed to allow simultaneous EEG and optical topography to be performed using an aqueous solution and an optically absorbing electric dipole target identical to those described in section 2.1.3. The results of this experiment not only proved the efficacy of the interface design but also showed, once again, that our opto-electrode probe design could yield an electrode contact impedance equivalent to that of standard, clinical cup electrodes. It also provided a further test of the electrical compatibility of the UCL optical topography and a commercial EEG system. The details of this experiment can be found in Cooper et al. 2009.

This interface has also been implemented in a cylindrical arrangement, which has allowed time-domain optical tomography and EEG to be performed simultaneously over the same volume. This phantom arrangement consisted of a cylindrical container, 70 mm in diameter and 110 mm in height. This container is constructed from the same polyester resin (Alec Tiranti Ltd., UK), and again was made optically turbid by the addition of ‘super-white’ resin pigment (Alec Tiranti Ltd., UK). In this

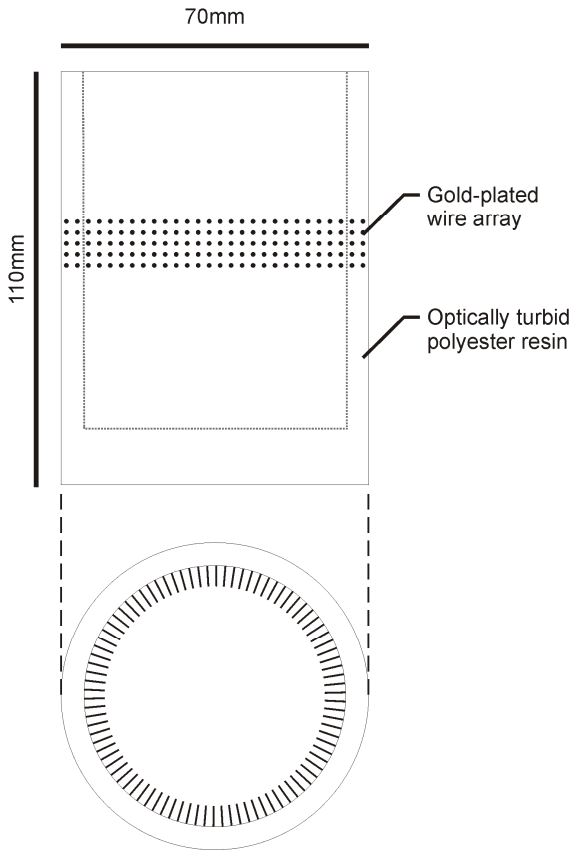

Figure 2.1.7. The design of the cylindrical, optically turbid and electrically conducting phantom.

construction, no additional absorber was added, rendering the optical properties of the phantom equal to $\mu_a = 0.0022$ mm^{-1} and $\mu_{s'} = 1$ mm^{-1}. The lengths of gold wire were spaced 2.5 mm apart around the surface of the cylindrical mould so as to form a ring. Five such rings, vertically spaced by 2.5 mm, form a conductive band 10 mm thick around the middle of the cylindrical container. This phantom design is shown in figure 2.1.7. Again, by filling this phantom container with the aqueous phantom solution described in section 2.1.3, and introducing an optically absorbing current dipole source (in this case reduced in diameter to 10 mm) we are able to provide a target for optical imaging and a source of EEG-equivalent variations in electrical potential difference.

2.1.4.2 Experimental Methods

A simultaneous EEG and NIR optical tomography experiment was performed using an array of twelve opto-electrodes evenly spaced around the external circumference of the cylindrical solid-surface phantom at the level of the conductive band. Each of these opto-electrodes acted as an active EEG recording electrode whilst a standard reference electrode was placed in contact with the aqueous solution. This reference position was chosen in order to maximise the number of active recording electrodes around the conduction band, and EEG data were re-referenced to the average of all recording electrodes before further analysis. The optically-absorbing, current dipole target was positioned level with the conductive band, 18 mm from the centre of the phantom, as shown in figure 2.1.8a.

EEG data were recorded using twelve channels of a Grass-Telefactor H2O 32-channel EEG recording system (Grass Technologies, Astro-Med Inc.) with a sample rate of 400 Hz. Data were acquired using the software package EEG TWin 2.6 (Grass Technologies, Astro-Med Inc.), and then analyzed offline using Matlab (The Mathworks Inc., USA) and EEGLab (SCCN, UC San Diego, USA). EEGLab was used to produce a topographic representation of the electrical potential field and a current dipole reconstruction of the recorded EEG data. (Note that EEGLab performs an independent component analysis of the EEG data, and then provides a dipole localisation and a topographic representation of each independent component. As our data was essentially a sine wave, only the primary independent component results are presented in figure 2.1.8. For more information see Delorme and Makeig 2004).

Optical tomographic data were obtained using UCL's 32-channel time domain imaging system (Schmidt et al. 2000). This system produces light pulses with a duration of 2 ps at 780 and 815 nm which are coupled sequentially to the object under investigation via a set of optical fibre connectors. Each connector consists of a detector fibre bundle and a source

fibre arranged co-axially. Diffusely scattered NIR light from the illuminated medium is detected using a series of microchannel plate PMTs, which, in conjunction with timing electronics and variable attenuators to prevent overexposure, enable the time of flight of each detected photon to be recorded. For this experiment, only twelve channels and connectors were required, each coupled to the ring-array via an opto-electrode probe. One complete data set was obtained prior to the dipole target being inserted into the phantom in order that an image of the change in optical absorption could be obtained. Images of the change in optical absorption coefficient were reconstructed using the non-linear reconstruction algorithms of the TOAST software package developed at UCL (Arridge et al. 2000a, Schweiger et al. 2003, Gibson et al. 2005).

2.1.4.3 Results

Figure 2.1.8 summarises the results of this phantom experiment. Figure 2.1.8a shows the experimental phantom geometry, with the red circle representing the size and position of the optically absorbing current dipole target. Figure 2.1.8b shows a topographic representation of the dipole field

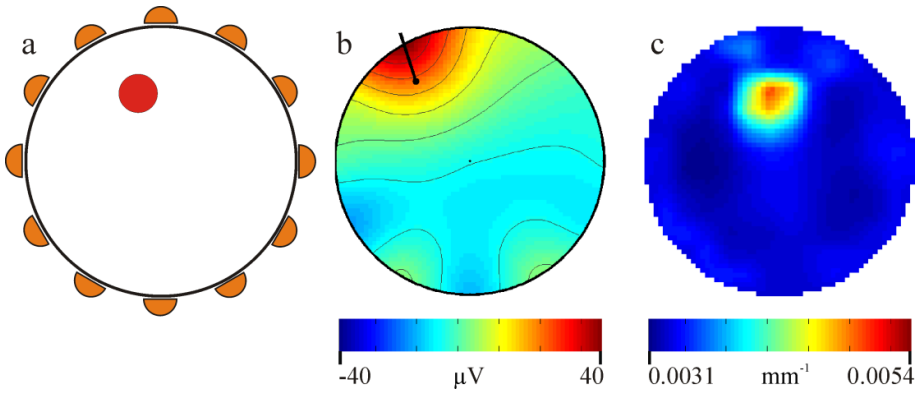

Fig. 2.1.8. The actual phantom geometry cross-section is shown in figure a, the red circle indicating the location of the optically absorbing, current-dipole target and the orange semi-circles show the position of the 12 opto-electrodes. Figure b shows the topography of the re-scaled, dominant independent component of the recorded EEG data and the resulting dipole reconstruction. Figure c shows the reconstructed image of change in optical absorption coefficient at 780 nm.

and the result of a current dipole localisation algorithm, performed using the EEGLab package for Matlab (Delorme and Makeig 2004). The error in the reconstructed dipole position is 8.1 mm. An accurate dipole localisation is to be expected given the electrical isotropy of the phantom, though this is confounded by the relatively small number of EEG electrodes used and the probable errors in phantom construction (slight variability in the length and position of the conducting wires, surface deformities, variation in electrical contact etc.). Figure 2.1.8c shows the reconstructed tomographic image of change in optical absorption coefficient at 780 nm. Note that the scale of the change in optical absorption is, once again, inaccurate: a common problem in optical image reconstruction techniques. The focal change in reconstructed absorption coefficient is accurately located, with a peak change at 3.3 mm from the actual target position. The dimensions of the focal change are also similar to that of the actual target, with a full-width at half maximum of 11.3 mm.

2.1.4.4 Discussion and conclusions

As one of a series of tests, these phantom studies have contributed significantly to the evaluation of our opto-electrode design and the phantom constructions themselves may well prove useful in future development of combined EEG and NIR imaging techniques. However, the best test of our EEG-NIR application methods can only be provided by an in-vivo experiment. Such an experiment is described in detail in the following section.

2.1.5 Motor Cortex Activation Study

2.1.5.1 Justification and experimental design

Performing an in-vivo experiment using the opto-electrode design was necessary to test two fundamental characteristics: whether the probe is capable of providing a good enough optical contact to observe the cerebral haemodynamics which are the basis of NIR imaging, and whether the opto-electrode can provide a good enough electrical contact to observe en-mass neuronal activity.

It was therefore necessary to perform an experiment which would produce a well defined electro-cortical response of a well documented form but that would also produce a well defined haemodynamic response over a known area of the cerebral cortex. The experiment was to be performed on an adult, and ideally needed to produce electro-cortical and haemodynamic responses which were significant enough to be observed in a single-subject study.

As it was necessary to know where and when the physiological responses were to occur, this experiment lended itself to a functional activation/ERP paradigm. However, finding a suitable functional stimulus was challenging. First there is the problem of timescale. Event-related potentials typically last anywhere between 50 and 1000 ms post-stimulus whilst the haemodynamic response usually peaks between 5 and 10 seconds post stimulus and can take another 15 seconds to return to baseline. As ERP paradigms typically require hundreds of repetitions of a stimulus in order to achieve a suitable signal-to-noise ratio, using a single stimulus event to provide both responses will force the experiment to become unsuitably time consuming. There is also the problem of the scale of the stimulus. Most well-documented ERP signals are in response to a very subtle, discrete stimulus, such as a single finger extension in motor cortex activation or a single tonal sound in auditory cortex studies. However, the most robust

functional activation stimulus in NIR studies consists of a repeated, continuous thumb-to-finger opposition task so as to activate the primary motor cortex (Franceschini et al. 2003, Everdell et al. 2005).

The first paradigm considered was a visual stimulus paradigm involving a checkerboard pattern reversing between black and white. A single reversal produces a known ERP (Odom et al. 2004) and regular reversals (at 2 Hz for example) for 20 seconds should produce a well-documented haemodynamic response (Zeff et al. 2007). However, this experiment was abandoned because of technical problems unrelated to the opto-electrode, specifically the excessive absorption of 670 nm light over the primary visual cortex. Because a finger-to-thumb opposition task has produced so many reliable and repeatable haemodynamic responses it was decided instead that the experiment should be designed to incorporate this stimulus. This required us to separate the stimuli for the NIR imaging and ERP aspects of the experiment. This was due to the technical difficulties of event marking an EEG trace for every finger-to-thumb movement, and because of the less well defined ERP it would produce.

The paradigm that was finally employed consisted of continuous, simultaneous EEG and NIR recording but with the experiment divided into two halves. The first consisted of fifteen, 30 second long periods of self-paced finger-to-thumb opposition of the dominant hand, interspersed with 30 seconds of rest. The start and end of each of these periods was controlled by a visual cue and time-locked to the UCL OT system. The second half consisted of 15 minutes of self-paced forefinger extensions, again, of the dominant hand. Each movement was time-locked to the EEG system using a simple, purpose-built break-beam optical trigger. The first half of this paradigm was designed to elicit the known haemodynamic motor cortex response as shown previously by Francescini et al. (2003) and Everdell et al. (2005), whilst the second half was designed to produce what's known as a Bereitschaftspotential (BP) or readiness potential. A BP

is an electrophysiological sign of the activation of the supplementary motor area of the motor cortex prior to a voluntary movement (Shibasaki and Hallett 2006) and is characterised by a slow negative deflection beginning between 2 to 3 seconds prior to movement. BPs are usually observed over both motor cortices, even if the stimulus is lateralised, but an additional feature (known as 'late BP') tends only to be seen over the hemisphere contralateral to the movement. Late BP consists of a marked increase in the rate of deflection ~500ms prior to movement. The BP was used for the in-vivo test of the opto-electrode design because it is very well documented, has an easily recognisable form and is usually easy to observe, even in single-subject trials.

As the stimulus and the expected vascular response are lateralised in this experimental design, it was necessary to construct an opto-electrode array which covered both the right and left motor cortices. As this experiment was intended to be as simple as possible, a symmetrical, relatively low-density array with 10 channels per wavelength, per hemisphere was built. Two 3 mm thick thermoplastic housings, each holding seven opto-electrodes, were constructed and attached to one another using a thin strap of velcro. This velcro strap was then run over the top of the head such that the central opto-electrode of the left and right housings were positioned over C3 on the left and C4 on the right motor cortex respectively. The array is shown in its approximate position on the head in figures 2.1.9a and 2.1.10a.

2.1.5.2 Experimental Methods

Optical data were recorded using the UCL Optical Topography (UCL OT) System, (Everdell et al. 2005) as described in section 2.1.3.2. Optical images were reconstructed using the linear reconstruction methods described in section 1.2. EEG recording was performed using a Neuroscan Synamps 32-channel EEG/ERP system with a sample rate of 2 kHz linked to the Scan 4.2 EEG acquisition software package (Compumedics Ltd., USA). Data were recorded over the range 0.01 to 70 Hz with a 50 Hz notch

filter to minimise the electrical interference at the mains frequency. Artifact rejection, baseline correction and averaging were performed offline within Scan 4.2.

The subject was a healthy, right handed, 24 year-old male volunteer. The opto-electrode contact sites were abraded prior to the study using an abrasive paste (NuPrep, Weaver and Company, USA) as described in section 1.2.2. The contact impedance of each channel was measured before the beginning of the paradigm and all were found to be (or quickly adjusted to be) below 5 kΩ. Note that a good electrical and a good optical contact were achieved despite the subject having a full, albeit short, head of hair.

The two opto-electrode housings were linked together over the top of the head and then secured into position using light bandaging. A ground electrode was placed at Cz and a common reference electrode was placed on the tip of the nose. The subject was instructed to keep his eyes closed for the second part of the experiment in order to minimise eye-movement artefacts on the EEG trace.

2.1.5.3 Results

Figures 2.1.9b to 2.1.9f show changes in optical absorption over the left (contralateral to movement) motor cortex with time at a depth of 10 to 15 mm, whilst figures 2.1.10b to 2.1.10f show the corresponding changes over the right (ipsilateral to movement) motor cortex. Each of these figures represents the difference in optical absorption between a sample data set and a reference data set. Each sample set is the mean of a specified 5 second long data 'bin' recorded during the movement task. The reference set was taken as the mean of the 20 second of data recorded prior to movement onset. All of these data are grand means over all 15 repetitions of the movement task. Note that absorption images (as opposed to images of haemoglobin concentrations)

Figure 2.1.9

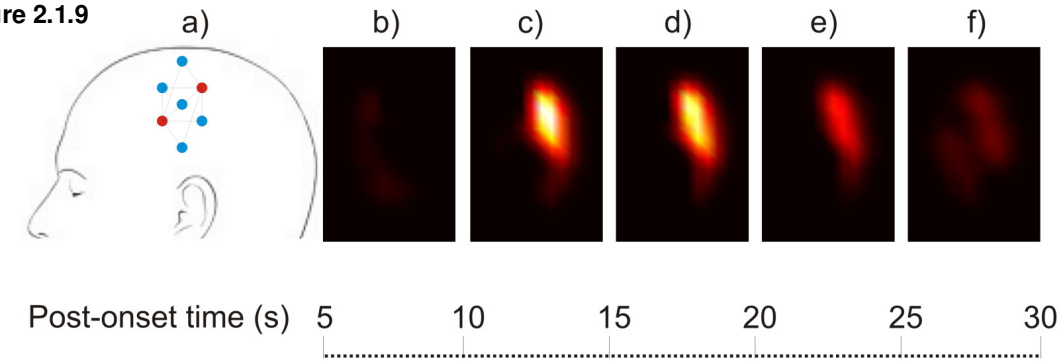

Figure 2.1.10

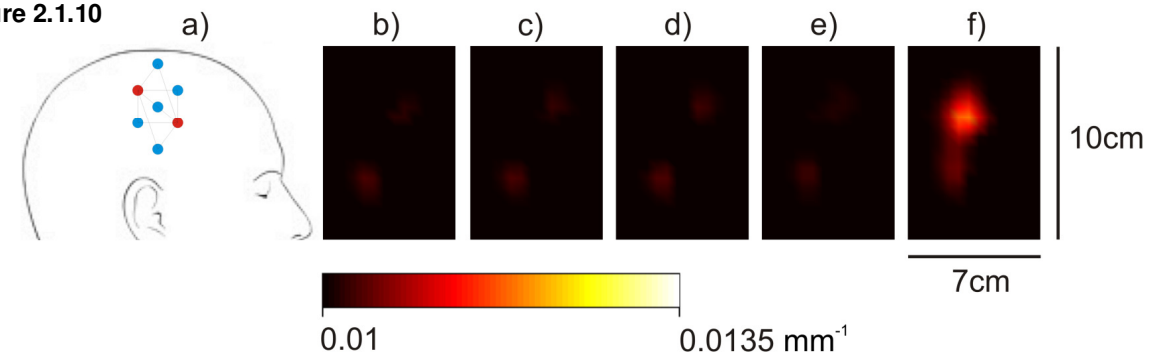

Figures 2.1.9 and 2.1.10. Figures 2.1.9a and 2.1.10a show the approximate positions of the opto-electrode arrays over the left (contralateral to movement task) and right (ipsilateral to movement task) motor cortices respectively. Red circles correspond to sources and blue circles to detectors, all positions were opto-electrodes. Figures 2.1.9 b-f and 2.1.10 b-f show the reconstructed images of mean changes in absorption at 770 nm for five second time windows beginning five seconds after the onset of the lateralised finger-opposition task, for the left and right opto-electrode arrays respectively. These images show the voxel layer at a depth of 10-15 mm. All are scaled to the maximum range across all 10 images.

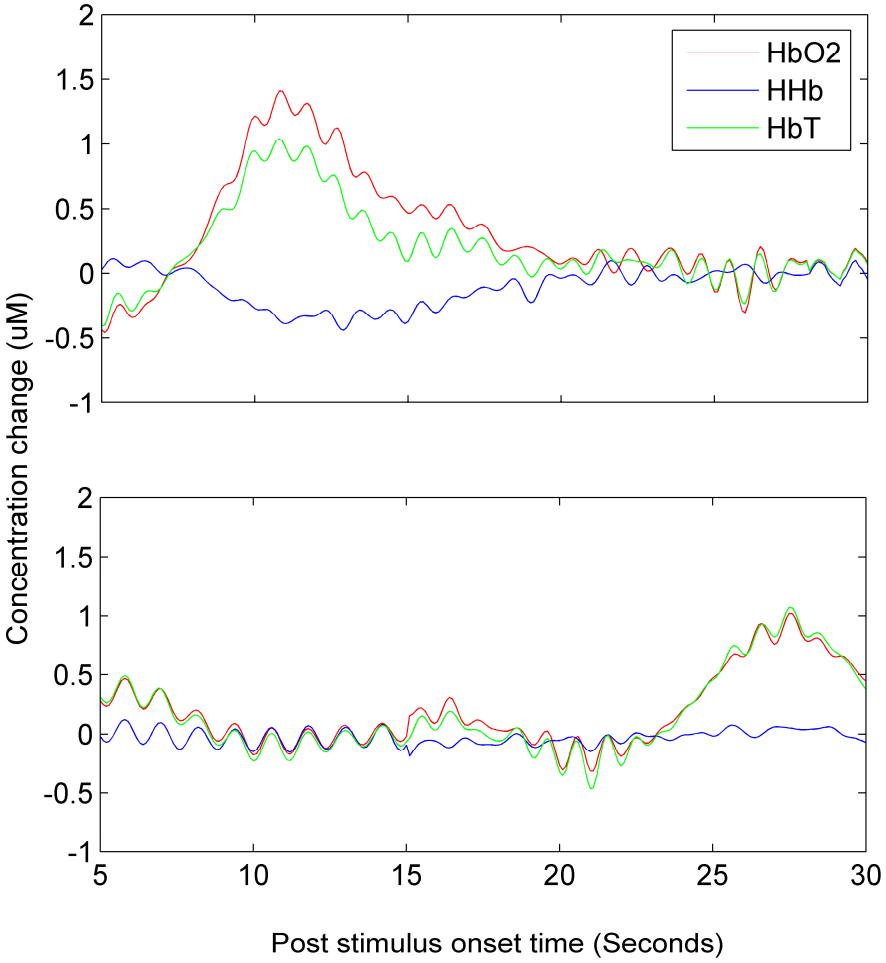

Figure 2.1.11. The changes in oxy and deoxyhaemoglobin concentration for two channels within the left (upper axes) and right (lower axes) optical imaging arrays, for the same period as depicted in figures 2.1.9 and 2.1.10. The lateralised finger-opposition task begins at time = zero. A perfect concordance between the dominant features of the reconstructed image series and the data from individual channels is not expected. However there is agreement in the approximate peak change positions for these single channels. Note that heart rate oscillations are clearly apparent despite these data being the average of 15 trials, which may be indicative of the fact that this functional response is of a relatively small scale.

are presented because of a technical failing in one of the optical topography channels at 850 nm, however figure 2.1.11 shows the comparable, average spectroscopic time course of changes in haemoglobin concentrations for a selected optical topography channel on each side of the head. These time courses show a typical contralateral haemodynamic response; with a

stimulus-locked increase in oxyhaemoglobin concentration and a decrease in deoxyhaemoglobin.

The optical imaging data shows a distinct change in absorption coefficient over the motor cortex contralateral to the hand performing the movement task. The absorption change peaks 10 to 15 seconds after the onset of the finger-to-thumb opposition task and slowly decays until returning to baseline completely within 5 seconds of the end of the stimulus period. With the exception of a relatively slight absorption coefficient change towards the end of the stimulus period, the ipsilateral optical images show only the effects of source noise.

Figure 2.1.12a shows the Bereitschaftspotentials recorded at the uppermost and central electrodes (approximately C1 and C3 respectively) over the motor cortex contralateral to the paced, voluntary finger extension. Figure 2.1.12b shows the equivalent data for the ipsilateral electrodes at approximately C2 and C4. These data are the average of 134 events, after 43 were visually rejected due to movement or other artefacts. Baseline correction was performed on the basis of the period from 3.5 to 3 seconds prior to movement. The characteristic slow-building negative deflection of a BP, beginning 2 seconds prior to movement, is very apparent over the contralateral electrodes (figure 2.1.12a) but, is not apparent over the equivalent ipsilateral electrodes (figure 2.1.12b), which shows only a post-movement positive deflection.

2.1.5.4 Discussion and conclusions

The reconstructed optical absorption images of figure 2.1.9 and 2.1.10 show an increase in optical absorption, which is dominant over the contralateral motor cortex and occurs on a timescale which means they are almost certainly physiological. These absorption changes, and the corresponding spectroscopic data of figure 2.1.11 are consistent with a contralateral

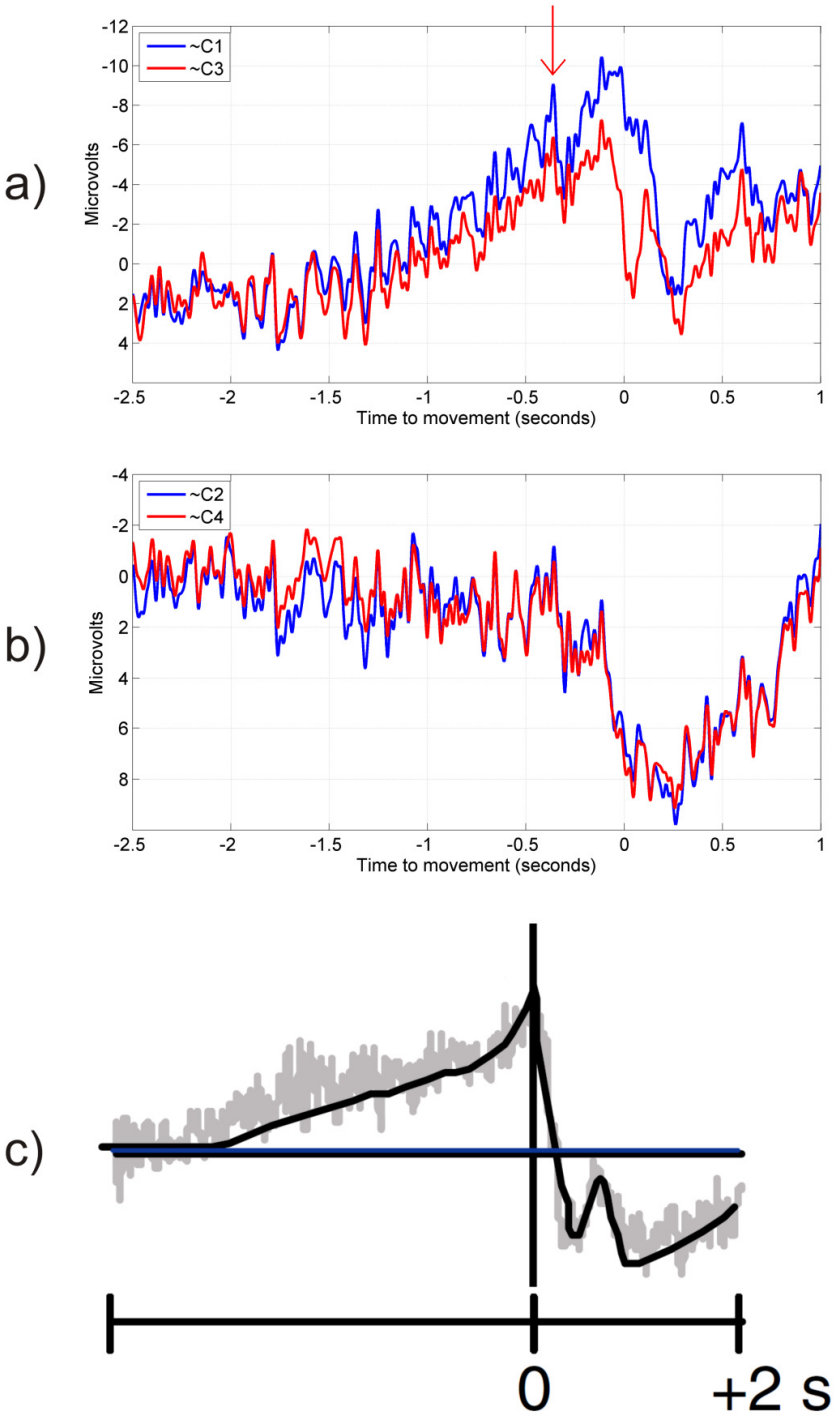

Figure 2.1.12. Figure a shows the BP recorded at the contralateral opto-electrodes positioned approximately at C1 and C3 using the lateralised finger extension task. The red arrow highlights a particular noise-spike which makes the division between early and late BP indisitinct. Figure b shows the corresponding ipsilateral signal which does not show a BP. Note the different scale. Figure c is a representative waveform which illustrates the expected form of the contralateral BP (Shibasaki and Hallett 2006).

functional response to lateralised motor cortex activation which has been shown in many previous studies (Franceschini et al. 2003, Everdell et al. 2005).

The reconstructed absorption changes reach a peak contralaterally at 10-15 seconds after stimulus onset from which time they slowly decay, despite the stimulus continuing until 30 seconds after onset. It is not unusual for the haemodynamic response to reach a peak at this time after stimulus, but in general we would expect the changes to become apparent earlier (at 3-5 seconds, see Obrig and Villringer 2003). Similarly, the observed change in absorption starts to decrease before the end of the stimulus period, suggesting some level of habituation to the stimulus. Given the limited scope of this single subject, proof-of-concept study it is difficult to establish the significance of these irregularities, but the spectroscopic time courses shown in figure 2.1.11 provide us with strong supporting evidence that these reconstructed absorption images do represent the result of functional activation as they are consistent with a stimulus-locked increase in cerebral blood flow.

Although the noise recorded during the ERP aspect of this experiment is significant, by examination of the raw data it is apparent that noise levels are not unusually excessive, and given the low contact impedances achieved, there is no evidence that the opto-electrode design is more susceptible to electrical noise than a standard clinical electrode. Because of the spike occurring at approximately -0.35 seconds in figure 2.1.12a (marked by the red arrow), the division between early and late BP is not well defined. However the apparent trend of an increase in gradient appears consistent with late BP, particularly for the opto-electrode at C1. For comparison, figure 2.1.12c shows a representative BP as compiled by Shibasaki and Hallett (2006).

Given that the aim of this study was to test whether the opto-electrode design is fundamentally suitable for in-vivo simultaneous EEG and NIR imaging studies, the conclusions that are drawn are not related to the nature or intricacies of the electro-cortical or vascular responses which were observed but rather the fact that they could be observed at all. Using the clinical abrasion methods it is possible to use a fixed array of many opto-electrodes and still achieve suitably low electrode contact impedances. Similarly, the opto-electrodes do not obstruct the transmission of light, and are not overly prone to movement artifacts in a manner which prevents their use in-vivo. The opto-electrode arrays need to be applied carefully, and it is particularly important that abrasion is performed thoroughly and in precisely the locations where each opto-electrode will make contact with the scalp. However, application of an opto-electrode array does not take significantly more time than the application of a standard EEG or optical imaging experiment.

Chapter 3

3.1 Functional Activation in the Neonate

3.1.1 Objectives and Experimental Design Considerations

The ultimate clinical goal of the work described in this thesis is the study of neonatal seizures, their diagnosis and their effects on cerebral haemodynamics. Prior to conducting studies of neurologically compromised infants, we set out to perform EEG-NIR imaging of functional activation in the healthy, term-age neonate. A primary motivation for this work was to validate the technology, and develop the methods of applying our system in a clinical environment. However, these studies also enable many scientific questions regarding neurovascular coupling and functional activation in the neonate to be addressed.

Functional activation in the neonate, and its relation to development has been a prolific application of NIR techniques (Meek et al. 1998, Hebden et al. 2002, Austin et al. 2006, Liao et al. 2010). This is despite the fact that neonates (particularly in a clinical setting) can be an intensely difficult group to study. Obtaining an acceptable rate of consent from new parents is a significant challenge, experiments must be flexible enough to cope with constant variations in the hospital environment and any research must ultimately be considered a low priority in comparison to the clinical (and even nutritional) needs of the subject.

The number of experimental paradigms which are suitable for application to newborn infants is small. Stimuli must be passive, and ideally robust with regard to the subject's varying sleep and behavioural state, their inability to interact and their tendency to move. The most commonly applied stimuli are visual, passive motor, somatosensory and auditory.

The haemodynamic response to functional activation in infants is known to be more variable than that of adults (Zaramella et al. 2001). The classic haemodynamic flow response, consisting of an increase in oxyhaemoglobin

and decrease in deoxyhaemoglobin concentration (which corresponds to a positive BOLD-fMRI signal) has been repeatedly seen in both fMRI and NIR functional studies of neonates (Erberich et al. 2006, Karen et al. 2008, Liao et al. 2010). However, there have also been many reports of stimulus-related haemodynamic responses in neonates consisting of an increase in oxyhaemoglobin and an increase in deoxyhaemoglobin (a negative BOLD-fMRI response) (Meek et al. 1998, Hoshi et al. 2000, Born et al. 2000) or even a decrease in oxyhaemoglobin and increase in deoxyhaemoglobin (Kusaka et al. 2004). This variability is believed to reflect the immaturity of neonatal vasculature and is an area of ongoing research (Colonnese et al. 2008, Zimmermann et al. 2010).

The studies presented in this section are intended to be a preliminary investigation into electro-cortical and haemodynamic responses in newborns, it is important to choose a stimulus which can provide a well understood and robust response in both EEG and optical topography (OT). The chosen stimulus must also lend itself to the intricate block paradigms necessary to perform simultaneous ERP and NIR imaging. The basis of these paradigms is, in general, that the event-related potential resulting from each individual stimulus can be recorded via EEG (or at least the *average* ERP can be, as the signal-to-noise ratio is usually too low to resolve single-stimulus ERPs) whilst the comparatively slow haemodynamic response to each block of repeated stimuli is recorded using NIR techniques. As described in section 1.3, the importance of simultaneous acquisition of functional NIR and ERP data (as opposed to sequential acquisition) is that the neurovascular coupling relationship can be studied in conditions where there is intra-stimulus and inter-stimulus variability in the evoked electro-cortical and/or haemodynamic responses. Such experimental designs have been used to study the neurovascular coupling relationship in cases of intra and inter-stimulus variability due to habituation (Obrig et al. 2002) and due to the effects of visual attention (Näsi et al. 2010). Such block-paradigms

require careful planning and extremely precise timing and event-marking.

To compare the electro-cortical and haemodynamic responses, it is important to be able to obtain enough ERPs within each block of stimuli to provide a reasonable ERP signal-to-noise ratio (SNR). If a reasonable SNR can only be obtained by averaging across all stimulation blocks, then any information about the variation of the neurovascular coupling relationship between those blocks will be lost. This would also negate the advantages of simultaneous (as opposed to sequential) EEG-NIR imaging.

As mentioned in section 1.1.4, hundreds of stimulus repetitions are usually necessary to produce a relatively low-noise ERP. One way of producing an experiment which is more robust with respect to the low signal-to-noise ratio of ERPs is to design an experiment which allows for analysis in the frequency domain. By presenting the stimulus at a known rate of repetition and performing a Fourier transform of the resulting EEG data, the variation of the spectral power at the rate of stimulation (and its harmonics) can provide a measure of the contribution of stimuli-related neuronal activity to the recorded EEG (Hermann et al. 2001, Koch et al. 2006, 2008).

Given all these considerations, it was decided that a flash-based visual stimulation was the most suitable. Flash stimuli can be controlled very precisely, and the haemodynamic and electro-cortical responses are well documented (Odom et al. 2004, Liao et al. 2010). Indeed, the presentation of a flash or stroboscopic stimulation is often part of a clinical EEG assessment, and this familiarity makes using such a stimulus for research purposes in a hospital environment somewhat less problematic. Flash stimulation is also entirely passive, and it has been shown that it can be performed through closed eyelids in adults as well as in neonates (Koch 2006 et al., Liao et al. 2010). This is particularly important, as maintaining attention, or even wakefulness, is almost impossible in newborn infants. The flash visual evoked potential (VEP) is known to change with sleep state

Author	Method	Subject age	Subject state	Stimulus	Result
Martin, 1999	BOLD-fMRI	Term to 12 years	Sedated	8 Hz red LED goggles	↑BOLD, ↓BOLD or no change
Altman, 2001	BOLD-fMRI	2 months to 9 years	Sedated	8 Hz white LED goggles	↓BOLD
Sie, 2001	BOLD-fMRI	18 months	Sedated	8 Hz red LED goggles	↓BOLD (17/28), no change (10/28), ↑BOLD (1/28)
Yamada, 2000; Morita, 2000; Muramoto, 2002	BOLD-fMRI	Term to 32 weeks	Sedated	8 Hz white light	↑BOLD ≥ 7 weeks ↓BOLD ≤ 8 weeks
Meek, 1998	NIRS	3 days to 14 weeks	Awake	5 Hz pattern reversal	↑HbO_2, ↑HHb
Hoshi, 2000	NIRS	4 to 5 days	Asleep	10 Hz white light	↑HbO_2, ↑HHb or ↓HHb or no change
Taga, 2004; Watanabe 2008	NIRS	2 to 4 months	Awake	14 Hz pattern reversal	↑HbO_2, ↓HHb
Kushaka, 2004	NIRS	1 to 4 months	Asleep	8 Hz white light	↓HbO_2, ↑HHb
Wolf, 2004	NIRS	Term	Unspecified	2-3 Hz red LED goggles	No change
Karen, 2008	NIRS	2 to 9 days	Asleep	1 Hz red LED goggles	↑HbO_2, ↓HHb
Liao, 2010	NIRS	Term to 3 days	Asleep	2 Hz LCD flash	↑HbO_2, ↓HHb

Table 3.1.1. A summary of previous visual stimulation paradigms in infants and their results. Note the variety of stimuli and haemodynamic response. Adapted from Liao et al. 2010.

(Apkarian et al. 1991), but this is true of all ERPs and although it is an undesirable variable, it is not necessarily a problem for our paradigm.

The development of the experimental arrangement, and the intricate stimulus paradigm required for an EEG-NIR study of flash stimulation in neonates is described below. Table 3.1.1 provides a summary of previous visual stimulation paradigms performed using NIR and fMRI methods.

3.1.2 Experimental Design and Development

3.1.2.1 Experimental arrangement and control

All EEG-NIR experiments were performed using UCL's Optical Topography System, as described in section 2, operating at 670 and 850 nm. This system was used in conjunction with a clinical EEG system based at the Neonatal Intensive Care Unit (NICU) of The Rosie Hospital, Cambridge, UK. Though designed primarily for clinical use, this EEG system (MicroMed SystemPlus SAM-FC1, MicroMed S.p.A. Italy) has a maximum acquisition rate of over 4 kHz and enough software flexibility to allow us to implement the system in an event-related potential experiment. However, the EEG system does not allow for any offline processing of ERP data without an additional software package, and this proved prohibitively expensive. Data were therefore exported in a raw format and offline data processing (including filtering, baseline correction, epoching and averaging) was performed using routines written using Matlab (The Mathworks, Inc., USA).

As was described above, any simultaneous EEG-NIR experiment, particularly when studying functional activation, requires extremely precise control of the timing of both the stimuli and each recording modality. It was determined that the simplest way to achieve this level of control was to use a single laptop computer to initiate both the flash stimulus and the corresponding event-marking signals that time-lock the EEG and optical topography systems to the stimulus. This necessitated the design and construction of bespoke LED stimulation goggles, which is described in detail in the following section. A diagram showing this experimental arrangement is shown in figure 3.1.2.

The paradigm control software was designed using the experimental toolbox Cogent 2000 (UCL, UK www.vislab.ucl.ac.uk/Cogent), which is used within the Matlab environment. Cogent is a framework which allows visual

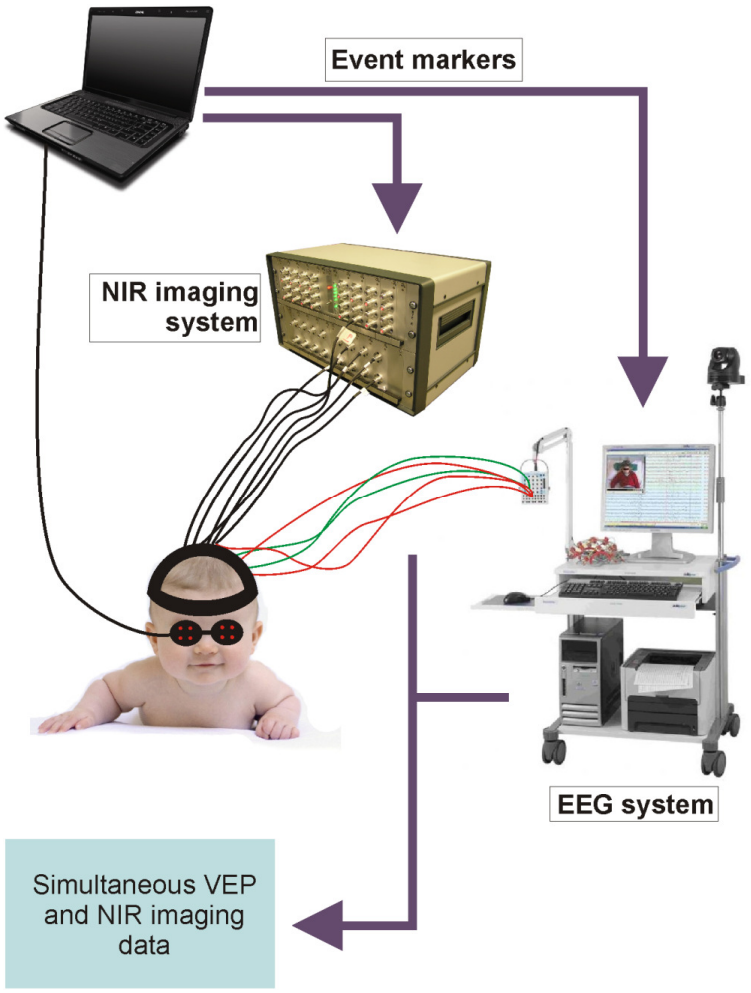

Figure 3.1.2. A diagram showing the basic experimental arrangement for EEG-NIR studies of flash-evoked functional activation.

and auditory stimuli, as well as digital signalling, to be performed with milli-second precision.

Event marking for the optical topography system is relatively straightforward, as it is designed to be used in such experimental arrangements. The sampling rate of the system is 10 Hz, and for each sample the system records a dedicated event-mark via an externally-triggered, serial-port connection. The event-marker can also be triggered by a manual keyboard input.

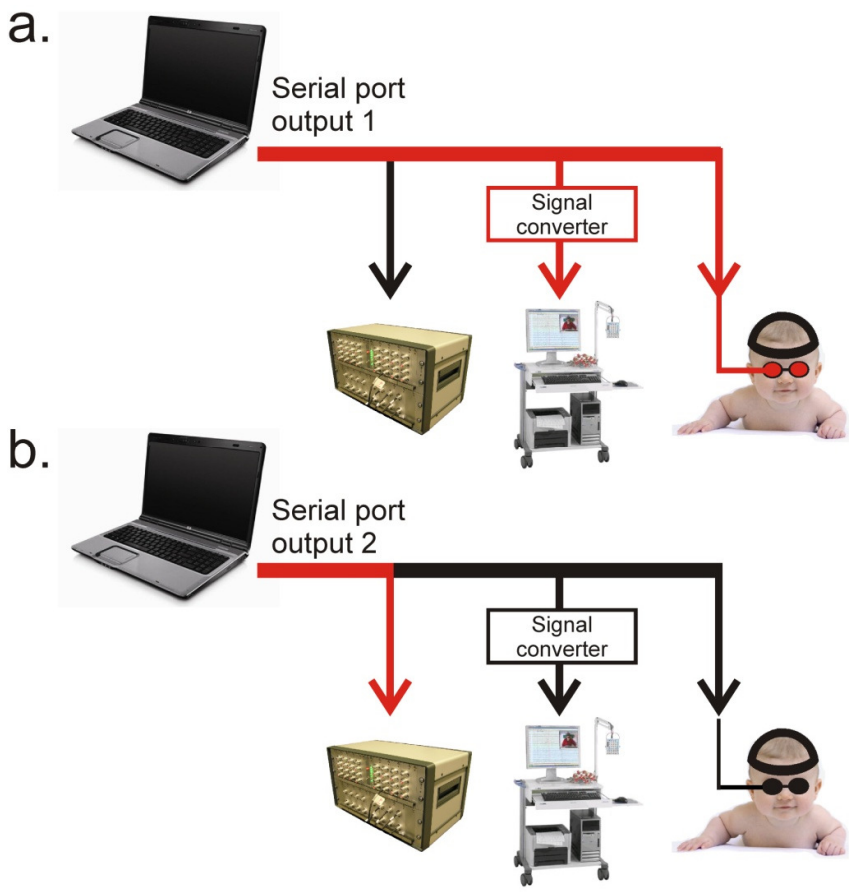

Figure 3.1.3. A representation of the triggering mechanisms for the optical topography system, EEG system and LED goggles under two different conditions. A particular serial port output from the control laptop will result in the simultaneous firing of the LED goggles and the positioning of an EEG event marker (figure a). A second type of serial port output results in event marking of the optical topography system only (figure b). The box labelled 'signal converter' interprets the incoming serial port output (an 8 bit ascii character) and converts it into a 0-5 Volt pulse to trigger the EEG system.

The time-locking of the EEG system is somewhat more complicated. It requires the transmission of a 0-5 Volt rising edge signal to an isolated USB triggering hub connected to the EEG computer. This incoming pulse is then recognised by the EEG SystemPlus software and a time-locked, ~2 mV spike is added to a recorded EEG channel of the user's choosing. It is therefore necessary to place an extra 'dummy' channel in each of our EEG montages to act as a triggering channel. The triggering spike is added to the chosen dummy EEG trace before any selected filters are applied, and

therefore the low pass filter setting must remain at 1000 Hz or higher whilst recording ERP data in order that the timing trigger itself is not filtered out. Despite being somewhat idiosyncratic, this event-marking procedure proved suitable, as recording of an incoming trigger occurs within one sample of the EEG system (which, for most experiments occurred at a rate of 2048 Hz). This triggering precision is above what it necessary to study event-related potentials.

As described above, performing a simultaneous ERP and optical topography study requires a carefully designed block paradigm, such that the ERP can be recorded in response to each individual stimulus, whilst the OT system records the haemodynamic response to a block of stimuli. The EEG data must therefore ideally be time-locked to each individual stimulus (or flash in this case), whilst the optical topography system need only be triggered at the beginning and end of each block of flashes. With these requirements in mind, it was decided that instigating each flash stimulus with the exact same laptop output used to provide the EEG trigger would be the easiest way to ensure synchronisation. A schematic of the triggering mechanisms is shown in figure 3.1.3.

3.1.2.2 Development of flash stimulation goggles

The design of flash stimulation goggles for application to infants in a clinical environment is subject to a number of different requirements. First, and most fundamentally, they must be able to elicit the flash evoked response, which is essentially a question of flash brightness and duration. Second, they must be electrically, optically and physically safe. Third, they must meet the standard of hygiene defined by the clinical unit's infection control team (an issue which is particularly important in the NICU). Fourth, they must be compact and easy to use in the limited space of a hospital ward, and fifth, they must not interfere in any way with our recording systems or the hospital's medical equipment.

Red-light LEDs, with a peak output at a wavelength of 625 nm (Kingbright OptoElectronics Ltd., UK) were selected to form the basis of the stimulation goggles. Flash VEP responses are commonly elicited by white or red light sources which stimulate the full field of view (Odom et al. 2004). Light emitting diodes are particularly suitable for this experiment because they can be easily controlled and have a fast, consistent response time at a known output luminance. Red LEDs were chosen because they are particularly suitable for illumination through closed eyelids, due to the relatively high transmission of red light through tissue. Using the published luminance values of previously designed LED stimulation goggles (Koch et al. 2006), the standards for flash stimulation (Odom et al. 2004, Marmor et al. 2004) and with knowledge of the British safety standards (BS EN 60825-1:2007) we determined that goggles consisting of 6 LEDs per eye, providing a total luminous intensity of 7.2 candela (Kingbright OptoElectronics Ltd., UK) for a duration of 10 ms per flash would safely produce the required response. Using a worst-case assumption that the output of all twelve LEDs was concentrated to a point source, the total output intensity would be 2.4 W/m^2, where the safety limit is 10 W/m^2.

Holding an LED stimulator in front of an infant's eyes is significantly easier than designing actual goggles and coupling them to the head. Our first prototype therefore consisted of the twelve LEDs described above soldered onto a rigid 25 x 100 mm printed circuit board. This board was electrically shielded and encased in disposable rubber insulation in order to aid disinfection. A shielded, twisted-pair cable was used to connect the LED circuit board (at the cot) to a shielded circuit box containing subsidiary electronics. This circuit box is placed next to the control laptop, which is either at a workstation or on a portable trolley depending on the location of the experiment. These subsidiary electronics receive the Cogent-controlled serial port output of the laptop and, if specified, provide a 20 mA, 10 ms duration current to the LEDs via the shielded cable. They also convert the

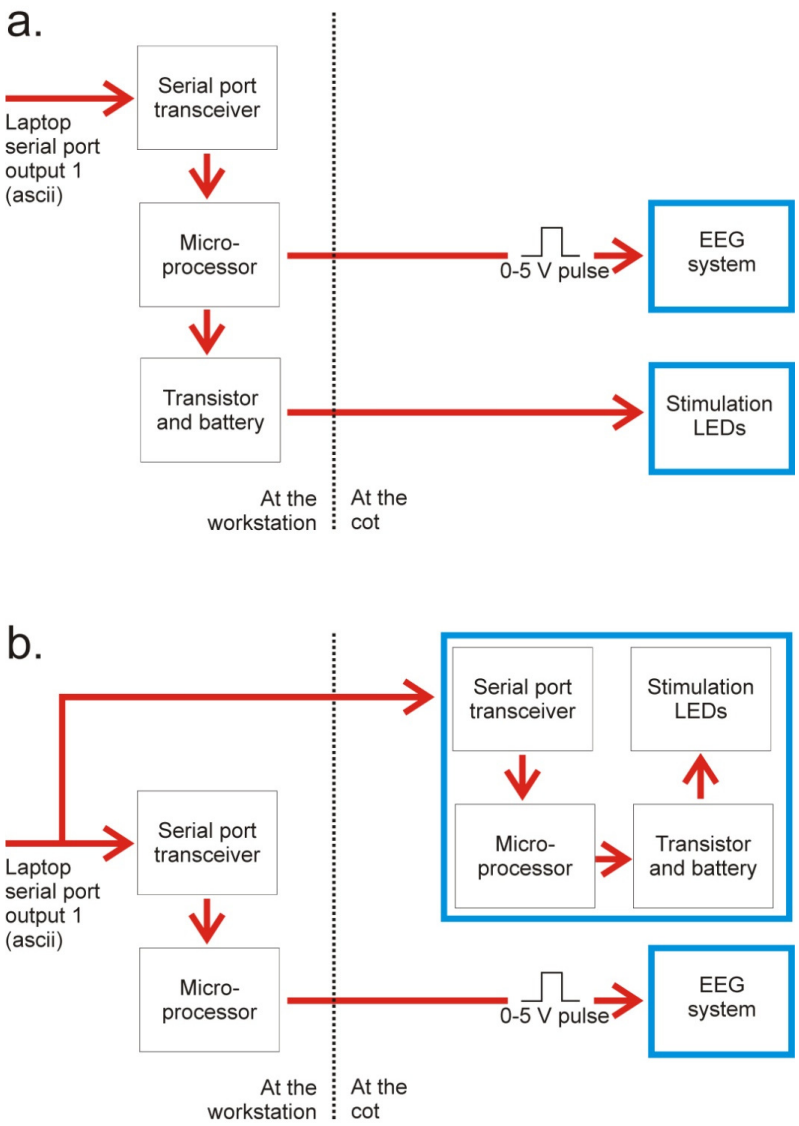

Figure 3.1.4. Schematic arrangements of the interpreting electronics, with respect to physical location, for the first LED goggle prototype (a) and the final design (b). Note how the final design relocates much to the electronics, and the power supply, to a position at the cot, where they form part of the goggles themselves.

laptop output into a 0-5 V pulse in order to trigger the EEG system, as discussed above. A diagram of this arrangement is shown in figure 3.1.4a.

This initial design was tested by performing a simple VEP experiment (i.e. EEG only) with an adult volunteer. A single, standard clinical EEG

electrode was attached to the head at Oz over the occipital lobe and referenced to Fz. The EEG was recorded at 2048 Hz with a bandpass filter operating from 0.5-1000 Hz with a 50 Hz notch filter. The contact impedance of this channel was maintained below 5 kΩ. The subject was placed in a dimly lit room and asked to hold the 'goggles' in front of his eyes, which were closed throughout the experiment. Stimulation was performed at 2 Hz but with a random jitter of between 0 and 250 ms added to each inter-stimulus interval. This helps to minimise the effects of

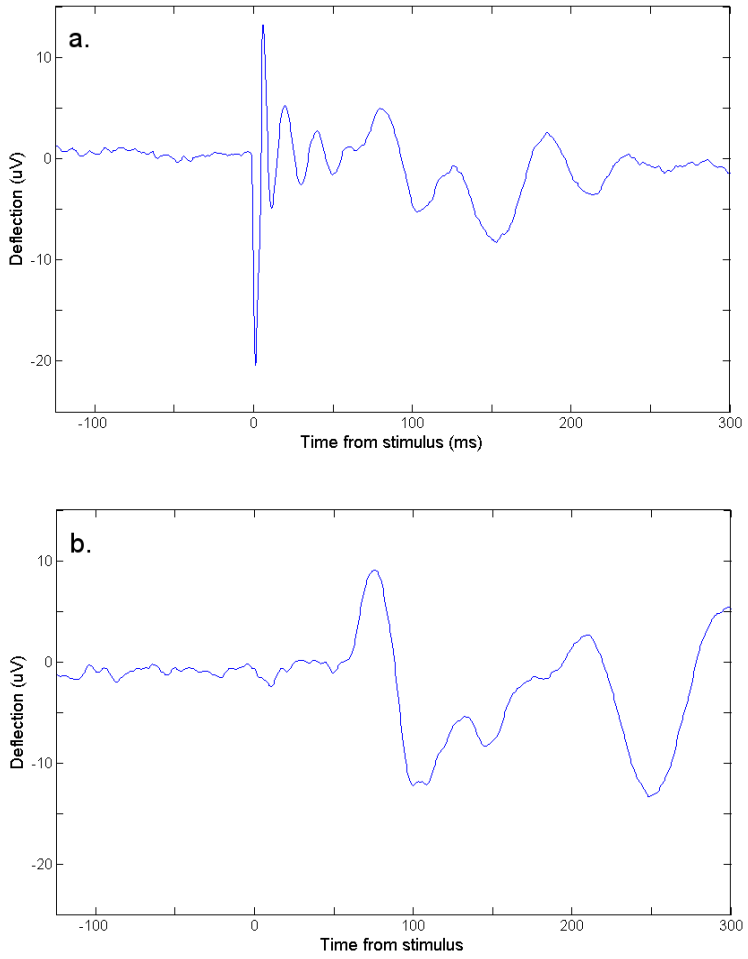

Figure 3.1.5. The adult flash VEPs obtained from the initial prototype LED goggles (a) and the final design (b). A large and distinct artifact is apparent at time = 0 in the upper trace, this artifact presents as an oscillation (or 'ringing') which decays by approximately time = 60 ms. A flash VEP waveform is apparent between 75 and 250 ms. There is no evidence of the time = 0 triggering artifact when using the re-designed goggles (b). These two VEPs were obtain using the same adult subject, and provide a good indication of the intra-subject variability of the flash VEP.

background electrical oscillations. The stimulus was presented in 12, ~30-second long blocks, with 20 seconds of rest in between. This additional complexity was unnecessary for a simple VEP experiment, but it allowed the block-paradigm software to be tested.

This experiment provided a (very large) 720-event data set. The data were exported in a raw format and, on the basis of the successfully obtained EEG event markers, cropped into 625 ms long epochs (125 ms pre-stimulus onset, 500 ms post-stimulus onset). Each epoch was de-trended using a linear extrapolation of the signal recorded over the first 125 ms. Of the 720 epochs, 54 were deemed to be corrupted by movement or other artifacts via visual inspection and were rejected. The remaining epochs were averaged and the resultant waveform is shown in figure 3.1.5a.

The result confirms that the goggle design is able to elicit the standard visual evoked potential. However, it is also very apparent that the process of providing the flash stimulus (or the process of time-locking the EEG system) is causing a substantial triggering artifact, almost certainly due to some form of electro-magnetic interference. The artifact consists of a classic 'ringing' effect associated with a rapid signal change despite all the components being independently isolated and shielded. After some investigation, the most likely source of this interference effect was found to be the transmission cable carrying the 20 mA current pulses from the subsidiary electronics to the goggles at the head. The use of optical fibres to carry the flash to the subject and thus negate the need for this cable was initially investigated, but eventually it was decided that the battery powering the LEDs (and the associated electronics) needed to be repositioned to form part of the goggles themselves. A representation of this arrangement is shown in figure 3.1.4b. Once completed, this new goggle design was tested using the same simple VEP paradigm described above. The result of this experiment is presented in figure 3.1.5b. A number of comparable

experiments was performed, none of which showed any further evidence of a stimulus interference artifact.

3.1.2.3 Preliminary data

Once all the triggering and stimulation methods had been perfected in adults, it was necessary to perform some preliminary experiments on infants before proceeding to a full EEG-NIR imaging paradigm. Most importantly, we had to test whether the LED goggles could elicit a VEP and a haemodynamic response in infants. Ethical approval was obtained from the Cambridgeshire Research Ethics Committee for all studies prior to subject recruitment. Two healthy neonates were therefore recruited to allow us to perform a simple flash-VEP experiment using the EEG system and, independently, a functional activation experiment using a limited number of optical topography channels. All the infants recruited to the studies described in this work were in-patients of The Rosie Hospital's Neonatal Unit. As a result, the majority of the infants available for recruitment were born prematurely, or had some condition at birth that necessitated in-patient care. The cohort cannot therefore be considered as simply healthy, term-age infants. However, no experiments were performed before the infants had achieved a good state of general health and were on the verge of being discharged.

The first infant had a gestational age of 36 weeks plus 3 days at the time of study. A single channel VEP experiment was performed, similar to that performed on an adult and described in the previous section. On the advice of our clinical research team, the experiment was timed to occur within an hour of the infant being fed. Newborn infants tend to be at their most docile immediately after a feed, and this makes application of the necessary equipment far easier. Performing these experiments is near impossible if the subject shows any significant agitation. The subject was in a quiet state in his cot, which was wheeled into a dimly-lit side-room where the EEG and

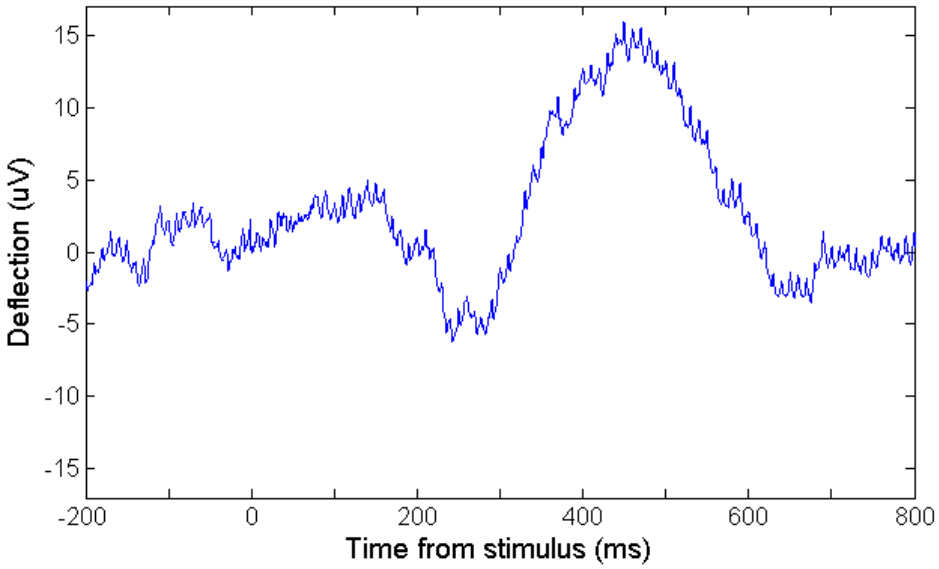

Figure 3.1.6. The grand average VEP response of one infant to the flash stimuli produced using our LED goggles, from a total of 133 responses. The flash occurs at time = 0, and a corresponding waveform is apparent from 150 to 650 ms. The signal to noise ratio, time scale and form is consistent with previous studies of the neonatal flash VEP. Note that the 100 Hz noise clearly present in the data corresponds to the 1st harmonic of the 50 Hz mains electricity frequency.

stimulation systems had been prepared. A single, standard clinical electrode was then affixed to 10-20 position Oz, and referenced to Fz. Before recording began we ensured that the contact impedance of this channel was below 5 kΩ and that the resulting EEG trace appeared continuous and relatively noise-free.

Once again, our LED goggles were operated using a block paradigm, which consisted of 12, 20-second long blocks of flash stimulation, interspersed by 30 seconds of rest. The inter-flash interval was 1.5 seconds plus a randomly assigned jitter of between 0 and 250 ms. This rate of stimulation is smaller than that used in adults because the neonatal flash VEP is known to have a significantly larger latency than that of adults, with features often persisting for longer than 500 ms post-stimulus (Ellingson 1986). The goggles were held approximately 1 cm in front of the subject's closed eyes by a Neonatologist member of the research team. The experiment lasted

approximately ten minutes and the subject remained in a still, quiet state throughout.

A total of 149 events were recorded, 16 of which were visually rejected due to movement or other artifacts. After each was de-trended the remaining data were averaged, and the result is shown in figure 3.1.6. A distinct deflection in response to the flash stimulus is apparent, with a timescale and shape consistent with a neonatal flash visual evoked potential. No triggering artifact is apparent.

The second healthy infant was the youngest infant studied in any of the experiments described in this work, with a corrected age of 35 weeks + 4 days, but again, was in a good state of general health by the time of the study. A simplified experiment was performed using two pairs of sources and two detectors of UCL's Optical Topography system, forming 4 near-infrared spectroscopy channels. The sources and detectors were fitted into a purpose built silicone-rubber array (figure 3.1.7). Silicone rubber is particularly suitable for optical topography arrays as it is rigid enough to maintain source-detector separations (which is important for accurate

Figure 3.1.7. The simplified, four-channel silicone rubber array design. The red circle represents a source pair (with output at both 690 and 850 nm) and the blue circles represent detectors. The grey regions are velcro pads which allow the array to be strapped to the head. The four channels (and separations) are S1-D1 (20 mm), S1-D2 (60 mm), S2-D1 (20 mm) and S2-D2 (20 mm).

measurement of concentration changes and image reconstruction) but flexible enough to conform to the head. It also has the advantage of being a very high-friction material; it tends to adhere to the skin and thus helps to reduce movement artifact.

The flash stimulation paradigm consisted of 12, 15-second blocks of LED stimulation at 8 Hz. This stimulation rate was chosen on the basis of previous successful studies (see table 3.1.1). The importance of the choice stimulation frequency is discussed further in section 3.1.2.4. The subject was initially asleep in her cot and the experiment was performed in a dimly lit room. The rubber array was centred over position Oz and attached to the head using a velcro strap. A layer of bandaging was then applied on top of the array and the optical fibres to provide extra support and minimise the effects of ambient light.

The experiment proceeded as before with the Neonatologist holding the LED goggles in front of the infant's closed eyes. After nine periods of stimulation, the subject began to wake up and move her head. It was decided that nine samples was probably sufficient and the experiment was stopped.

The data were band-pass filtered between 0.02 and 1.2 Hz (using a 5^{th} order Butterworth filter) in order to remove slow variations due to instrumental instability and vasomotion and the fast variations caused by the cardiac pulse. Each of the nine epochs was then separated and visually inspected. One epoch was rejected due to a significant movement artifact. It was also apparent from the raw data that a small triggering artifact occured on some optical topography channels. This feature had been identified previously in the use of UCL's Optical Topography System, and is an electrical artifact which can be easily removed by ensuring that the computer providing the event marker (i.e. the laptop in this case) is isolated from the mains electricity supply. This was performed for every subsequent experiment,

and the effect was not significant enough to undermine the experiment described here. Data were converted from measures of change in absorbance to measures of change in chromophore concentration using the Beer-Lambert law with a differential pathlength factor of 5.13 (Duncan et al. 1995), as described in section 1.2. The baseline was taken as the average of the 10 seconds of data immediately preceding the beginning of each stimulus block. The average changes in concentration of HbO_2, HHb and HbT for all four channels are shown in figure 3.1.8.

Comparing the five seconds of mean data around the peak change in each channel to the 10 seconds of mean data prior to stimulus onset, all four channels show a very significant increase in oxyhaemoglobin (two-tailed student t-test with a confidence level of 99 %). The signal-to-noise ratio (SNR) of all four channels is good. Using the changes in concentration of

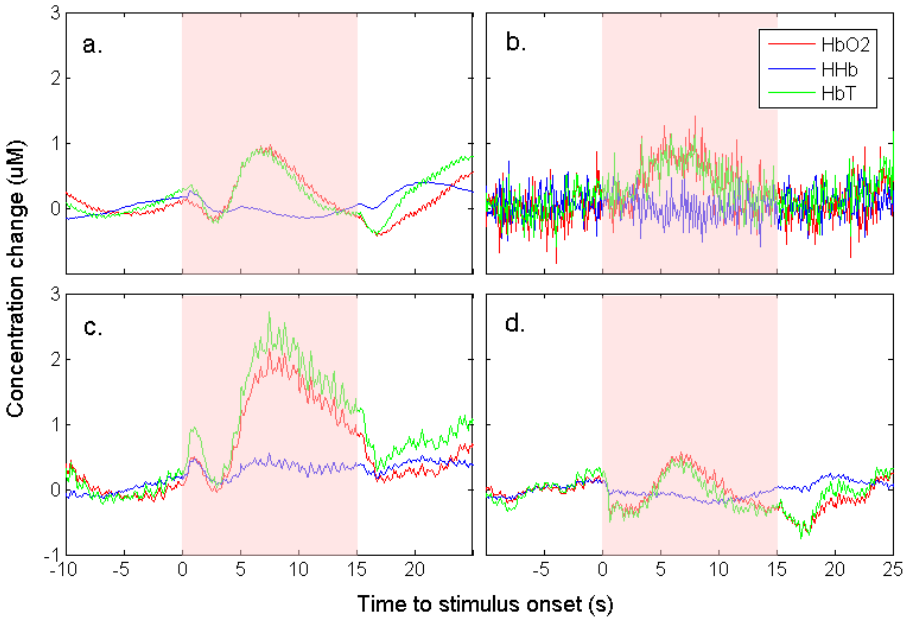

Figure 3.1.8. The average of nine haemoglobin concentration changes for 15 seconds of LED goggle flash stimulation at 8 Hz (represented by the shaded region) for channels 1-4 (axes a-d) as defined in figure 3.1.9. Channels 1, 3 and 4 show a rapid change between 0 and 3 seconds which is known to be an artifact. All four channels show a significant increase in oxyhaemoglobin concentration, peaking at 7 seconds post-stimulus onset.

HbO_2 the signal to noise ratios of channels 1-4 are 15.0, 7.98, 18.5 and 13.9 dB respectively. The SNR of channel 2 is surprisingly high, given its 60 mm source-detector separation. The changes in deoxyhaemoglobin concentration are more subtle. The SNR of deoxyhaemoglobin changes for channels 1-4 are 2.07, 1.56, 12.8 and 6.00 dB respectively. However, only channels 1, 2 and 4 show a significant (as defined above) decrease in HHb concentration. This is consistent with a typical haemodynamic flow response. Channel 3, which shows the largest change in HbO_2, exhibits a significant increase in HHb concentration.

This dataset provides strong evidence that the flash stimulation provided by our LED goggle arrangement is able to induce a haemodynamic response in newborn infants. Despite the apparent spatial variation in deoxyhaemoglobin signal (which is not necessarily unexpected given previous visual stimulation experiments performed in infants (table 3.1.1)), measures of oxyhaemoglobin concentration show a consistent and significant change which is time-locked to the onset of flash stimulation. These changes are significant on both sides of the sagital sinus, suggesting that flash stimulation produces bilateral changes in cerebral blood flow over a relatively large area of the visual cortex. Again, this is consistent with previous studies (Yamada et al. 2000).

3.1.2.4 Paradigm development

Having proven that our experimental arrangement is able to elicit both VEPs and functional haemodynamic responses, we set about designing a paradigm which would enable us to study the macroscopic neurovascular coupling associated with flash responses in the neonatal brain. It is important to note that it is conceivable for a study of the relationship between VEPs and the haemodynamic response to be performed using sequential data acquisition. However, because the electro-cortical and haemodynamic responses in infants are so variable, and the neurovascular coupling relationship

throughout these variations is itself of interest, a simultaneous method is preferable.

Ideally such a paradigm should include some form of variation in stimulus presentation in order to induce different electro-cortical and haemodynamic responses. The consistency (or otherwise) of the neurovascular coupling relationship throughout these variations can then be studied. For a flash stimulation experiment, there are four possible variables: flash brightness, flash duration, stimulation rate (number of flashes per second) and the duration of each block of flashes. The variation of brightness and duration of each flash would require further alterations to the electronics described in section 3.1.2.2, and therefore it was decided that these would remain constant.

Varying the duration of the stimulus block is an interesting experimental paradigm as it relates to the issue of habituation. In adults it has been shown that continuing stimulation for longer periods (anything greater than ~15 seconds) can result in the haemodynamic response returning to a steady baseline before the stimulus block has come to an end (Hathout et al. 1994, Condon et al. 1997). This has raised questions about whether the cerebral flow response habituates despite the level of stimulus-related neuronal activity remaining constant; i.e. is there a decoupling of the neurovascular relationship (Frahm et al. 1996)? At present it is accepted that there are linear and non-linear aspects to the relationship between neuronal activity and localised changes in CBF (Krüger et al. 1999, Miller 2001).

In 2002, Obrig et al. set about explicitly comparing the simultaneously-recorded VEP and functional haemodynamic response in adults during extended (1 minute long) stimulation periods in an EEG-NIRS experiment. Their results tentatively suggested that a linear relationship between the amplitude of certain VEP features and changes in HbO_2 and HHb concentration appeared to be maintained throughout habituation. No similar

experiments have been performed in young infants, and the result of such a study would not only be important from the perspective of the development of neurovascular coupling mechanisms but also with respect to habituation itself, which is an important feature of neurological development (Colombo and Mitchell 2009, Nakano et al. 2009). However, in order to pursue any such paradigm it would first be helpful to know which flash stimulation frequency is optimal for the production of both functional haemodynamic responses and visual evoked potentials.

As is apparent from table 3.1.1, there has been a large variety of stimulation rates applied in previous studies of infant visual activation, ranging from 1 Hz to 14 Hz. As far as the author is aware, there has been no study (using any modality) which has sought to determine how the functional haemodynamic response varies with flash stimulation rate in infants. Given the number of NIRS studies of the flash response in neonates, and the continued popularity of such paradigms, it seems a relevant question to seek to answer.

In adults, the flash VEP has a total duration of approximately 300 ms after the flash. In infants it is significantly longer; as much as 750 ms (Ellingson 1986, Odom et al. 2004). The result of repetitive flash stimulations at a rate faster than ~3 Hz in adults and ~1.5 Hz in infants is that these visually-evoked components begin to smear together and form an oscillation. This is known as the steady-state visual evoked potential or SSVEP. This response is well documented and quite striking in adults (Vialatte et al. 2010) but has also been studied repeatedly in infants (Taylor and McCulloch 1992, Birca et al. 2006, Pieh et al. 2009).

An experiment designed around SSVEPs and the variation of stimulus repetition rate lends itself to analysis in the frequency domain, which allows event-related EEG components to be identified even in cases where the

time-domain signal-to-noise ratio is low (Victor and Mast 1991, Isler et al. 2007, Pieh et al. 2009).

Adding further motivation for such an experiment is the fact that a comparable paradigm has been applied in adults. In 2006, Koch et al. recorded the SSVEP and the resulting haemodynamic response in adults to flash stimulation at rates between 1 and 25 Hz. The most striking result of this study was the fact that a peak in SSVEP amplitude at the alpha wave frequency is not associated with a peak in the haemodynamic response. It was hypothesised that this was because groups of neurons that are already synchronously firing to produce the spontaneous alpha wave do not show an increased metabolic demand when recruited to contribute to the SSVEP. The authors of this study went on to examine the relationship between an individual's alpha frequency and their electro-cortical and haemodynamic responses to steady state flash stimulation (Koch et al. 2008). As described in section 1.2, newborn infants do not exhibit background activity comparable to the alpha wave; they have no posterior dominant rhythm. Instead they exhibit global, mixed, low-frequency background oscillations. Whether any discrepancy exists between peak frequency of the SSVEP and the haemodynamic response in infants is unknown, though previous studies show that a haemodynamic response can be observed for stimulation at 8 Hz (table 3.1.1), despite the corresponding SSVEP being somewhat variable (Pieh et al. 2009).

A study of the neurovascular coupling relationship in response to a varying rate of flash stimulation in infants would ideally cover a range of ~1-15 Hz. This would encompass the stimulation frequencies employed in the majority of NIRS and fMRI studies, and also the range over which Koch et al. discovered a decoupling of the SSVEP and haemodynamic responses in adults. However, the paradigm must not exceed a duration of around 15-20 minutes, as it is unrealistic to expect a newborn infant to remain cooperative for any longer. Given this limit, a balance must be achieved between the

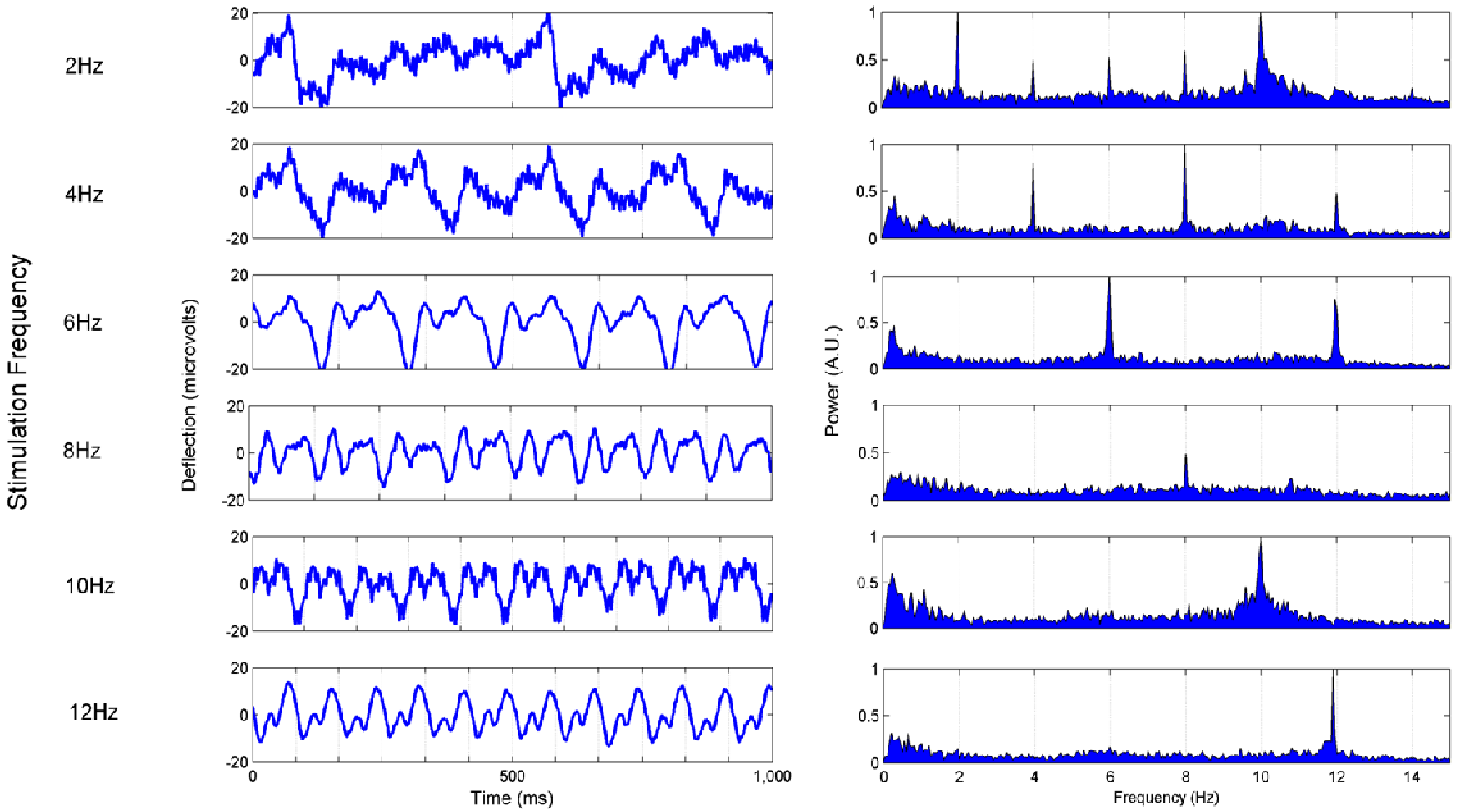

Figure 3.1.9. The SSVEPs recorded from EEG channel Oz-Fz for six stimulation frequencies in an adult, presented in the time domain (each 20 second stimulation block is cut into 1-second epochs, grouped by stimulation frequency then averaged) and the frequency domain (the normalised average power spectra produced from each 20-second stimulation block, right column).

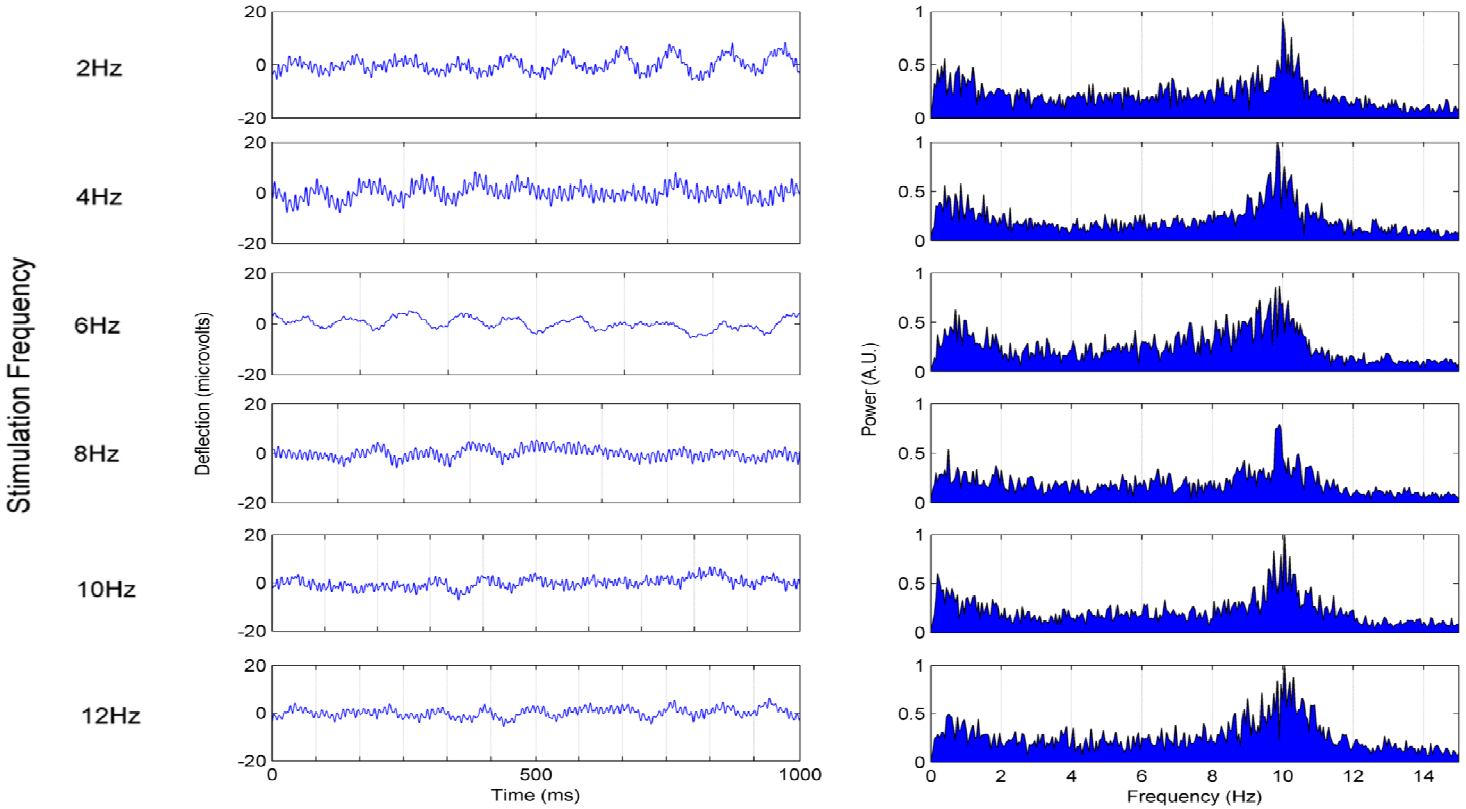

Figure 3.1.10. The data recorded using the same stimulation paradigm which resulted in the data shown in figure 3.1.8 but with the goggles placed above the eyes so as to not be visible. The absence of a signal provides an explicit proof that the results presented in figure 3.1.9 are not the result of electrical interference.

number of different stimulation frequencies employed and how many times a block of a given stimulation frequency can be repeated. A good number of block repetitions is essential if a reasonable signal-to-noise ratio is to be obtained in both VEP and optical topography measurements.

Three, 20-second long blocks of stimulation at rates of 2, 4, 6, 8, 10 and 12 Hz, randomly ordered and interspersed with 30 seconds of rest constitutes a paradigm with a total duration of 15 minutes. One disadvantage of the analysis of SSVEP data in the frequency domain is that any stimulation-locked noise (i.e. any remnants of the trigger artifact described in section 3.1.2.2) will be indistinguishable from SSVEP signal. The data shown in figures 3.1.9 and 3.1.10 were recorded in a single adult, using a single EEG channel (Oz-Fz) and the block paradigm described above. The presented time-domain data were obtained by cutting the three 20-second long stimulation blocks at each frequency into 1-second epochs and taking a mean of these epochs. The average power spectra are the means of the power spectra of each 20-second long stimulation block. These experiments were performed partly as a test of the stimulation paradigm and partly to identify any remaining interference artifacts. They are presented here to show the distinctive nature of SSVEP responses in adults, and also the suitability of frequency domain analysis. This result is consistent with previous studies of the adult SSVEP (e.g. Koch et al. 2006).

3.1.2.5 Array design and application methods

One of the aims of this visual activation experiment was to show that the methods described in section 2 for simultaneous EEG and NIR imaging were applicable to the neonate. Without explicit testing, it is difficult to know what practical difficulties may be encountered when attempting to apply such complicated apparatus to an infant in a clinical setting. Such difficulties are likely to be more pronounced when studying neurologically damaged infants in intensive care.

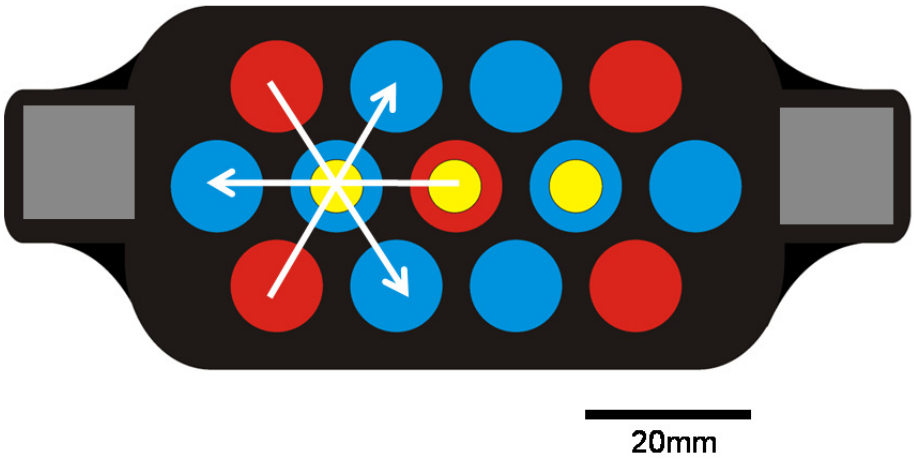

Figure 3.1.11. The silicone-rubber EEG-NIR imaging visual cortex array. Red circles represent NIR imaging sources and the blue circles detectors. Those probes with yellow centres are opto-electrodes. The grey areas represent velcro connectors to allow the array to be strapped to the head and the white arrows explicitly show three optical topography channels which sample the volume beneath one of the opto-electrodes.

The EEG-NIR imaging array designed for this visual activation experiment is shown in figure 3.1.11. This array was designed using the rules set out in section 1.2.3.3 which optimise diffuse optical imaging arrays. However, it was also important to maintain the visual cortex 10-20 electrode locations as closely as possible, to be consistent with previous neonatal VEP studies.

The final array design consisted of 13 probes; 10 standard optical fibre bundles and 3 opto-electrodes. Five probes were optical source fibres emitting both 670 and 850 nm light, and the remaining 8 were detector fibres. The array was designed around a central opto-electrode which was coupled to 10-20 position Oz using the methods described in section 2. Either side of this central probe were two more opto-electrodes positioned approximately at O1 and O2. These positions were approximate because a single array was used for multiple subjects. The array was maximally accurate (i.e. the positions O1 and O2 were exact) for an infant with a head circumference of 36 cm, which is a relatively large term infant. The

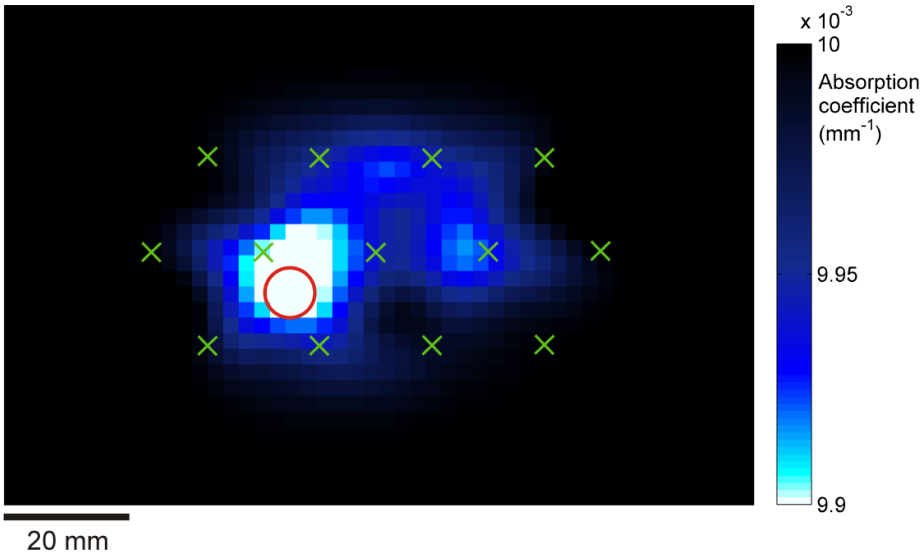

Figure 3.1.12. A reconstructed image of the change in absorption coefficient at 670 nm, obtained from a dynamic phantom using the imaging array shown in figure 3.1.11. This image represents a depth of 15-18 mm. The array positions are indicated by the green crosses, whilst the red circle shows the position and size of the phantom target.

positioning was less accurate for smaller infants, but even for an infant with a 30 cm head circumference, the location error would be only 3 mm.

The array contained a total of 40 source-detector pairs, of which 18 had a separation of 18 mm, 10 had a separation of 36 mm, 8 had a separation of 47 mm and 4 had a separation of 65 mm. Although the longer separations were unlikely to yield useful data (as not enough light can traverse that distance through tissue) this array still provided relatively dense, over-lapping sampling of the occipital lobe. The smallest separation (18 mm) was shorter than is optimal for sampling of the cerebral cortex. However, as our previous in-vivo study (section 3.1.2.3) and recent in-vivo and theoretical work (Taga et al. 2007, Heiskala et al. 2009) have both suggested that 20 mm is a suitable source-detector separation to sample the neonatal cortex, we believe the compromise made between the size of the array and the length of the shortest separation was reasonable.

As an explicit test of the suitability of this array design for NIR optical imaging, we performed a simple imaging experiment using the UCL optical topography system and a solid, dynamic phantom. The phantom consists of an epoxy resin with comparable optical properties to bulk tissue ($\mu_a = 0.01$ mm^{-1} and $\mu_s' = 1$ mm^{-1}) (Hebden et al. 2008). Embedded within the resin, at a depth of approximately 15 mm is a spatially discrete region containing a thermally-activated pigment, which becomes less absorbing as it is heated. By passing current through a resistor at the centre of the region of pigment a localised change in optical absorption is produced, which is designed to mimic changes in cortical haemoglobin concentration. An image of a change in optical absorption within this phantom was produced using our visual cortex array, and is shown in figure 3.1.12.

Image reconstruction was performed using the linear methods described in section 1.2.3.2. To evaluate the suitability of the geometrical arrangement of optical sources and detectors standard optical fibre probes were used in all positions. The reconstructed image shows a relatively focal decrease in optical absorption at 670 nm, the reconstructed pixel with the minimum value of optical absorbance was 3.8 mm from the centre of the phantom target. This result confirms that the density and arrangement of sources and detectors in this array is suitable for optical topography.

The process of applying the combined EEG-NIR imaging array involves several stages and is not just a question of strapping it to the head of the subject. The opto-electrode contact sites have to be carefully abraded, and it can be difficult to correctly position an opto-electrode over the abraded site when the opto-electrode is part of an extended array. This difficulty is addressed by the following procedure. First, the standard optical fibre probes (i.e. the 10 outer positions of figure 3.1.11) are fitted into the silicone rubber array, whilst the three central positions are left empty. The Oz position is located, and the array is centred over it, using adjustable velcro straps to hold the array in place. The three opto-electrode contact sites are

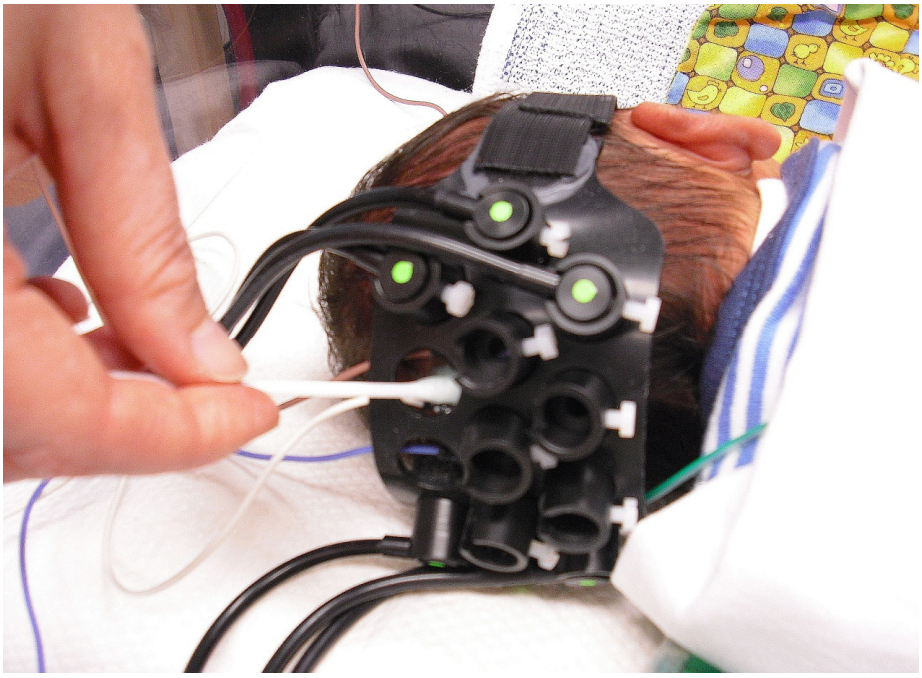

Figure 3.1.13. A photograph showing the abrading of an opto-electrode contact site through an empty position in the imaging array. Note that the clinician in the photo is only demonstrating the application process, as the three opto-electrodes had already been applied before the photograph was taken. A number of the optical fibres (black cables) have yet to be fitted into the array, as sometimes it was easier to fit them after the process of abrasion. The three electrode leads (brown, white, blue can be seen emerging from the array.

Figure 3.1.14. A photograph of an infant during the combined EEG-NIR imaging study. Note the layer of bandaging applied over the array and the goggles held in front of the subject's eyes.

then abraded through the empty probe positions using a cotton bud and an abrasive paste (NuPrep, Weaver and Co., USA) as per standard, clinical EEG application (see figure 3.1.13). Following the abrasion of a contact site, the translucent electrode coupling gel (Et Medical Devices, Italy) is introduced into an opto-electrode, which is then slotted into the relevant empty array position. This approach ensures that each opto-electrode is located exactly over the site that has been abraded, minimising electrode contact impedance. Once all the probes have been attached, a reference electrode is placed at Fz and a ground electrode at approximately Cz. The electrode leads are connected to the appropriate EEG system inputs and a layer of bandaging is strapped around the head of the subject, over the imaging array (figure 3.1.14). This helps to achieve a good optical contact, as well as minimise movement artifacts and the effects of ambient light.

3.1.3 Results

A total of six healthy subjects with a mean corrected age of 37.6 weeks were recruited from The Rosie Hospital Neonatal Unit, with informed consent being obtained from all parents in advance of each study. A summary of the medical histories of these infants is given in table 3.1.15. In all six infants we performed an EEG-NIR imaging experiment with varying-frequency flash stimulation, using the visual cortex imaging array described in the previous section. In two of the six infants (referred to as OEV_01 and OEV_02) we employed a paradigm of six stimulation frequencies (2,4,6,8,10 and 12 Hz). Three blocks of 20-second long stimulation were performed at each frequency, in a randomised order and interspersed with 30 seconds of rest. In the remaining four infants (OEV_03 to OEV_06) we employed a simplified paradigm using six blocks of 20-second long stimulation at only three frequencies: 2, 5 and 8 Hz.

All six studies were completed successfully, with all subjects remaining relatively still and quiet throughout. Only one infant (OEV_05) was observed to open their eyes during the course of the study. The contact impedance of each opto-electrode was measured prior to the start of recording using the EEG SystemPlus software. We aimed to achieve contact impedances below 5 kΩ in each case, though in some infants this proved difficult despite repeated application of all electrodes and opto-electrodes. The highest contact impedance recorded was 9.8 kΩ, but this did not produce an excessively noisy EEG trace and so the experiment was continued. EEG data were recorded with a sample rate of 2048 Hz, with a band pass filter from 0.3 to 1000 Hz and a 50 Hz notch filter.

Optical data were inspected for movement artifacts before being band-pass filtered (5^{th} order Butterworth filter, 0.02-1.2 Hz) and cropped into 60 second-long epochs on the basis of the position of each stimulus block. The optical dataset from infant OEV_02 was completely rejected because of excessive artifacts, which were likely to be the result of poor coupling of

Infant	Age at birth (Weeks + days)	Age at study (Weeks + days)	Previous pathology	Drug regime	Condition	Behavioural state during study	Experiment performed
OEV_01	35	36+3	Duplex kidney	Antibiotics	Stable, self-ventilating	Soundly asleep, almost no movement	Full, six-frequency paradigm
OEV_02	36+1	36+4	Hypothermia and hypoglycaemia	Vitamin supplement	Stable, self-ventilating	Soundly asleep, almost no movement	Full, six-frequency paradigm
OEV_03	34+3	36+3	Respiratory distress	Antibiotics, vitamin supplement	Stable, self-ventilating	Variable, some movement	Reduced three-frequency paradigm
OEV_04	37	39+5	Intrauterine growth retardation, hypoglycaemia	Vitamin supplement	Stable, self-ventilating	Asleep, minimal movement	Reduced three-frequency paradigm
OEV_05	37	39+5	Laryngomalacia	Vitamin supplement	Stable, self-ventilating	Variable, eyes open at some points. Some movement.	Reduced three-frequency paradigm
OEV_06	35+4	36+3	None	Vitamin supplement	Stable, self-ventilating	Asleep, minimal movement	Reduced three-frequency paradigm

Table 3.1.15. A summary of relevant information for each of the six flash-stimulus EEG-NIR imaging subjects.

certain optical channels to the scalp. Once cropped, each epoch was individually inspected for artifacts before being allowed to contribute to the mean result.

The EEG data were exported in a raw format and visually inspected for any gross artifacts before being low-pass filtered with a threshold of 40 Hz. This filter is applied in order to further reduce any 50 Hz electrical mains interference (although the notch filter removes most of the 50 Hz component, its harmonics are often still apparent). Using the associated triggers, the EEG dataset was separated into 20-second long blocks coinciding with flash stimulation, and these blocks were then divided into twenty, 1-second long epochs. The 20-second long blocks were used to produce power spectra at each stimulation frequency using a fast Fourier transform. Power spectra were also obtained for the EEG data in the absence of any visual stimuli, using the latter 20 seconds of data from each 30 second rest period. The 1-second long epochs were averaged together after being subjected to a simple threshold artifact rejection algorithm, which excludes epochs where the peak-to-peak amplitude exceeds 300 μV. This threshold was chosen on the basis of inspection of previous infant EEG recordings, and was found to provide reasonably accurate identification of larger (i.e. movement) artifacts. These data processing methods are exactly that performed on the adult SSVEP data presented in figures 3.1.9 and 3.1.10.

In order to assess the significance of any SSVEP response in the frequency domain, it is necessary to compare the power spectra recorded during rest periods with the power spectra recorded during periods of stimulation. Because of the significant natural variation in EEG content in infants, the absolute scale of power spectra calculated from different periods of data can vary significantly. Therefore, before stimulus and non-stimulus power spectra can be compared, each is scaled by its total power content (i.e. the

power at each frequency is divided by the sum of the power at all frequencies).

The total power contained in a 0.5 Hz window, centred at each flash stimulation rate (and it's first two harmonics) is then calculated for each stimulus block and each of the three EEG channels. The same calculation is performed for each non-stimulus power spectrum (of which there are 18; one for each rest block). The resulting frequency-specific stimulus and non-stimulus power contributions can then be compared using a suitable hypothesis test (i.e. a student t-test, with a confidence level of 95 % or above).

3.1.3.1. Infant OEV_01

The SSVEP data obtained for the varying-frequency stimulation paradigm in infant OEV_01 are shown in figure 3.1.16. Out of a total of sixty, the numbers of 1-second epochs automatically rejected for each stimulation rate (2,4,6,8,10 and 12 Hz) were 10,1,1,6,1 and 3 respectively. The first feature to note about this dataset is that the response appears quite indistinct. This is particularly true of the time-domain data (left column), as any frequency components related to the stimulation rate are not apparent in these averages. The frequency domain data (each axis of which is the average of three power spectra, one for each of the 20-second long stimulation blocks) exhibits some observable response at 2 Hz and 4 Hz stimulation rates, although it is much less apparent than in the adult studies. The statistical analysis described above for the SSVEP data of infant OEV_01 (figure 3.1.16) indicates that there is a power increase associated with 2 Hz stimulation, but it only reaches significance for the electrode position Oz, and not for positions O1 and O2 (at a confidence level of 95 %). There is also a significant increase in power measured at all electrodes for 4 Hz flash stimulation, but not for any higher stimulation rates at any electrode. The SSVEP data obtained with infant OEV_02 show a very similar result; with only 2 and 4 Hz stimulation rates producing a significant response.

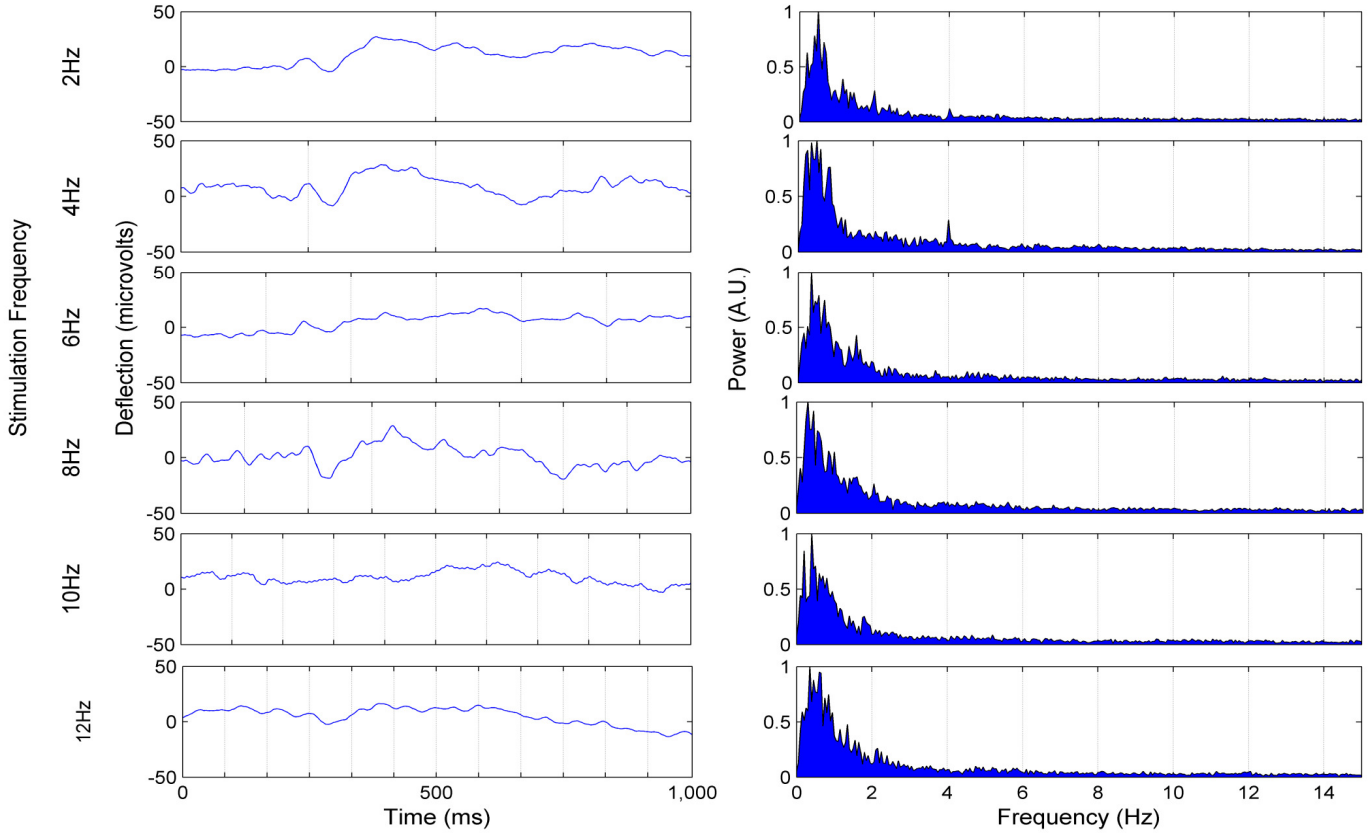

Figure 3.1.16. SSVEP data recorded in channel Oz-Fz in infant OEV_01 for six flash stimulus frequencies presented in the time domain (left column; each 20 second stimulation block is cut into 1-second long epochs which are grouped by stimulation frequency and averaged) and frequency domain (right column; the average of the power spectrum of each 20 second stimulation block). Note the lack of any consistent stimulus-locked response.

Although SSVEPs in infants are known to be significantly less distinct than those in adults (Ellingson 1986, Pieh et al. 2009), these datasets exhibit a lower signal-to-noise ratio than is expected.

Figure 3.1.17 shows the average changes in oxy, deoxy and total haemoglobin recorded in a representative channel of the optical topography array for each of the 6 stimulus frequencies used with subject OEV_01.

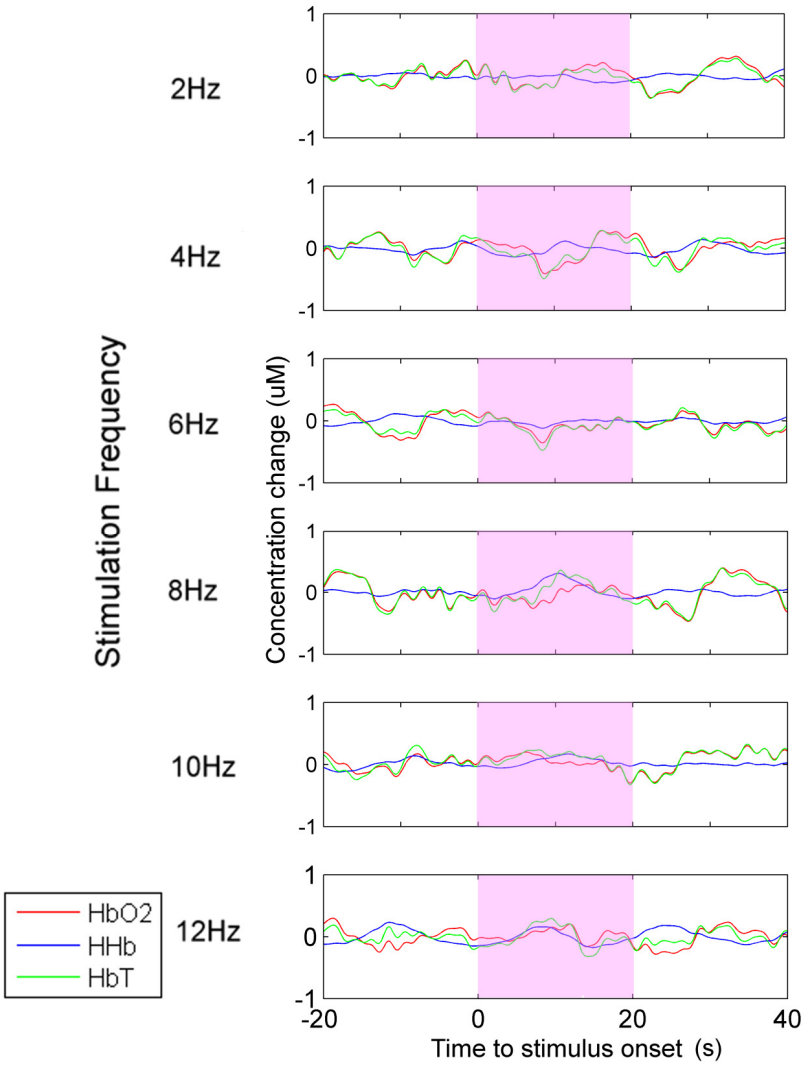

Figure 3.1.17. The average haemoglobin concentration changes for a representative channel for all six flash stimulation rates in subject OEV_01. The shaded regions are the periods of stimulation.

There is no distinct haemodynamic response to flash stimulation at any frequency. This is unexpected given the large test response described in section 3.1.2.3. Still present in the average data are relatively large (~0.2 μM) spontaneous oscillations in haemoglobin concentrations, which suggests that the number of stimulus trials may be too small.

As described previously, the haemodynamic response to visual stimulation in neonates is highly variable, so a null-result in one infant is not necessarily indicative of a failure of the experimental paradigm. One concern with all optical topography experiments is ensuring that the light that is detected has actually passed through the tissue of the subject, rather than being reflected directly into the detector. This requires that good optical isolation and a tight fit to the scalp are maintained.

Whether or not an optical channel is sampling tissue can be easily established by observing the presence of a subject's heart rate in the optical topography data. Figure 3.1.18 shows the normalised power spectrum of the same optical topography channel shown in figure 3.1.17. This clearly indicates that the heart rate is being recorded. An additional consideration is related to array design and the dynamic range of the optical system. As described previously, a major factor in the design of any optical-topography array is the balance between source-detector separation and obtaining a level of light incident at the detector which is large enough to exceed the level of background noise but is small enough not to saturate the detector. This also affects whether the array is sampling the intended volume of tissue, as the more channels which are saturated or not recording enough light, the lower the sampling density of the array. Figure 3.1.19 shows the mean intensity recorded across each channel as a function of source-detector separation for the optical topography dataset recorded from infant OEV_01. It shows that the shortest separations are not saturating the detectors, whilst many channels exceed the noise floor (of approximately 3×10^{-4}) for separations as large as 47 mm.

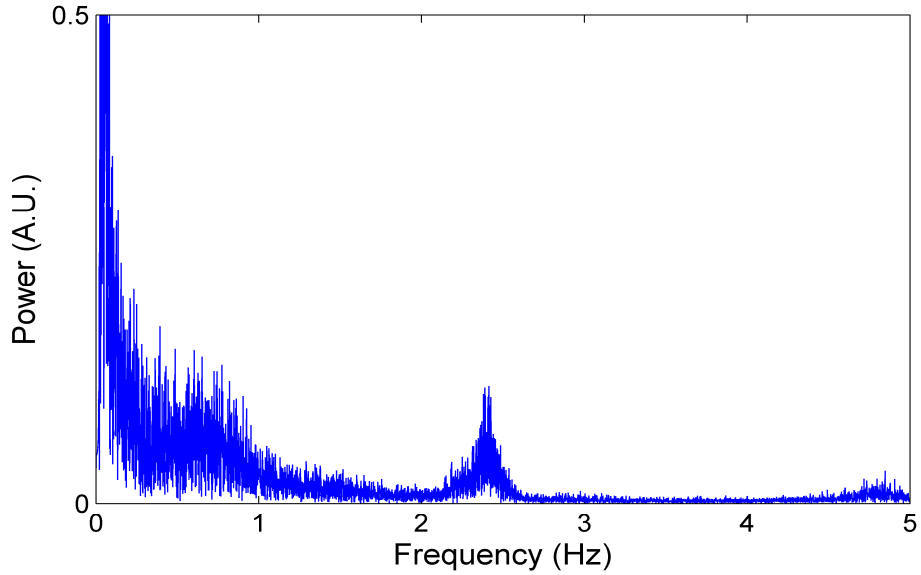

Figure 3.1.18. The normalised power spectrum of a representative optical topography channel. The contribution of the cardiac pulse is very apparent at around 2.4Hz. The activity below 1 Hz will include respiration rate and vasomotion.

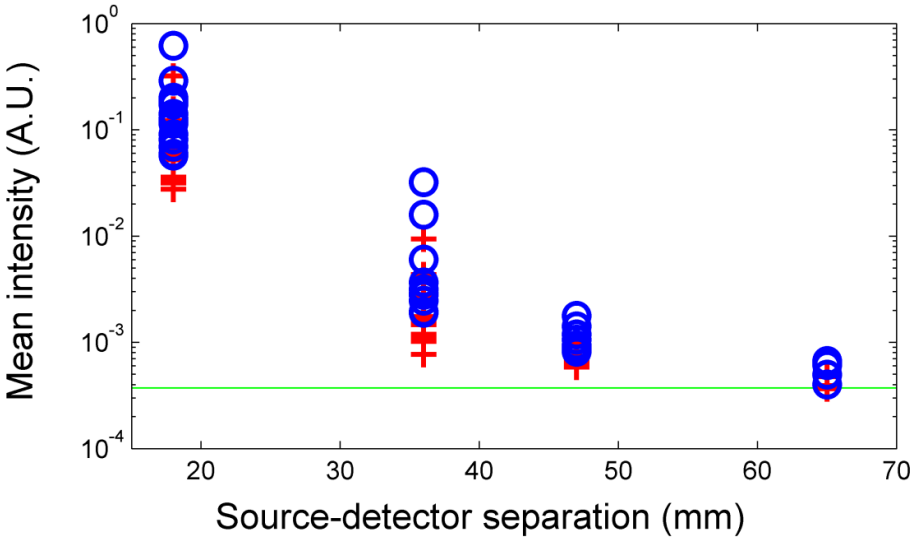

Figure 3.1.19. A plot of mean intensity against source-detector separation for the 40 channels of the visual cortex array. This is taken from the optical topography dataset of infant OEV_01. The red crosses are 670 nm sources and the blue circles are 850 nm sources. Channels which are partially saturated will show an intensity of greater than ~1-1.5 (A.U.), whilst complete saturation causes the detector to shut down and produce an intensity measure of approximately zero. The approximate noise floor is represented by the green line. It is therefore apparent that no channels are saturating, and a reasonable level of light is incident for all 36 mm channels, and many 47 mm channels.

3.1.3.2 Infants OEV_03 to OEV_06

As the signal-to-noise ratios for both recording modalities appear less than expected for infant OEV_01 (and partially in infant OEV_02), the paradigm was simplified for the remaining four infants. By reducing the number of different stimulus rates from six to three, the number of stimulus blocks for each stimulus rate could be doubled. This yields 120, one-second long SSVEP epochs and six optical topography trials for each stimulation frequency. The paradigm was therefore redesigned to include only three flash stimulation frequencies: 2, 5 and 8 Hz.

Figure 3.1.20 shows the time-domain SSVEP results of the reduced-paradigm performed in four infants (OEV_03-OEV_06). Figure 3.1.21 shows the corresponding frequency domain data. The results of the EEG processing and statistical analysis for each infant at each stimulation frequency and for each EEG channel are shown in table 3.1.22. In general, this reduced paradigm produced a much improved SSVEP signal-to-noise ratio, as can be seen in the form (and scale) of the average 1-second epochs shown in figure 3.1.20. Statistically significant changes in stimulation-frequency power were found at all three stimulation frequencies, in all infants except OEV_05.

The average changes in oxy, deoxy and total haemoglobin concentration for a representative channel of the visual cortex array, for all four infants and all three stimulation frequencies are presented in figure 3.2.23. Again, there appears to be no distinct haemodynamic response observable in any of these four infants, at any stimulation frequency. The level of background haemodynamic oscillations present in this mean data is not clearly less than that obtained in infant OEV_01, despite having doubled the number of blocks of flash stimulation at each frequency. This is likely due to the fact that movement artifacts were more abundant in the optical topography data of infants OEV_03-OEV_06 (which is consistent with their noted

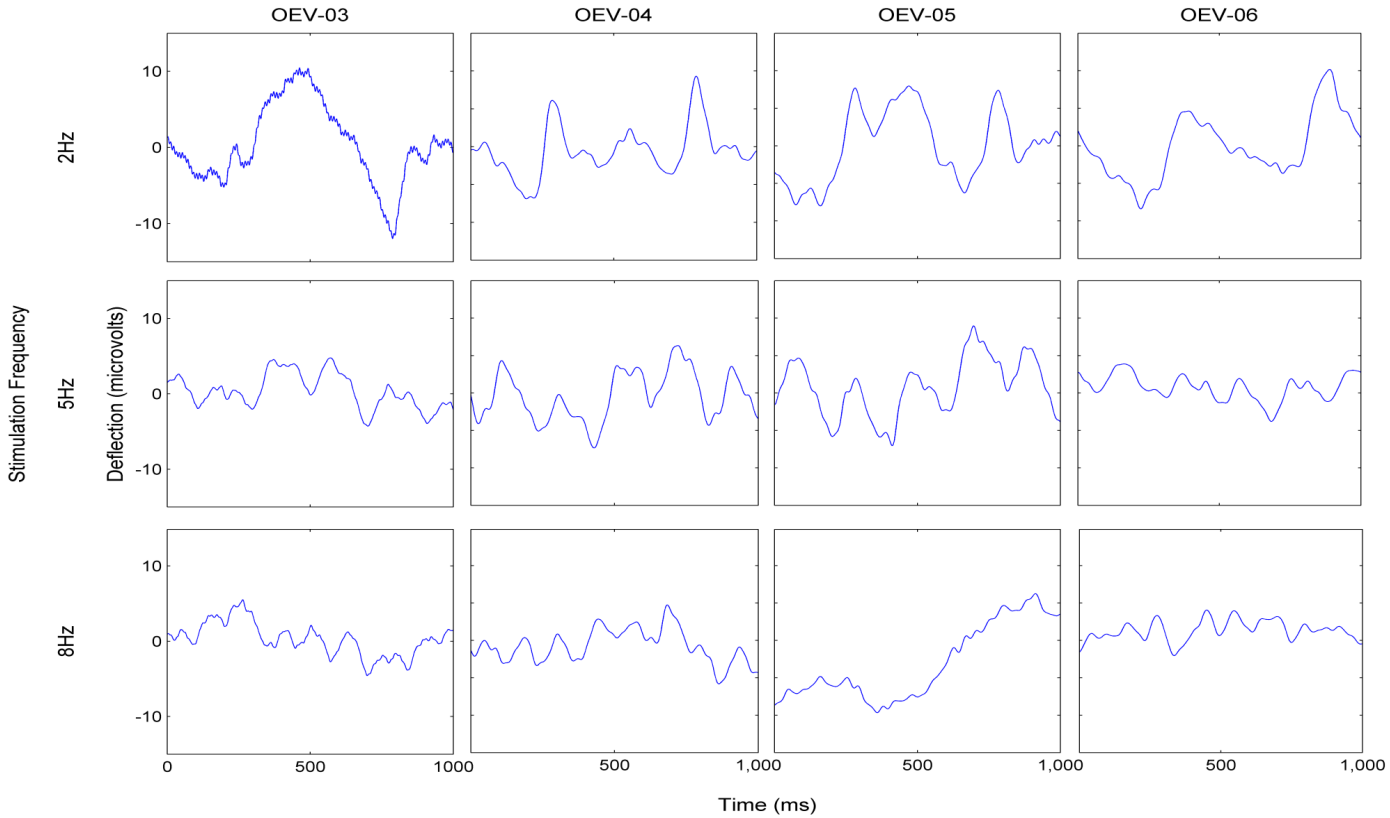

Figure 3.1.20. The average 1-second stimulation epochs for all four subjects and all three stimulation frequencies recorded over Oz-Fz (the 20 second stimulation blocks are cut into 1-second epochs, grouped by stimulation frequency and averaged). Note that the signal-to-noise ratio for all infants (particularly OEV_04) is much improved in this reduced paradigm.

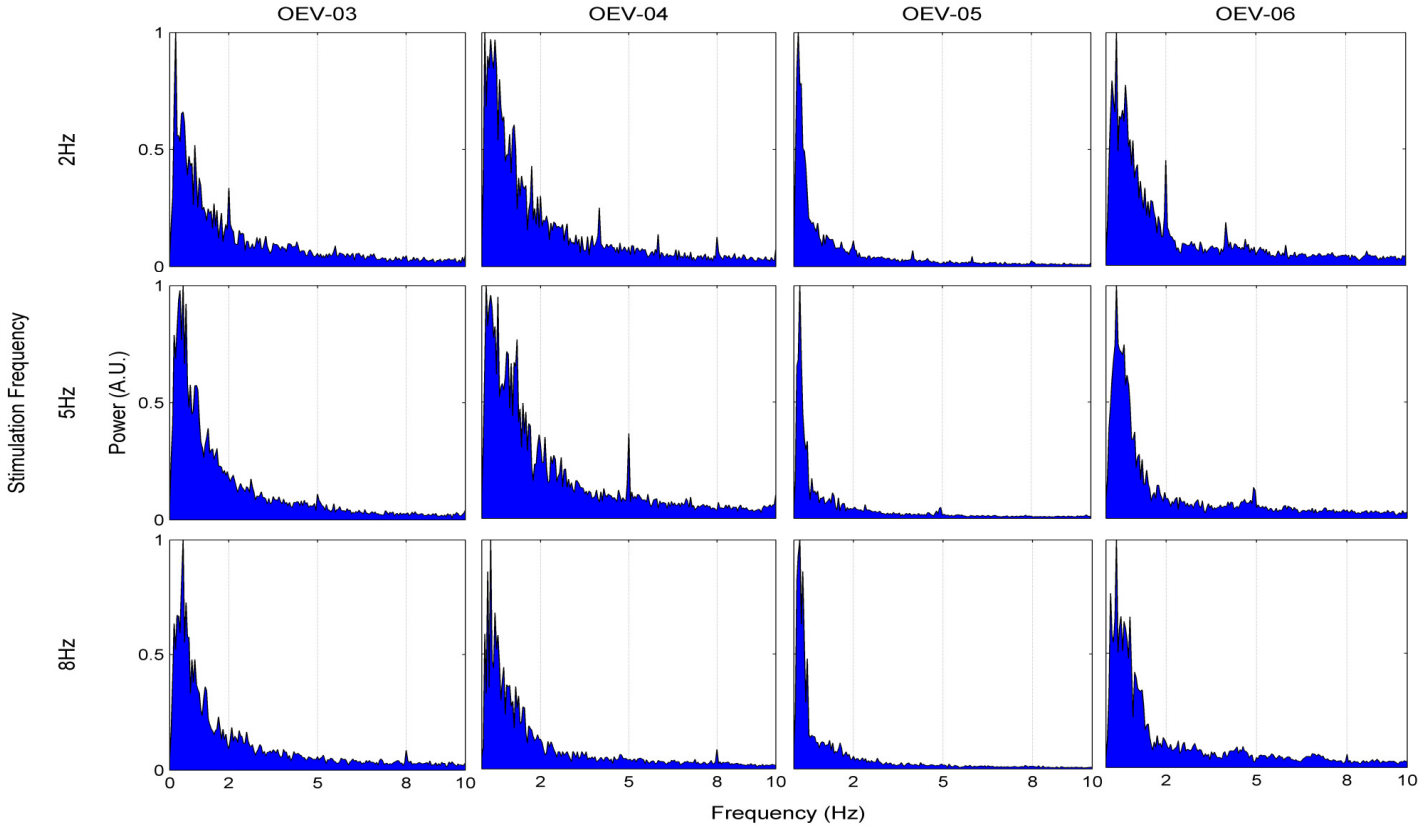

Figure 3.1.21. The mean within-stimulus power spectra for all four subjects and all three stimulation frequencies of the reduced paradigm recorded over Oz-Fz. Note that peaks corresponding to the stimulation frequency are apparent in all infants at nearly all stimulation frequencies.

	Stimulation Frequency (Hz)	Number of epochs rejected	Power increase significant at 95%? Y/N (p-value, 2 s.f.) O1	Oz	O2
OEV_03	2	9	Y (4.2e-3)	Y (5.2e-3)	Y (8.4e-4)
	5	6	Y (1.1e-6)	Y (8.1e-3)	Y (6.3e-5)
	8	3	Y (8.5e-4)	Y (1.0e-3)	Y (3.4e-3)
OEV_04	2	3	N (7.3e-2)	Y (4.3e-2)	Y (1.7e-2_
	5	1	Y (6.1e-6)	Y (3.7e-5)	Y (1.4e-4)
	8	2	Y (1.6e-2)	Y (2.4e-2)	N (1.7e-1)
OEV_05	2	2	N (3.3e-1)	N (2.7e-1)	N (2.3e-1)
	5	4	N (3.2e-1)	N (4.8e-1)	N (3.3e-1)
	8	7	N (9.7e-1)	N (9.7e-1)	N (9.3e-1)
OEV_06	2	2	Y (2.4e-4)	Y (1.8e-4)	Y (2.5e-4)
	5	2	Y (2.6e-3)	Y (1.1e-3)	Y (1.4e-3)
	8	2	N (2.7e-1)	N (1.7e-1)	N (1.5e-1)

Table 3.1.22. The results of the automatic EEG threshold epoch rejection algorithm and the statistical analysis of SSVEP data described above. Whether the power increase was significant (at the 95 % confidence level) is highlighted and the p-values are provided in each case. Only OEV_05 shows no significant response at any frequency, despite fundamental and harmonic peaks being apparent in the corresponding power spectrum data at a stimulation frequency of 2 Hz.

behavioural state). This resulted in an average block rejection ratio of approximately 27 %. Once again, the frequency content of each optical topography dataset was examined, and the heart rate was present for all four datasets, suggesting that optical isolation was not a significant issue.

In order to compare the SSVEP and haemodynamic responses, we were hoping to obtain a response in each individual infant, or even in individual trials as was the case for the data presented in section 3.1.2.3. As this is clearly not the case for infants OEV_03-OEV_06, the grand average

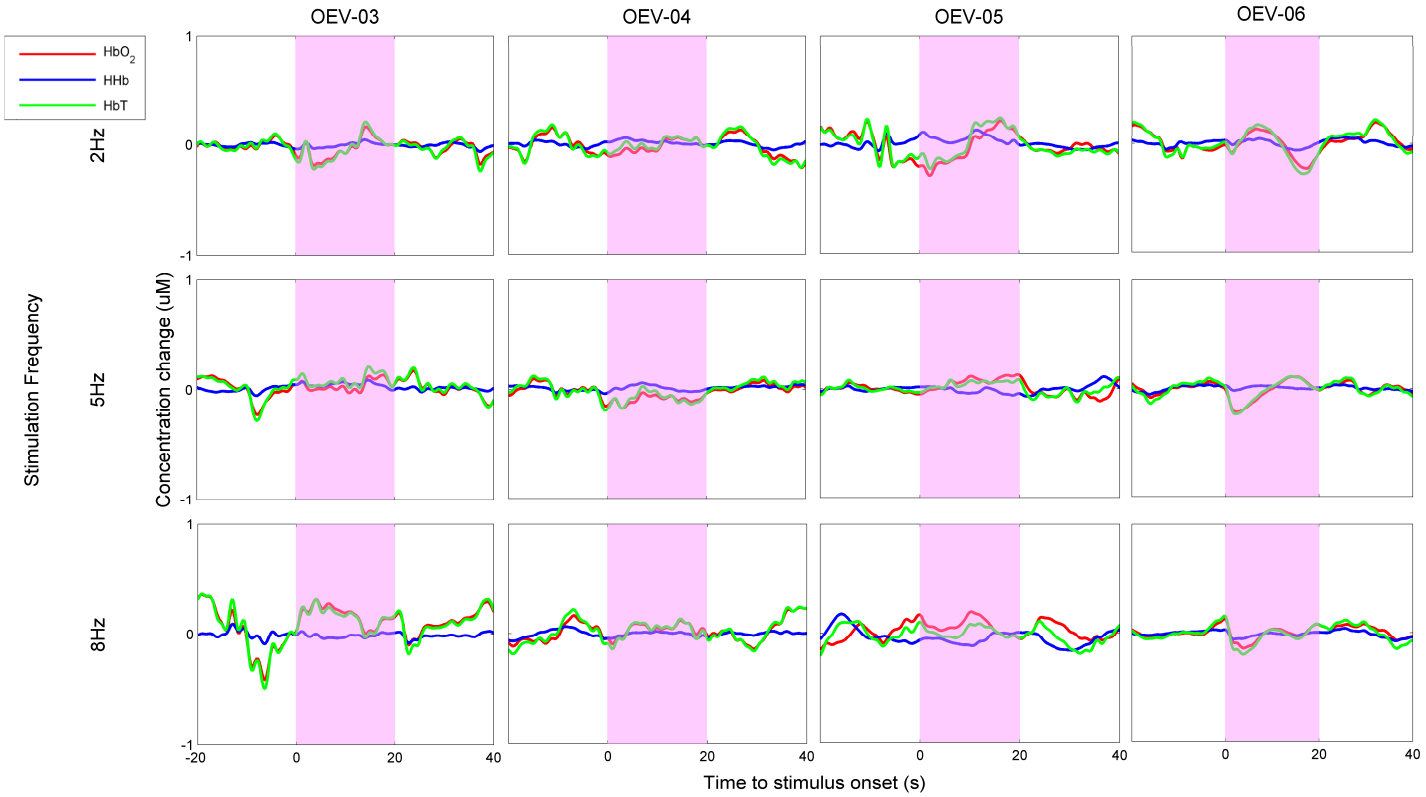

Figure 3.1.23. Representative channels showing the average of the haemodynamic response to 20 seconds of flash stimulation, arranged by stimulation frequency and subect. The shaded regions are stimulus periods.

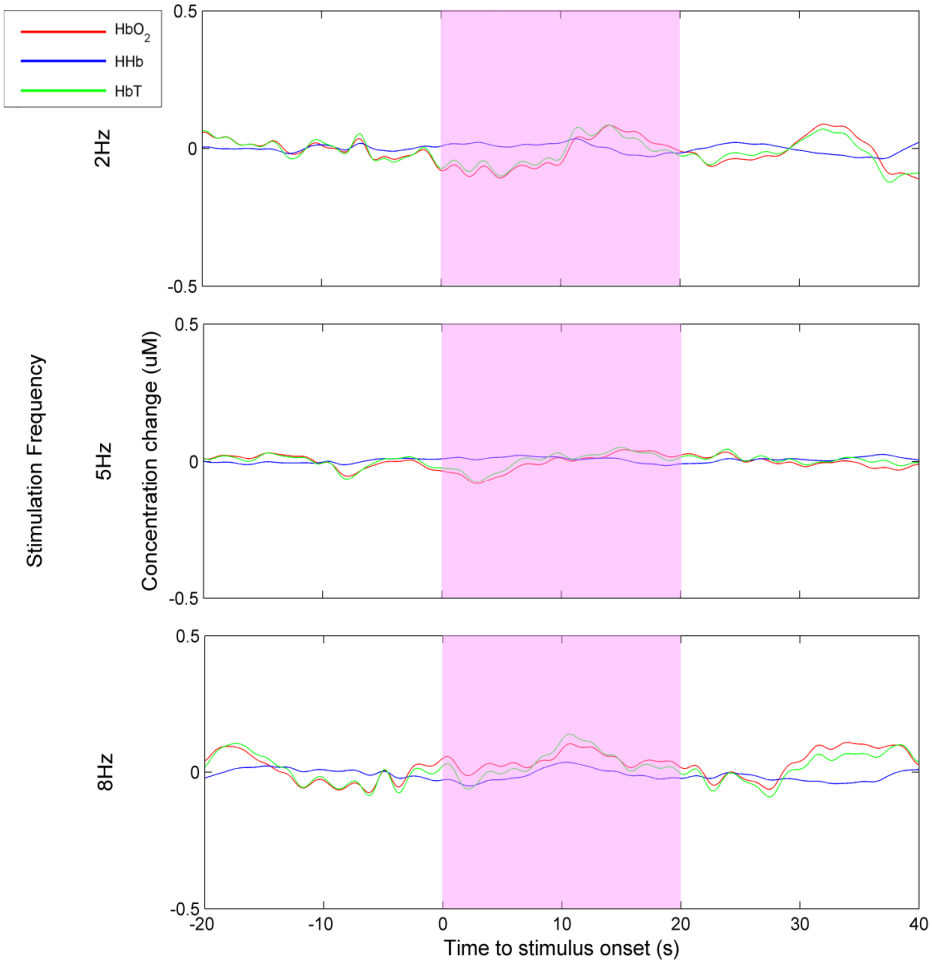

Figure 3.1.24. The grand average of the haemoglobin concentration changes resulting from 20 seconds of flash stimulation at 2, 5 and 8 Hz. For all accepted trials across five infants. A single representative channel is presented. The shaded region represents the period of stimulus. Note that the scale is half that of previously presented haemoglobin concentration changes.

haemodynamic response across all recorded infants was calculated to determine if any signal was present but hidden by background physiological oscillations.

The grand average of the haemoglobin concentration changes recorded at a single optical topography channel, for each stimulation frequency, calculated using data from infants OEV_03-OEV_06 (and from OEV_01 at

2 and 8 Hz stimulation rates) is shown in figure 3.1.24. The absence of any response strongly suggests that the small number of repetitions of each stimulus block is not to blame for the absence of an observable haemodynamic response.

3.1.4 Discussion and Conclusions

This series of experiments had two objectives. The first was to serve as a prelude to future experiments with neurologically compromised infants; to explicitly prove that the EEG-NIR imaging application methods described in section 2 could be applied to newborn infants in a clinical setting. This is not simply a question of the effectiveness of our opto-electrode design, but also of the suitability of the silicone rubber array, the process of application, the mechanisms for time-locking EEG and NIR imaging data and all offline data processing and analysis methods. In this regard, this series of experiments was very successful. As the research team became more skilled in the application of the sensing array to the head, the time taken to complete the process was reduced. In the latter studies, all equipment was applied, and the experiment was completed within as little as 30 minutes. The opto-electrodes were not dramatically more challenging to apply than standard EEG-electrodes, and provided a comparable quality of electrical contact.

In many ways, this series of functional experiments is more practically demanding than the continuous EEG-NIR imaging of a neurologically damaged infant in intensive care. Although studies in intensive care will present different challenges (due to the necessity of constant nurse access, the prevalence of other equipment, subject ventilation etc.) they will not involve stimulation, and will not require such an intricate event-marking procedure. Furthermore, because sedation is common, movement artifacts are likely to be significantly reduced, if not absent entirely. This complex flash stimulation paradigm therefore provides an excellent test of our EEG-NIR imaging arrangement, in preparation for studies of more vulnerable infants.

The second objective of this series of experiments was to study how the steady-state visual evoked potential and the functional haemodynamic response are related to flash stimulation rate, and to one another, in newborn

infants. Although statistically significant stimulus-related electro-cortical activity was successfully recorded in the majority of infants, at the majority of stimulation frequencies, the failure to record any haemodynamic responses prevents the second objective being achieved.

Clearly, our inability to observe a haemodynamic response to flash stimulation in these infants is either because of a failure of the array to sample the relevant volume of tissue or because the response was too subtle or absent altogether. As described above, the functional haemodynamic response to visual stimulation in neonates is highly variable. There have been several fMRI and NIRS studies using similar stimuli in which many infants exhibited no stimulus-related changes (Martin et al. 1999, Sie et al. 2001, Wolf 2004). However, there have also been many studies where a reliable response was obtained, in a large proportion of subjects. In the recent study by Liao et al. (2010) seven of the nine infants studied exhibited a significant increase in oxyhaemoglobin concentration.

Given that we were able to obtain both a VEP and a haemodynamic response when performing EEG and NIR imaging sequentially, the failure to obtain a haemodynamic response with simultaneous recording could be indicative of the inherently sub-optimal NIR imaging acquisition associated with simultaneous EEG-NIR. The array design is specific to this study, and has not been explicitly tested for its suitability for imaging of the infant visual cortex. However, its design is based on well established principles and was successful during phantom testing. All expected source-detector separations produced a signal within the dynamic range of the system and the heart rate was apparent in the dataset of each infant. It is also unlikely that any activation was missed because of poor positioning of the array, as it is large enough to cover a substantial proportion of the occipital lobe. It is important to note that this series of experiments have failed to simultaneously observe a VEP and a functional haemodynamic response, despite such features being

It is impossible to determine whether no haemodynamic response was produced or whether we were simply unable to observe it. However, we believe it unlikely that a response of the expected scale could have been produced in the expected region of the visual cortex without our optical topography array detecting it.

3.2 Neonatal Seizures

3.2.1 Objectives and Experimental Design Considerations

As described in section 1.1.3.3, seizures are particularly prevalent in newborn infants, and is a common result of a variety of conditions including hypoxic ischemia, stroke and hypoglycaemia. The long term objectives of the application of a combined EEG-NIR imaging method to seizures in neonates are two-fold. The first is that it will allow the haemodynamics of ictal events in neonates to be studied and characterised. This will improve our understanding of how the neonatal cerebrovascular system is affected during and after seizure events, which may have an impact on treatment. This is difficult to achieve with any pre-existing modality. The use of EEG-fMRI is nearly impossible in this patient group because of their extreme vulnerability, and propensity for movement. There is also the important issue of the study of ictal as opposed to inter-ictal events. As described in section 2.1.4, the majority of EEG-fMRI studies of epileptic activity have been of inter-ictal features. Given the erratic, mixed-frequency nature of neonatal EEG (particularly in neurologically damaged patients) it is often very difficult to discern inter-ictal epileptiform activity from the background EEG. The study of the haemodynamic response to transient inter-ictal spikes is therefore a significant challenge. Ictal EEG-fMRI in neonates is possible, but the seizure events would have to be subclinical to avoid movement contamination, and it is likely that recording would have to extend over a prohibitively long period of time. A combined EEG-NIR imaging arrangement can avoid these issues; it can be applied at the cot-side and, if the application methods and equipment can be perfected, there is nothing to prevent recording continuing for many hours at a time.

The second long term objective is related to diagnosis. It is known that near-infrared imaging methods can detect focal and generalised seizures (Roche-Labarbe et al. 2008, Gallagher et al. 2008). It is also accepted that certain cases of electro-clinical dissociation provide evidence for a failure of

EEG sensitivity to seizure events (Lieb et al. 1976, Mizrahi and Kellaway 1987, Weiner et al. 1991, Pinto and Giliberti 2001). Such cases are more common after the administration of anti-epiletic drugs, which suggests that these treatments may be suppressing epileptic discharges in certain areas of the brain but not others (Scher et al. 1994). We believe it is possible that a combined EEG-NIR imaging system (particularly one with significant depth sensitivity) will offer improved detection of neonatal seizures.

There has been little research published pertaining to the cerebral haemodynamics of ictal (or inter-ictal) events in newborn infants. Although there are several studies which have measured increased cerebral blood flow velocity using transcranial Doppler ultrasound (e.g. Boylan et al. 1999), to the author's knowledge there is only one paper which describes combined EEG and near-infrared spectroscopy (Wallois et al. 2009) and none which employs EEG-fMRI in the study of neonatal seizures. Our first goal was therefore to perform EEG-informed optical topography, in order to begin to characterise any haemodynamic pattern associated with EEG-defined ictal events in the neonate.

As mentioned above, EEG-fMRI studies of epileptic haemodynamics in adults have generally been limited to the investigation of inter-ictal features, because ictal events during recording are rare. Our initial studies of seizures in newborns is likely to have the same difficulty. However, it is common for infants to continue to seize after the initial diagnosis and treatment with anti-convulsant drugs. The study by Painter et al. (1999) showed that, when treated with phenobarbital or phenytoin, electrographic seizures were successfully controlled in fewer than half of infants. Phenobarbital is still the first line of treatment of neonatal seizures in the UK.

3.2.1.1 The patient group and recruitment

Although seizures are also common amongst pre-term infants, these experiments focussed on the term age infant. The two most common causes

of seizures in the term infant are hypoxic-ischemic encephalopathy (HIE) and focal arterial infarction (or 'stroke') (Levy et al. 1985, Scher et al. 1993, Rennie et al. 2008). Term infants who are diagnosed with seizures and HIE have often suffered asphyxia due to complications at birth. Infants born in a good or only mildly depressed state, who then develop seizures in the first few days of life are likely to have suffered a stroke. Seizures in response to HIE are varied in form, but are often generalized, whilst stroke infants will usually exhibit focal seizures associated with the location of the infarct. The middle cerebral arteries, which rise from the internal carotid arteries through the Sylvian fissure and supply much of the lateral cerebral cortices and temporal lobes, are involved in at least 75 % of perinatal strokes (Rennie et al. 2008).

At the Rosie Hospital, Cambridge, UK, infants who have suffered birth asphyxia are usually subject to examination using a cerebral function monitor (i.e. amplitude-integrated EEG) within the first 12 hours of life, which allows seizures to be identified electrographically and can aid assessment of the severity of any underlying cerebral insult. In other infants, seizures are almost always diagnosed by clinical observation of abnormal rhythmic movements of the limbs and face. The cerebral function monitor is usually applied soon after this clinical diagnosis. Once seizures have been diagnosed, some form of structural neuroimaging is usually performed (usually cranial ultrasound, CT or MRI) and a full EEG examination is always undertaken.

Treatment with anti-convulsant drugs is recommended if 3 or more seizure events are observed within an hour, or if there is a single prolonged seizure lasting 3 minutes or more. A loading dose of between 20 and 30 mg/kg of phenobarbital is the first anti-convulsant treatment to be administered, and though it depends on the infant's state, this will usually occur within 2 hours of the initial diagnosis. If seizures persist, a second dose of phenobarbital (a maximum of 20 mg/kg) can be provided. If this still fails to control the

seizures, clonazepam or phenytoin will be administered as well. Anti-convulsant drugs, and seizures themselves, are both known to cause respiratory depression in infants. As a result the majority of infants found to be seizing are soon mechanically ventilated if this is not already the case.

In this series of experiments, we sought to recruit any infant diagnosed with seizures by clinical or electrophysiological methods, and perform combined EEG and NIR-imaging as soon as possible after diagnosis. This was very challenging because the recruitment of such critically ill infants requires great sensitivity with respect to the parents and family of the infant as well as to the infants themselves. On average, the NICU of The Rosie Hospital will admit between 1 and 3 suitable seizure-diagnosed term infants a month. Given the logistical difficulties of the experimental arrangement, the limited number of research staff (who are not on the unit at all times) and issues of recruitment, it is not surprising that obtaining a good number of subjects, and studying them at the relevant time, for a suitable duration, is a serious challenge.

3.2.1.2 Experimental arrangement

The experimental arrangement necessary for EEG-informed optical topography of neonates diagnosed with seizures is not dissimilar to that applied to functional activation in the previous section. The most fundamental difference is that there is no stimulus or block paradigm. Instead, passive, simultaneous EEG and optical topography monitoring are performed for as long as deemed suitable by the attending Neonatologist. Synchronisation of the EEG and optical topography recordings is still essential, but the time-locking of stimulus events with milli-second precision is not. The triggering mechanisms described in section 3.1.2 are still applicable to the continuous monitoring of seizing infants, but the stimulation goggles can simply be removed. A regular output from the control laptop which triggers both the EEG and optical topography systems can be used to explicitly ensure synchronisation.

It is also possible to synchronise the EEG and OT systems without the use of a control laptop. If recording is started simultaneously in both modalities, the datasets will be synchronous with an accuracy related to the error in the clocks of both systems. Any drift in the clock of either system will cause the two datasets to become increasingly desynchronised over time. To assess this, the control laptop was used to send two time-markers, exactly 30 minutes apart, to both the EEG and OT systems. Any drift in either system could them be calculated by comparing the number of actual data samples recorded in this 30 minutes period. The EEG system was recording at 256 Hz, so one would expect to find $30 \times 60 \times 256 = 460800$ data samples within the 30 minutes period. Similarly, there should be $30 \times 60 \times 10 = 18000$ data samples for the optical topography system, which runs at 10 Hz. The EEG time marking was found to be very precise, with 460796 samples recorded, corresponding to a drift of -0.016 seconds over a 30 minute period. The optical topography system recorded 18011 data samples, corresponding to an error of +1.1 seconds over a 30 minute period. This is quite large, and significant enough to affect the accuracy of any experiment, particularly when recording extends for an hour or more, which is our intention here. However, the UCL Optical Topography System also assigns a time reading to every output data sample. The drift in this measure was found to be only +0.013 seconds over the 30 minute period. Assuming a maximum permissible drift of 0.5 seconds (which is a suitable bench mark given that the accuracy of manual synchronisation of the start of recording will be approximately 0.5 seconds) recording can occur for upto ~19 hours and remain reasonably synchronous without externally controlled time markers.

This information is useful because the use of the laptop to time-lock the EEG and OT systems requires extra space, which is always at a premium when working in the intensive care environment. Even so, the laptop was employed to synchronise the systems whenever possible during continuous

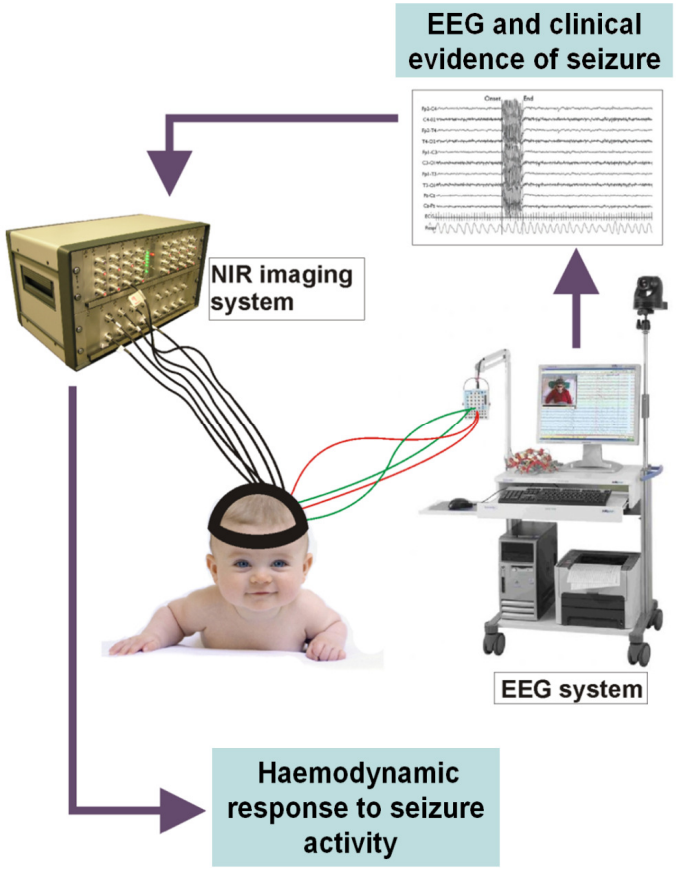

Figure 3.2.1. A simplified schematic illustrating the experimental arrangement for EEG-NIR imaging of seizures in newborn infants. Note that the laptop, which can be used to explicitly synchronise the EEG and OT systems is not shown.

EEG-NIR imaging of infants suffering from seizures. The experimental arrangement is summarised in figure 3.2.1.

3.2.1.3 Array design

The design of a suitable dual-modality EEG and optical topography array was absolutely critical for this series of experiments. Once again, there are several competing issues. The array must be suitable for NIR image reconstruction, and ideally cover as large a proportion of the scalp as is possible. The array must also be comfortable, flexible and adjustable, so that it can be applied to different subjects. It must satisfy the regulations regarding hygiene and disinfection set out by the Neonatal Intensive Care

Unit. Ideally, the array must also allow the 9-electrode, clinical neonatal EEG montage to be maintained, so as to allow the resulting EEG data to be inspected by clinical electrophysiologists and compared to standard EEG recordings.

The UCL Optical Topography System has a total of 32 sources (16 at 670 nm and 16 at 850 nm) and 16 detectors, though for the duration of this project, 4 of the modular detectors were in use elsewhere, leaving only 12. Once again, an optical topography 'channel' consists of one pair of co-located sources and one detector, both of which necessitate a single optical fibre to be coupled to the scalp. Thus, for a given number of optical fibres, the maximum number of channels is obtained when there are an equal number of paired sources and detectors. As 12 detectors are available, the first array designs were based on a total of 24 optical fibre positions.

If arranged to cover the entire scalp, 24 optical fibre positions would not provide a sampling density large enough to produce adequate imaging resolution. Given the prevalence of temporal lobe stroke in newborn infants, it was decided that producing a bilateral array which covered the temporal lobes and as much of the surrounding regions as possible would be the best use of a limited number of channels. As was shown in figure 1.1.7b, the standard neonatal EEG montage consists of 9 electrode positions. Given the size of the average term infant, and wishing to include as many optical channels as possible, the final array design contained 11 optical fibre positions on each side on the head (reduced from 12 for reasons of bulk and curvature of the head). Of these 11 positions, three are opto-electrodes, corresponding to 10-20 positions T3, C3 and O1 on the left and T4, C4 and O2 on the right. The array contains 5 source pairs and 6 detectors on each side, forming a maximum of 30 channels, allowing optical images to be reconstructed independently for each side of the head. These 30 channels

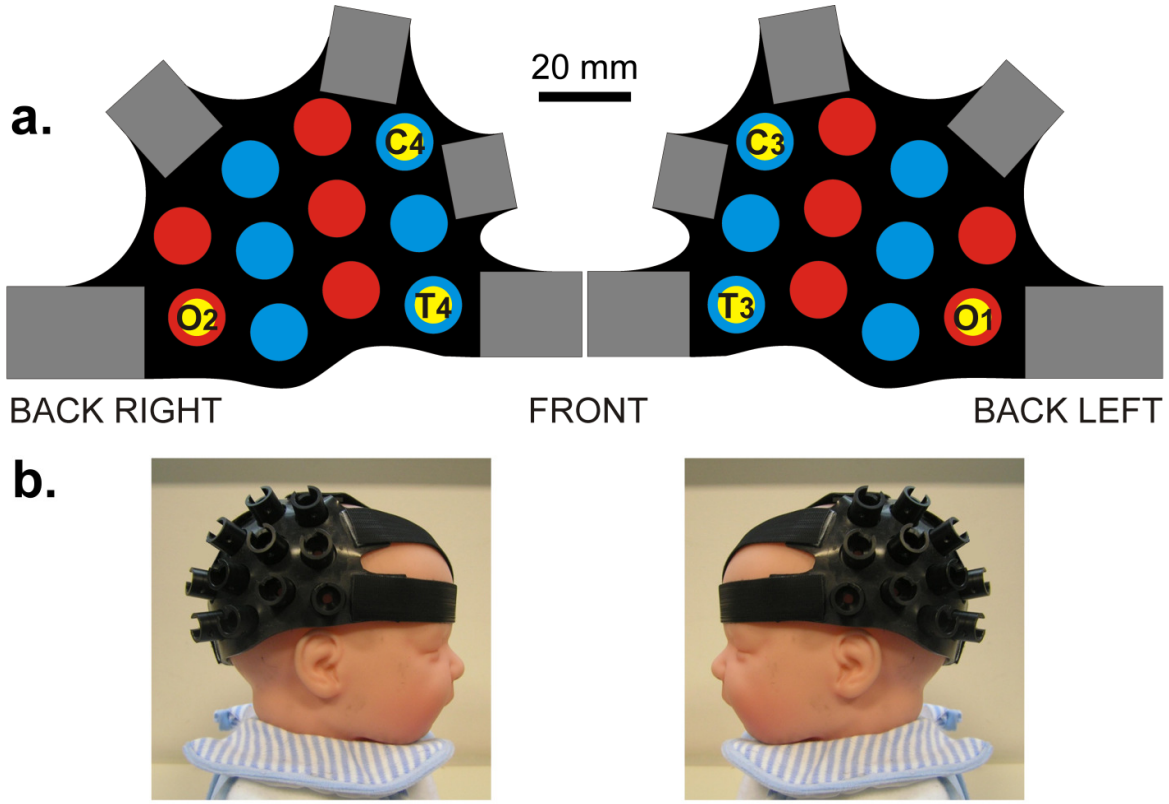

Figure 3.2.2. The top figure (a.) shows a schematic of the imaging array, with sources, detectors and opto-electrodes represented by red, blue and yellow circles respectively, and the relevant 10-20 positions indicated. The lower figure (b.) is a photograph of the imaging array (without optical fibres attached) showing its position on the head of a term-size doll.

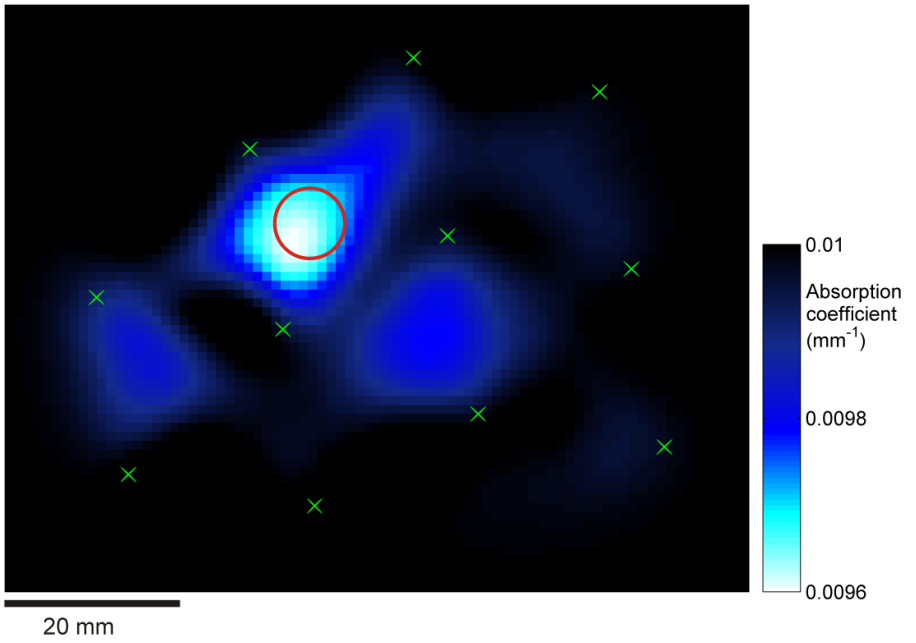

Figure 3.2.3. A reconstructed image of the change in absorption coefficient at 670 nm, obtained from a dynamic phantom using one side of the imaging array shown in figure 3.2.2. This image corresponds to a depth of 15-18 mm. The array positions are indicated by the green crosses, whilst the red circle shows the position and size of the phantom target.

include various separations ranging from 20 mm to 65 mm. The array design is partially based on the staggered row layout used repeatedly at UCL (Everdell et al. 2005, Correia at al. 2009) but altered for reasons of ergonomics. The final array design is shown in figure 3.2.2.

This arrangement of NIR sources and detectors was tested using the same solid, dynamic optical imaging phantom described in section 3.1.2.5. Linear image reconstruction was performed to produce an image of the change in optical absorption coefficient of the electrically activated phantom. The result is shown in figure 3.2.3. Once again, a focal decrease in optical absorption is seen, with the minimum occurring 3.0 mm from the actual target centre. This provides explicit proof that this array layout can produce sensible optical images.

The application method is similar to that employed for the visual cortex array described in section 3.1.2.5. The opto-electrode positions T3 and T4 are located exactly and the array, minus the opto-electrode probes, is positioned and fixed to the head. As with the visual cortex array, all other opto-electrode positions will be approximate, and their accuracy will depend on the size of the infant. The array is designed to be maximally accurate for infants with a head circumference of the term average of 35 cm. The O1 and O2 positions will have the largest positioning error, but it will not exceed 10 mm in an infant with a head circumference in the normal term range. The remaining electrodes which complete the 9-electrode neonatal EEG montage (F3, F4 and Cz) are standard clinical electrodes applied in the usual way. Reference and ground electrodes are also applied, both at the midline close to Fz.

3.2.2 Initial Results

Over a period of 8 months, four seizure-diagnosed infants were recruited and studied at The Rosie Hospital NICU. The general health and neurological condition of these infants was varied, as was the nature of their seizures. A summary of the relevant information regarding medical condition and the experiment performed is provided in table 3.2.4

All experiments were performed using the UCL Optical Topography System as described previously. All data were analysed offline using bespoke methods developed using Matlab (The Mathworks Inc., USA). The clinical EEG system described in the previous section was also employed. Recording settings consisted of a sample rate of either 2048 or 256 Hz, a band pass filter of 0.3-70 Hz and a notch filter at 50 Hz. The higher sample rate was used for previous studies of the visual cortex, and this was maintained for all infants except OES_04. A sample rate of 256 Hz is perfectly adequate for clinical EEG monitoring and minimises the size of the resulting data files. All resulting EEG data were inspected and interpreted by an experienced electrophysiologist.

The first infant (OES_01) was studied before the full array design (described the previous section) was completed. A simplified experiment was performed using two pairs of opto-electrodes, positioned so as to form two near-infrared spectroscopy channels centred approximately over 10-20 positions T5 and T6. Four EEG channels were formed by referencing each opto-electrode to Fz. These probes were applied using a silicone-rubber strap array similar to that shown in figure 3.1.7. The remaining three infants (OES_02-OES_04) were all studied using the full NIR imaging array and full neonatal EEG montage described in section 3.2.1.3.

3.2.2.1 Infant OES_01

The first infant had been diagnosed with left-sided seizures on the fourth day of life and was treated with phenobarbital, which was maintained for several days. A left-sided stroke was suspected and later confirmed by MRI. A simplified EEG-NIR experiment was performed on day 9. The reduced array, containing four opto-electrodes, was applied with little difficulty. Electrode contact impedances were measured on commencement of recording, and were all found to be less than 5 kΩ. The EEG and OT systems were explicitly synchronised using a regular pulse from the control laptop. Recording continued for 45 minutes at which point it was decided to remove the apparatus, because of the need to perform certain clinical procedures.

The EEG data were inspected by an experienced electrophysiologist, who reported that the trace was continuous and of a mixed low frequency. The EEG appeared generally suppressed, with possible signs of asymmetry. No ictal or definite inter-ictal features were observed in this 45 minute period of recording. A representative segment of the EEG recording is shown in figure 3.2.5.

Although there were no ictal or inter-ictal features apparent in the EEG recording, the raw optical intensity data were still carefully inspected. Although it was expected that all measurements would show only background physiological oscillations, we found that the channel positioned over the left side (the side of the stroke) of the infant's head exhibited a series of large, slow changes in optical intensity. These events are dominated by an increase in intensity, well above the noise level of each measurement, at both 670 and 850 nm. These increases continue for a period of between 10 and 40 seconds before reaching a peak and slowly returning to the apparent baseline. Each of these events lasts for a total of 50-120 seconds. These features occur regularly throughout the 45 minute

Infant	Age at birth (Weeks + days)	Age at seizure diagnosis	Age at study	Seizure form	Related condition	Drug regime	Ventilation	Experiment performed
OES_01	42+1	4 days	9 days	Clonic, left-sided movements. Left-sided seizures confirmed by aEEG	Left middle and posterior cerebral artery infarct confirmed by MRI	Phenobarbital	High frequency oscillatory ventilation	Simplified bilateral NIRS and reduced-electrode EEG
OES_02	38+5	20 hours	5 days	Clonic movements of legs. Generalised seizures confirmed by aEEG	Suspected sepsis at birth. MRI shows widespread infarction in both cerebral hemispheres	Phenobarbital, phenytoin, clonazepam infusion.	Conventional mechanical ventilation	Full EEG-OT with clinical, 9-electrode EEG montage
OES_03	38+1	3 days	6 days	Generalised seizures confirmed by aEEG	Hypoglycaemia. MRI shows bilateral abnormal signal intensity within posterior parietal and occipital lobes	Phenobarbital and clonazepam infusion	Conventional mechanical ventilation	Full EEG-OT with clinical, 9-electrode EEG montage
OES_04	38+5	1 day	13 days	Generalised seizures confirmed by aEEG	Severe neonatal encephalopathy. MRI shows large right temporal haemorrhagic stroke	Phenobarbital, phenytoin, clonazepam and midazolam infusion.	Conventional mechanical ventilation	Full EEG-OT with clinical, 9-electrode EEG montage

Table 3.2.4. A summary of relevant information for each of the four seizure-diagnosed infants studied.

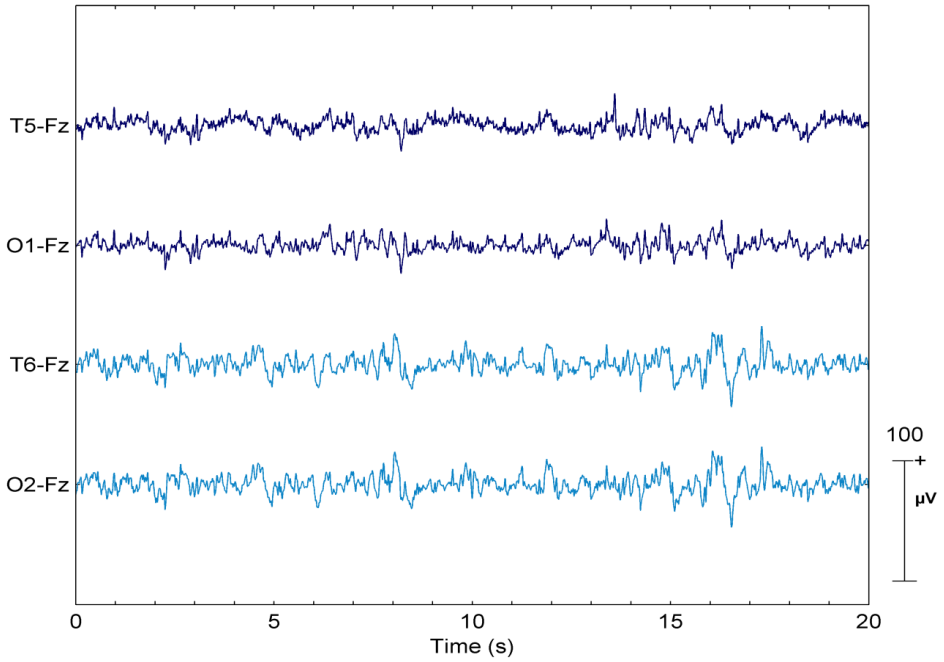

Figure 3.2.5. A twenty second period of the EEG trace from infant OES_01. The trace shows continuous, but suppressed, mixed frequency activity. Left sided channels are shown in a darker blue.

optical data set, with as many as 21 being apparent on visual inspection (though, as they vary in size, visual inspection is a poor assessment). Two of these features can be clearly seen in the raw optical data displayed in figure 3.2.6. In general, near infrared spectroscopy artifacts are relatively easily to identify by visual inspection. Movement tends to result in very rapid and random variations in optical intensity which are rarely mistaken for physiological features. Similarly, any form of electrical interference, or changes in background light conditions tend to result in an increase in high-frequency noise content. The time-scale of these events is a strong indicator that they have a physiological basis, and they do not resemble any artifact previously observed in the use of the UCL Optical Topography Systems.

The seemingly spontaneous nature of these features, which are not concurrent with any changes in EEG activity, causes a problem with respect

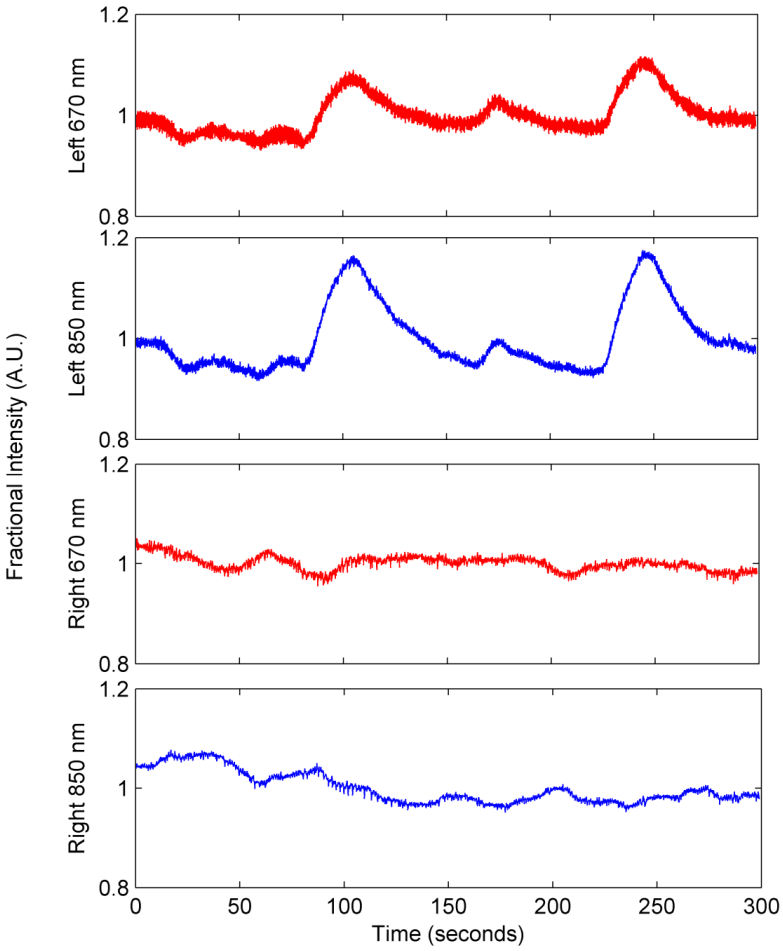

Figure 3.2.6. A section of raw optical intensity data (each scaled to its mean over this period) for each recorded source-detector pair for infant OES_01. The measurements over the left side (top two plots) exhibit two large, slow changes from the apparent baseline which are not present over the right side (lower two plots). These events exhibit an intensity variation of greater than 10 % of the mean, which is large compared to the physiological oscillations normally observed. These data have not been filtered, and the apparent thickness of each line is due to the heart rate.

to the processing of this near-infrared spectroscopy data. Without a defined 'start point' it is impossible to define a meaningful baseline optical intensity. Without a baseline, these changes in intensity cannot be converted to changes in haemoglobin concentrations and the majority of the physiological information is lost. Although one could use mean intensity as an estimate of baseline, this is likely to produce an inaccurate measure of the form and scale of changes in concentration of oxy and deoxyhaemoglobin. This problem is addressed in section 3.2.3.

3.2.2.2 Infant OES_02

Infant OES_02 was the first to undergo the application of the full optical topography and 9-electrode EEG array described in section 3.2.1.3. Details of the medical condition of this infant are given in table 3.2.4. Clinical seizures were diagnosed on day 1 and appeared generalised. Initial treatment with phenobarbital was unsuccessful, and phenytoin and clonazepam were added. The EEG-NIR imaging experiment was performed on day 5. Despite the complexity of application process (and having to abrade contact sites for 6 opto-electrodes, 3 standard electrodes, a reference and a ground electrode), all equipment was attached and ready within approximately 30 minutes. Contact impedances were all found to be below 5 kΩ at the first measure, and no electrode required re-application. The EEG system settings were as described above. The infant's ECG was also recorded using a dedicated channel of the EEG system. In this experiment, the laptop was not used to provide an external timing signal. Instead, the EEG and optical topography systems were started simultaneously (within a manual error of approximately 0.5 seconds). Recording took place for just over 90 minutes. The resulting EEG trace was bilaterally symmetric but discontinuous, with long periods of generalised, almost complete suppression and periods of low-amplitude mixed frequency activity. Once again, no ictal, or definite inter-ictal features could be identified in this recording. A representative section of the EEG of infant OES_02 is shown in figure 3.2.7.

On inspection of the optical topography data, several features comparable in scale and duration to those identified in infant OES_01 were apparent. These occurred over a number of different channels, to differing degrees, on both the left and right sides of the head. Although not completely identical (which one would expect if they were of a non-physiological origin), they consisted of a large increase in intensity from the baseline, well above the apparent level of heart rate and other physiological oscillations. Each of these events lasted between 40 and 90 seconds and occurred repeatedly

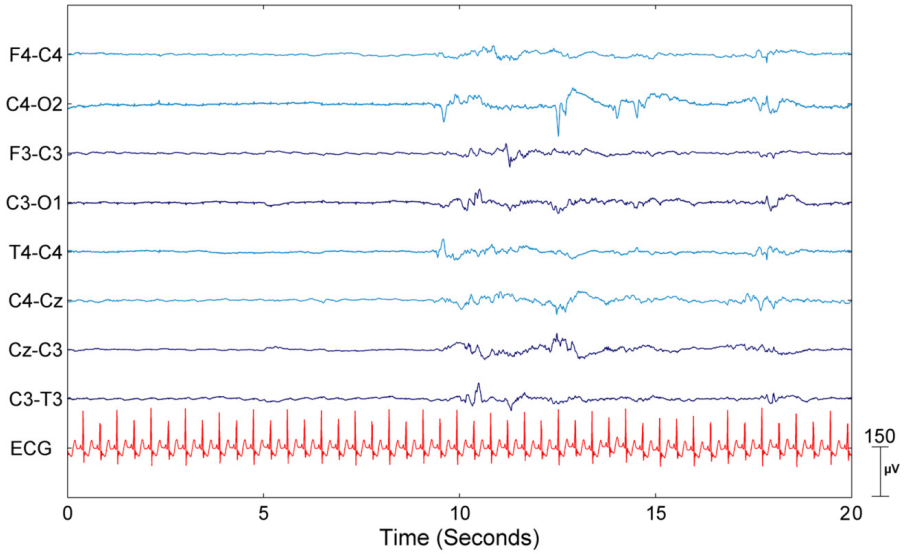

Figure 3.2.7. A twenty second period of the EEG trace of infant OES_02. The trace is clearly discontinuous, with periods of generalised suppression and burst of mixed frequency activity. A single-channel ECG is also presented

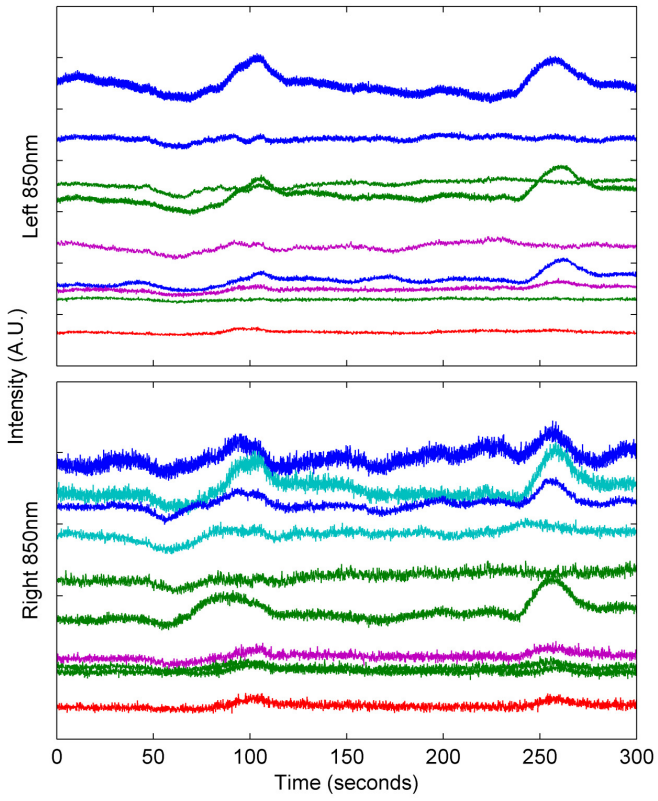

Figure 3.2.8. A section of raw optical intensity data from infant OES_02. A selection of 850nm channels from both the left side (upper plot) and right side (lower plot) are presented. Two large, slow changes are again visible, over several channels and on both sides of the head. Colours are arbitrary.

throughout the 90 minutes of recording. On visual inspection, as many as twenty such events were visible. An example of the raw data from a selection of optical topography channels from infant OES_02 is shown in figure 3.2.8.

3.2.2.3 Infant OES_03

Generalised seizures were diagnosed on the third day of life, and were confirmed by aEEG. Further details are given in table 3.2.4. Again, seizures in this infant were persistent, and a combination of anti-convulsants was administered. A full EEG-NIR imaging experiment was performed on day six. In the study of this infant, application of the dual-modality array proved problematic. The opto-electrode at position T3 persistently recorded a high contact impedance. Despite repeated re-application, we were not able to reduce this value below 14 kΩ. On inspection of the EEG trace, it was apparent that all channels which included electrode C3 were excessively noisy, despite C3 registering a contact impedance below 5 kΩ. Electrode C3 is essential to 4 of the 8 channels in the clinical neonatal montage. The experiment was continued in the hope that offline analysis would still yield a meaningful interpretation of the EEG trace. Recording occurred for just over one hour, and synchronisation was performed manually. Figure 3.2.9 shows a section of the recorded EEG, with four excessively noisy channels due to electrode C3. By altering the EEG montage, it is possible to remove electrode C3 and obtain 6 EEG channels of a reasonable quality (figure 3.2.10). The EEG trace from infant OES_03 was analysed by a clinical electrophysiologist who reported that it contained bilaterally symmetric, somewhat discontinuous activity but without burst suppression, ictal or definitively inter-ictal activity. Once again, the optical topography data appeared to contain some large, slow variations similar to those of the previous two infants. Approximately six very large events were apparent, along with as many as 10 events with a shorter duration and smaller amplitude.

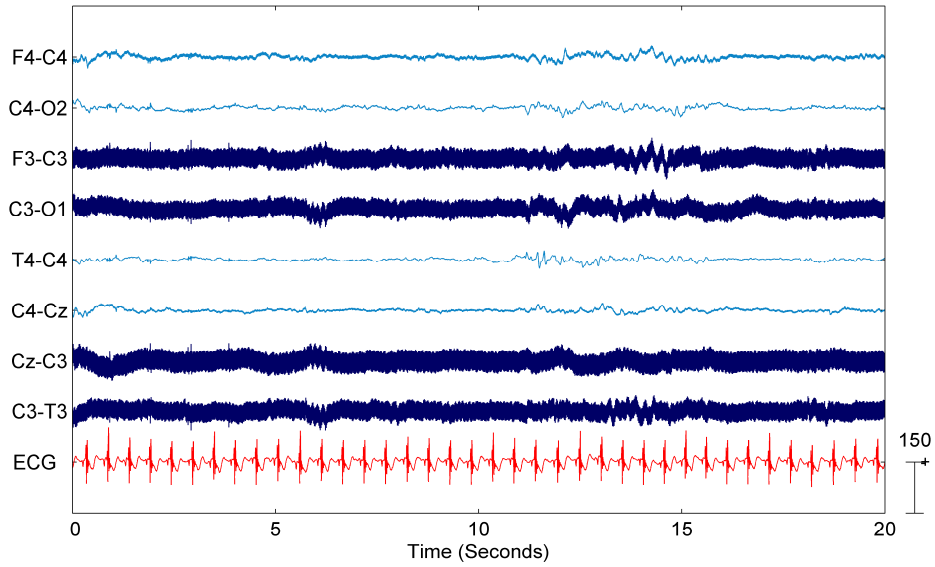

Figure 3.2.9. A twenty second period of the EEG trace of infant OES_03. Electrode C3 is clearly excessively noisy, this is despite it having a reasonable contact impedance. The only contact impedance above the 5 kΩ threshold was that of electrode T3.

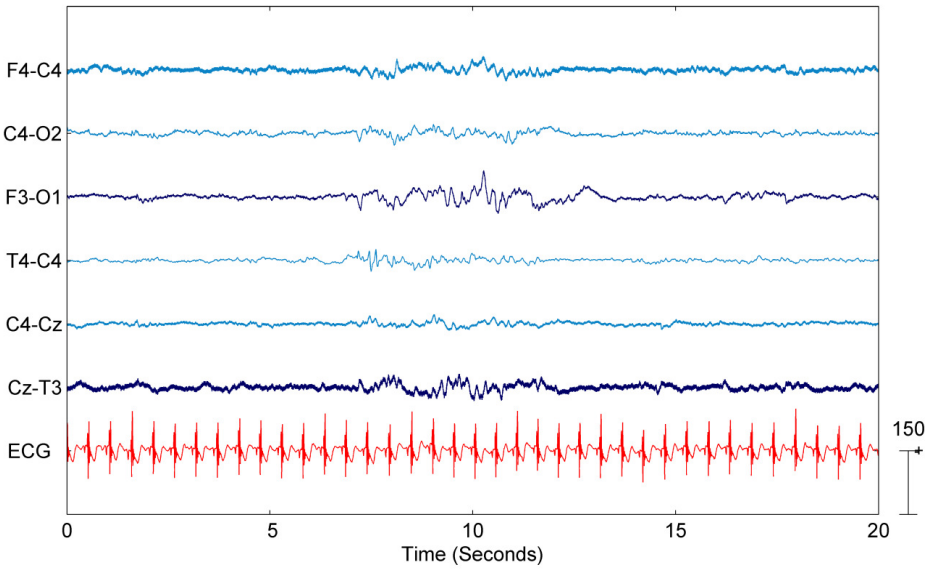

Figure 3.2.10. The same twenty seconds of data (though offset by ~5 seconds as presented in figure 3.2.9, but re-montaged so as to remove electrode C3. Despite its high contact impedance, the channel containing electrode T3 is not excessively noisy. This period of EEG shows an example of a burst of activity interspersed with a generally suppressed EEG.

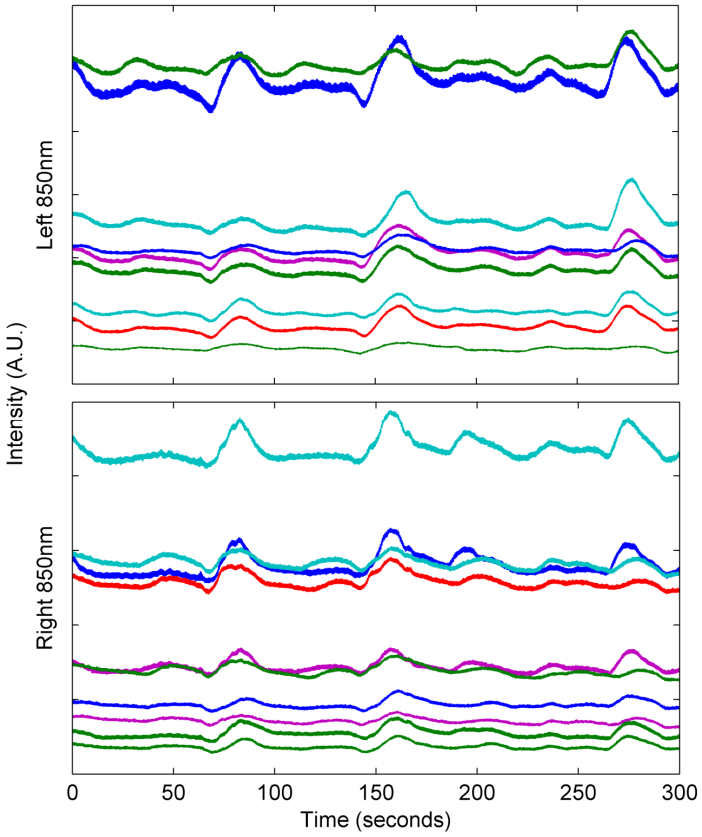

Figure 3.2.11. A section of raw optical intensity data for infant OES_03. Once again there appear to be several slow, significant features present over several channels on both sides of the head. These particular examples are of a relatively short duration and small amplitude.

An example of a period of raw intensity data from infant OES_03 is shown in figure 3.2.11.

3.2.2.4 Infant OES_04

In this infant, general seizures were diagnosed on the first day of life and confirmed by aEEG. Several neurological conditions including hypoxic ischemia and a right-sided haemorrhagic stroke were later identified using, among other methods, MRI. Seizures were not responsive to initial treatment with phenobarbital and phenytoin, clonazepam and midazolam were administered. The full EEG-NIR imaging experiment was not

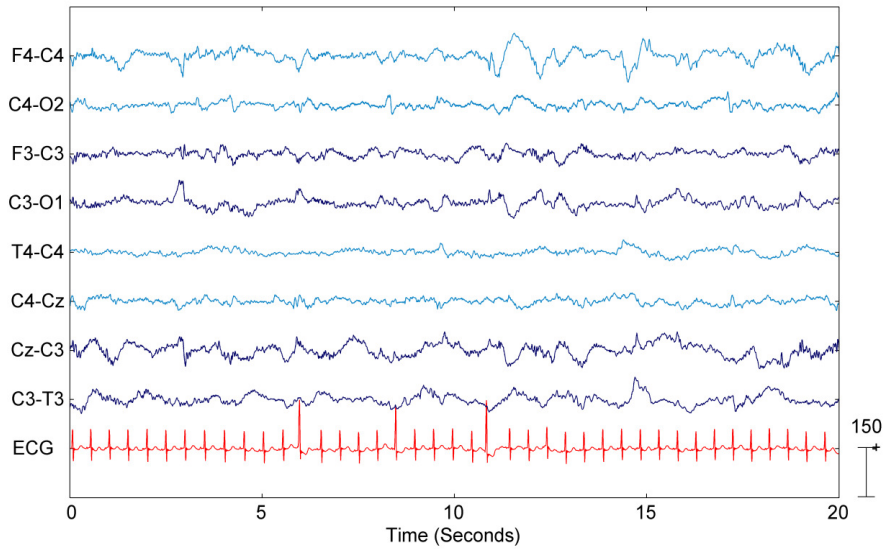

Figure 3.2.12. A section of the EEG trace of infant OES_04. Note the continuous mixed frequency nature of the recording and it's relatively high amplitude compared to the EEG traces of infants OES_01, OES_02 and OES_03.

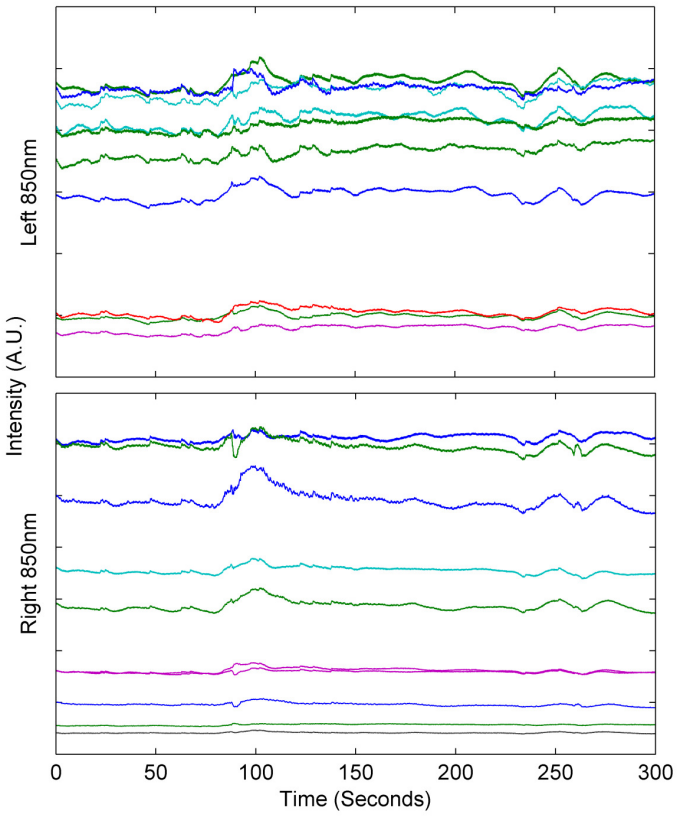

Figure 3.2.13. A section of raw optical intensity data from infant OES_04. The upward trend at ~ 90 seconds represents the only feature which is comparable to those observed in infants OES_01-OES_03.

performed until day 13, at which time the infant was still being treated with anti-convulsants. Whereas infants OES_01 to OES_03 were completely sedated throughout recording, infant OES_04 showed some signs of consciousness. Some movement was apparent.

The application of the dual-modality sensing array was successful, and no contact sites required attention after the initial application. All recorded contact impedances were found to be below 5 kΩ. Recording took place for just under 70 minutes.

On examination of this infant's EEG, the electrophysiologist reported continuous, symmetrical, mixed-frequency activity. Presumably because this infant was less sedated, the EEG showed no signs of suppression. Artifacts relating to movement of the head and eyes were apparent regularly throughout the EEG trace. There is no evidence of seizures, and despite there being several spike-like discharges, none were categorically epileptiform. A period of the EEG trace from infant OES_04 is shown in figure 3.2.12.

Despite the successful application of the array, and obtaining a good quality EEG recording, the optical topography data exhibited long periods of signal corruption. The first 30 minutes of data shows continuous artifact, which appear somewhat like movement artifact. However, movement would also be present in the EEG data which is not the case. After approximately 30 minutes, this artifact suddenly disappears, only to re-appear for the last 10 minutes of recording. The likely explanation is that there was a significant change in ambient lighting conditions. A relatively bright light incident on the front panel of the optical topography system (or on the array itself) can cause a significant increase in background noise. This is particularly true with fluorescent lighting of the type found in the neonatal intensive care unit. No changes in light conditions were noted during recording, but this seems to be the most likely explanation. The 30 minutes of data which were

not corrupted by this artifact were examined in the same way as was performed for the previous three infants. During this period there is one feature which is similar in form to those found repeatedly in the datasets of infants OES_01 to OES_03. This feature is shown in figure 3.2.13. It contains more high-frequency components than were observed in the earlier datasets, and it is not consistent in form across different channels. These factors suggest that this feature may be movement-related.

3.2.3 Data Processing: Movement and Event identification

The aim of these studies was to show that simultaneous EEG-NIR imaging methods could be used successfully in the study of seizure events in newborn infants. The successes and failures of this series of experiments will be discussed in section 3.2.5, but it is apparent that these datasets do not allow for EEG-informed optical imaging of ictal events. Rather, the most interesting aspect of these datasets is found in the optical data alone.

The haemodynamic events observed in the raw optical intensity data were not expected, and (at least to the knowledge of the author and his collaborators) constitute an abnormality. As mentioned above, the spontaneous nature of these changes in optical intensity causes a problem. Without being able to define a meaningful baseline, it is not possible to convert changes in intensity to changes in concentration of oxy and deoxyhaemoglobin. In order to define a meaningful baseline, and establish whether these features are significant and consistent, it is necessary to determine a fixed, automated approach to the event identification. Such an approach is then applicable to age-matched control data, and it should be possible to establish whether these events are associated with neurological damage or whether they are a normal, but as yet undocumented, feature of neonatal cerebral haemodynamics.

There are many approaches to the identification of specific features within a given NIR dataset. Independent component analysis (ICA) is a form of blind source-separation, which for N data channels will identify the N most statistically independent components which are present in a dataset has become a common approach to processing multi-channel NIR imaging data (Hyvärinen and Oja 2000). If a model waveform of the haemodynamic feature can be produced, then cross-correlation methods, which provide a measure of the similarity of two waveforms, can be applied to identify features in a dataset which correspond to that model waveform. Cross-

correlation methods have recently been used to identify resting-state functional networks in the brain using NIR imaging (White el al. 2009).

Because the features identified in the unprocessed optical data appeared to be robust and large (relative to the noise level of each channel), it was decided that it would be most appropriate to develop a simple, automated approach to event identification. If such simple methods failed to suitably identify the features of interest, then more intricate signal analysis methods (such as ICA and cross-correlation) could then be pursued.

The simple approach consisted of two operations. The first was to locate and reject periods of optical topography data which were corrupted by movement artifact, and the second was to identify the features of interest. Before either of these operations was performed the dataset was pre-filtered using a pass-band Butterworth filter between 0.005 and 2 Hz, to eliminate very slow trends in laser diode source power and high-frequency noise and heart rate oscillations.

3.2.3.1 Movement artifact identification

There remains no community-wide approach to movement and artifact identification in NIR data. This is partly due to the variety of data types and the variation in signal to noise ratio between and within experiments and subjects. Scholkmann et al. (2010) recently suggested that a relative increase in standard deviation is a good indicator of corruption by movement. Data recently obtained at University College London have suggested that a rate of change in haemoglobin concentrations of 0.6 μM/s represents an upper limit for physiological phenomena. Features which exhibit faster changes in haemoglobin concentration must, therefore, be due to movement or other artifacts (C Elwell and C Cooper, personal communication). In order to identify periods of movement in the optical data of our infants, we defined a process which incorporates both of these approaches. Using both an absolute threshold (of rate-of-change in

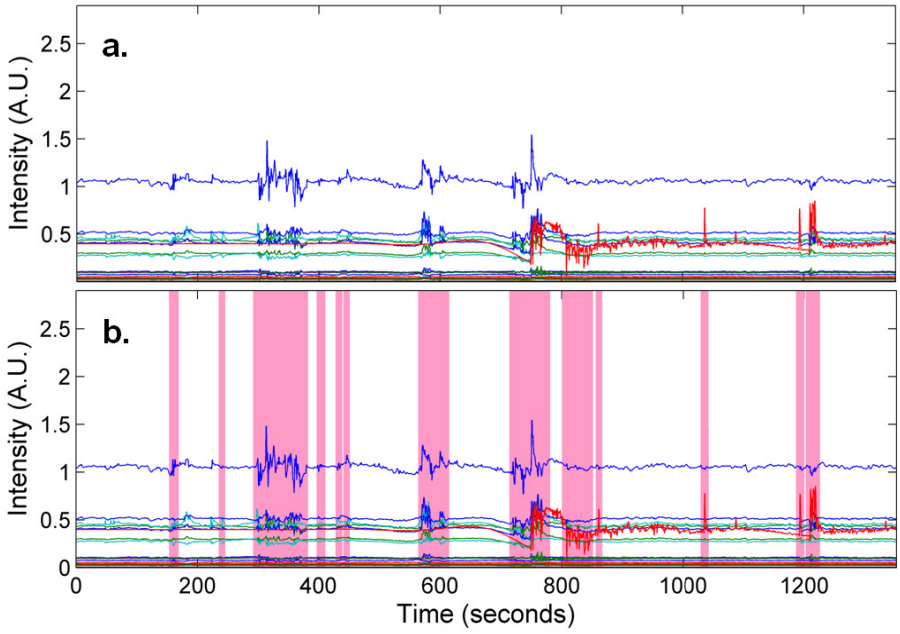

Figure 3.2.14. A period of optical topography data, with several periods of obvious movement artifact is shown in figure a. Figure b shows the result of the movement artifact detection algorithm. The shaded regions are identified as movement-corrupted and excluded from further analysis.

haemoglobin concentration) and a relative measure (the increase in standard deviation relative to the dataset mean) produced the most consistently accurate results.

The movement identification algorithm proceeds as follows. First a rolling standard deviation ( ) is calculated for each time-point (t) for five second-long 'windows' of optical intensity data for each channel (n) at both wavelengths, as is the mean standard deviation ($_n$) across each channel for the duration of the recording. Second, a baseline intensity is calculated for each channel by low-pass filtering the (already filtered) intensity data to remove any features with a duration comparable to the observed haemodynamic events. Changes in total haemoglobin concentration are then calculated for the entire optical data set using these 'DC' baseline

intensities. This data is then differentiated to give the rate of change in total haemoglobin concentration ($Hb'(t)$).

If a given data point, for any channel, is found to occupy a data window with a standard deviation greater than *x* times the mean standard deviation, whilst the rate of change of total haemoglobin exceeds a threshold of *y* (i.e. $SD_n(t) > x \times \overline{SD}$ AND $Hb'(t) > y$) then the five seconds of data before and after that data point, for all channels, are identified as movement corrupted. As part of the purpose of this process is to establish that the haemodynamic events present in the optical data are of a physiological origin, the movement rejection algorithm is deliberately over sensitive. After some trial and error, the values of the parameters *x* and *y* selected were 4.5 (dimensionless) and 0.3 μM/s respectively. Figure 3.2.14 shows an example of this movement identification algorithm being applied to a functional activation dataset recorded previously using the UCL Optical Topography System.

It is important to note also that EEG data can be an excellent indication of movement corruption. Although the presence of movement in the EEG traces of our infants was not included in the automated approach to artifact detection, a manual inspection of the EEG data recorded during the period around each identified event was performed. The results of these inspections are discussed in section 3.2.4.

3.2.3.2 Event identification

Following the removal of as many non-physiological features as possible from the data, the next step is to identify the features of interest. Because the purpose of this process is to perform identical operations on data from our four neurologically damaged infants and on data from healthy control infants, we can define an 'event' as specifically as we wish without affecting the independence of the result. Events were identified by simply searching for a variation in optical intensity from the mean 'DC' baselines.

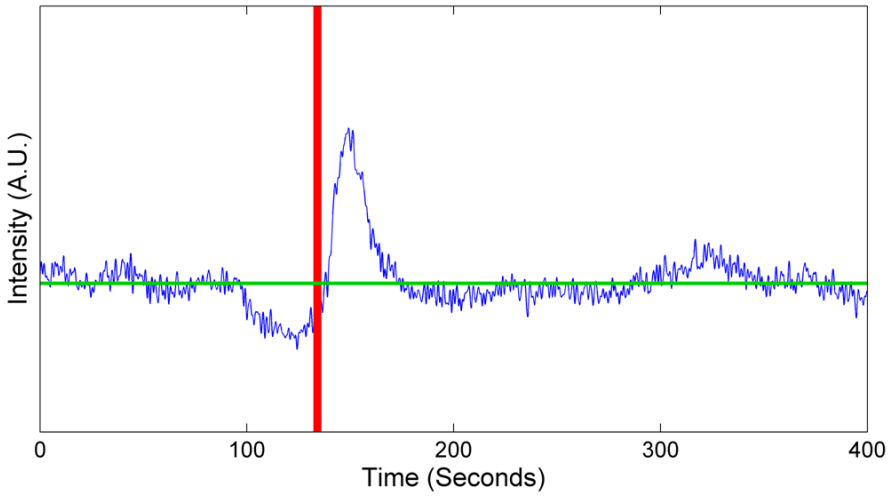

Figure 3.2.15. An illustration of the event location algorithm. If the mean of 15 seconds of data exceeds a mean baseline (represented by the green line), the algorithm marks the beginning of that 15 seconds (the red line). This is an example taken from infant OES_01.

As the observed features appeared large (relative to background variations), slow (typically > 30 seconds), and dominated by an increase in intensity, the identification algorithm looked for periods where the mean intensity of 15 seconds of data exceeded the baseline intensity by 8 %, in at least one channel at one wavelength. When an event is identified, the following 100 seconds of data are skipped to prevent a single event being identified more than once. Note that as we are defining the polarity of the change, the mean of identified events will naturally have a dominant direction. However, an identical process is performed on both sample and control data, so irrespective of how specifically the events are defined, we are able to determined whether those events are common to both subject groups. This process was also performed by defining events as a decrease in intensity. The results of this event identification were very similar, due to of the bi-phasic nature of the events themselves (see section 3.2.4). The event location process was performed independently for data from each side of the head so that any lateralisation could be identified. The process is illustrated in figure 3.2.15.

3.2.4 Haemodynamic Event Results

3.2.4.1 Control subjects

As the primary purpose of this process is to determine whether or not these haemodynamic features are abnormal, it is clearly necessary to obtain a significant quantity of optical topography data from healthy, term-aged infants. Obtaining true controls, which allow a particular variable to be isolated in a statistically meaningful fashion, is essentially impossible within the limits of this work. This is because of the variety of underlying pathologies, medications, states of consciousness and medical histories of our neurologically damaged infants, and because of their relatively small number. Nevertheless, it is possible to determine whether the observed features are common to healthy term infants.

Two infants were recruited at The Rosie Hospital with corrected ages of 40+5 and 38+6 (weeks + days). These infants were in a good state of general health at the time of study, although the first infant (OEC_01) had been born very prematurely. An optical topography experiment, identical to those performed in infants OES_01 to OES_04, but without the addition of EEG recording or the use of opto-electrodes, was performed in these two infants. Data were recorded for as long as possible, which, given their relatively active state, was no more than 25 minutes.

In addition to these two control experiments, the data obtained from the functional visual cortex experiments of infants OEV_01 and OEV_3-OEV_6 (see section 3.1) were also subjected to the same process of movement rejection and event location. Although these optical topography data-sets were obtained from the occipital (as opposed to temporal) lobe, during a functional stimulation paradigm, their use as control data, to represent normal neonatal cerebral haemodynamics, seems appropriate.

In order to further augment the control data sample, we obtained 12 datasets recorded as part of an auditory stimulation paradigm in newborn infants. This series of experiments was performed at the Laboratoire de Science Cognitive et Psycholinguistique (LSCP) in Paris, as part of an investigation into the development of language in infants. These 12 data-sets were recorded using a UCL Optical Topography System, identical to that used in our studies. Although the array design was different, these experiments also targeted regions in and around the temporal lobes. Subjects were infants born approximately at term (> 37 weeks) and with no known medical complications. Studies were performed before the subjects had reached the age of 3 days. Each experiment provides approximately 20 minutes of neonatal optical topography data, which puts the total length of our control datasets at over 6 hours.

3.2.4.2 Processing results

The movement rejection and event identification processes described in section 3.2.3 were performed on the optical topography datasets of all four neurologically damaged infants. These processes were performed independently for the left and right sides of the head. The resulting defined events were classed as left-sided, right-sided or global. Global events are those for which an event was independently identified on both the left and right sides of the head within a period of 25 seconds. An event which is defined as left or right-sided is not necessarily completely lateralised, it means only that one side did not exceed the intensity threshold necessary to be classified as an event.

The movement and event location algorithms were also applied to all control datasets, although independent analysis of left and right sides of the head was only possible for infants OEC_01 and OEC_02.

Infant	Experiment type	Percentage rejected by movement algorithm	Number of defined events (left, right, global)	Number of rejections due to EEG movement	Number of accepted events (left, right, global)	Number of accepted events per hour
OES_01	EEG-OT of seizures	0	5 (5,0,0)	0	5 (5,0,0)	7.32
OES_02	EEG-OT of seizures	5.13	22(11,7,4)	0	22 (11,7,4)	15.82
OES_03	EEG-OT of seizures	0.52	11 (5,0,6)	0	11 (5,0,6)	10.82
OES_04	EEG-OT of seizures	0*	1 (1,0,0)	1	0	0
OEV_01	EEG-OT of VEP	0	1	0	1	3.41
OEV_03	EEG-OT of VEP	15.24	1	0	1	3.42
OEV_04	EEG-OT of VEP	15.10	3	1	2	6.82
OEV_05	EEG-OT of VEP	5.12	0	0	0	0
OEV_06	EEG-OT of VEP	17.75	0	0	0	0
OEC_01	OT control	23.15	2(1,0,1)	N/A	2(1,0,1)	5.33
OEC_02	OT control	28.08	4(4,0,0)	N/A	4(4,0,0)	12.08
LSCP_01	OT of auditory	25.84	1	N/A	1	2.88
LSCP_02	OT of auditory	13.41	2	N/A	2	5.53
LSCP_03	OT of auditory	10.58	2	N/A	2	6.22
LSCP_04	OT of auditory	19.73	4	N/A	4	11.67
LSCP_05	OT of auditory	13.51	6	N/A	6	16.56
LSCP_06	OT of auditory	6.02	5	N/A	5	9.70
LSCP_07	OT of auditory	9.53	1	N/A	1	3.27
LSCP_08	OT of auditory	18.01	0	N/A	0	0
LSCP_09	OT of auditory	17.68	5	N/A	5	9.89
LSCP_10	OT of auditory	8.78	5	N/A	5	9.04
LSCP_11	OT of auditory	13.30	2	N/A	2	4.46
LSCP_12	OT of auditory	21.98	6	N/A	6	13.01

Table 3.2.16. The results of the movement rejection and event identification processes for all neurologically damaged and control infants. (*This value is the result of the automated process after a total of 52.72 % was removed manually due to the noise issue described above).

When an event position is identified, an epoch consisting of 100 seconds of data before and after that event position is selected. Changes in oxy and deoxyhaemoglobin concentrations, and reconstructed optical images, can then be produced using a period prior to the identified event position as baseline. The baseline period was selected as the average of the first 40 seconds of each epoch (i.e. from -100 to -60 seconds relative to the identified event position).

A summary of the results of the movement rejection and event location processes is given in table 3.2.16. This table includes the results of applying our processing algorithms to the data from our 4 neurologically damaged infants and all 19 control infants.

For each event identified in the optical topography data, it was important to inspect the corresponding period of an infant's EEG. This allows any EEG patterns or discharges which are time-locked to the haemodynamic events to be identified. It also provides an additional assessment of movement artifact. Because no movement rejection algorithm can be completely accurate, there are likely to be cases where movement is occurring but remains unidentified. For each identified haemodynamic event, the corresponding EEG was inspected. If movement was apparent in the EEG data, that haemodynamic event was rejected from the subsequent averages. The number of defined events rejected in this manner is given in table 3.2.16. Of the neurologically damaged infants (OES_01 to OES_04) this procedure only resulted in the rejection of one event; that of OES_04. This rejected feature was the only event identified in this infant's optical topography data and was shown in its raw form in figure 3.2.13. The corresponding, movement-corrupted period of EEG data is shown in figure 3.2.17. The presence of movement artifact in this infant's data is consistent with the observation that this infant was relatively conscious compared to infants OES_01, OES_02 and OES_03.

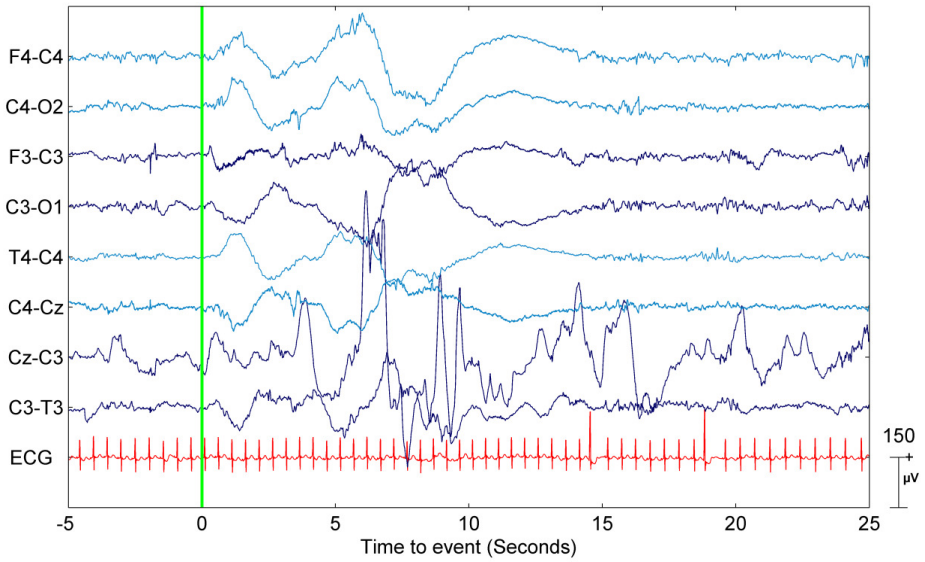

Figure 3.2.17. The period of EEG data corresponding to the only defined haemodynamic event for infant OES_04. The event start point is represented by the green vertical line. Movement corruption across all EEG channels is clearly apparent for at least 15 seconds. The corresponding haemodynamic event was thus rejected.

Figure 3.2.18 shows three examples of the haemodynamic events identified in infants OES_01, OES_02 and OES_03. The single channel which showed the largest change is presented. These are single events rather than averages and give a good indication of the signal-to-noise ratio of these features. Figure 3.2.19 shows the mean changes in haemoglobin concentrations for all events in infants OES_01 and OES_03, organised by lateralisation (left-sided, and left-sided and global respectively). A single channel from each side of the head is presented in each instance. Similarly figure 3.2.20 shows the mean of all left-sided, right-sided and global events in infant OES_02. All these mean events exhibit a similar bi-phasic pattern. Oxyhaemoglobin concentration increases significantly, reaching a peak at an average (and standard deviation) of 26.2 (12.5) seconds after the beginning of its departure from the baseline value. It then decreases very rapidly, reaching a minimum well below the initial baseline value after 55.5 (13.3) seconds. The average total HbO_2 event duration is 103.4 (19.7) seconds. Deoxyhaemoglobin concentration (HHb) follows a similar pattern,

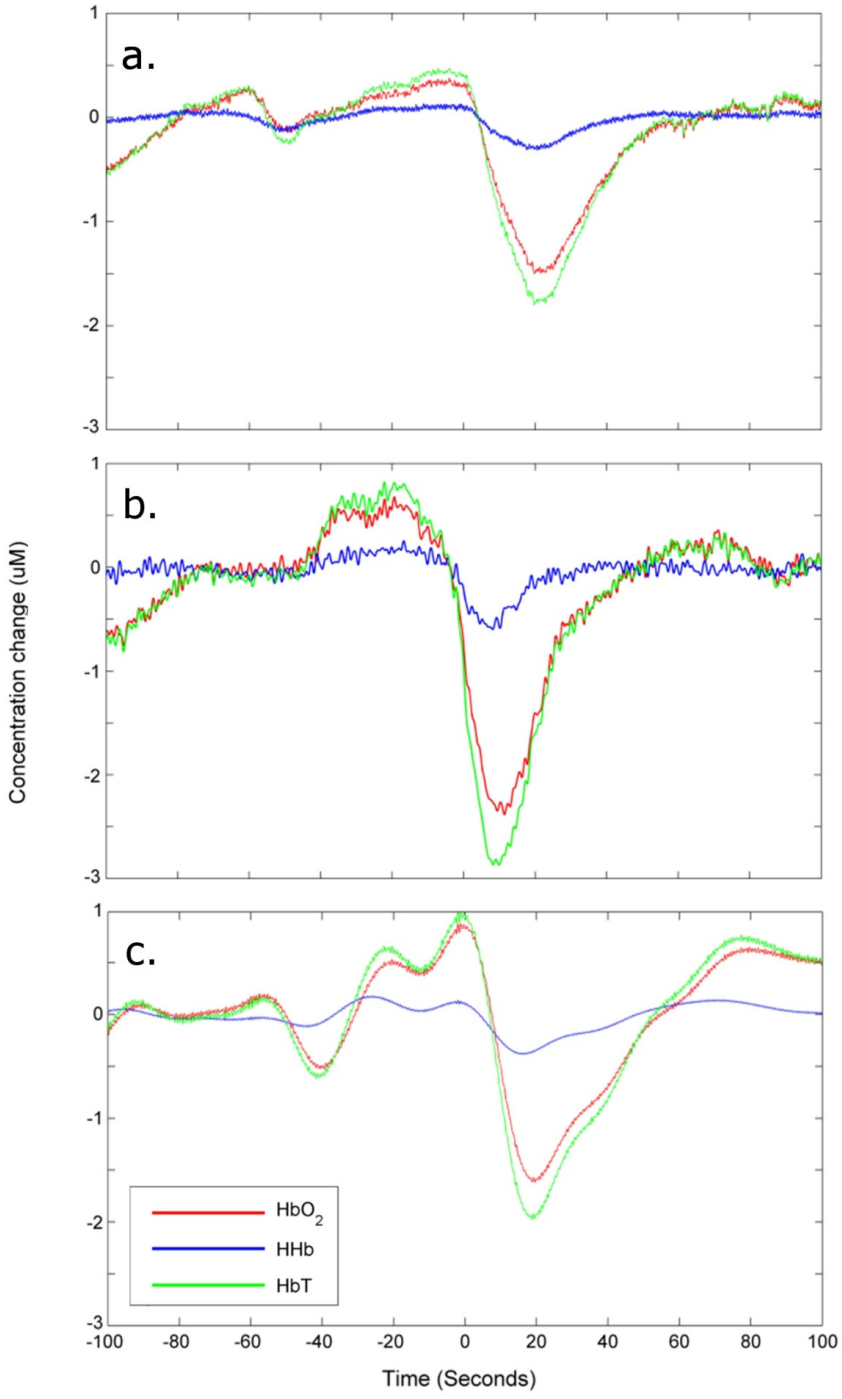

Figure 3.2.18. Three single events defined in infants OES_01 (a), OES_02 (b) and OES_03 (c). The channel which exhibited the largest concentration change in presented for each.

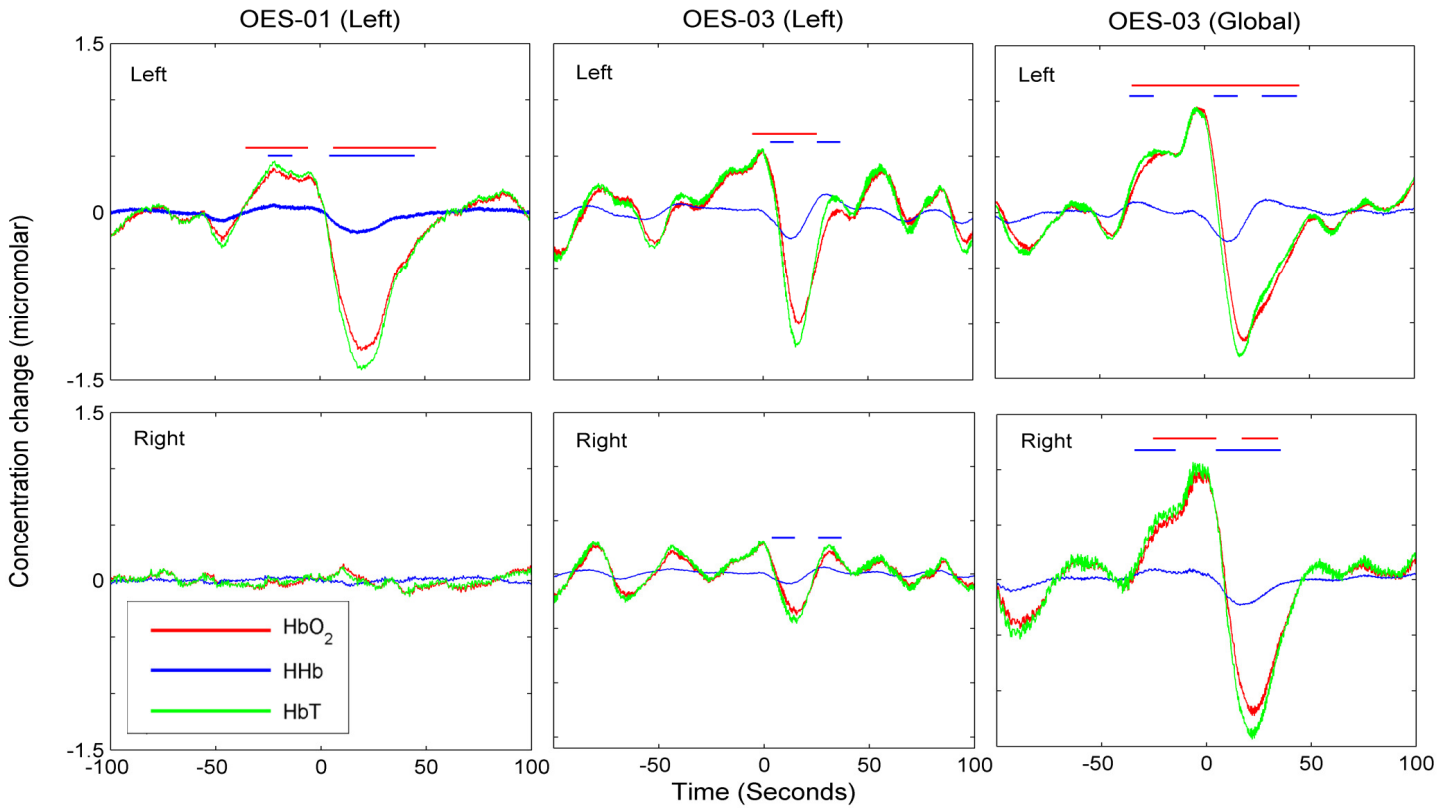

Figure 3.2.19. The mean events for OES_01 (all of which were left sided) are shown in the left column. The mean left-sided and global events in infant OES_03 are shown in the centre and right columns. The channel with the largest response over each side of the head is presented in each instance. The blue and red horizontal bars indicate periods of significant variation from the defined baseline (-100 to -60 seconds) of HHb and HbO_2 respectively (at 95 % confidence level).

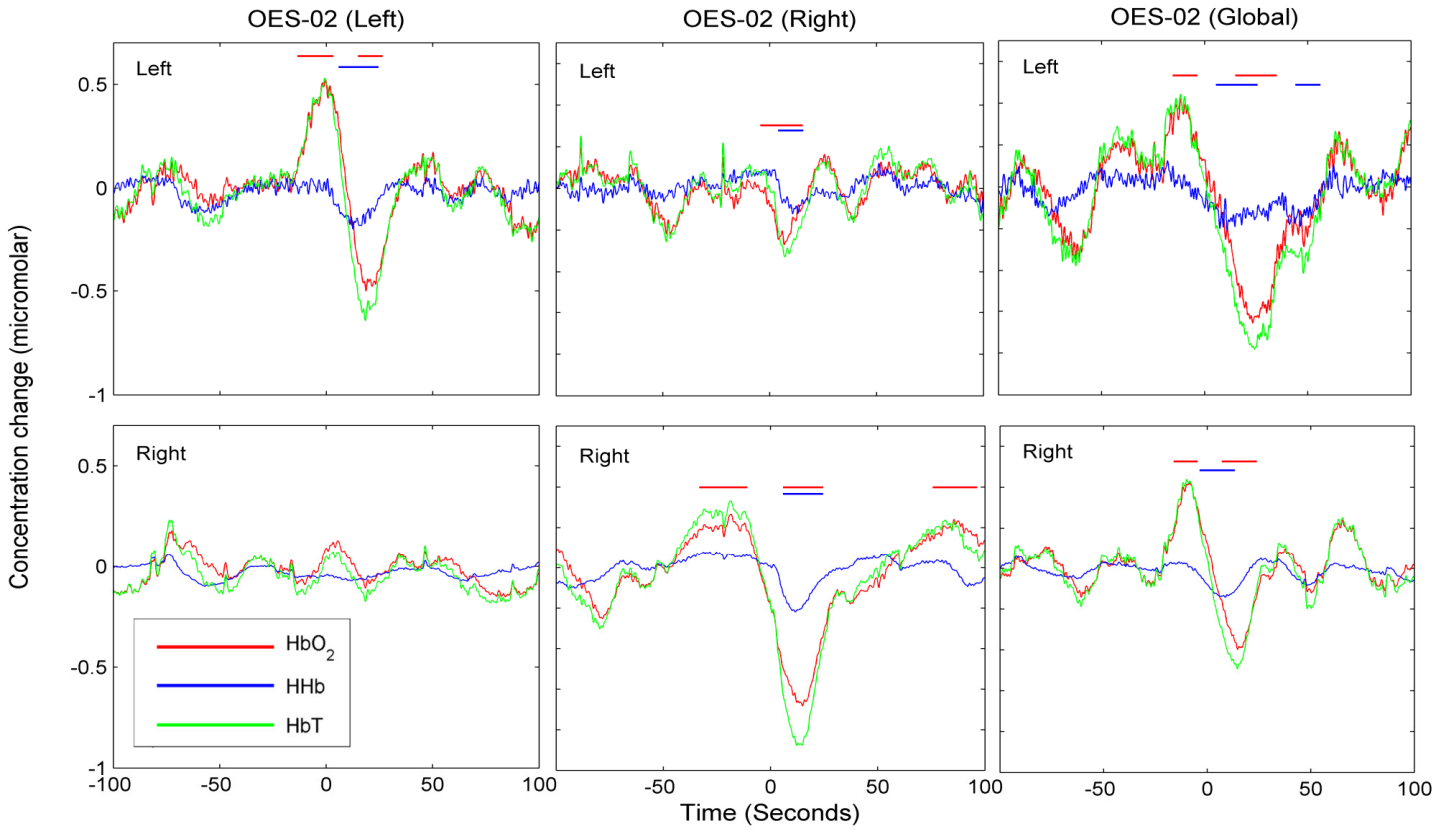

Figure 3.2.20. The mean of all left-sided, right-sided and global events identified in infant OES_02 are shown in the left, centre and right columns respectively. Again, the channel with the largest variation is shown for each side of the head, and periods of significant variation in HHb and HbO_2 are marked with blue and red horizontal bars.

Infant	Time to maximum (s)		Time to minimum (s)		Max-to-min time (s)		Return time (s)		Total duration (s)		Inter-event interval (s)
	HbO_2	HHb	HbO_2	HHb	HbO_2	HHb	HbO_2	HHb	HbO_2	HHb	
OES_01	16.5	16.8	58.6	56.7	42.1	39.9	66.9	62.1	125.5	118.8	467.0
OES_02	31.2	30.2	53.9	49.7	22.7	19.5	43.5	42.7	97.4	92.4	381.3
OES_03	30.9	28.6	54.1	50.0	23.2	21.5	33.4	13.5	87.5	63.5	332.4
Mean	26.2	25.2	55.5	52.1	29.3	27.0	49.2	48.0	103.4	91.6	393.6

Table 3.2.21. Details of the duration of each feature of the all defined haemodynamic events. These figures are based on the channel with the largest variation for the grand average for each infant, i.e. after averaging across all left-sided, right-sided and global events. Return time is the time between the minimum and a return to baseline.

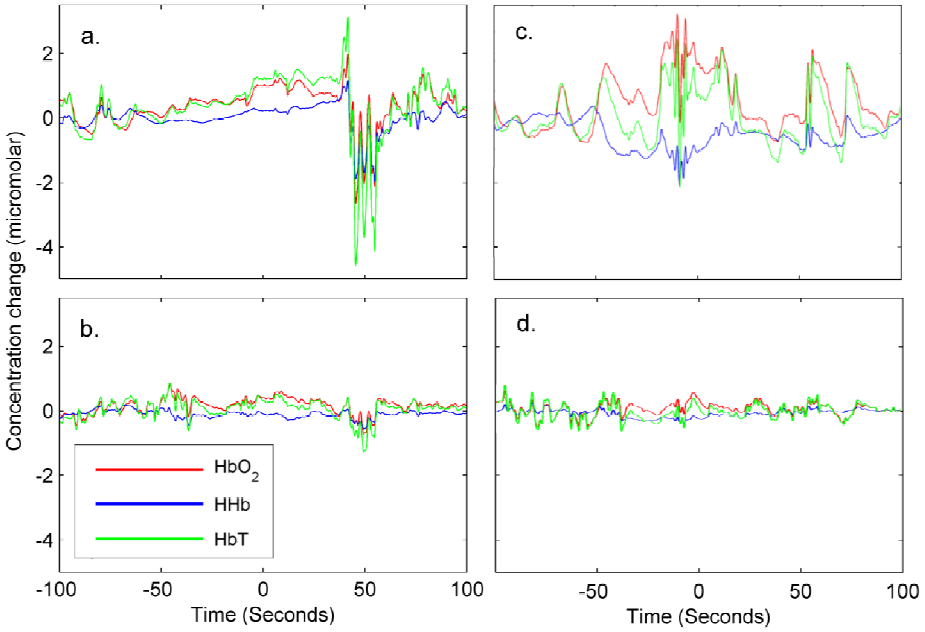

Figure 3.2.22. A single and the mean events identified in infant OEC_01 are shown in figures a and b. A single and the mean events identified in infant OEC_02 are shown in figures c and d. These are typically of all the events identified in all control infants. They appear to be of a non-physiological origin and none show the bi-phasic pattern of the events defined in infants OES_01 to OES_03.

though does not generally exhibit as significant a change. The deviations from baseline of HbO_2 and HHb occur slightly out of phase, with HbO_2 changes lagging behind those of HHb. Deoxyhaemoglobin concentration returns to its baseline value more quickly than HbO_2, such that the average total HHb event duration is 91.6 (27.7) seconds. The average inter-event interval in the neurologically damaged infants is 393.6, but varies significantly, with a standard deviation of 306 seconds. The minimum interval was 109 seconds, whilst the maximum was 1277 seconds (or just over 21 minutes). Information regarding the time course of the mean events in each infant OES_01 to OES_03 is given in table 3.2.21.

For every identified event, the corresponding period of EEG was examined. Although this process consisted only of a careful visual inspection, it was apparent that there were no consistent or significant variations in these infant's EEG recordings before, during or after any of these haemodynamic

features. Although the EEG traces of OES_02 and OES_03 were discontinuous, no significant bursts of electro-cortical activity were found to consistently coincide with the defined haemodynamic events.

Similarly the ECG of infants OES_02 and OES_03 were examined and were found to exhibit a steady heart rate throughout the recording. The mean (and standard deviation) of the heart rate of each infant were 137 (3.9) and 121 (4.2) bpm respectively, and no large or consistent variations were found to be concurrent with the events identified in the optical topography data.

Figure 3.2.22 shows the single-channel haemoglobin concentration changes for a single defined event and the mean of all events in control infant OEC_01, which are very likely to be non-physiological. Although not all are presented for the sake of brevity, the 49 events defined across all control infants appear, without exception, to be of a non-physiological origin. None exhibit the slow increase, rapid decrease and slow return to baseline of HbO_2 concentration which is characteristic of the events defined in infants OES_01, OES_02 and OES_03.

3.2.4.3 Image reconstruction and analysis

As the full dual-modality imaging array was applied in the studies of infants OES_02 and OES_03, the recorded events can be reconstructed to produce three-dimensional images of changes in HbO_2 and HHb concentration. These images are able to provide information about the spatial features of the defined haemodynamic events and provide a further test of their physiological and cortical origin.

Images were reconstructed by dividing each 200-second long event period into 10-second blocks. Each of these blocks of data was used to produce an image of changes in optical absorption at each wavelength, from a baseline defined as the mean of the first 40 seconds of each event period.

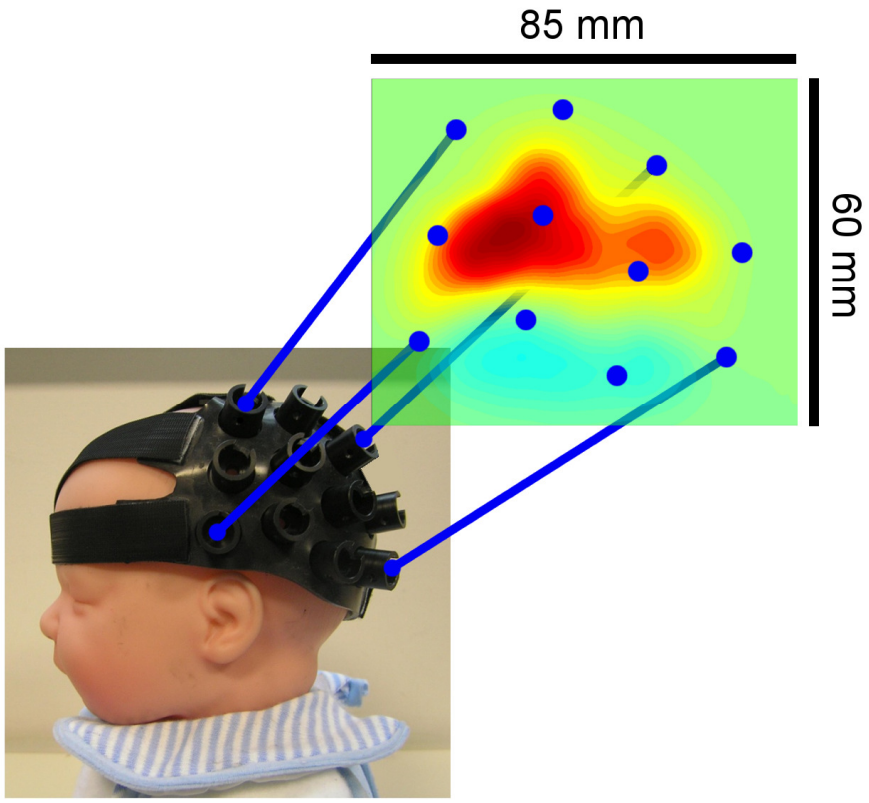

Figure 3.2.23. A representation of how the images presented below map to the curved surface of the head. This figure presents a left-sided image. Right sided images are identical but mirrored about the vertical.

The linear image reconstruction methods described in section 1.2 were employed using a cuboidal finite element mesh. The resulting images were therefore planar, despite the head and imaging array being significantly curved. Each three-dimensional, reconstructed image therefore represents a 'flattened' version of a curved, non-cuboidal volume. Each image contains $40 \times 40 \times 20$ voxels, each of which is a 3 mm cube. Figure 3.2.23 indicates how each 2D image (which represents one layer of the reconstructed 3D image) maps onto the curved surface of the head. The reconstructed images of changes in optical absorption were converted into images of changes in oxy and deoxyhaemoglobin concentrations using the Beer-Lambert law and the coefficients defined by Matcher et al. (1995).

Image reconstruction was performed for all individual events defined in infants OES_02 and OES_03, and for the mean events across each infant and each lateralisation (i.e. left-sided, right-sided and global). After reconstruction each image was rescaled to the correct aspect ratio.

Figure 3.2.24 shows a series of reconstructed images for one right-sided event identified in infant OES_02. In these reconstructions a slow increase in HbO_2 followed by significant decrease is apparent over the right side. The peak increase in HbO_2 concentration occurs over the right temporal region in the -20 to -10 second image. This same position is subsequently the location of the largest decrease in HbO_2 concentration, occurring in the 20-30 second image. The scale of these changes is large, with a peak increase of 13.8 μM. Though the scale of linear reconstructions is often unreliable (as discussed in section 1.2.3.3) one would expect the reconstructed changes to be significantly larger than the changes measured channel-by-channel because of the partial volume effect, and this is indeed the case in all reconstructed events.

Note that for the majority of events in both infants, the reconstructed changes in HHb concentration were similar in spatial content, but were consistently of a smaller-scale than those of HbO_2. They are therefore not presented here.

Figure 3.2.25 shows the series of images reconstructed from the mean of all left-sided events in infant OES_02. Again, a slow increase in HbO_2 concentration, followed by a sudden decrease is apparent. Whilst the peak increase and decrease in HbO_2 concentration occur over the left side, there is clearly some global contribution to these features, as a similar biphasic pattern is apparent over the right side. Note that the scale of these changes is still large compared to functional activation, but is significantly smaller than the single event shown in figure 3.2.24.

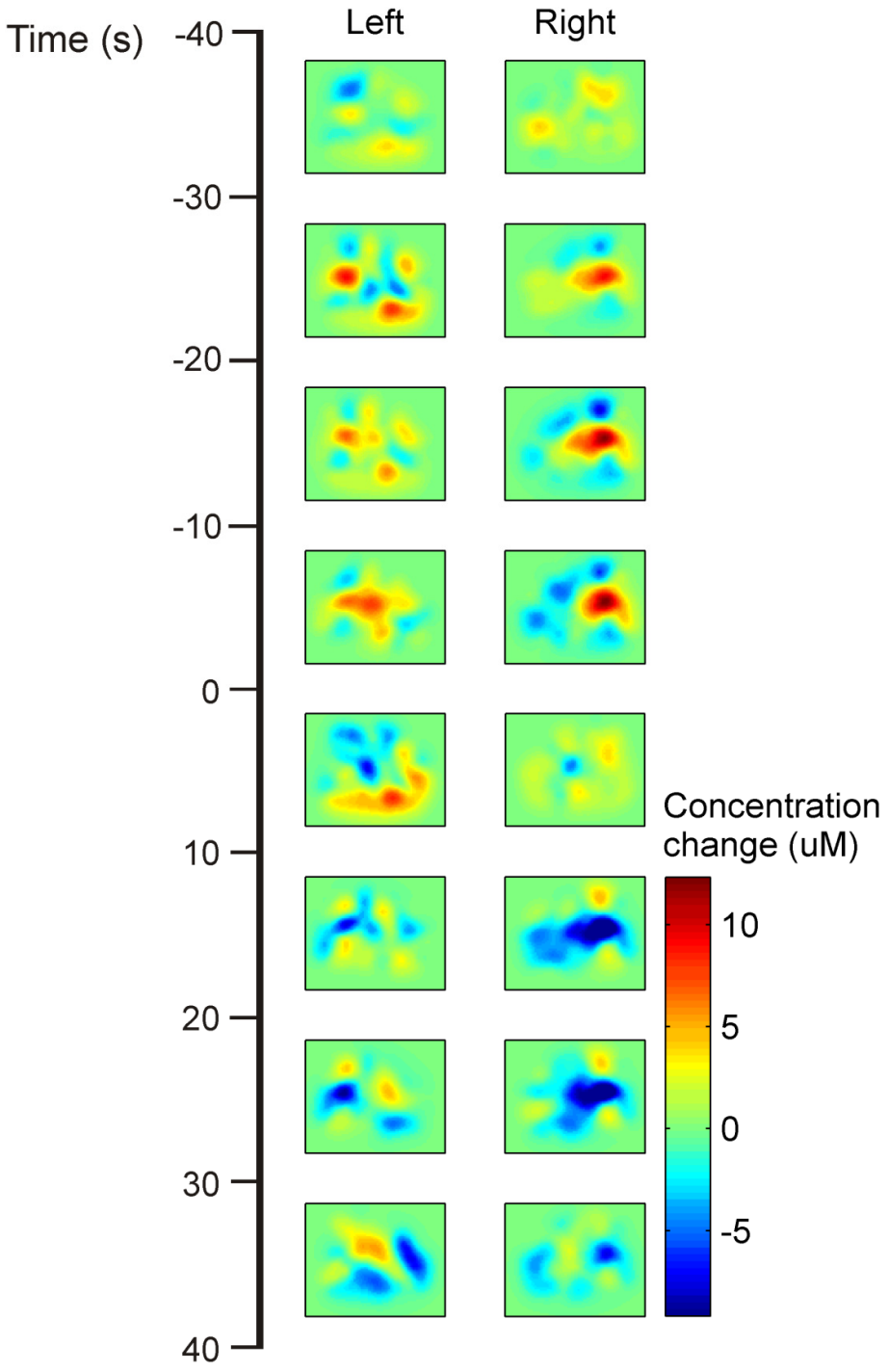

Figure 3.2.24. A series of reconstructed images of HbO_2 concentration for a single event in infant OES_02. Each image is the result of comparing the average of ten seconds of data with baseline. The timescale is such that zero is the start position of the event as defined by the event location algorithm. These images represent a depth of 9-12 mm, which was the site of the peak change in HbO_2 concentration for this event. The reconstructed concentration changes of this event were among the largest for infant OES_02.

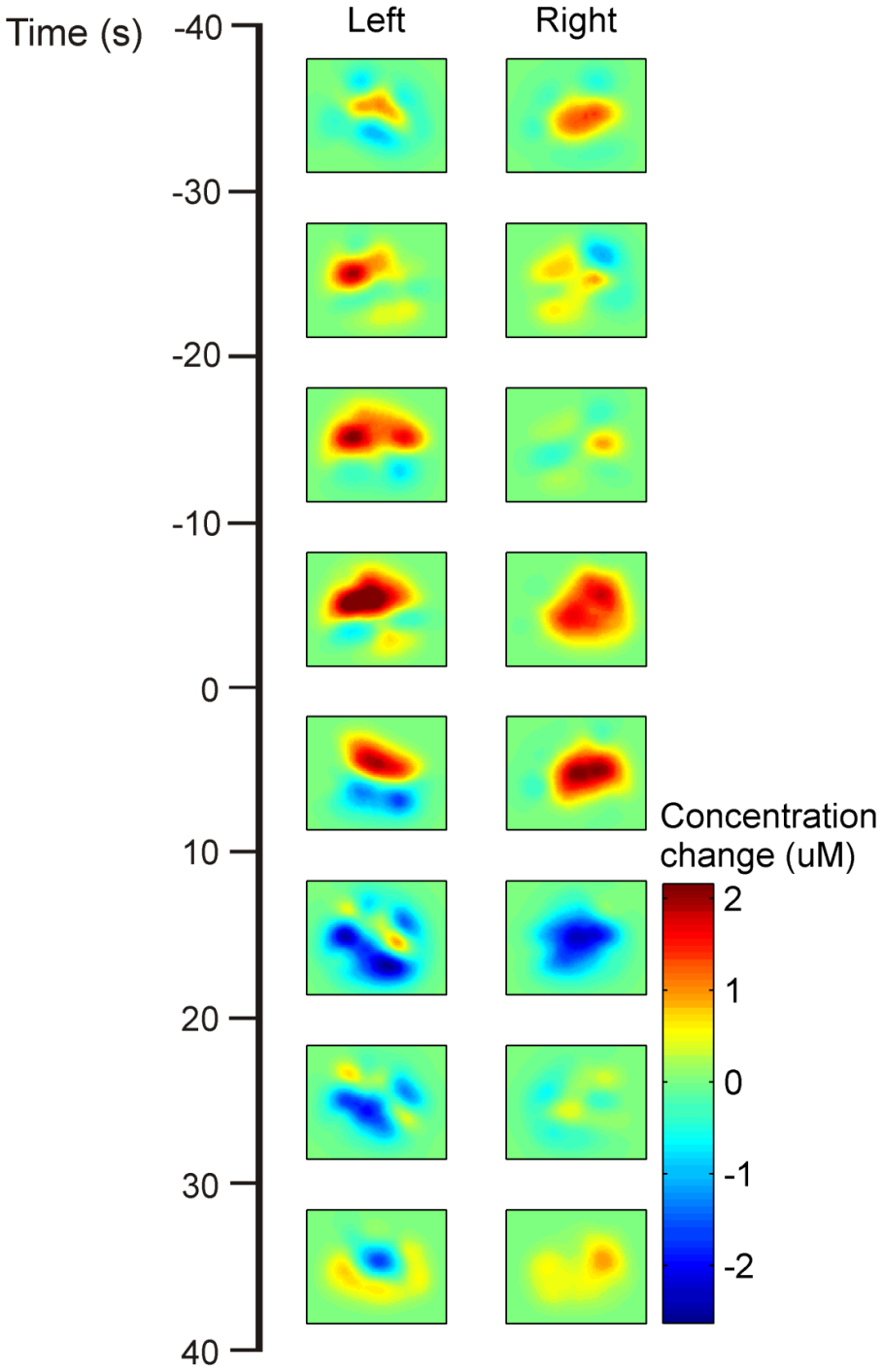

Figure 3.2.25. The reconstructed images of the mean optical topography data for all left-sided events in infant OES_02. These images show the changes in HbO_2 concentration at a depth of 15-18 mm.

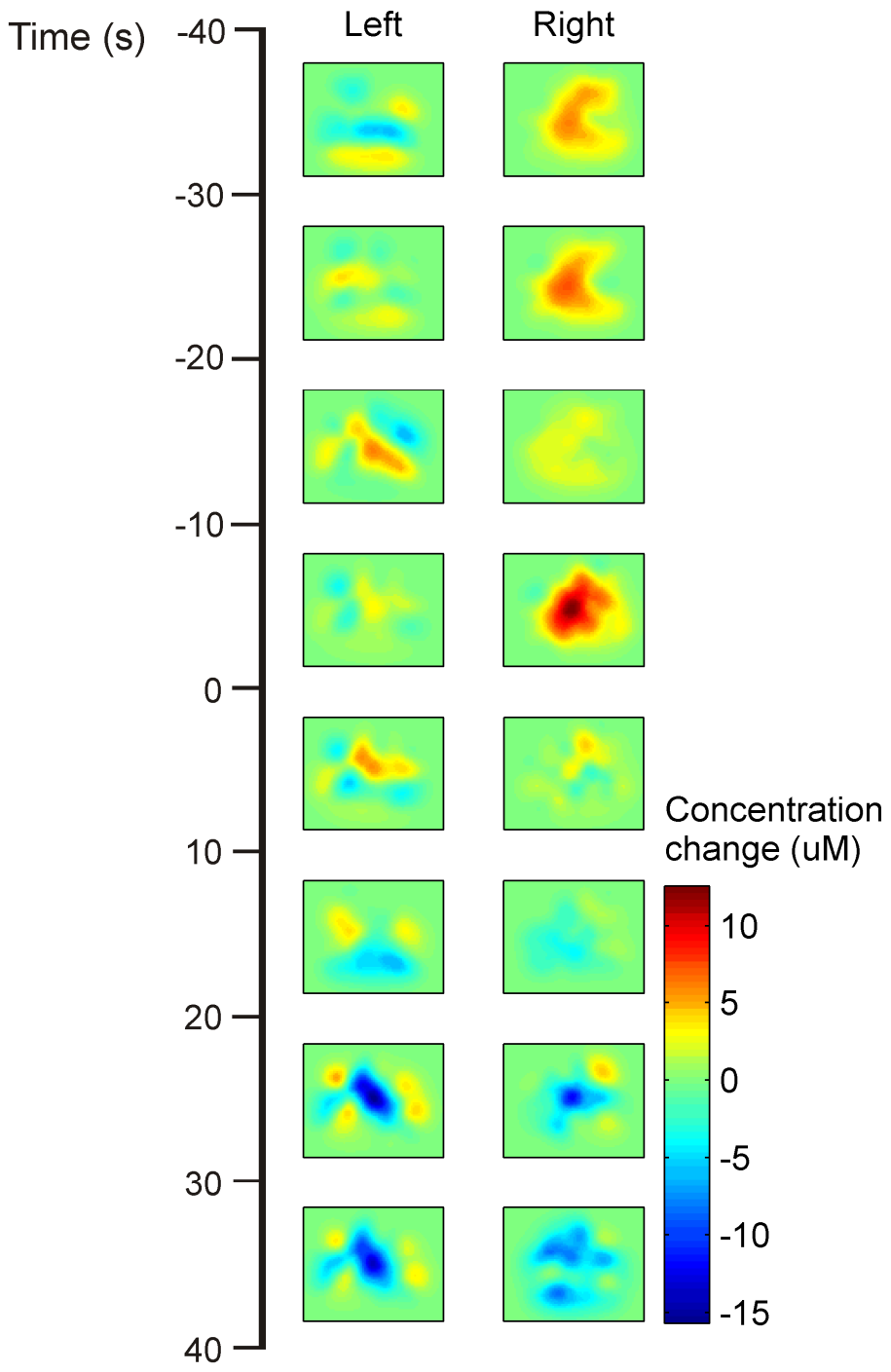

Figure 3.2.26. The reconstructed image series of a single, global event identified in infant OES_03. These images show the changes in HbO_2 concentration at a depth of 12-15 mm.

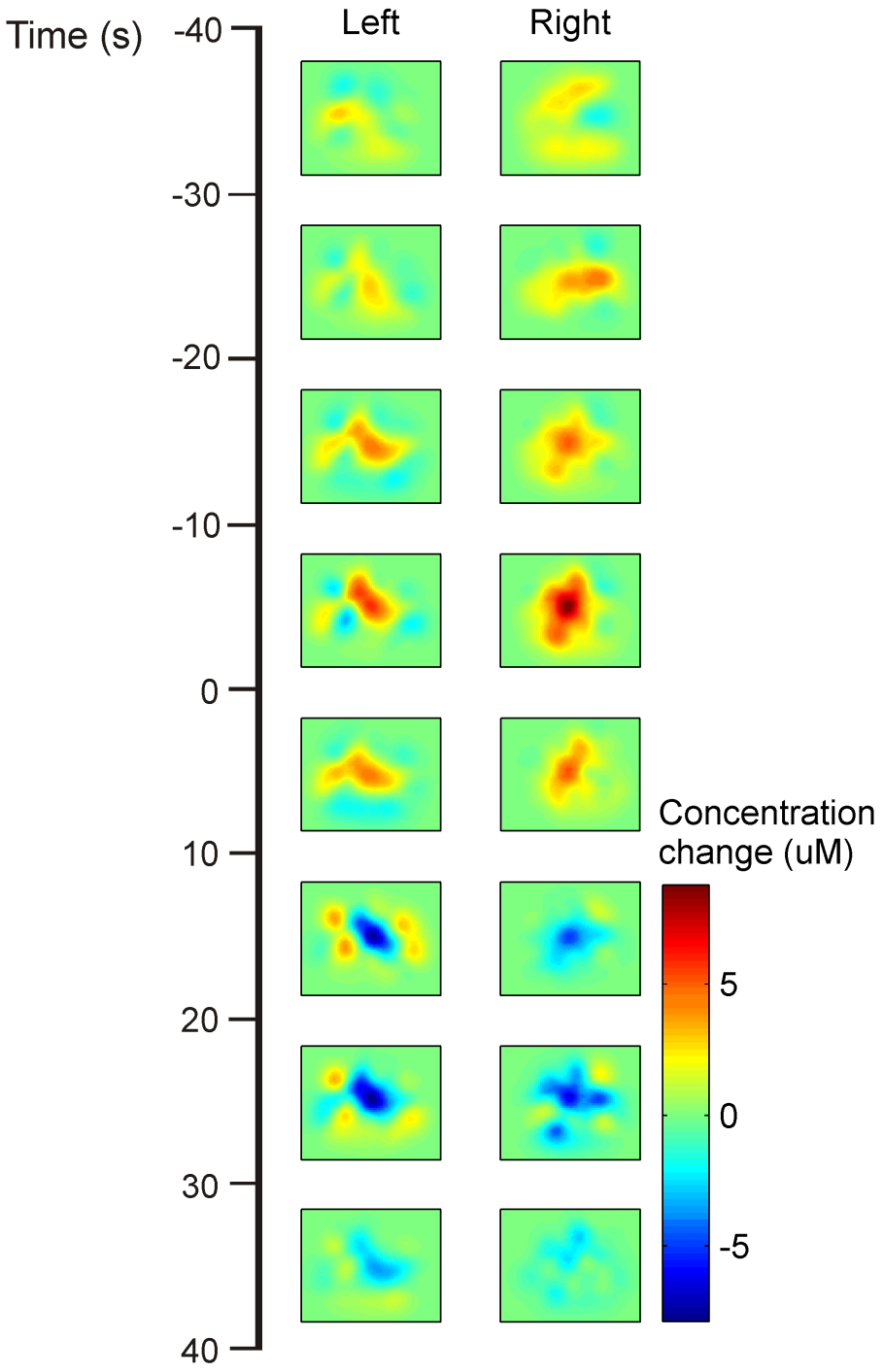

Figure 3.2.27. The reconstructed images of the mean optical topography data for all global events identified in infant OES_03. These images show the changes in HbO_2 concentration at a depth of 12-15 mm.

Figure 3.2.26 shows an example of the images reconstructed for a single, global event identified in infant OES_03. The peak increase in HbO_2 concentration occurs over the right hemisphere in the -10 to zero second image. The same site subsequently exhibits a large decrease in HbO_2 concentration in the 20-30 and 30-40 second images. Figure 3.2.27 shows the average of all global events in infant OES_03, and is perhaps the best example of the slow increase, and sudden decrease in HbO_2 concentration which characterise these haemodynamic events.

The reconstructed images of all 33 defined events in infants OES_02 and OES_03 exhibit a peak haemoglobin concentration change (i.e. the

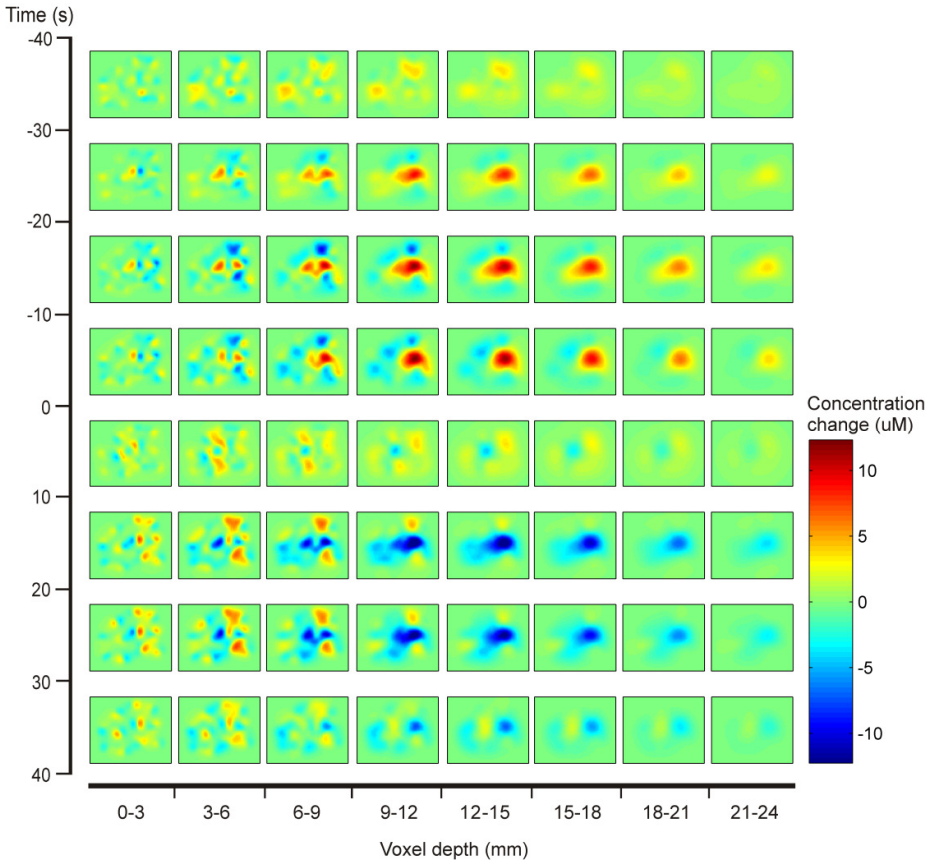

Figure 3.2.28. The reconstructed HbO_2 image series for a single event in infant OES_02, on right side of the head, as a function of time and depth. Once again, time is relative to the defined event start point. The column furthest to the left is the most superficial layer.

maximum positive or negative change in HbO_2 or HHb concentration) at a depth of 6-9 mm or greater. This is significant because noisy or corrupted data often produce reconstructed images in which the largest variations occur at the surface, which obviously cannot be the case if the dominant changes are of a cerebral origin.

Figure 3.2.28 shows the reconstructed images for a single event in infant OES_02 as a function of depth. The superficial layers show many point-like reconstruction artifacts which are associated with the source and detector positions of the array. The characteristic increase and subsequent decrease in HbO_2 concentration is only dominant in the layers at a depth of 9-12 mm and deeper. This dataset is typical of the majority of defined events and provides further evidence that these features have a cortical origin. The depth of the peak change in haemoglobin concentration for all of the 33 events identified in infants OES_02 and OES_03 is provided in figure 3.2.29.

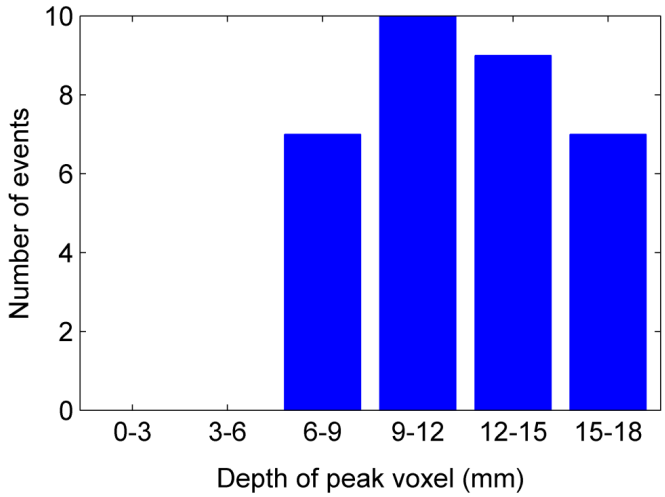

Figure 3.2.29. A histogram of the depth of the voxel which exhibits the largest change (either positive or negative) in HbO_2 or HHb concentration in the reconstructed images of each identified event.

3.2.5 Discussion and Conclusions

These experiments are the first example of the use of full-montage neonatal EEG simultaneously with NIR optical topographic imaging. They provide an explicit proof that high quality EEG data can be obtained simultaneously with NIR topographic images of a large proportion of neonatal cerebral cortex.

The studies presented here have established that simultaneous EEG-NIR imaging of neurologically injured neonates in intensive care is achievable. The continued application of EEG-NIR imaging to the study of neonatal seizures is now a question of addressing two particular issues. The first is the issue of delay between diagnosis and experiment. To maximise the number of ictal events which can be recorded, it is necessary to begin EEG-NIR recording as soon as possible after diagnosis, ideally within an hour. There is no fundamental reason why this cannot be realised. The most significant barrier is likely to be obtaining parental consent in such difficult circumstances in a suitably short period of time. The second issue is the duration for which the system can be applied. Ideally recording would continue for many hours. The factors preventing this are the cumbersome nature of the EEG and optical topography systems, each of which requires its own trolley and power supply, the inconvenience to medical staff caused by the imaging array, and the ability to maintain a good electrical contact for extended periods.

Despite failing to record any electrographic seizures, this series of experiments has resulted in the identification of a consistent, repeated, transient haemodynamic event which is present in the optical topography data of three out of four neurologically compromised infants, but is completely absent in 19 healthy age-matched controls. These events consist of an initial increase, then dramatic fall in HbO_2 and HHb concentrations which can be either localised or global and have an average total duration of approximately 95 seconds.

The optical data sets used as controls were not ideal. The studies of OEC_01 and OEC_02 employed the same arrangement of optical sources and detectors as was used in our brain injured infants, which meant that identical areas of the cortex were sampled. Data sets OEV_01 and OEV_03-OEV_06 were collected with simultaneous EEG recording, but these interrogated a different region of the brain, and were obtained during a study (albeit an unsuccessful one) of functional activation. The experiments which resulted in data sets LSCP_01-LSCP_12 were performed using an identical optical topography system, interrogating the temporal regions of the head. However, these data sets were also part of a functional activation paradigm, although this paradigm was also unsuccessful in obtaining a functional response.

The fundamental purpose of using these control data (and employing an automated approach to data processing) was not to isolate a particular variable; the small sample number and the variety of neurological conditions and medications of the brain-injured group render this impossible. Instead, the aim was simply to establish whether or not these haemodynamic events are common amongst term-age infants. The results presented above strongly suggest they are not.

The fact that any 'events' were identified in the control datasets at all represents a failure of the sensitivity of the movement artifact algorithm and a failure of the specificity of the event identification algorithm. The process by which all events were identified (whether within the neurologically damaged infants or in controls) was an objective process. However, because these algorithms still selected periods of apparently non-physiological variations in the control data (see figure 3.2.22), the eventual comparison between the sample and control datasets remained subjective. The differences between the events identified in the neurologically damaged infants and those of the control infants, though very clear, were assessed visually in a subjective manner. This subjective approach could be made

more robust by employing multiple observers to blindly separate physiological from non-physiological data, though this approach is not usually considered necessary because artifacts are, in general, very distinct from physiological variations. Identification of non-physiological variations in NIR data by visual inspection is still the most common and widely accepted approach within the NIR imaging community (Scholkmann et al. 2010).

Ideally all subjectivity would be removed from the analysis, either by improving the artifact and event identification processes or perhaps by employing a different analysis technique altogether. As mentioned previously, Independent Component Analysis (ICA) would be particularly suited to this task, although the limited number of channels recorded in infant OES_01 would result in the ICA problem being under-determined. If we assume that the NIR signal consists of four independent components: respiration, heart rate, movement effects and the haemodynamic events of interest (though in reality there will be other components, such as vasodilation and blood pressure oscillations) then four independent measurements are required in order for conventional ICA algorithms to be employed. Although under-determined solutions have been presented (Bofill and Zibulevsky 2001). Despite the fact that there remains an element of subjectivity in the approach to event identification performed here, we do not believe that this is a significant failing. The events identified in all 19 control datasets were markedly distinct from the slow features observed in the neurologically damaged infants.

The haemodynamic events indentified appear robust and repeated across three out of four of our brain-injured sample, and significant evidence has been presented that these features are of a physiological origin. The fact that these data can be reconstructed to produce meaningful images, (which consistently exhibit a peak change at a cortical depth) is a strong indication that these events are due to variations in cerebral haemoglobin

concentrations and not due to artifact or physiological changes in superficial tissues. The absence of any events in infant OES_04, who was examined 12 days after the initial seizure diagnosis, was only lightly sedated and exhibited little EEG abnormality, is a further indication that these haemodynamic events are not an artifact inherent to the paradigm.

The haemodynamic events we have identified are consistent in their form, but they do not exhibit the variations in HbO_2 and HHb concentration which are commonly associated with a simple change in regional cerebral blood flow. The classical increased flow response to functional stimulation in adults consists of an increase in HbO_2 and a concurrent decrease in HHb concentration, producing a positive BOLD-fMRI signal (Obrig and Villringer 2003). Studies of functional activation using BOLD-fMRI and diffuse optical techniques have shown the haemodynamic response in newborn infants to be highly variable. Whilst the neonatal functional response is still associated with an increase in regional CBF, many studies have reported an increase in both oxy and deoxyhaemoglobin concentrations (Meek et al. 1998, Hoshi et al. 2000, Muramoto et al. 2002). Immaturity of the cerebrovascular system, (and therefore a different balance between local $CMRO_2$ and CBF) is one possible explanation for this discrepancy.

The large initial increase in HbO_2 concentration exhibited by these haemodynamic events is almost certainly related to an increase in regional cerebral blood flow. The subsequent decrease in HbO_2 concentration may be associated with a sudden decrease in CBF or may be indicative of an inability to meet an increase in regional metabolic demand. The additional complexity of the flow-metabolism relationship in the developing brain makes a detailed interpretation of these haemodynamic variations (particularly those of HHb concentration) very difficult.

The origin of these events is, as yet, undetermined. Without other physiological measures it is impossible to know for certain whether these

events represent localised changes in cerebral blood flow due to activity in the brain itself (i.e. changes in the rate of neuronal metabolism) or whether they are caused by systemic variations in blood pressure.

Because the brain is extremely sensitive to ischemic and haemorrhagic injury, the relationship between blood pressure and cerebral blood flow is regulated in the healthy brain to ensure that CBF is held constant over a range of blood pressures. The mechanism which governs this relationship is known as cerebral autoregulation. In the adult, CBF is held approximately constant for a range of mean arterial blood pressures (MABP) from ~60 mmHg to 150 mmHg (Kandel et al. 2000). Beyond this range, CBF varies approximately linearly with MABP. It has long been suggested that autoregulation mechanisms are poorly developed in newborn infants and can be severely impaired by neurological damage (Lou et al. 1979, Tyszczuk et al. 1998, Munro et al. 2004, Papademetriou et al. 2010).

The fundamental mechanism of autoregulation is arteriolar dilation and constriction. Arterioles are small-diameter vessels which extend from the arteries to the capillary bed (Paulson at al. 1990, Kandel at al. 2000). The ability to regulate CBF under conditions of fluctuating blood pressure can therefore vary significantly from one region of the brain to another. Localised impairment of autoregulation has been demonstrated in studies of ischemic stroke (Paulson et al. 1990, Reinhard et al. 2008).

The haemodynamic events identified in infant OES_01 were completely lateralised, occurring only over the side of the brain which had suffered an extensive ischemic stroke. Infants OES_02 and OES_03 each exhibited both lateralised and global events. Neither had suffered a focal or lateralised neurological injury. The location of these haemodynamic events is therefore consistent with the neuropathology of each infant, but this fact does not necessarily help to determine whether these events are of a cerebral or systemic origin.

The heart rate of infants OES_02 and OES_03 was measured throughout each experiment and was found to remain approximately constant. Though far from conclusive, this observation does not suggest the presence of significant and repeated fluctuations in systemic blood pressure. However, if we assume such fluctuations were present, and that inhomogeneous impairment to cerebral autoregulation could allow such fluctuations in blood pressure to result in lateralised and focal haemodynamic variations, is it possible to predict the form that these variations would take? Studies of neurologically damaged infants have suggested that compromised cerebral autoregulation results in a strong correlation between MABP and CBF (Munro et al. 2004, Wong et al. 2010). Systemic variations in blood pressure would not be concurrent with an alteration of $CMRO_2$. In the event of a significant variation in blood pressure, we may therefore expect to see changes in cerebral haemoglobin concentrations associated with a purely flow-driven response (i.e. HbO_2 increases whilst HHb decreases and vice versa). Although this argument is extremely speculative (and does not take account of the affects of an immature cerebrovascular system), such a flow response is not consistent with the haemodynamic events we have identified.

Although the aetiology of the brain injury was heterogeneous, the diagnosis of seizures and the application of the anti-epileptic drug phenobarbital are the only features common to all the infants in which these haemodynamic events were identified. Studies of partial seizures in adults using single photon emission computed tomography (SPECT), have consistently reported a sustained ictal increase in regional CBF followed by a significant decrease relative to the inter-ictal state (Duncan 1997). This has been confirmed using ictal EEG-fMRI (Salek-Haddadi et al. 2002). It has also been observed that the transition from hyperperfusion to hypoperfusion occurs approximately 90 seconds after the onset of a seizure, irrelevant of

the seizure duration (Avery et al. 2000), suggesting the existence of a metabolic mechanism which limits CBF.

A study using EEG-NIRS in children aged from 1.5 months to 16 years, and suffering from a variety of forms of epilepsy reported a haemodynamic response to electrographic and electro-clinical seizures which consisted of an increase in both HbO_2 and HHb concentration in certain cases (Haginoya et al. 2002). The only published study which has observed the haemodynamic response to neonatal seizures is that of Wallois et al. in 2009, which was described in section 2.1.3. They used the onsets of seizure-like EEG discharges to isolate haemodynamic features which consisted of an increase in HHb and HbO_2, followed by an undershoot of HHb only, and a slow return to baseline. Twenty of these features were observed in a 2-hour recording and they lasted an average of 171 seconds. The author was recently made aware of earlier, unpublished data in which EEG-informed near-infrared spectroscopy of neonatal seizures in three infants showed a large, slow increase in HbO_2 and HHb concentrations followed by a significant undershoot of both, in a manner almost identical to the haemodynamic events identified in infants OES_01-OES-03 (Wallois and Roche-Labarbe, personal communication).

Neonatal seizures are typically brief but recurrent. In 1987 Clancy and Legido recorded electrographic seizures in 42 infants and determined a mean ictal duration of 137 seconds with a mean inter-ictal interval of 480 seconds. The mean (and standard deviation) HbO_2 event duration and inter-event interval of the features identified in infants OES_01, OES_02 and OES_03 were 103.4 (19.7) and 393.6 (306) respectively.

The suitability of phenobarbital as a default treatment for neonatal seizures is still the subject of debate, as it successfully controls seizures in fewer than half of infants (Painter et al. 1999, Scher 2003). The persistence of electrographic seizures when all clinical symptoms have been suppressed is

a common feature of treatment with phenobarbital and suggests the preferential suppression of particular cortical activity (Scher et al. 2003). In large doses, phenobarbital is known to cause a generalised suppression of EEG activity but its effect on cerebral haemodynamics is unknown.

These factors have led to the suggestion that the haemodynamic events we have identified could represent a response to transient seizure activity in groups of neurons which, due to their location or the effects of anti-epileptic medication, do not produce observable electrographic discharges. Although there is evidence to support this idea, the small sample size and the variety of associated neuropathologies renders any such hypothesis highly speculative.

Irrelevant of whether these haemodynamic features are the result of localised and global failures in autoregulation, are related to seizures or are due to some as yet unknown phenomena, further investigation is undoubtedly warranted.

Chapter 4

4.1 Further Work and Future Prospects

This thesis has presented a number of technological advances and experimental applications which have contributed to the development of simultaneous EEG and NIR imaging techniques, particularly with respect to clinical application. However, there are many important issues which warrant further study. The majority of these arise directly from the experimental work described above. Others, however, are essential to the future prospects of EEG-NIR but have remained beyond the scope of this thesis. These issues are briefly discussed below.

4.1.1 System Development and Application Methods.

There are a number of specific hardware developments which would make our EEG-NIR imaging system easier to employ in a clinical setting. For example, the components of the two systems could be mounted on a single trolley, which would save space and minimise the inconvenience caused to the neonatal unit. A further step would be to use a single control computer, rather than one for each modality. This would simplify data acquisition and synchronisation. However, both of these developments require a dedicated EEG system, which is not currently available.

To perform EEG-NIR imaging of neonatal seizures routinely, further improvements to the imaging array are required. A major step would be to decrease the diameter, height and weight of the optical fibres. The fibres used in the experiments described here are right-angled (i.e. the direction of fibre terminus is at 90° to the fibre cable, as can be seen in figure 2.2.1), which makes their application significantly easier. However, they are still relatively large. The fibre housing is 14 mm in diameter and 19 mm in height. Their large diameter places a lower limit on the size of each opto-electrode, and this ultimately limits the sampling density of the dual-modality array. The sensing arrays are also relatively cumbersome and heavy. The use of right-angled fibres, with similar optical transmission

properties but a greatly reduced height and diameter would make long-term EEG-NIR recording significantly easier.

4.1.2 Data Co-registration and Integration

Co-location of one or more of the EEG electrodes with a given optical fibre position makes spatial co-registration of the resulting EEG-NIR imaging data as straight-forward as possible. However, the methods presented here do not constitute an optimum integration of these two forms of data. Pursuing such an integration has remained beyond the scope of this work.

An important step towards maximising the amount of information extracted from simultaneous EEG-NIR data would be to produce a robust and accurate method of registering the position of the sensing imaging array to the cerebral cortex. This has been a goal of diffuse optical imaging methods for many years, and there have been a number of advances (for example see Ye et al. 2009). Except in cases where structural imaging of the brain is performed simultaneously, all such methods consist of two stages. The first is to measure the position of the optical imaging array with respect to the bony landmarks of the head (on which the international 10-20 system is based). The second is to use these landmarks to map the position of the imaging array to the cortex, using a generic or individual structural MRI or CT image. Both of these procedures introduce inaccuracies, particularly the manual location of the 10-20 positions. Superior approaches include the use of photogrammetry techniques, which can produce accurate models of the head surface and the position of the optical imaging array relative to that surface in real time. Such systems can also be used to monitor movement of the subject and produce accurate, head-shaped finite element meshes which aid image reconstruction.

Any approach to data integration must take account of the fact that observable electro-cortical activity and the corresponding haemodynamic

responses can be de-coupled. Significant, synchronous neuronal activity, which (due to depth or neuronal orientation (Conners and Gutnick 1990)), is invisible to scalp EEG is still likely to produce a haemodynamic response. It is also likely that many significant neuronal activations do not produce an observable increase in CBF. The assumption that the increased metabolic activity of a localised group of neurons will produce an exactly co-located haemodynamic response has also been proven to be invalid (Disbrow et al. 2000, Bénar et al. 2006).

Although there are many possible approaches, constraining EEG dipole source localisation on the basis of NIR images is one potentially suitable method of integrating the information apparent in each modality. If a robust spatial concordance can be achieved between a series of NIR images and the corresponding dipole source localisation, it should be possible to take advantage of the high temporal resolution of EEG to look for dynamic changes within a given region of increased cerebral blood flow during a period of activation. Comparable methods are currently under investigation for use in EEG-fMRI (see for example Toma et al. 2002, Vuillemoz et al. 2010), and it is likely that many of these approaches will also be applicable to EEG-NIR techniques.

4.1.3 Neurovascular Coupling and Functional Activation

The simultaneous recording of NIR images and event-related potentials provides a more complete picture of functional processing in the brain than can be achieved with either technique alone. The limited number of studies which have employed EEG-NIR methods to investigate neurovascular coupling have so far concluded that the magnitude of the haemodynamic response to cortical activation generally has a linear relationship with the magnitude (which can be defined in various ways) of the corresponding event-related potentials (Obrig at al. 2002, Näsi et al. 2010). Therefore, the simultaneous recording of ERPs can potentially explain much of the intra and inter-subject variability of functional haemodynamic responses.

Many aspects of neurovascular coupling are still the subject of active research. Simultaneous EEG and NIR techniques can be used to observe a measure of both the input and output of the neurovascular coupling mechanism, on a relatively macroscopic scale. The utility of EEG-NIR imaging will therefore be found in the testing of models of neurovascular coupling from beginning to end. Using EEG-NIR methods, such experiments can be performed efficiently and simply on a wide variety of subjects, which will allow alterations of neurovascular coupling mechanisms to be investigated in cases of neurological disease.

4.1.4 Continuation of Functional Activation in Neonates

Although the main purpose of the functional activation studies presented here was as a proof-of-concept, functional activation in newborns and children is an important potential application of EEG-NIR imaging techniques. There are many functional processes in the developing brain which are poorly understood, even with respect to the areas of the brain which are involved. This is particularly true in the study of auditory processing and language development, studies of which are difficult to perform using fMRI methods. Indeed, one specific application of EEG-NIR

imaging which was not discussed in this thesis is the study of language impairment in young children. Whilst EEG studies have shown there to be distinct differences in the processing of certain linguistic stimuli in infants with specific language impairment, the exact areas of the brain where these discrepancies are apparent is still unknown (Fonteneau and Van der Lely 2008).

Despite the failure of the visual stimulus experiments to elicit a haemodynamic response, there are many visual and auditory stimulation paradigms which may yield important information about functional processing in the developing brain. One obvious application would be to perform an EEG-NIR visual stimulation paradigm, similar to that described above, to explicitly investigate the discrepancies in haemodynamic response which have been observed in studies of neonatal functional activation (see section 3.1.1). The addition of EEG recording would allow changes in the ERP and in the subject's sleep state to be isolated and removed as variables, which may help to clarify the nature of the neonatal functional activation.

4.1.5 Continuation of Studies of Neonatal Seizures

The studies described in this thesis have led to the discovery of a potentially important haemodynamic feature, but they have not facilitated the characterisation of the haemodynamic features of neonatal seizures. However, it has been explicitly demonstrated that EEG-NIR imaging is suitable for the neonatal intensive care unit. Successfully performing EEG-informed NIR imaging of neonatal seizures is now a question of instigating relatively minor alterations to the experimental paradigm.

As described in section 3.2.5, in order to study ictal events, it is essential to begin EEG-NIR recording as soon as possible after seizure diagnosis, and to continue recording for as long as possible. Achieving this is a question of expansion and improved organisation of the clinical research team, though it

would also be significantly aided by the technical developments described above.

If the scale of the project were increased, it may be beneficial to not recruit infants who have been diagnosed, but instead recruit a large number of infants who are at risk of developing seizures (i.e. those who have suffered some ischemic insult at birth) and perform EEG-NIR imaging as continuously as possible for the first 12-24 hours of life. Although this would produce many negative results, it would significantly increase the likelihood of observing ictal seizure events, and may avoid some of the confounding issues related to the administration of anti-epileptic drugs.

One further technological development would be to replace the UCL Optical Topography System with and instrument able to perform whole-head, 3D optical tomography. Such technology is available and has been successfully employed in the neonatal intensive care unit on multiple occasions (Hebden et al. 2002, Austin et al. 2006). Although it would introduce additional experimental complexities, such a system would have the advantage of being able to probe all depths of the neonatal brain. Although highly speculative, it is possible that a combined EEG-optical tomography system would provide a method of studying sub-cortical lesions and seizure foci and provide an assessment of the limitations of clinical EEG and anti-epileptic drugs in the monitoring and treatment of neonatal seizures.

The haemodynamic feature identified in section 3.2 also warrants specific and detailed investigation. The size of the sample group of neurologically compromised infants is too small to make any precise determinations of the aetiology, prevalence or importance of these features. Further experiments, both with seizure-diagnosed and healthy control infants are certainly required. With an increased number of subjects would come better isolation of particular disorders. For example, those infants suffering seizures as a

result of stroke would need to be separated from those who have suffered global hypoxic ischemia, and any variation in the location or form of the biphasic haemodynamic features (if present at all) may inform us as to their physiological origin. The approach to the data processing of these haemodynamic features also needs to be improved in order to remove the remaining subjectivity in the rejection of movement artifacts and identification of events. This can be achieved by improving the sensitivity and specificity of the algorithms presented in section 3.2, by employing multiple observers in order to negate this subjectivity or by developing the use of other signal processing methods. It is likely that independent component analysis would be particularly well suited to this task, particularly when employing the high number of data channels associated with NIR optical topography.

Overall, this thesis represents a first step towards the optimisation of EEG-NIR imaging. The technique presents numerous, significant advantages and many are yet to be fully exploited. Further advances are required, particularly in terms of imaging arrays and data integration, but there are no fundamental obstacles to EEG-NIR becoming a routine neuroimaging technique, for both research and clinical applications.

References

Al-Asmi, A et al. 2003. “fMRI activation in continuous and spike-triggered EEG-fMRI studies of epileptic spikes.” *Epilepsia* 44(10): 1328-1339.

Allen, P J et al. 2000. “A Method for Removing Imaging Artifact from Continuous EEG Recorded during Functional MRI.” *NeuroImage* 12(2): 230-239.

Altman, N R, and B Bernal. 2001. “Brain activation in sedated children: auditory and visual functional MR imaging.” *Radiology* 221(1): 56-63.

Apkarian, P et al. 1991. “Effects of behavioural state on visual processing in neonates.” *Neuropediatrics* 22(2): 85-91.

Arridge, S R. 1995. “Photon-measurement density functions. Part I: Analytical forms.” *Applied Optics* 34(31): 7395-7409.

Arridge, S R. 1999. “Optical Tomography in Medical Imaging.” *Inverse Problems* 15: R41-R93.

Arridge, S R et al. 1992. “The theoretical basis for the determination of optical pathlengths in tissue: temporal and frequency analysis.” *Physics in Medicine and Biology* 37(7): 1531-60.

Arridge, S R et al. 2000a. “A method for three-dimensional time-resolved optical tomography.” *International Journal of Imaging Systems and Technology* 11(1): 2-11.

Arridge, S R et al. 2000b. “A finite element approach for modeling photon transport in tissue.” *Medical Physics* 20(2 Pt 1): 299-309.#

Arthurs, O J et al. 2000. “Linear coupling between functional magnetic resonance imaging and evoked potential amplitude in human somatosensory cortex.” *Neuroscience* 101(4): 803-806.

Attwell, D, and C Iadecola. 2002. “The neural basis of functional brain imaging signals.” *Trends in Neurosciences* 25(12): 621-625.

Austin, T et al. 2006. “Three dimensional optical imaging of blood volume and oxygenation in the neonatal brain.” *NeuroImage* 31(4): 1426-1433.

Avery, R A et al. 2000. “Decreased cerebral blood flow during seizures with ictal SPECT injections.” *Epilepsy Research* 40(1): 53-61.

Aydin, E D et al. 2002. “A comparison between transport and diffusion calculations using a finite element-spherical harmonics radiation transport method.” *Medical Physics* 29(9): 2013-2023.

Bear, M F et al. 2007. *Neuroscience: exploring the brain*. Lippincott Williams & Wilkins.

Bénar, C G. et al. 2006. “EEG-fMRI of epileptic spikes: Concordance with EEG source localization and intracranial EEG.” *NeuroImage* 30(4): 1161-1170.

Bénar, C G. et al. 2007. “Single-trial analysis of oddball event-related potentials in simultaneous EEG-fMRI.” *Human Brain Mapping* 28(7): 602-613.

Ben-Ari, Y. 2002. “Excitatory actions of gaba during development: the nature of the nurture.” *Nat Rev Neurosci* 3(9): 728-739.

Berger, H. 1929. “Über das Elektrenkephalogramm des Menschen.” *Archiv für Psychiatrie und Nervenkrankheiten* 87(1): 527-570.

Birca, A et al. 2006. “Interaction between the flash evoked SSVEPs and the spontaneous EEG activity in children and adults.” *Clinical Neurophysiology* 117(2): 279-288.

Boas, D A. 1997. “A fundamental limitation of linearized algorithms for diffuse optical tomography.” *Optics Express* 1(13): 404-413.

Boas, D A et al. 1994. “Scattering of diffuse photon density waves by spherical inhomogeneities within turbid media: analytic solution and applications.” *PNAS USA* 91(11): 4887-4891.

Boas, D A et al. 2002. “Three dimensional Monte Carlo code for photon migration through complex heterogeneous media including the adult human head.” *Optics Express* 10(3): 159-170.

Boas, D A et al. 2003. “Can the cerebral metabolic rate of oxygen be estimated with near-infrared spectroscopy?.” *Physics in Medicine and Biology* 48(15): 2405-2418.

Boas, D A et al. 2004. “Improving the diffuse optical imaging spatial resolution of the cerebral hemodynamic response to brain activation in humans.” *Optics Letters* 29(13): 1506-1508.

Bofill, P and M Zibulevsky, 2001. “Underdetermined blind source separation using sparse representations.” *Signal Processing* 81(11): 2353-2362

Bonmassar, G et al. 1999. “Visual evoked potential (VEP) measured by simultaneous 64-channel EEG and 3T fMRI.” *Neuroreport* 10(9): 1893-7.

Bonmassar, G. et al. 2001. “Spatiotemporal Brain Imaging of Visual-Evoked Activity Using Interleaved EEG and fMRI Recordings.” *NeuroImage* 13(6): 1035-1043.

Bonmassar, G et al. 2002. “Motion and Ballistocardiogram Artifact Removal for Interleaved Recording of EEG and EPs during MRI.” *NeuroImage* 16(4): 1127-1141.

Born, A P et al. 2000. “Functional magnetic resonance imaging of the normal and abnormal visual system in early life.” *Neuropediatrics* 31(1): 24-32.

Bouchard, M B et al. 2009. “Ultra-fast multispectral optical imaging of cortical oxygenation, blood flow, and intracellular calcium dynamics.” *Optics Express* 17(18): 15670-15678.

Boylan, G et al. 1999. “Cerebral blood flow velocity during neonatal seizures.” *Archives of Disease in Childhood. Fetal and Neonatal Edition* 80(2): F105-F110.

Boylan, G et al. 2002. “Phenobarbitone, neonatal seizures, and video-EEG.” *Archives of Disease in Childhood Fetal and Neonatal Edition* 86(3): F165-F170.

Bradford, H F. 1995. “Glutamate, GABA and epilepsy.” *Progress in Neurobiology* 47(6): 477-511.

Bradford, H F et al. 1978. “Glutamine--a major substrate for nerve endings.” *Journal of Neurochemistry* 30(6): 1453-1459.

Buchheim, K et al. 2004. “Decrease in haemoglobin oxygenation during absence seizures in adult humans.” *Neuroscience Letters* 354(2): 119-122.

Buxton, R B et al. 1998. “Dynamics of blood flow and oxygenation changes during brain activation: The balloon model.” *Magnetic Resonance in Medicine* 39(6): 855-864.

Casse, R et al. “Positron Emission Tomography and Epilepsy.” *Molecular Imaging & Biology* 4(5): 338-351.

Chance, B. et al. 1998. “Phase measurement of light absorption and scatter in human tissue.” *Review of Scientific Instruments* 69(10): 3457-3481.

Clancy, R R, and A Legido. 1987. “The exact ictal and interictal duration of electroencephalographic neonatal seizures.” *Epilepsia* 28(5): 537-541.

Clancy, R R et al. 1988. “Occult Neonatal Seizures.” *Epilepsia* 29(3): 256-261.

Cohen, L B. 1973. “Changes in neuron structure during action potential propagation and synaptic transmission.” *Physiological Reviews* 53(2): 373-418.

Colombo, J, and D W Mitchell. 2009. “Infant visual habituation.” *Neurobiology of Learning and Memory* 92(2): 225-234.

Colonnese, M T et al. 2008. “Development of hemodynamic responses and functional connectivity in rat somatosensory cortex.” *Nat Neurosci* 11(1): 72-79.

Condon, B et al. 1997. “Habituation-like Effects Cause a Significant Decrease in Response in MRI Neuroactivation During Visual Stimulation.” *Vision Research* 37(9): 1243-1247.

Connors, B W, and Michael J. Gutnick. 1990. “Intrinsic firing patterns of diverse neocortical neurons.” *Trends in Neurosciences* 13(3): 99-104.

Cooper, R J et al. 2009. “A tissue-like optically turbid and electrically conducting phantom for simultaneous EEG and near-infrared imaging.” *Physics in Medicine and Biology* 54(18): N403-408.

Correia, T et al. 2009. “A quantitative assessment of the depth sensitivity of an optical topography system using a solid dynamic tissue-phantom.” *Physics in Medicine and Biology* 54(20): 6277-6286.

Culver, J P et al. 2003. “Three-dimensional diffuse optical tomography in the parallel plane transmission geometry: Evaluation of a hybrid frequency domain/continuous wave clinical system for breast imaging.” *Medical Physics* 30(2): 235-247.

Danos, P et al. 2001. “EEG Alpha Rhythm and Glucose Metabolic Rate in the Thalamus in Schizophrenia.” *Neuropsychobiology* 43(4): 265-272.

Dehghani, H et al. 2009. “Depth sensitivity and image reconstruction analysis of dense imaging arrays for mapping brain function with diffuse optical tomography.” *Applied Optics* 48(10): D137-D143.

Delorme, A, and S Makeig. 2004. “EEGLAB: an open source toolbox for analysis of single-trial EEG dynamics including independent component analysis.” *Journal of Neuroscience Methods* 134(1): 9-21.

D'Esposito, M et al. 2003. “Alterations in the BOLD fMRI signal with ageing and disease: a challenge for neuroimaging.” *Nat Rev Neurosci* 4(11): 863-872.

Di Russo, F et al. 2003. “Source Analysis of Event-related Cortical Activity during Visuo-spatial Attention.” *Cerebral Cortex* 13(5): 486 -499.

Diaz, G A et al. 2006. “Near infrared spectroscopy in the management of status epilepticus in a young infant.” *European Journal of Paediatric Neurology* 10(1): 19-21.

Disbrow, E A et al. 2000. “Functional MRI at 1.5 tesla: A comparison of the blood oxygenation level-dependent signal and electrophysiology.” *Proceedings of the National Academy of Sciences of the United States of America* 97(17): 9718-9723.

Duncan, A et al. 1995. “Optical pathlength measurements on adult head, calf and forearm and the head of the newborn infant using phase resolved optical spectroscopy.” *Physics in Medicine and Biology* 40(2): 295-304.

Duncan, J S. 1997. “Imaging and epilepsy.” *Brain* 120(2): 339 -377.

Ebersole, J S. 2003. “EEG dipole analysis.” In *Presurgical Assessment of the Epilepsies with Clinical Neurophysiology and Functional Imaging*, Elsevier, p. 471-490.

Elisee, J P et al. 2010. “Combination of Boundary Element Method and Finite Element Method in Diffuse Optical Tomography.” *Biomedical Engineering, IEEE Transactions on* 57(11): 2737-2745.

Ellingson, R J. 1986. “Development of visual evoked potentials and photic driving responses in normal full term, low risk premature, and trisomy-21 infants during the first year of life.” *Electroencephalography and Clinical Neurophysiology* 63(4): 309-316.

Engel, J. 2006. “ILAE classification of epilepsy syndromes.” *Epilepsy Research* 70: 5-10.

Engel, J et al. 2008. *Epilepsy: A Comprehensive Textbook*. Lippincott Williams & Wilkins.

Erberich, S G et al. 2006. “Somatosensory lateralization in the newborn brain.” *NeuroImage* 29(1): 155-161.

Everdell, N L et al. 2005. “A frequency multiplexed near-infrared topography system for imaging functional activation in the brain.” *Review of Scientific Instruments* 76(9): 093705-5.

Firbank, M et al. 1995. “An improved design for a stable and reproducible phantom material for use in near-infrared spectroscopy and imaging.” *Physics in Medicine and Biology* 40(5): 955-961.

Fisher, R S et al. 2005. “Epileptic Seizures and Epilepsy: Definitions Proposed by the International League Against Epilepsy (ILAE) and the International Bureau for Epilepsy (IBE).” *Epilepsia* 46(4): 470-472.

Flock, S T et al. 1992. “Optical properties of intralipid: A phantom medium for light propagation studies.” *Lasers in Surgery and Medicine* 12(5): 510-519.

Fonteneau, E, and H K J van der Lely. 2008. “Electrical Brain Responses in Language-Impaired Children Reveal Grammar-Specific Deficits.” *PLoS ONE* 3(3): e1832.

la Fougère, C et al. 2009. “PET and SPECT in epilepsy: A critical review.” *Epilepsy & Behavior* 15(1): 50-55.

Fox, P T, and M E Raichle. 1986. “Focal physiological uncoupling of cerebral blood flow and oxidative metabolism during somatosensory stimulation in human subjects..” *PNAS USA* 83(4): 1140-1144.

Frahm, J et al. 1996. “Dynamic uncoupling and recoupling of perfusion and oxidative metabolism during focal brain activation in man.” *Magnetic Resonance in Medicine* 35(2): 143-148.

Franceschini, M A, and D A Boas. 2004. “Noninvasive measurement of neuronal activity with near-infrared optical imaging.” *NeuroImage* 21(1): 372-386.

Franceschini, M A et al. 2000. “On-line optical imaging of the human brain with 160-ms temporal resolution.” *Optics Express* 6(3): 49-57.

Franceschini, M A et al. 2003. “Hemodynamic evoked response of the sensorimotor cortex measured noninvasively with near-infrared optical imaging.” *Psychophysiology* 40(4): 548-560.

Franceschini, M A et al. 2010. “The effect of different anesthetics on neurovascular coupling.” *NeuroImage* 51(4): 1367-1377.

Gallagher, A et al. 2008. “Non-invasive pre-surgical investigation of a 10 year-old epileptic boy using simultaneous EEG-NIRS.” *Seizure: the journal of the British Epilepsy Association* 17(6): 576-82.

Gibson, A P et al. 2005. “Recent advances in diffuse optical imaging.” *Physics in medicine and biology* 50(4): R1-43.

Ginley, D S. 2010. *Handbook of Transparent Conductors*. Springer.

Glass, H C et al. 2009. “Clinical Neonatal Seizures are Independently Associated with Outcome in Infants at Risk for Hypoxic-Ischemic Brain Injury.” *The Journal of Pediatrics* 155(3): 318-323.

Glauser, T A, and R R Clancy. 1992. “Adequacy of Routine EEG Examinations in Neonates With Clinically Suspected Seizures.” *J Child Neurol* 7(2): 215-220.

Gloor, P. 1985. “Neuronal generators and the problem of localization in electroencephalography: application of volume conductor theory to electroencephalography.” *Journal of Clinical Neurophysiology* 2(4): 327-354.

Goldman, R I et al. 2002. “Simultaneous EEG and fMRI of the alpha rhythm.” *Neuroreport* 13(18): 2487-92.

Gotman, J. 2008. “Epileptic networks studied with EEG-fMRI.” *Epilepsia* 49(s3): 42-51.

Gotman, J et al. 2005. “Generalized epileptic discharges show thalamocortical activation and suspension of the default state of the brain.” *Proceedings of the National Academy of Sciences of the United States of America* 102(42): 15236 -15240.

Gotman, J et al. 2006. “Combining EEG and fMRI: A multimodal tool for epilepsy research.” *Journal of Magnetic Resonance Imaging* 23(6): 906-920.

Gratton, G. 1997. “Attention and probability effects in the human occipital cortex: an optical imaging study.” *Neuroreport* 8(7): 1749-1753.

Gratton, G et al. 2006. “Effects of measurement method, wavelength, and source-detector distance on the fast optical signal.” *NeuroImage* 32(4): 1576-1590.

Grimm, C et al. 1998. “A comparison between electric source localisation and fMRI during somatosensory stimulation.” *Electroencephalography and Clinical Neurophysiology* 106(1): 22-29.

Haginoya, K et al. 2002. “Ictal cerebral haemodynamics of childhood epilepsy measured with near-infrared spectrophotometry.” *Brain* 125(9): 1960 -1971.

Hamandi, K et al. 2006. “EEG-fMRI of idiopathic and secondarily generalized epilepsies.” *NeuroImage* 31(4): 1700-1710.

Hathout, G M et al. 1994. “MR imaging signal response to sustained stimulation in human visual cortex.” *Journal of Magnetic Resonance Imaging: JMRI* 4(4): 537-543.

Hawco, C S et al. 2007. “BOLD changes occur prior to epileptic spikes seen on scalp EEG.” *NeuroImage* 35(4): 1450-1458.

Hebden, J C, and David T. Delpy. 1994. “Enhanced time-resolved imaging with a diffusion model of photon transport.” *Optics Letters* 19(5): 311-313.

Hebden, J C et al. 2002. “Three-dimensional optical tomography of the premature infant brain.” *Physics in Medicine and Biology* 47(23): 4155-4166.

Hebden, J C et al. 2008. “An electrically-activated dynamic tissue-equivalent phantom for assessment of diffuse optical imaging systems.” *Physics in Medicine and Biology* 53(2): 329-337.

Heiskala, J et al. 2009. “Significance of background optical properties, time-resolved information and optode arrangement in diffuse optical imaging of term neonates.” *Physics in Medicine and Biology* 54(3): 535-554.

Herrmann, C S. 2001. “Human EEG responses to 1-100 Hz flicker: resonance phenomena in visual cortex and their potential correlation to cognitive phenomena.” *Experimental Brain Research* 137(3-4): 346-353.

Hoge, R D et al. 2005. “Simultaneous recording of task-induced changes in blood oxygenation, volume, and flow using diffuse optical imaging and arterial spin-labeling MRI.” *NeuroImage* 25(3): 701-707.

Horovitz, S G, and John C. Gore. 2004. “Simultaneous event-related potential and near-infrared spectroscopic studies of semantic processing.” *Human Brain Mapping* 22(2): 110-115.

Horovitz, S G et al. 2008. “Low frequency BOLD fluctuations during resting wakefulness and light sleep: A simultaneous EEG-fMRI study.” *Human Brain Mapping* 29(6): 671-682.

Hoshi, Y et al. 2000. “Hemodynamic responses to photic stimulation in neonates.” *Pediatric Neurology* 23(4): 323-327.

Hyvärinen, A and E Oja, 2000. “Independent component analysis: algorithms and applications.” *Neural Networks* 13(4-5): 411-430

Iadecola, C. 2004. “Neurovascular regulation in the normal brain and in Alzheimer's disease.” *Nat Rev Neurosci* 5(5): 347-360.

Isler, J R et al. 2007. “Frequency Domain Analyses of Neonatal Flash VEP.” *Pediatric Research* 62(5): 581-585.

Jäger, L et al. 2002. “Focal Epileptiform Activity in the Brain: Detection with Spike-related Functional MR Imaging: Preliminary Results1.” *Radiology* 223(3): 860 -869.

Jöbsis, F F. 1977. “Noninvasive, infrared monitoring of cerebral and myocardial oxygen sufficiency and circulatory parameters.” *Science (New York, N.Y.)* 198(4323): 1264-7.

Johnston, M V. 1995. “Neurotransmitters and vulnerability of the developing brain.” *Brain and Development* 17(5): 301-306.

Kandel, E et al. 2000. *Principles of Neural Science*. 4th ed. McGraw-Hill Medical.

Karen, T et al. 2008. “Hemodynamic response to visual stimulation in newborn infants using functional near-infrared spectroscopy.” *Human Brain Mapping* 29(4): 453-460.

Kaufmann, C et al. 2006. “Brain activation and hypothalamic functional connectivity during human non-rapid eye movement sleep: an EEG/fMRI study.” *Brain* 129(3): 655-667.

Kennan, R P et al. 2002. “Simultaneous Recording of Event-Related Auditory Oddball Response Using Transcranial Near Infrared Optical Topography and Surface EEG.” *NeuroImage* 16(3, Part 1): 587-592.

Klem, G H et al. 1999. “The ten-twenty electrode system of the International Federation. The International Federation of Clinical Neurophysiology.” *Electroencephalography and Clinical Neurophysiology. Supplement* 52: 3-6.

Kobayashi, E et al. 2006. “Temporal and extratemporal BOLD responses to temporal lobe interictal spikes.” *Epilepsia* 47(2): 343-354.

Koch, S P et al. 2006. “Synchronization between Background Activity and Visually Evoked Potential Is Not Mirrored by Focal Hyperoxygenation: Implications for the Interpretation of Vascular Brain Imaging.” *J. Neurosci.* 26(18): 4940-4948.

Koch, S P et al. 2008. “Individual alpha-frequency correlates with amplitude of visual evoked potential and hemodynamic response.” *NeuroImage* 41(2): 233-242.

Krakow, K. et al. 1999. “EEG-triggered functional MRI of interictal epileptiform activity in patients with partial seizures.” *Brain* 122(9): 1679 -1688.

Krakow, K et al. 2001. “Spatio-temporal imaging of focal interictal epileptiform activity using EEG-triggered functional MRI.” *Epileptic Disorders* 3(2): 67-74.

Krüger, G et al. 1999. “Simultaneous monitoring of dynamic changes in cerebral blood flow and oxygenation during sustained activation of the human visual cortex.” *Neuroreport* 10(14): 2939-2943.

Kusaka, T et al. 2004. “Noninvasive optical imaging in the visual cortex in young infants.” *Human Brain Mapping* 22(2): 122-132.

Laufs, H. 2008. “Endogenous brain oscillations and related networks detected by surface EEG-combined fMRI.” *Human Brain Mapping* 29(7): 762-769.

Laufs, H et al. 2003. “EEG-correlated fMRI of human alpha activity.” *NeuroImage* 19(4): 1463-1476.

Leahy, R M et al. 1998, “A study of dipole localization accuracy for MEG and EEG using a human skull phantom.” *Electroencephalography and Clinical Neurophysiology* 107(2): 159-173.

Lemieux, L et al. 2001. “Event-Related fMRI with Simultaneous and Continuous EEG: Description of the Method and Initial Case Report.” *NeuroImage* 14(3): 780-787.

Levy, S R et al. 1985. “Seizures and cerebral infarction in the full-term newborn.” *Annals of Neurology* 17(4): 366-370.

Liao, S M et al. 2010. “Neonatal hemodynamic response to visual cortex activity: high-density near-infrared spectroscopy study.” *Journal of Biomedical Optics* 15(2): 026010-9.

Lieb, J P et al. 1976. “A Comparison of EEG Seizure Patterns Recorded with Surface and Depth Electrodes in Patients with Temporal Lobe Epilepsy.” *Epilepsia* 17(2): 137-160.

Linden, D E J et al. 1999. “The Functional Neuroanatomy of Target Detection: An fMRI Study of Visual and Auditory Oddball Tasks.” *Cerebral Cortex* 9(8): 815 -823.

Logothetis, N K. 2008. “What we can do and what we cannot do with fMRI.” *Nature* 453(7197): 869-878.

Lou, H C et al. 1979. “Impaired autoregulation of cerebral blood flow in the distressed newborn infant.” *The Journal of Pediatrics* 94(1): 118-121.

Luck, S J. 2005. *An Introduction to the Event-Related Potential Technique*. MIT Press.

Lui, Z et al. 2006. “Integration of EEG/MEG with MRI and fMRI.” *Engineering in Medicine and Biology* 25(4): 46-53.

Mandelkow, H et al. 2006. “Synchronization facilitates removal of MRI artefacts from concurrent EEG recordings and increases usable bandwidth.” *NeuroImage* 32(3): 1120-1126.

Mangun, G R et al. 1998. “ERP and fMRI measures of visual spatial selective attention.” *Human Brain Mapping* 6(5-6): 383-389.

Marmor, M F et al. 2004. “Standard for clinical electroretinography (2004 update).” *Documenta Ophthalmologica* 108(2): 107-114.

Martin, E et al. 1999. “Visual processing in infants and children studied using functional MRI.” *Pediatric Research* 46(2): 135-140.

Matcher, S J et al. 1995. “Performance Comparison of Several Published Tissue Near-Infrared Spectroscopy Algorithms.” *Analytical Biochemistry* 227(1): 54-68.

Mayhew, S D et al. 2010. “EEG signatures of auditory activity correlate with simultaneously recorded fMRI responses in humans.” *NeuroImage* 49(1): 849-864.

Maynard, D et al. 1969. “Device for continuous monitoring of cerebral activity in resuscitated patients..” *British Medical Journal* 4(5682): 545-546.

Meek, J H et al. 1995. “Regional Changes in Cerebral Haemodynamics as a Result of a Visual Stimulus Measured by near Infrared Spectroscopy.” *Proceedings: Biological Sciences* 261(1362): 351-356.

Meek, J H et al. 1998. “Regional hemodynamic responses to visual stimulation in awake infants.” *Pediatric Research* 43(6): 840-843.

Miller, K L et al. 2001. “Nonlinear temporal dynamics of the cerebral blood flow response.” *Human Brain Mapping* 13(1): 1-12.

Mirmiran, M et al. 2003. “Development of fetal and neonatal sleep and circadian rhythms.” *Sleep Medicine Reviews* 7(4): 321-334.

Mizrahi, E M, and Peter Kellaway. 1987. “Characterization and classification of neonatal seizures.” *Neurology* 37(12): 1837.

Morita, T et al. 2000. “Difference in the metabolic response to photic stimulation of the lateral geniculate nucleus and the primary visual cortex of infants: a fMRI study.” *Neuroscience Research* 38(1): 63-70.

de Munck, J C et al. 2007. “The hemodynamic response of the alpha rhythm: An EEG/fMRI study.” *NeuroImage* 35(3): 1142-1151.

Munro, M J et al. 2004. “Hypotensive Extremely Low Birth Weight Infants Have Reduced Cerebral Blood Flow.” *Pediatrics* 114(6): 1591-1596.

Muramoto, S et al. 2002. “Age-dependent change in metabolic response to photic stimulation of the primary visual cortex in infants: functional magnetic resonance imaging study.” *Journal of Computer Assisted Tomography* 26(6): 894-901.

Murray, D M et al. 2008. “Defining the gap between electrographic seizure burden, clinical expression and staff recognition of neonatal seizures.” *Archives of Disease in Childhood. Fetal and Neonatal Edition* 93(3): F187-91.

Nakano, T et al. 2009. “Prefrontal Cortical Involvement in Young Infants’ Analysis of Novelty.” *Cerebral Cortex* 19(2): 455 -463.

Näsi, T et al. 2010. “Correlation of visual-evoked hemodynamic responses and potentials in human brain.” *Experimental Brain Research* 202(3): 561-570.

Niedermeyer, E, and F H Lopes Da Silva. 2004. *Electroencephalography: Basic Principles, Clinical Applications and Related Fields*. 5th ed. Lippincott Williams and Wilkins.

Noesselt, T et al. 2002. “Delayed Striate Cortical Activation during Spatial Attention.” *Neuron* 35(3): 575-587.

Nunez, P L, and R B Silberstein. 2000. “On the relationship of synaptic activity to macroscopic measurements: does co-registration of EEG with fMRI make sense?.” *Brain Topography* 13(2): 79-96.

Obrig, H, and A Villringer. 2003. “Beyond the Visible[mdash]Imaging the Human Brain With Light.” *J Cereb Blood Flow Metab* 23(1): 1-18.

Obrig, H et al. 2002. “Habituation of the Visually Evoked Potential and Its Vascular Response: Implications for Neurovascular Coupling in the Healthy Adult.” *NeuroImage* 17(1): 1-18.

Odom, J V et al. 2004. “Visual evoked potentials standard (2004).” *Documenta ophthalmologica. Advances in ophthalmology* 108(2): 115-23.

Painter, M J et al. 1999. “Phenobarbital compared with phenytoin for the treatment of neonatal seizures.” *The New England Journal of Medicine* 341(7): 485-489.

Papademetriou, M D et al. 2010. “Cerebral and peripheral tissue oxygenation in children supported on ECMO for cardio-respiratory failure.” *Advances in Experimental Medicine and Biology* 662: 447-453.

Paulson, O B et al. 1990. “Cerebral autoregulation.” *Cerebrovascular and Brain Metabolism Reviews* 2(2): 161-192.

Pieh, C et al. 2009. “Maturation of steady-state flicker VEPs in infants: fundamental and harmonic temporal response frequencies.” *Documenta Ophthalmologica. Advances in Ophthalmology* 118(2): 109-119.

Pinto, L C, and P Giliberti. 2001. “Neonatal seizures: background EEG activity and the electroclinical correlation in full-term neonates with hypoxic-ischemic encephalopathy. Analysis by computer-synchronized long-term polygraphic video-EEG monitoring.” *Epileptic Disorders* 3(3): 125-132.

Portas, C M et al. 2000. “Auditory Processing across the Sleep-Wake Cycle: Simultaneous EEG and fMRI Monitoring in Humans.” *Neuron* 28(3): 991-999.

Rector, D M et al. 1997. “Light scattering changes follow evoked potentials from hippocampal Schaeffer collateral stimulation.” *Journal of Neurophysiology* 78(3): 1707-1713.

Reinhard, M et al. 2008. “Cerebral Autoregulation Dynamics in Acute Ischemic Stroke after rtPA Thrombolysis.” *Cerebrovascular Diseases* 26(2): 147-155.

Rennie, J et al. 2004. “Non-expert use of the cerebral function monitor for neonatal seizure detection.” *Archives of Disease in Childhood Fetal and Neonatal Edition* 89(1): F37-F40.

Rennie, J et al. 2008. “Neonatal Cerebral Investigation.” *Cambridge University Press* ISBN-13: 9780521838481.

Ritter, P, and A Villringer. 2006. “Simultaneous EEG-fMRI.” *Neuroscience & Biobehavioral Reviews* 30(6): 823-838.

Roche-Labarbe, N et al. 2007. “Coupled oxygenation oscillation measured by NIRS and intermittent cerebral activation on EEG in premature infants.” *NeuroImage* 36(3): 718-27.

Roche-Labarbe, N et al. 2008. “NIRS-measured oxy- and deoxyhemoglobin changes associated with EEG spike-and-wave discharges in children.” *Epilepsia* 49. 1871-1880.

Rosa, M J et al. 2010. “Estimating the transfer function from neuronal activity to BOLD using simultaneous EEG-fMRI.” *NeuroImage* 49(2): 1496-1509.

Rugg, M D, and M G H Coles. 1996. *Electrophysiology of Mind: Event-related Brain Potentials and Cognition*. New edition. OUP Oxford.

Salek-Haddadi, A et al. 2002. “Simultaneous EEG-Correlated Ictal fMRI.” *NeuroImage* 16(1): 32-40.

Salek-Haddadi, A et al. 2003a. “EEG quality during simultaneous functional MRI of interictal epileptiform discharges.” *Magnetic Resonance Imaging* 21(10): 1159-1166.

Salek-Haddadi, A et al. 2003b. “Studying spontaneous EEG activity with fMRI.” *Brain Research Reviews* 43(1): 110-133.

Salek-Haddadi, A et al. 2003c. “Functional magnetic resonance imaging of human absence seizures.” *Annals of Neurology* 53(5): 663-667.

Salek-Haddadi, A et al. 2006. “Hemodynamic correlates of epileptiform discharges: An EEG-fMRI study of 63 patients with focal epilepsy.” *Brain Research* 1088(1): 148-166.

Sanchez, R M, and F E Jensen. 2001. “Maturational Aspects of Epilepsy Mechanisms and Consequences for the Immature Brain.” *Epilepsia* 42(5): 577-585.

Scarff, C J et al. 2004. “Simultaneous 3-T fMRI and high-density recording of human auditory evoked potentials.” *NeuroImage* 23(3): 1129-1142.

Schaul, N. 1998. “The fundamental neural mechanisms of electroencephalography.” *Electroencephalography and Clinical Neurophysiology* 106(2): 101-107.

Scher, M S et al. 1993. “Ictal and Interictal Electrographic Seizure Durations in Preterm and Term Neonates.” *Epilepsia* 34(2): 284-288.

Scher, M S. 2003. “Neonatal seizures and brain damage.” *Pediatric Neurology* 29(5): 381-90.

Scher, M S et al. 2003. “Uncoupling of EEG-clinical neonatal seizures after antiepileptic drug use.” *Pediatric Neurology* 28(4): 277-280.

Schmidt, F E W et al. 2000. “A 32-channel time-resolved instrument for medical optical tomography.” *Review of Scientific Instruments* 71(1): 256.

Schmitz, C H et al. 2002. “Instrumentation for fast functional optical tomography.” *Review of Scientific Instruments* 73(2): 429-439.

Schmitz, C H et al. 2005. “Design and implementation of dynamic near-infrared optical tomographic imaging instrumentation for simultaneous dual-breast measurements.” *Applied Optics* 44(11): 2140-2153.

Scholkmann, F et al. 2010. “How to detect and reduce movement artifacts in near-infrared imaging using moving standard deviation and spline interpolation.” *Physiological Measurement* 31(5): 649-662.

Schreckenberger, M et al. 2004. “The thalamus as the generator and modulator of EEG alpha rhythm: a combined PET/EEG study with lorazepam challenge in humans.” *NeuroImage* 22(2): 637-644.

Schweiger, M, and S R Arridge. 1999. “Optical tomographic reconstruction in a complex head model using a priori region boundary information.” *Physics in Medicine and Biology* 44(11): 2703-2721.

Schweiger, M et al. 2003. “Computational aspects of diffuse optical tomography.” *Computing in Science & Engineering* 5(6): 33-41.

Sheth, S A et al. 2004. “Linear and Nonlinear Relationships between Neuronal Activity, Oxygen Metabolism, and Hemodynamic Responses.” *Neuron* 42(2): 347-355.

Shibasaki, H, and M Hallett. 2006. “What is the Bereitschaftspotential?.” *Clinical Neurophysiology* 117(11): 2341-2356.

Sie, L T L et al. 2001. “Functional MRI of Cortex in Sedated 18 Month-Old Infants with or Without Periventricular Leukomalacia.” *Developmental Medicine & Child Neurology* 43(07): 486-490.

Silverstein, F S. 2009. “Do Seizures Contribute to Neonatal Hypoxic-Ischemic Brain Injury?.” *The Journal of Pediatrics* 155(3): 305-306.

Silverstein, F S, and F E. Jensen. 2007. “Neonatal seizures.” *Annals of Neurology* 62(2): 112-120.

Steinhoff, B J et al. 1996. “Ictal near infrared spectroscopy in temporal lobe epilepsy: a pilot study.” *Seizure* 5(2): 97-101.

Steriade, M. 2000. “Corticothalamic resonance, states of vigilance and mentation.” *Neuroscience* 101(2): 243-276.

Stott, J J et al. 2003. “Optode Positional Calibration in Diffuse Optical Tomography.” *Applied Optics* 42(16): 3154-3162.

Swann, J W et al. 1989. “Postnatal development of GABA-mediated synaptic inhibition in rat hippocampus.” *Neuroscience* 28(3): 551-561.

Taga, G et al. 2004. “Hemodynamic responses to visual stimulation in occipital and frontal cortex of newborn infants: a near-infrared optical topography study.” *Pathophysiology* 10(3-4): 277-281.

Taga, G et al. 2007. “Effects of source-detector distance of near infrared spectroscopy on the measurement of the cortical hemodynamic response in infants.” *NeuroImage* 38(3): 452-460.

Tak, S et al. 2010. “Quantification of CMRO(2) without hypercapnia using simultaneous near-infrared spectroscopy and fMRI measurements.” *Physics in Medicine and Biology* 55(11): 3249-3269.

Tao, J X et al. 2005. “Intracranial EEG substrates of scalp EEG interictal spikes.” *Epilepsia* 46(5): 669-676.

Taylor, M J, and D L McCulloch. 1992. “Visual evoked potentials in infants and children.” *Journal of Clinical Neurophysiology* 9(3): 357-372.

Thees, S et al. 2003. “Dipole source localization and fMRI of simultaneously recorded data applied to somatosensory categorization.” *NeuroImage* 18(3): 707-719.

Thibeault-Eybalin, M P et al. 2009. “Neonatal seizures: do they damage the brain?.” *Pediatric Neurology* 40(3): 175-180.

Thornton, R et al. 2010. “EEG correlated functional MRI and postoperative outcome in focal epilepsy.” *Journal of Neurology, Neurosurgery & Psychiatry* 81(8): 922 -927.

Tidswell, T et al. 2001. “Three-Dimensional Electrical Impedance Tomography of Human Brain Activity.” *NeuroImage* 13(2): 283-294.

Toet, M C, and P M A Lemmers. 2009. “Brain monitoring in neonates.” *Early Human Development* 85(2): 77-84.

Toet, M C et al. 2002. “Comparison Between Simultaneously Recorded Amplitude Integrated Electroencephalogram (Cerebral Function Monitor) and Standard Electroencephalogram in Neonates.” *Pediatrics* 109(5): 772-779.

Toma, K et al. 2002. “Generators of Movement-Related Cortical Potentials: fMRI-Constrained EEG Dipole Source Analysis.” *NeuroImage* 17(1): 161-173.

Tyszczuk, L et al. 1998. “Cerebral Blood Flow Is Independent of Mean Arterial Blood Pressure in Preterm Infants Undergoing Intensive Care.” *Pediatrics* 102(2): 337-341.

Tyvaert, L et al. 2008. “Different structures involved during ictal and interictal epileptic activity in malformations of cortical development: an EEG-fMRI study.” *Brain* 131(8): 2042 -2060.

Uchida-Ota, M et al. 2008. “Intrinsic correlations of electroencephalography rhythms with cerebral hemodynamics during sleep transitions.” *NeuroImage* 42(1): 357-368.

Vanhatalo, S, and K Kaila. 2006. “Development of neonatal EEG activity: From phenomenology to physiology.” *Seminars in Fetal and Neonatal Medicine* 11(6): 471-478.

Vialatte, F B et al. 2010. “Steady-state visually evoked potentials: Focus on essential paradigms and future perspectives.” *Progress in Neurobiology* 90(4): 418-438.

Victor, J D, and J Mast. 1991. “A new statistic for steady-state evoked potentials.” *Electroencephalography and Clinical Neurophysiology* 78(5): 378-388.

Villringer, A et al. 1994. “Noninvasive assessment of cerebral hemodynamics and tissue oxygenation during activation of brain cell function in human adults using near infrared spectroscopy.” *Advances in Experimental Medicine and Biology* 345: 559-65.

Vulliemoz, S et al. 2010. “The combination of EEG source imaging and EEG-correlated functional MRI to map epileptic networks.” *Epilepsia* 51(4): 491-505.

Wallois, F et al. 2009. “Haemodynamic changes during seizure-like activity in a neonate: A simultaneous AC EEG-SPIR and high-resolution DC EEG recording.” *Neurophysiologie Clinique/Clinical Neurophysiology* 39(4-5): 217-227.

Warach, S et al. 1996. “EEG-triggered echo-planar functional MRI in epilepsy.” *Neurology* 47(1): 89-93.

Wasterlain, C G et al. 1993. “Pathophysiological mechanisms of brain damage from status epilepticus.” *Epilepsia* 34 Suppl 1: S37-53.

Watanabe, E et al. 2000. “Noninvasive cerebral blood volume measurement during seizures using multichannel near infrared spectroscopic topography.” *Journal of Biomedical Optics* 5(3): 287-290.

Watanabe, E et al. 2002. “Focus Diagnosis of Epilepsy Using Near-Infrared Spectroscopy.” *Epilepsia* 43(s9): 50-55.

Watanabe, H et al. 2008. “Functional activation in diverse regions of the developing brain of human infants.” *NeuroImage* 43(2): 346-357.

Weiner, S P et al. 1991. “Neonatal seizures: Electroclinical dissociation.” *Pediatric Neurology* 7(5): 363-368.

White, B R et al. 2009. “Resting-state functional connectivity in the human brain revealed with diffuse optical tomography.” *NeuroImage* 47(1) 148-156.

Wolf, M. 2004. “Near infrared Spectrophotometry Detects the Neuronal Activation Induced by Tactile, Auditory and Visual Stimulation.” *Pediatric Research* 56(3).

Wong, F Y et al. 2008. “Impaired Autoregulation in Preterm Infants Identified by Using Spatially Resolved Spectroscopy.” *Pediatrics* 121(3): e604-611.

Yamada, H et al. 2000. “A milestone for normal development of the infantile brain detected by functional MRI.” *Neurology* 55(2): 218-223.

Ye, J C et al. 2009. “NIRS-SPM: Statistical parametric mapping for near-infrared spectroscopy.” *NeuroImage* 44(2): 428-447.

Zaramella, P et al. 2001. “Brain auditory activation measured by near-infrared spectroscopy (NIRS) in neonates.” *Pediatric Research* 49(2): 213-219.

Zeff, B W et al. 2007. “Retinotopic mapping of adult human visual cortex with high-density diffuse optical tomography.” *Proceedings of the National Academy of Sciences* 104(29): 12169-12174.

Zimmermann, B et al. 2010. “The Confounding Effect of Systemic Physiology on the Hemodynamic Response in Newborns.” *OSA Biomedical Optics*.